Microwave Electronics

Design and Analysis of Printed UWB Antenna with Dual Band-Notched Characteristics

A thesis submitted by

SARAH JACOB

in partial fulfillment of the requirements for the degree of

DOCTOR OF PHILOSOPHY

Under the guidance of

Prof. P. MOHANAN

Department of Electronics
Faculty of Technology
Cochin University of Science and Technology
Cochin-22, India

November 2015

Design and Analysis of Printed UWB Antenna with Dual Band-notched Characteristics

Ph.D. Thesis under the Faculty of Technology

Author

Sarah Jacob,
Research Scholar,
Department of Electronics,
Cochin University of Science and Technology,
Cochin- 682022.
Email: sarahjacob12@gmail.com

Supervising Guide

Dr. P. Mohanan,
Professor,
Department of Electronics,
Cochin University of Science and Technology,
Cochin – 682022.
Email: drmohan@gmail.com

November 2015

DEPARTMENT OF ELECTRONICS
COCHIN UNIVERSITY OF SCIENCE AND
TECHNOLOGY
COCHIN-22, INDIA.

Dr. P. Mohanan
Professor
E-mail: drmohan@cusat.ac.in

Certificate

This is to certify that this thesis entitled "**Design and Analysis of Printed UWB Antenna with Dual Band-notched Characteristics**" is a bonafide record of the research work carried out by Smt. Sarah Jacob under my supervision in the Department of Electronics, Cochin University of Science and Technology. The results embodied in this thesis or parts of it have not been presented for any other degree.

I further certify that the corrections and modifications suggested by the audience during the pre-synopsis seminar and recommended by the Doctoral Committee of Smt. Sarah Jacob are incorporated in the thesis.

Cochin-22,   **Dr. P. Mohanan**
November 2015.   (Supervising guide)

Declaration

I hereby declare that the work presented in this thesis entitled "**Design and Analysis of Printed UWB Antenna with Dual Band-notched Characteristics"** is a bonafide record of the research work done by me under the supervision of Dr. P. Mohanan, Professor, Department of Electronics, Cochin University of Science and Technology, India and that no part thereof has been presented for the award of any other degree.

Cochin-22,
November 2015.

Sarah Jacob,
Research Scholar.

Acknowledgement

I remember with gratitude…

First and foremost, I would like to express my sincere thanks to my supervisor, Professor P. Mohanan. He has given me valuable ideas and suggestions with his insightful knowledge and rich research experience which guides me in the right direction. I am very much indebted to his efforts of helping me to complete this dissertation.

I thank from the bottom of my heart Dr. K. Vasudevan, Emeritus Professor, former Dean, Faculty of Technology, CUSAT for his timely support and constant encouragements through all my years at the department.

I am grateful to Prof. C. K. Aanadan, former Head, Department of Electronics for his whole-hearted support and extending the facilities of the Department of Electronics for my research.

A special and sincere acknowledgement goes to Dr. P. R. S. Pillai, Emeritus Professor, Department of Electronics for the advice and care rented during these years.

My sincere thanks to Dr. M. H. Supriya, Professor and Head, Department of Electronics for her valuable suggestions and supports.

In this context let me also thank Dr. Tessamma Thomas, Dr. James Kurien and all other faculty members of Department of Electronics for the help and assistance extended to me. I thank all the non-teaching staff and technical staff at the Department of Electronics for their sincere cooperation and valuable helps.

I remember with gratitude, Dr. S. Mridula, School of Engineering, CUSAT for her guidance and encouragement towards my research. Special thanks to Dr. Binu Paul and Mrs. Anju Pradeep for their whole-hearted support and helps.

▓▓▓ Abstract ▓▓▓

The thesis deals with the design of two types of compact printed antennas suitable for Ultra-wide Band (UWB) applications in WiMAX/WLAN environment; truncated circular disc monopole antenna and a modified rectangular slot antenna. Through structure modifications, these antennas are made to support overlapping multiple modes to provide UWB response.

The analyses of these antennas are performed using standard simulation tools used in industry/academia and the characteristics are verified with experimental results. Based on the current patterns and parametric studies, design equations for the proposed antennas on any substrates are deduced and validated using simulation tools. Then techniques to circumvent interference from co-existing narrow band services (WiMAX and WLAN) are also discussed for both the antennas.

As far as the design of UWB system is considered, one of the major criteria is the transmission of narrow pulses with minimum dispersion in addition to compact size and stable gain. So these antennas required linear phase response in frequency domain or excellent transient response in time domain. Both the time domain and frequency domain characterisation of the antennas are elaborately discussed in the thesis.

▐▐▐ Contents ▐▐▐

List of Abbreviations

BPSK	Binary Phase Shift Keying
BW	Band Width
CPW	Co-planar Waveguide
CR	Cognitive Radio
CST	Computer Simulation Technology
DGS	Defected Ground Structure
SIR-DGS	Stepped Impedance Resonator-DGS
DSSS	Direct Sequence Spread Spectrum
EBG	Electromagnetic Band Gap
CLV-EBG	Corner-Located vias EBG
ELV-EBG	Edge Located vias EBG
EMI/EMC	Electromagnetic Interference/ Compatibility
FCC	Federal Communication Commission
FDTD	Finite Difference Time Domain
FWHM	Full Width Half Maximum
Gbps	Giga bits per second
HF	High Frequency
IFFT	Inverse Fast Fourier Transform
IRA	Impulse Radiating Antennas
LNA	Low Noise Amplifier
LOS	Line of Sight
NLOS	Non-LOS
LTI	Linear Time Invariant
MIMO	Multiple-input-Multiple-output

ML	Meander line
MEMS	Micro Electro Mechanical Systems
MMIC	Monolithic Microwave Integrated Circuits
OFDM	Orthogonal Frequency Division Multiplexing
PAM	Pulse Amplitude Modulation
PCB	Printed Circuit Board
PPM	Pulse Position Modulation
PSD	Power Spectral Density
RL	Return loss
RF	Radio Frequency
SNR	Signal to Noise Ratio
SRR	Split-Ring Resonator
C-SRR	Complementary-SRR
UWB	Ultra-wide Band
DS-UWB	Direct Sequence-UWB
I-UWB	Impulse-UWB
VNA	Vector Network Analyser
VSWR	Voltage Standing Wave Ratio
WiMAX	Worldwide Interoperability for Microwave Access
WLAN	Wireless Local Area Networks
WPAN	Wireless Personal Area Networks

…..ೞಐ…..

List of Symbols

t - time

τ – pulse width

f – frequency

ω – angular frequency $(= 2\pi f)$

θ – elevation angle

φ – azimuth angle

c – velocity of light

λ – wavelength

Γ – reflection coefficient

η – efficency

τ_g - group delay

τ_r – ringing duration

ϕ – signal phase

Z_o - free space impedance (120π)

G - gain

S_{11} - return loss

S_{21} - antenna transfer function

Chapter 1

INTRODUCTION

This chapter encapsulates the broad band wireless communication technologies which throw light into the development of new technology called "Ultra-wide Band" (UWB). UWB signal waveforms and the transmission schemes are described. It further highlights the features of UWB which make it a leading standard for high speed data communication over short distance. A brief history of various UWB antennas developed from time to time is discussed. Motivation behind the present work is described and the chapter is concluded with the organization of the thesis.

1.1 Broad Band Wireless Technologies

Generally wireless broad band refers to technology that use point to point or point to multipoint services to transmit signals between hub and end-user receiver [1]. Broad band wireless services employ radio

waves to transmit and receive data directly to and from the potential users. It guarantees high-speed connection over the air. Higher frequencies have the advantages of wide bandwidth, reduced antenna size and ease of installation as compared to lower frequencies. But high frequency systems suffer from range limitations under poor weather conditions, eg. rain and fog.

Broad band wireless technologies can be classified into different types depending on their features. Each wireless technology is designed to serve a specific application. The requirements for each application are based on different parameters such as data rate, distance and power. Classification of wireless technologies based on the distance coverage [2] is shown in Fig. 1.1.
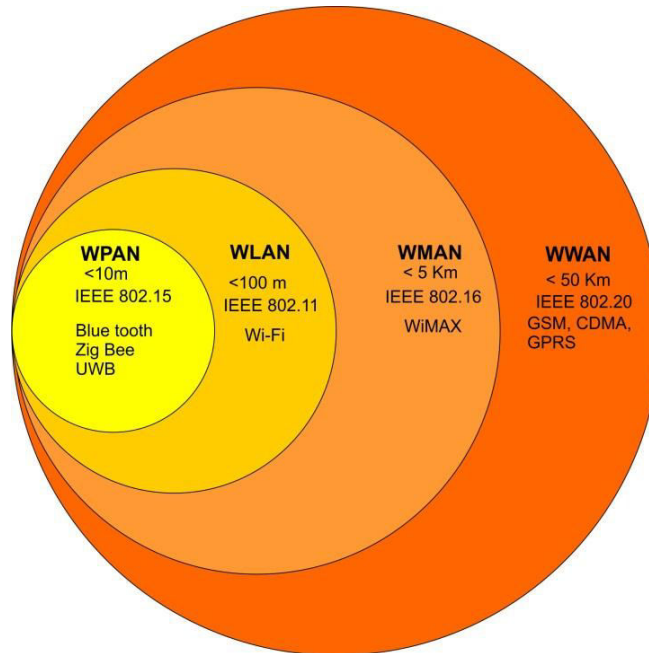
Fig.1.1: Classification of broadband wireless technologies

Wireless Local Area Networks (WLANs), with a transmission radius of the order of hundreds of meters, and Wireless Personal Area Networks (WPANs), with a transmission range of the order of tens of meters or less, are rapidly established as popular applications of wireless technology. For the above networks, the demand for high data rate is continually increasing [3]. In addition to the IEEE 802.11 WLAN products (Wi-Fi) and Bluetooth-based IEEE 802.15 WPAN products, there is a great variety of wireless networking products for home and commercial applications [4]. So in recent years, the WPAN aimed to provide reliable and high speed wireless connections between computers, portable devices and consumer electronics within a short range.

According to Shannon-Hartley channel capacity theorem, channel capacity C in bps is given by

$$C = BW * log_2(1 + SNR) \text{ ....(1.1)}$$

where BW is the bandwidth and SNR is the signal to noise ratio. From (1.1), the capacity increases linearly with BW and logarithmically with SNR, so the bit rate can be increased to the required level by simply increasing the bandwidth rather than the transmitter power $(SNR = \frac{P_t}{P_N})$. Moreover, increasing the transmitter power beyond certain limits may adversely affect the normal functioning of the portable devices and living objects. As such large bandwidth is the best solution to achieve high data rate.

New generation wireless mobile radio systems serve many users with the target to provide a wide range of applications to all the users. This is not easy to achieve because of the constraints on the available spectrum and power. The future wireless technologies will face the problem of spectral scarcity as the number of mobile devices increases and the co-existence of wireless devices will become a major issue. So an innovative technology that can co-exist with devices operating at various frequency bands is required [5].

These demands for high data rate and co-existence of wireless devices led to the formation of IEEE 802.15.3 Task Group for development of a standard for high-rate WPANs [6] and then of a new study group (IEEE 802.15.SG3a—now a task group, IEEE 802.15.3a) to consider an alternative high-rate physical layer that possibly will be implemented using Ultra-wide Band technology (UWB) [7].

1.2 Ultra-wide Band (UWB) Technology

UWB is a wireless communication technology which transmits large amounts of data using low power narrow radio pulses/ impulses of duration less than 1 nanosecond. Since it does not require a high frequency carrier to deliver data over a short distance, it is also known as carrier-free, impulse or base-band radio.

According to Federal Communication Commission's (FCC's) definition, UWB is the one for which the fractional bandwidth is greater than 20% or occupying an instantaneous bandwidth of at least 500 MHz [8]. Fractional bandwidth B_f is a factor used to classify narrowband,

wideband or ultra-wideband and is defined as the ratio of signal bandwidth B_s to the centre frequency f_c

$$B_f = \frac{B_s}{f_c} = \frac{2(f_h - f_l)}{f_h + f_l} \quad .... (1.2)$$

where f_h and f_l are the upper and lower edge frequencies of the operating band respectively.

UWB technology offers a promising solution to the radio frequency (RF) spectrum scarcity by allowing new services to co-exist with other wireless narrow band systems [5]. The transmitted power of UWB devices is controlled by the regulatory agencies to make these narrow band systems immune to the UWB interferences. The low power (approximately 0.5 mW) UWB signal is made to spread over a wide band width of 7.5 GHz (3.1–10.6 GHz allotted by FCC) resulting in a power spectral density of -41.3 dBm/MHz which is much less than other wireless narrow band systems. This makes the UWB signals appear as background noise to these wireless systems thus permit to co-exist with them. Therefore, the UWB systems are allowed to co-exist with other technologies only under stringent power constraints.

UWB was initially developed for military applications, so very narrow development took place in the commercial area. A considerable outpouring of research interest has occurred since 2002, when FCC has recommended unlicensed/commercial use of UWB spectrum. Subsequently, UWB attracted researchers and industrialists because of its potential for high speed data communication over short distance.

UWB offers attractive solution for many wireless communication areas including wireless telemetry, telemedicine and wireless sensor networks. The development of UWB has been carried out for many years in the laboratories and now it has been regarded as the leading standard of WPAN technology which allows high speed wireless transmission of data to multiple devices within a distance of 10 m from the host device [9] - [10] as shown in Fig. 1.2.

Fig. 1.2: UWB communication scenarios
(from www.exuberantsolution.com)

A brief overview of UWB history, FCC emission limits, concepts of UWB signal waveforms, single band and multiband transmission schemes, advantages and applications are presented in the following sections.

1.2.1 UWB History

UWB radio is an old and at the same time a new technology also. In 1887, Hertz generated the first UWB signals, which was in the form of sparks and radiated using wide-band loaded dipoles. At that time, short pulses were the easiest waveforms to generate [11].

The work by Hertz is refined by Guglielmo Marconi into a transatlantic radio system in 1901 where the spark gap radio transmitters were used to transmit Morse code sequences across the Atlantic Ocean. Spark-gap transmitter generates impulse signals with very wide bandwidth. However, the benefits of a large bandwidth and possibility of multi-user systems were not considered at that time [12]. Later on, the communication systems concentrated more on the carrier-based narrow band systems, which allowed many stations to share a band of frequencies (multiplexing) with the technology available at that time [11].

In the 1950s, the pulse based transmission gained interest in military applications with the implementation of impulse radars.

Approximately fifty years after Marconi, contributions to the development of UWB commenced in the late 1960's with the pioneering contributions of Harmuth at Catholic University of America, Ross and Robbins at Sperry Rand Corporation, Paul van Etten at the USAF's Rome Air Development Centre and in Russia [13].

Harmuth published papers, 1969-1984, on the basic design for UWB transmitters and receivers. Ross and Robbins (R&R), 1972-1987,

pioneered the use of UWB signals in a number of application areas, including communications and radar. Ross's US patent (1973) is a landmark in UWB communications [13].

UWB radar system for penetrating the ground was designed by Morey in 1974 and became a commercial success at Geophysical Survey Systems, Inc. (GSSI). Other subsurface UWB radar designs were also introduced [14]. Van Etten's empirical testing of UWB radar systems in 1977 resulted in the development of system design and antenna concepts [15].

Development of sample and hold receivers for commercial applications (mainly for oscilloscopes) in the late 1960s, was also an aid to the developing UWB field [16]. Other advances in the development of the sampling oscilloscope were made at the Hewlett Packard Company. These approaches were adopted into UWB designs later.

In 1960s, the original research on pulse transmitters, receivers and antennas were performed by both Lawrence Livermore National Laboratory (LLNL) and Los Alamos National Laboratory (LANL). LLNL expanded its laser-based diagnostics research into pulse diagnostics. Thus the basic designs for UWB signal systems were available by the early 1970s. By 1975, the construction of UWB communications/ radar systems could be possible using the components purchased from Tektronix. In 1978 Bennett & Ross summarised the pulse generation methods [13].

The USAF held a program in UWB system development during the period 1977-1989, headed by Col. J. D. Taylor. At that time, a number of synonymous terms such as: impulse, carrier-free, baseband, large-relative-bandwidth radio/radar signals etc. were used to refer the UWB technology. The term "ultra-wide band", was not applied to these systems until about 1989, appeared in a publication of Department of Defense in the United States (U.S.) [13].

By 1990's, over 50 patents were issued on topics related to UWB technology such as UWB pulse generation/ reception and applications such as communications, radar, automobile collision avoidance, positioning systems, liquid level sensing and altimetry [17].

By the late 1990s, UWB technology and its development had advanced greatly. Commencing with a conference held at W.J. Schafer Associates [18] and one at LANL in 1990 [19], there have been numerous meetings held on impulse radar/radio.

The first patent with the exact phrase "UWB antenna" was filed on behalf of Hughes in 1993.

In 1994, T.E. McEwan, then at LLNL, invented the Micro power Impulse Radar (MIR) which provided for the first time a UWB operating at ultra low power, besides being extremely compact and inexpensive [20]-[21]. This was the first UWB radar to operate on only microwatts of battery drain.

In earlier times, from 1960 to 1990's, this technology was restricted to highly protected military applications. Development in

modern digital systems and high speed semiconductor technology made UWB suitable for various commercial applications. This led to the increased demand for the commercialization of UWB spectrum among the developers of UWB systems. Since UWB signals occupy a large frequency range, spectrum overlap with other conventional narrowband systems will occur. Promoters of the technology claimed that the UWB emissions would not interfere with other narrowband services. In February 2002, Part 15 rules which govern the unlicensed radio devices are amended by FCC to include the operation of UWB devices with strict power emission limits [8]. A substantial growth in UWB systems took place after the FCC allocated a bandwidth of 7.5 GHz, i.e. from 3.1 GHz to 10.6 GHz for commercial applications.

1.2.2 FCC Emission limits

In order make co-existing narrow band radio services unaffected by UWB signals, FCC has assigned emission masks between 3.1 GHz to 10.6 GHz for commercial UWB devices. The maximum allowed power spectral density for these devices is –41.3dBm/MHz or 75 nW/MHz which is same as the level of unintentional radiators (FCC Part 15 class) such as televisions and computer monitors [22].

Based on the FCC regulations, UWB devices are classified into three major categories; communication, imaging and vehicular radar. Since the thesis deals with antennas for communication devices, emission limits applicable to the communication devices alone is discussed here. Short-range communication systems including wireless personal area networks and measurement systems are grouped under this category.

Extensive use of UWB devices in home, offices and public places enhanced the growth of communication devices.

For indoor and outdoor UWB communication devices different emission limits has been assigned by FCC. The spectral mask for indoor devices is 10 dB more than that for outdoor devices, between 1.61 GHz to 3.1 GHz and 10.6 GHz to 29 GHz, as shown in Fig. 1.3 and Table 1.1. This is to protect various other Government systems in the 1.61 GHz to 3.1 GHz band and satellite systems above 10.6 GHz.
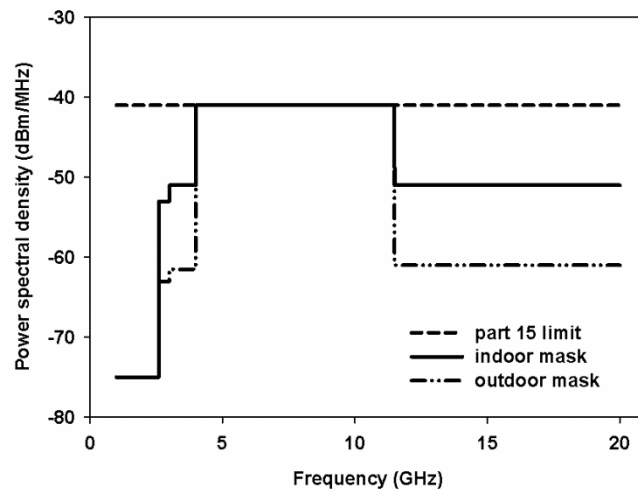
Fig. 1.3: UWB indoor/outdoor emission limits for communication systems

Table 1.1: UWB emission limits for communication devices [8]

Power spectral density (dBm/MHz)		Operational bandwidth (GHz)					
		0.96-1.61	1.61-1.99	1.99-3.1	3.1-10.6	10.6-22.0	22.0-29.0
	Indoor	-75.3	-53.3	-51.3	-41.3	-51.3	-51.3
	Outdoor	-75.3	-63.3	-61.3	-41.3	-61.3	-61.3

According to FCC regulations, indoor UWB devices must be of handheld equipment and are restricted to peer-to-peer operations inside buildings. As per FCC's rule use of fixed infrastructure and antennas mounted outdoor are not allowed for UWB communications in outdoor environments. Therefore, outdoor UWB communications are restricted to handheld devices. These devices are permitted to send information only to their associated receivers. In addition, these devices must stop emission within 10 seconds on non-receipt of acknowledgement from an associated receiver [23]-[24].

1.2.3 UWB Signal Waveforms

All the pulses with spectra wider than 500 MHz can be used as the UWB signals. Practically, pulses which have no DC component are considered to avoid the wastage of transmitted power. Owing to unique spectral properties, a family of Rayleigh (differentiated Gaussian) pulses $s_n(t)$ are widely used as the source pulses in the UWB systems [25] and is given by

$$s_n(t) = \frac{d^n}{d^n t}\left[e^{-\left(\frac{t}{\tau}\right)^2}\right]$$ ....(1.3)

where t represents time and τ is the pulse width.

Gaussian monocycle, the first derivative of Gaussian pulse was the original proposal for UWB radar and communication systems [26] and is given by

$$s_1(t) = \frac{t}{\tau}e^{-(t/\tau)^2}$$ ....(1.4)

where t represents time and τ is the pulse width. But its Power Spectral Density (PSD) for different values of pulse width (τ) does not fully fall into the UWB band defined by the FCC.

(a)

(b)
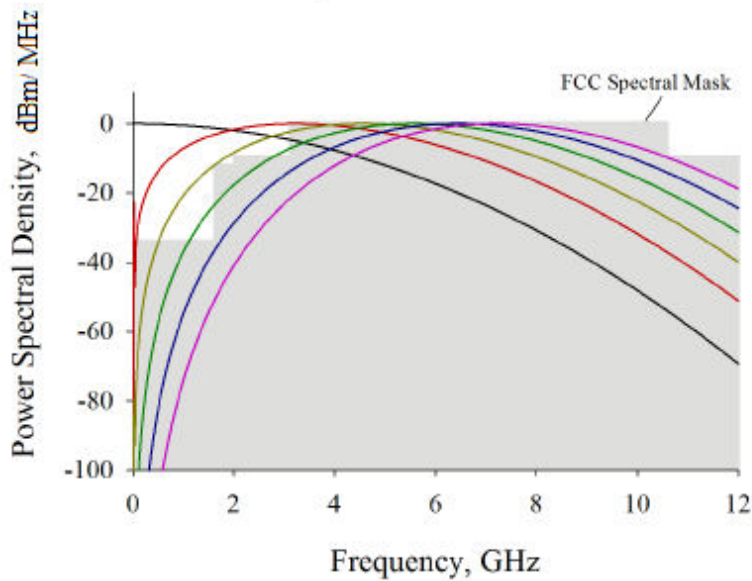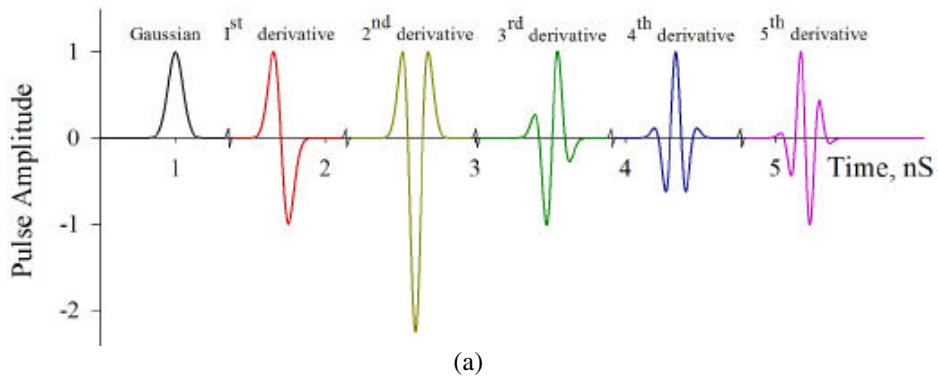
Fig. 1.4: Family of Rayleigh pulses (a) wave forms and (b) power spectral density

Family of Rayleigh pulses and the corresponding PSD are shown in Fig. 1.4. For Rayleigh pulses up to third order, the PSDs at frequencies lower than 3.1 GHz is not within the FCC mask. As the order of the pulse increases, PSD moves to higher frequencies. By choosing the order and a suitable pulse width, a pulse that satisfies the FCC masks can be obtained. Some higher order Rayleigh pulses such as fourth order Rayleigh pulse with $67 < \tau < 76\ ps$ and fifth order Rayleigh pulse with $72 < \tau < 91\ ps$ can match the UWB band directly [25].

1.2.4 Transmission Schemes

Single band and multiband are two possible technologies for transmission of signals over the UWB spectrum [5], [27]. The single band technique supports the idea of impulse radio, the initial approach to UWB technology. It uses narrow pulses so that their spectra occupy a large portion of the UWB band as in Fig. 1.5 (a). Since the pulse width is very narrow, typically in picoseconds, it can provide high resolution of multi path in UWB channels. Pulse Amplitude Modulation (PAM) or Pulse Position Modulation (PPM) is employed to modulate the UWB waveforms. Here continuous radio frequencies are not used in the modulation process as in narrow band and wide band technologies. Time hopping schemes are used to support multiple users.

Direct Sequence-UWB (DS-UWB) is a single band approach which transmits and receives data using narrow UWB pulses combined with Direct Sequence Spread Spectrum (DSSS) technique. Data representation in this approach is based on simple Binary Phase Shift Keying (BPSK) modulation and can achieve data rates in excess of 1 Gbps. The Rake

receivers are used to receive the signal from multiple paths in a multipath channel. Simple Impulse-UWB (I-UWB) systems are inexpensive to construct as it does not require any up and down conversion and result in reduced complexity in transceivers. To mitigate the effects of narrow band interferers, notch filters are required in impulse radios.
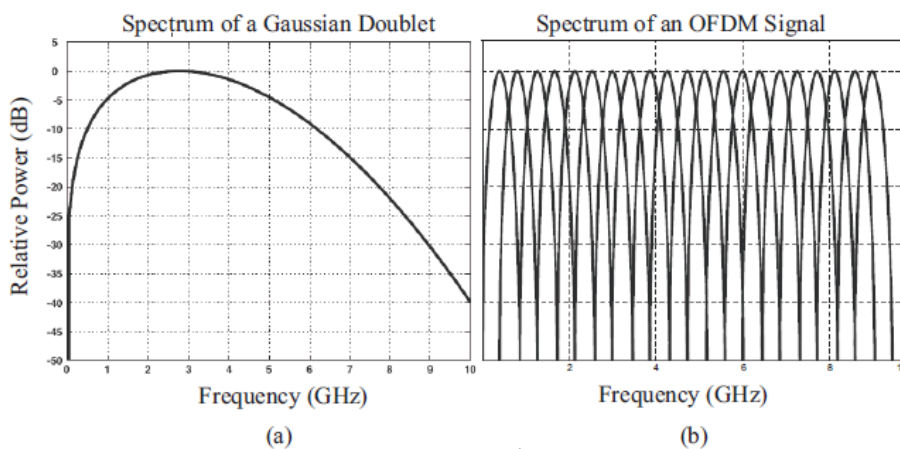
Fig. 1.5: Comparison of (a) impulse radio and (b) multi band UWB spectrum

The multiband technique divides the available UWB frequency spectrum (3.1 GHz to 10.6 GHz) into several small and non-overlapping bands with bandwidths greater than 500 MHz to satisfy the FCC's definition of UWB signals as shown in Fig. 1.5 (b). This method is similar to the narrowband frequency-hopping technique. Each of the source pulses is designed to occupy only one sub-band. By dividing the UWB spectrum into several frequency bands it is possible to avoid transmission over certain bands, such as 802.11a at 5 GHz, so as to prevent potential interference. In the multiband approach, since the pulses are not too narrow, the synchronisation requirements are not too

critical as in single band UWB transmission. A number of modulation methods have been proposed by industry leaders for the multiband approach; however, Orthogonal Frequency Division Multiplexing (OFDM), which was initially proposed by Texas Instruments, offers improved performance for high data rate applications [27].

1.2.5 Advantages of UWB

The spectral properties of narrow pulses used in UWB technology offers several advantages over narrow band and wide band communication systems. This section describes some of the benefits that UWB brings to wireless communications [27], [28]-[29].

High channel capacity:

Channel capacity, or data rate, is defined as the maximum amount of data that can be transmitted per second over a communications channel. From Shannon-Hartley's capacity formula (1.1), a data rate of Gigabits per second (Gbps) can be obtained with UWB signals. High data rate is available only for short ranges of less than 10 m because of the FCC's emission limit on UWB transmissions. This makes UWB systems a perfect candidate for high speed, short-range wireless applications such as WPANs.

Operate with low SNR:

Again from Shannon-Hartley's formula (1.1), it is clear that UWB systems are able to offer large channel capacity even in the midst of noisy environment since the data rate depends linearly on bandwidth and logarithmically on the SNR .

RF spectrum sharing:

As the emissions level of UWB is below the noise floor of co-existing narrow band users as in Fig. 1.6, they are able to share spectrum with these services with minimal or no interference. Thus offers a promising solution to the scarcity in RF spectrum. This co-existence brings the advantage of avoiding expensive spectrum licensing fees that providers of all other radio services must pay.
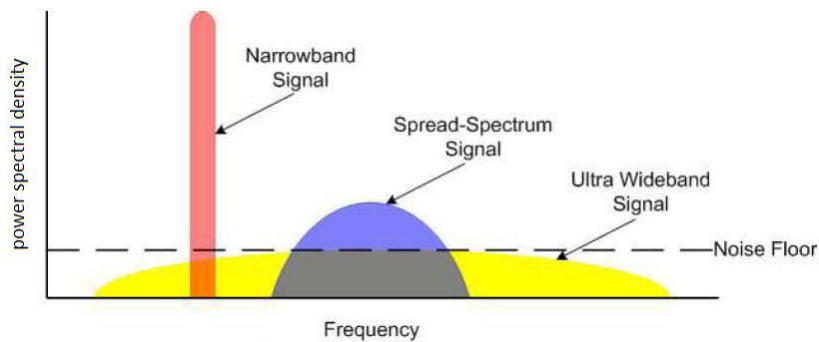
Fig. 1.6: Coexistence of UWB signals with narrowband and wideband signals in the RF spectrum [30]

Immunity to intercept and detection:

In military communications, there are many potential threats about the security of the signal. UWB communications systems have an inherent immunity/ low probability to detection and intercept because of their low average transmission power. Ultra-wide band communications spread transmitting power across a wide spectrum of frequency, resulting in power spectral density lower than the noise floor of the other wireless services. So the UWB signals are relatively resistant to intentional and unintentional jamming, because no jammer can jam every frequency in the UWB spectrum at once.

Robustness against multipath propagation:

Signals from the transmitter reach the receiver by direct or Line Of Sight (LOS) and indirect (Multipath/NLOS) path. Multipath propagation results from the multiple reflections of the transmitted signal from various surfaces such as buildings, trees, mountains etc. This causes the degradation in the resultant signal at the receiver end when LOS and NLOS are out-of -phase. On the other hand, since the UWB pulses are narrow pulses of duration less than nanoseconds the reflected pulses (NLOS) will not get the sufficient time to overlap with the LOS pulses at the receiver end, so the chances of signal degradation is reduced.

Ranging and imaging capability:

Signals in the lower band of the UWB spectrum are able to penetrate a variety of materials, even the walls. This penetration property improves the coverage of the UWB radios and makes these systems useful for applications such as through - the - wall communication and ground penetrating radars.

Simple transceiver design:

Since the I-UWB transmission is carrier less, it requires fewer RF components than carrier based transmission like narrowband and wideband technologies. There is no need for mixers and local oscillators to translate the modulated signal to the required frequency band; consequently there is no need for a carrier recovery stage at the receiver end. Further, the transmission of low-power pulses eliminates the need for a power amplifier in UWB transmitters.

1.2.6 Applications of UWB

UWB technology offer major developments in three wireless application areas: communications, radar and positioning or localization. A brief summary of UWB applications [24], [31]-[32] are listed in Table 1.2.

Table 1.2: Summary of UWB applications

Areas	Applications	
	Military	**Commercial**
Data Communications	Covert military communication Wireless sensor networks (detection of biological agents, tracking of enemies on battlefield)	Local and personal area networks (computer peripherals sending messages to the same computer from anywhere in the given range) Wireless streaming video distribution (home networking) Wireless sensor networks (health and habitat monitoring, environment observation, home automation)
Radar	High resolution radar Through-wall imaging (for law enforcement, fire-fighters) Ground-penetrating radar (for rescue operations) Surveillance and monitoring	Medical imaging (remote heart monitoring) Ground-penetrating radar (detection of electrical wiring, studs, etc. on construction sites) Automotive industry (collision avoidance, road side assistance)
Localization	Personnel identification Lost children Prisoner tracking	Inventory tracking Tagging and identification (RFID) Asset management

Short range wireless data communication technologies currently available are Bluetooth, UWB, ZigBee and Wi-Fi which are corresponding to the IEEE 802.15.1, 802.15.3, 802.15.4, and 802.11a/b/g standards respectively. Comparison of these technologies [24], [33] are summarised in Table 1.3.

Table 1.3: Comparison of short range data communication technologies

Technology	WLAN			Bluetooth	UWB	ZigBee
IEEE standard	802.11a	802.11b	802.11g	802.15.1	802.15.3a	802.15.4
Frequency (GHz)	5	2.4	2.4	2.4	3.1 – 10.6	2.4
Max. data rate (Mbps)	54	11	54	1	> 100	250 Kbps
Max. range (meters)	100	100	100	10	10	50
Band width (MHz)	22	22	22	1	500 - 7500	2

1.3   Development of UWB Antennas

The antenna is an essential part of any wireless system since it provides transition between guided wave and free-space wave. According to the IEEE standard definitions for antenna, an antenna is defined as a means for radiating or receiving radio waves.

UWB antenna belongs to the class of broad band antennas which operate over wide bandwidth. The term bandwidth refers to two types of definition; impedance bandwidth and pattern bandwidth. Impedance

bandwidth relates the parameters input impedance, voltage standing wave ratio (VSWR), and return loss while the pattern bandwidth to radiation pattern, gain and polarisation.

A brief history of UWB antennas is presented in [34] – [35].

Several advances in antennas were patented in 1897 by Lodge and new terms such as matching, tuning and impedance were added to the antenna theory. In 1898, Oliver Lodge [36] firstly introduced the concept of UWB antenna design like spherical dipoles, square plate dipoles, triangular or "bow-tie" dipoles and biconical dipoles. After that, a number of types of UWB antennas were developed in the following several years such as conical monopole, biconical dipole incorporating a tapered feed, coaxial horn, volcano smoke antenna etc.

Biconical dipole antenna in Fig. 1.7 (a) was the first UWB antenna introduced by Oliver Lodge. The input impedances of the infinitely long bi-cone is uniform and real. They can offer real constant impedances and consistent pattern properties over a frequency bandwidth greater than 10:1. Rumsey's principle suggests that the pattern properties of an antenna will be frequency independent if the antenna shape is specified only in terms of angles. Infinite bi-conical antenna is a good example whose shape is completely described by angles.
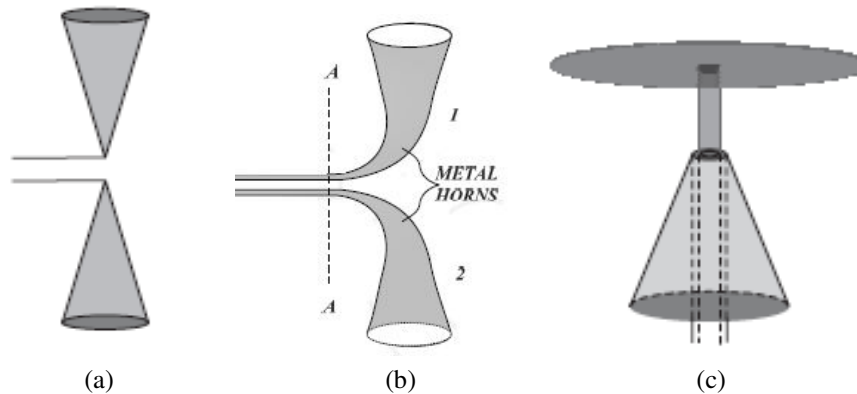
Fig. 1.7: (a) Bi-conical (b) Tapered feed bi-conical and (c) Discone

In 1939 Carter [37] improved Lodge's original design by incorporating a tapered feed as Fig. 1.7 (b), one of the key steps towards the design of broadband antennas.

Discone antennas are obtained by introducing variation to the basic geometry of the bi-conical antenna. Discone comprises a disk and a cone as shown in Fig. 1.7 (c). The antenna performance as a function of frequency is similar to a high-pass filter. Below an effective cutoff frequency it becomes inefficient and produces severe standing waves in the feed line. At cut-off, the slant height of the cone is approximately $\frac{\lambda}{4}$. They have relatively constant input impedance, satisfactory radiation pattern and gain over wide bandwidths with beam widths tending to become smaller. The antenna gain is larger with increasing frequency and that may be highly desirable and useful.
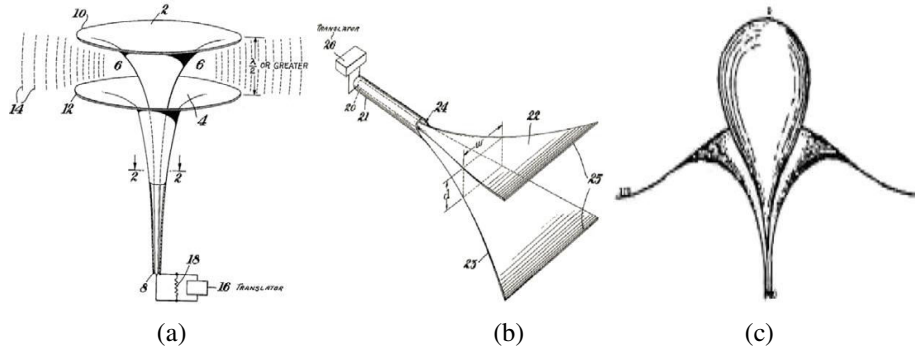
Fig. 1.8: (a) omni-directional coaxial horn (b) directional coaxial horn and (c) volcano smoke antenna

During the period 1940's, coaxial transitions became one of the design techniques for antenna researchers and designers. At that time coaxial horns were the most well-known UWB antenna. L. N. Brillouin [38] developed omni-directional and directional coaxial horns, as shown in Fig. 1.8 (a) and (b). But these two antennas are difficult to manufacture and install because of their bulky structure.

In 1940, J. C. Kraus [39] also developed an antenna similar to the coaxial horn called as volcano smoke antenna as in Fig.1.8 (c), which played a significant role as the foundation of television development. Investigations carried out on this antenna showed that this bulging monopole-like structure yields an impedance bandwidth ratio ($\frac{f_h}{f_l}$) of 5:1.

Even though the conventional UWB antennas were widely used in the broadcast communication applications, they are not suitable for applications in modern communication systems due to their solid (3D) structure, high manufacturing cost and difficulty in integration with the systems.

Last decade, some novel types of onmi-directional UWB antennas such as planar monopole antenna and printed monopole antenna, have been developed to meet the demands of wireless systems such as miniaturisation and low fabrication cost. They can provide almost the same bandwidth and radiation performances as the conventional UWB antennas with much smaller volumes by using certain techniques.

The planar monopole antenna was firstly reported in 1976 by G. Dubost and S. Zisler [40]. This was realized by replacing a conventional wire monopole with a planar monopole. The planar monopole is located above a ground plane and fed using coaxial probe. After that several planar monopole antennas with bandwidth ratio varying from 2:1 to more than 10:1 have been developed as in Fig. 1.9. Bandwidth comparison of several planar monopoles with regular geometries such as rectangular, square, circular and elliptical was carried out [41]. Among these the circular and elliptical monopoles exhibit much wider bandwidth exceeding of 10:1. A trapezoidal planar monopole proposed by Evans [42] achieved a bandwidth ratio exceeding of 11:1. Besides the regular structures, Suh [43] proposed an interesting structure, the Planar Inverted Cone Antenna (PICA), which can provide an impedance bandwidth ratio of more than 10:1.
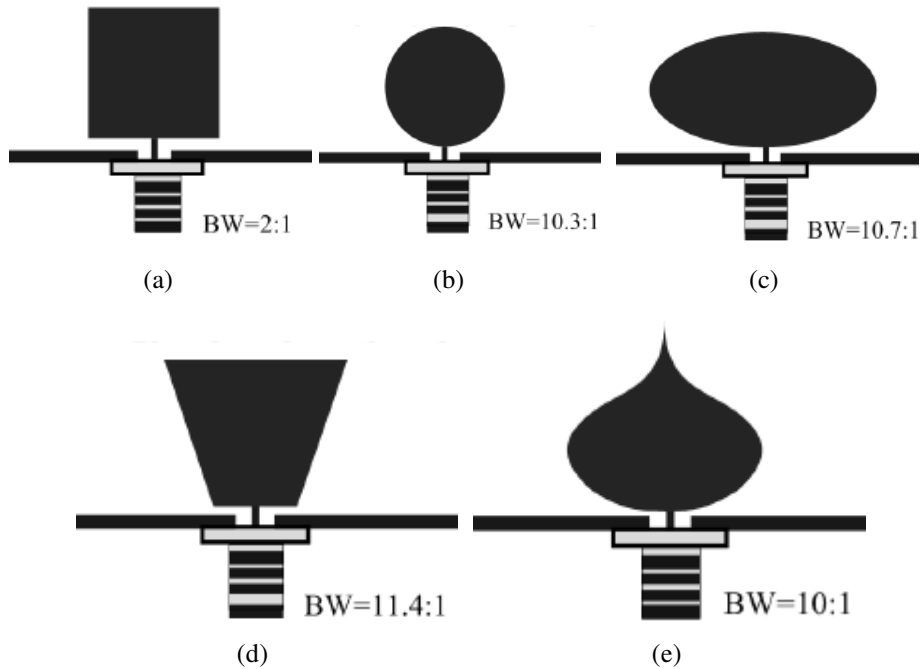
Fig. 1.9: various geometries of planar monopole antennas [35]

The planar monopoles mentioned above require a perpendicular ground plane, resulting in large volume and inconvenience for integration with portable wireless devices. So the printed monopole antennas are more popular in portable wireless devices due to their compact size and ease of integration with Monolithic Microwave Integrated Circuits (MMICs). The printed UWB monopole antenna usually consists of a monopole patch and a ground plane. Both of them are printed on the same side of a substrate with Co-planar Waveguide (CPW) line or on opposite sides with microstrip line to excite the patch.

Printed antennas became more attractive due to their features such as wide impedance bandwidth, good radiation properties, simple

structure and the ease of fabrication. Studies on various printed monopole antennas performed mainly focussed on microstrip or CPW fed monopole and slot type antennas. A detailed literature review of the same is done in the second chapter of this thesis.

1.4   Motivation of the Present Work

Even though many significant developments has been taken place in the UWB technology in past years still there are concerns which make this field live even today. One of the concerns is related to UWB antenna designs which have a considerable effect on the performance of the UWB systems. Here we discuss the technical and practical design goals for an antenna as far as the UWB system is considered.

By definition, UWB system operates in the frequency range of 3.1 GHz - 10.6 GHz, i.e., it extends over a bandwidth of 7.5 GHz. So attaining a wide impedance bandwidth is the main challenge in the UWB antenna design. As the UWB communication system is considered the PSD of the system must comply with the FCC's emission limits to ensure the co-existence with the other wireless services. Then for effective signal reception, antennas with high radiation efficiency is required because the transmit power spectral density is excessively low. Any excessive losses incurred by the antenna could degrade the performance of the system.

Freedom in transmitter and receiver location is another important requirement in data communication applications where many computer peripheral devices communicate with the same computer from anywhere

within a specified area. To meet this condition, antenna with nearly omni- directional radiation patterns are desirable. Because of omni-directional pattern, the gain of the antenna will be less compared to directional antenna; anyway a flat gain response with gain between 2 dBi and 5 dBi is desired. Moreover, to improve the ease of integration with these peripheral devices most of which are portable, low profile antennas are highly appreciated.

UWB signals are narrow pulses with duration less than a nanosecond. The capability of the antenna to handle these pulses efficiently is evaluated in terms two important parameters, group delay and antenna transfer function. Constant group delay and flat antenna transfer function are required to reproduce the transmitted pulses faithfully at the receiver end. Since the signal itself carries the useful information, receiving the pulses with minimum distortion is the prime goal for an efficient UWB antenna.

One of the main operational challenges of UWB systems is their coexistence with narrow band wireless services such as IEEE 802.16 standard for Worldwide Interoperability for Microwave Access (WiMAX) system (3.3–3.6 GHz) and IEEE 802.11a standard for WLAN system (5.15–5.825 GHz). Fig. 1.10 illustrates the PSD of the UWB and some existing narrowband services.
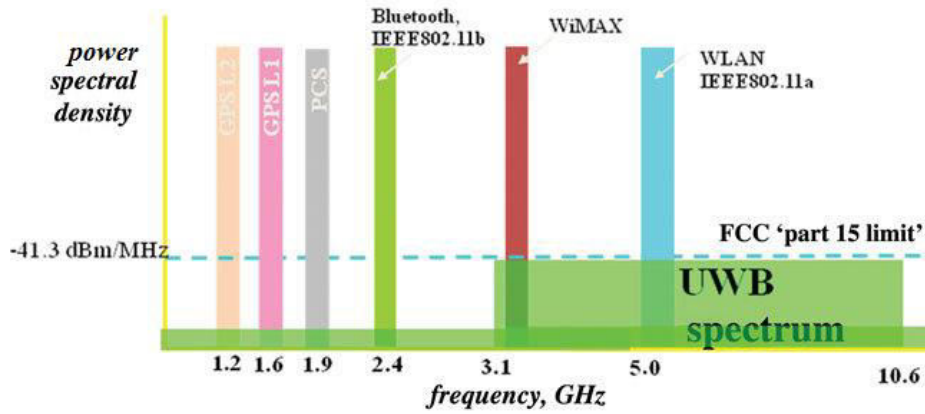
Fig. 1.10: PSD of UWB and other existing narrow band services (www.theiet.org)

UWB communication systems operating in the frequency band from 3.1 to 10.6 GHz with an emission limit of -41.3 dBm/MHz closing to the thermal noise floor for commercial applications could easily be interfered by the co-existing communication systems; WiMAX and WLAN. Thus a band-notch filter is needed in UWB systems to avoid the possibility of this interference. But, the use of a separate filter circuit will increase the complexity of the UWB systems and require more space when integrated with other microwave circuits in the wireless devices. Instead of that, it is possible to design the UWB antenna itself as a band notched one i.e., by incorporating resonant structure within the designed antenna to notch out the undesired bands. A detailed literature review of the same is done in Chapter 2 of this thesis.

Since the UWB communication system mainly involves the communication between portable devices antennas with reduced sizes are required. Size of the antenna is one of the crucial design issues

because it affects the gain and bandwidth. So the design of compact antennas with wide impedance bandwidth and pattern bandwidth (omnidirectional pattern with acceptable gain) is a challenging task.

The printed monopole antennas are promising candidate for UWB applications due to their simple structure, low profile, ease of fabrication. This thesis investigates wide band performance of compact printed antennas where two different CPW fed antenna structures are considered. In order to obtain the wide impedance bandwidth without increasing the antenna size, certain matching techniques are applied to the proposed UWB antennas. The thesis provides simple design formulas for the fabrication of the proposed antennas on commercially available microwave substrates which could be useful in consumer electronics applications.

The objective of the thesis is to develop compact dual band notched UWB antennas suitable for WLAN and WiMAX environment. So the proposed UWB antenna structures are modified by incorporating notch structures operating at WLAN and WiMAX bands. The transient characteristics of both the antennas are also studied in order to confirm its suitability for pulse communication applications.

1.5 Thesis Organisation

The thesis is divided into six chapters

Chapter 1 is an introductory chapter, which defines various broad band technologies and their demands which lead to high rate PAN or

UWB technology. Then continues with the evolution of UWB and UWB definition, highlighted the advantages and applications of the technology. Discussed various UWB antennas developed in early stages and concludes with challenges in the UWB antenna design. Considering the design requirements, printed antennas are identified as a suitable choice for UWB communication devices.

Chapter 2 presents the review of the printed monopole and slotted antennas which mainly deals with various bandwidth enhancement techniques used for realising UWB response followed by a detailed review on various band notching techniques employed in UWB antennas.

Chapter 3 deals with the methodology for the analysis of the proposed antennas. This includes structure simulation studies in Computer Simulation Technology (CST) - Microwave Studio, fabrication by photolithography and measurements using vector network analyser (VNA). Both electrical and transient parameters of the antenna are defined; the theory and measurement procedures are also discussed.

Chapter 4 and 5 describes the proposed printed antennas; monopole antenna and slotted antenna. For both the antennas CPW feeding method is selected because of easy fabrication, better integration with monolithic microwave circuits, less dispersion and less losses. The simulated radiation patterns at different resonant frequencies are analysed and found remains omni-directional even at higher resonances unlike most of UWB antennas reported. Design

equations for the fabrication of the proposed structures on commercially available substrates have been developed and verified with CST simulation.

Chapter 4 presents a compact dual band-notched truncated circular disc monopole antenna of size 25 mm x 20 mm (L x W). The antenna exhibits wide band performance in terms of both input impedance and radiation patterns. Moderate gain response even with this compact size is an advantage over other similar designs. The resonant slots, folded U-slot and U-slot etched on the radiating patch notch out the corresponding bands effectively.

Chapter 5 illustrates the characteristics of dual band-notched slotted antenna of size 30 mm x 27 mm. Various impedance enhancement techniques such as extending ground plane to form slot structure, inserting slits and bevelling the ground plane are employed to attain UWB response. This antenna also exhibits wide pattern bandwidth with flat gain response. To reject the WiMAX and WLAN bands, a meandered (Z-shaped) parasitic element is etched on the radiating aperture and quarter wavelength stubs are attached to the upper edge of the ground plane respectively.

Time domain analyses are carried out to verify the suitability of the proposed antennas for pulse communication applications. The influence of the antenna on UWB pulse transmission is examined by performing antenna transfer function measurements. The radiated pulse derived from the measured transfer function is compared against the simulated results

obtained using the time domain capabilities of CST. Another important parameter called 'fidelity' which is a measure of pulse distortion due to the antenna as a function of direction is also investigated.

Finally, the thesis is concluded in Chapter 6 by highlighting the results of the research work along with a brief description on the scope for future study.

References

[1]   http:// www.tutorialspoint.com "Wireless Introduction".

[2]   R. Prasad, OFDM for Wireless Communications Systems, Artech House Publishers, 2004.

[3]   L. Miller, "Why UWB? A Review of Ultra wideband Technology" National Institute of Standards and Technology, 2003.

[4]   http://www.wlana.com/direct/matrix.htm, web pages of the Wireless LAN Association (WLANA)

[5]   H. Arslan, Z. N. Chen and M-G.D.Benedetto, "Ultra Wideband Wireless Communication", Wiley publishers, 2006.

[6]   J. Karaoguz, "High-Rate Wireless Personal Area Networks," IEEE Communications Magazine, vol. 39, no. 12, pp. 96–102, 2001.

[7]   http://www.ieee802.org/15/pub/TG3a.html, web pages of the alternate high-rate physical layer Task Group of IEEE 802.15

[8]   Federal Communications Commission, "Revision of Part 15 of the Commission's Rules Regarding Ultra-Wideband Transmission Systems," First Report and Order, ET Docket 98-153, FCC 02-48, 2002. http://www.fcc.gov.

[9]   Y. Rahayu, T. A. Rahman, R. Ngah and P.S. Hall, "Ultra Wideband Technology and Its Applications", 5th IFIP International Conference on Wireless and Optical Communications Networks, 2008.

[10]   P. Withington, "Ultra-wideband RF—A Tutorial," presentation to the IEEE 802 Plenary meeting, 2000. http://grouper.ieee.org/groups/802/15/pub/2000/Mar00/

[11]   M. Z. Win, D. Dardari, A. F. Molisch, W. Wiesbeck and J. Zhang, "History and Applications of UWB", Proceedings of IEEE vol. 97, no. 2, pp. 198-202, 2009.

[12]   "Ultra-Wideband: Past, Present and Future" Research project supported by the European Commission, EUWB consortium, 2009, www.bitgear.rs/pdf/EUWB-WhitePaper.pdf

[13]   T. W. Barrett, "History of UltraWideBand (UWB) Radar & Communications: Pioneers and Innovators", Progress In Electromagnetics Symposium (PIERS2000), 2000.

[14]   D.L. Moffatt & R.J Puskar, "Subsurface electromagnetic pulse radar", Geophysics, vol. 41, pp. 506-518, 1976.

[15]   P. Van Etten, "The present technology of impulse radars", Int. Radar Conf. Proc., pp. 535-539, 1977.

[16]   Tektronix, Inc., S.W. Millikan Way, P.O. Box 500, Beaverton, Oregon 97005: Instruction Manual: Type S-2 Sampling Head, 1968.

[17]   R. J. Fontana, "A Brief History of UWB Communications" Multispectral Solutions, Inc. Kluwer Academic/Plenum Publishers, 2000. http://www.multispectral.com/history.html.

[18]   T.W. Barrett, "Impulse (Time-Domain) Radar Technology" Assessment Colloquium W.J. Schafer Associates, 1988.

[19]   B. Noel, "Ultra-Wideband Radar", Proceedings of the First Los Alamos symposium, CRC Press, Boca Raton, FL, 1991.

[20] T.E. McEwan, "Ultra-wideband radar motion sensor" U.S Patent 5,361,070 dated November 1, 1994.

[21] T.E. McEwan, Re-examination Certificate (4084th) B1 5,361,070, Certificate Issued dated May 16, 2000.

[22] "Part 15 Rules for Unlicensed RF Devices", Federal Communications Commission, 2002. http://www.fcc.gov/oet/info/rules/

[23] K. Siwiak and D. M. Keown, "Ultra-Wideband Radio Technology" John Wiley & Sons, Ltd, 2004.

[24] L. Zhu, S. Sun and R. Li, "Microwave band pass filters for wideband communication", John Wiley & Sons, 2012.

[25] Z. N. Chen, "Considerations for Source Pulses and Antennas in UWB Radio Systems," IEEE Transactions on Antennas and Propagation, vol. 52, no. 7, 2004.

[26] J. D. Taylor, 'Introduction to Ultra-Wideband Radar Systems", CRC Press, Boca Raton, FL, 1995.

[27] F. Nekoogar, "Ultra-Wideband Communications: Fundamentals and Applications", Prentice Hall, 2005.

[28] M. Ghavami, L. B. Michael and R. Kohno, "Ultra Wideband Signals and Systems in Communication Engineering", John Wiley and Sons, 2004.

[29] D. Porcino and W. Hirt, "Ultra-wideband radio technology: potential and challenges ahead", IEEE Commun. Mag., vol. 41, no. 7, pp. 66–74, 2003.

[30] N. Cravotta, "Ultrawideband: the next wireless panacea?" 2002, www.edn.com

[31] I. Oppermann, M. Hamalainen and J. Iinatti, "UWB Theory and Applications," John Wiley & Sons, 2004.

[32] R. J. Fontana, "Recent System Applications of Short-Pulse UWB Technology," IEEE Transactions on Microwave Theory and Techniques, vol. 52, no. 9, pp. 2087-2104, 2004.

[33]   J. S. Lee, Y. W. Su and C. C. Shen, "A Comparative Study of Wireless Protocols: Bluetooth, UWB, ZigBee, and Wi-Fi", The 33rd Annual Conference of the IEEE Industrial Electronics Society (IECON), pp. 46-51, 2007.

[34]   W. Wiesbeck and G. Adamiuk, "Antennas for UWB Systems", Proceedings of International ITG Conference on Antennas, pp. 66-71, 2007.

[35]   X.L. Liang, "Ultra-Wideband Antenna and Design", In Tech publishers, 2012.

[36]   Lodge, "Electric telegraphy", U.S. Patent 609, 154, August 1898.

[37]   P.S. Carter, "Wideband, short wave antenna and transmission line system", U.S. Patent2, 181, 870, December 1939.

[38]   L.N. Brillouin "Broad Band Antenna", U.S. Patent 2, 454, 766, November 1948

[39]   L. Paulsen, J.B West, W.F Perger and J. Kraus, "Recent investigations on the volcano smoke antenna", IEEE Antennas and Propagation International Symposium (Digest), 2003.

[40]   G. Dubost and S. Zisler "Antennas a Large Band", New York: Masson, 1976.

[41]   N.P. Agrawall, G. Kumar and K.P. Ray, "Wide-band Planar Monopole Antennas", IEEE Transactions on Antennas and Propagation vol. 46, no. 2, pp. 294-295, 1998.

[42]   J.A. Evans and M.J. Ammann, "Planar Trapezoidal and pentagonal monopoles with impedance bandwidth in excess of 10:1", IEEE Antennas and Propagation International Symposium (Digest), 1999.

[43]   S.Y. Suh, W.L. Stutaman and W.A. Davis, "A new ultra wideband printed monopole antenna the Planar Inverted Cone Antenna (PICA)", IEEE Transactions on Antennas and Propagation, vol. 52, no.5, pp. 1361-1365, 2004.

.....ෂ෬.....

Chapter 2

LITERATURE REVIEW

Design and analysis of a CPW-fed monopole and a slot antenna for UWB applications is the subject of this thesis. This chapter deals with the literature review on various mechanisms employed to achieve wide impedance bandwidth with monopole and slot antennas. Different methods available in the literature to achieve multiple band-notched functions are also discussed. Each section of this chapter is concluded with a brief description of the proposed antennas i.e., monopole, slot and dual-band notched antennas.

2.1   Printed UWB Monopole Antennas

Monopole antennas are the one of the most popular antennas employed in wireless communication systems. Monopole antenna geometry consists of a quarter wavelength thin wire mounted vertically at the centre of a perfectly conducting, infinitely thin, circular ground plane in free space. Radius of the ground plane varies from a fraction of

a wavelength to many wavelengths. Electrical properties of these antennas depend on the parameters of the thin wire and ground plane.

Due to the increased demands for frequency band and shorter waves, "thin-wire" quarter wave antenna dominated the market. In 1939, Carter reinvented bi-conical antenna and conical monopoles by incorporating tapered transition between feed probe and the radiating element to create a wide band response, one of the key steps towards the design of broadband antennas [1]-[2]. Even though these designs exhibit frequency-independent impedance matching and radiation performance across a wide operating bandwidth, suffer from large volume.

Later in 1976, planar monopole antennas were realised by replacing the thin wire of a conventional monopole with a planar element. The bow-tie antenna is the planar version of a bi-conical antenna for which the volume is reduced by replacing three-dimensional bi-conical radiators with their planar versions. The disc and polygonal planar monopole antennas are the variations of bow-tie antennas; in which largest dimension determine their lowest operating frequency. Different monopole shapes have already been mentioned in Chapter 1, section 1.3. Among various planar monopole antennas, the square planar monopole is having simple geometry which possesses an impedance bandwidth ratio of 2:1. From the antenna geometry, the feed gaps formed between the edges of the upper and bottom radiators or ground plane, the feed point location and the shape of the monopole's bottom, all may affect the impedance matching. Thus, several techniques

such as bevelling [3], use of shorting pins [4], combining bevelling and shorting [5], offset feed [6], double feed [7], trident-shaped feed [8] and notching [9] etc. were proposed to expand the bandwidth of the square monopole antenna. Designs such as double or three feeds not only widen the impedance bandwidth, but also improve the stability of radiation pattern. All the antennas mentioned above need a perpendicular metallic ground plane. Since the UWB technology focussed more on the consumer electronic devices for short-range wireless connections, the antennas mentioned above are too bulky to use in portable/ mobile devices.

Design concerns for antennas and source pulses in UWB wireless communication systems were first presented in 2003, which discriminated the existing UWB antenna design from the conventional ones from a system point of view [10] – [11]. The suggestions of design thoughts have significantly affected the later designs.

By printing the antennas on the printed circuit board (PCB), it is possible to develop low cost compact antennas which can easily be embedded into portable devices or integrated with other RF circuits. It consists of a monopole patch and a ground plane, both printed on the same side of a substrate for CPW line or on the opposite sides for microstrip line to feed the monopole.

Printed antennas are widely used in wireless communications due to its features like low cost, light weight and ease of fabrication but it offers narrow band width. Many attempts have been made to widen the

bandwidth of printed antennas. Since the bow-tie antennas are one of the promising candidates for UWB applications several printed designs have been attempted with bow-tie shapes. But the conventional printed bow-tie antenna [12] is not sufficient to cover the UWB frequency band. A double-sided printed bow-tie antenna, which presents stable characteristics over the UWB frequency band, is presented [13].

Microstrip fed broad band rectangular printed monopole antenna with a partial ground plane [14] is introduced in 2004. By employing two steps at the lower corners and a single slot on the patch, the antenna is made to operate from 3.2 GHz to 12 GHz. Since then many monopole with varying geometries for the patch and ground plane have been developed to realise the UWB bandwidth.

A novel design of a printed circular disc monopole fed by a microstrip line is proposed [15]. The effect of feed gap and the ground plane width on the operating bandwidth of the antenna are studied. It produces an ultra-wide bandwidth from 2.78 to 9.78 GHz with radiation patterns similar to those of a traditional monopole. Further investigation of this structure is presented [16] where it analyses the effect of disc dimension on bandwidth of the antenna and the time domain performance of the antenna. It is concluded that the first resonant frequency is directly associated with the dimension of the circular disc because the current is mainly distributed along the edge of the disc. CPW- fed version of the circular disc is proposed [17] and demonstrated the optimal design of this type of antenna can achieve an ultra wide bandwidth ranges from 2.64 GHz to more than 12 GHz.

Knight's helm shaped double-sided printed antenna with partial ground plane [18] employed two techniques to obtain good impedance match; cutting two slots on the rectangular patch and a tapered transition between the rectangular patch and the feed line. Consistent omni-directional radiation pattern is observed for frequencies from 4 GHz to 10 GHz.

A small microstrip-fed monopole antenna, which consists of a rectangular patch and a truncated ground plane, is presented [19]. To achieve the broad impedance bandwidth, a pair of notches is placed at the two lower corners of the patch and a notch is embedded in the truncated ground plane. The designed antenna satisfies the 10 dB return loss condition from 3.1 to 11 GHz and provides monopole-like radiation patterns.

The design, fabrication and measurement of a printed planar triangular monopole antenna on a FR-4 printed circuit board (PCB) is reported [20] for which the measured VSWR is less than 2 from 4.2 GHz to 7.2 GHz.

A CPW fed U-shaped monopole antenna [21] is analysed by using the finite-difference time-domain (FDTD) method. The parameters and shape of the antenna are determined by utilizing the genetic algorithm to achieve an ultra-wide bandwidth characteristic. The measured frequency response shows an impedance bandwidth of 7.25 GHz or 104.7% over 3.3 to 10.55 GHz for VSWR less than 2.

Technique for enhancing the bandwidth of a microstrip fed elliptical monopole is discussed [22]. The ultra-wideband property for the proposed antenna is achieved by cutting a slot on the truncated ground opposite to the microstrip line. The slot width is more effective in determining the matching bandwidth than slot length. It is also seen that the impedance bandwidth performance of the antenna with increase in major axis of the ellipse has similar effect of bevelling the lower edge of the radiating element. The same technique of cutting rectangular slot in the truncated ground plane is used to improve the impedance characteristics of a printed rectangular monopole antenna [23].

The impedance bandwidth of a rectangular monopole with truncated ground is increased by inserting a narrow slit near the lower right corner of the printed monopole [24]. The use of a narrow slit allows additional surface current paths [25] and thus a wideband characteristic can be achieved by adjusting the height of the slit.

A novel design which combines the stepped-patch approach with a number of resonating elements to achieve a bandwidth (VSWR < 2; gain > 1 dBi) of more than 150% is discussed [26]. The gain and bandwidth of the antenna are improved systematically by adding resonators of different lengths along the line. These resonators are arranged both vertically and horizontally and are fed through direct electrical connection.

The impedance bandwidth of monopole antenna presented [27] is improved by adding slit on one side of the monopole. By introducing a

tapered transition between the monopole and the feed line and adding two-step staircase cut in the ground plane improved bandwidth can be achieved. The slit is placed to create additional path for the surface current and results in bandwidth when the dimensions are properly chosen. The tapered transition and two-step staircase cut results in good impedance match i.e. make the VSWR less than 1.75 for the entire operating band. The antenna operates over a bandwidth of 2.8 to 22 GHz with a compact size of 16 mm × 19 mm.

A new geometry of branch type UWB monopole antenna discussed [28] consists of an L-shaped monopole and an I-shaped open stub monopole connected at the end of a CPW feed line. The UWB bandwidth ranges from 3.0 to 11.0 GHz is achieved by merging of three resonant frequencies associated with the current paths controlled by the structural parameters of monopole antennas. The proposed antenna generates the omnidirectional radiation patterns.

Printed elliptical monopole antennas with two possible ways of feeding, along the major axis and along the minor axis are studied [29]. Approximate formula to calculate lower band edge frequency is derived and variation in bandwidth with ellipticity ratio is also investigated. The measured bandwidth ratio of printed elliptical configuration is 12.4:1 with an ellipticity ratio of 1.1.

In printed UWB antennas with finite ground plane, the electric currents present on both the radiator and the ground plane. So the impedance bandwidth and radiation patterns of the antennas are

affected by the shape and size of the ground plane also, especially when the antenna becomes small in size [30] – [31]. This has been one of the most challenging design issues in small antennas. A technique to reduce the ground-plane effect on the performance of a small printed UWB antenna by cutting a rectangular notch vertically from the printed radiator and asymmetrically attaching a strip to the radiator is presented [32].

The planar binomial curved monopole antenna is investigated [33] where the impedance bandwidth of the proposed antenna can significantly be improved by selecting the suitable binomial function of order N and the gap width G between the antenna and ground plane. A stable omnidirectional radiation pattern was also obtained for the whole impedance bandwidth.

UWB antennas with the radiating elements are formed by the intersection of two ellipses or two circles are described [34]. To avoid the time consuming trial-and-error approach, simple design formulas for this type of radiators are presented and are validated. The time domain test of transmission between two identical antennas at different orientations are done and confirmed from the fidelity factor.

CPW-fed open crescent patch antenna consists of an open annulus strip as a ground plane and an open crescent patch in the inner space of the annulus as a radiating element is studied [35]. The radius of the inner crescent patch and the inner radius of the outer annulus are adjusted carefully to obtain optimal impedance bandwidth of 129 %, which covers 3 to 14 GHz.

Design and construction of a compact Ultra Wide Band (UWB) antenna using stepped impedance matching technique on the microstrip feed line to improve the impedance bandwidth is proposed [36]. The antenna parameters in frequency domain are investigated to show its capability as an effective radiating element. Furthermore, time domain Gaussian pulse excitation analysis in UWB systems is also demonstrated.

A novel technique to enhance the bandwidth of the conventional planar triangular monopole antenna is [37] presented. With two symmetrical corrugations extended from the flat ground plane, a significant improvement on the impedance bandwidth up to 4:1 can be achieved. The proposed antenna design is a modification from the conventional volcano smoke antenna (VSA) in which a smooth transition from the feed line to the radiator yields a wideband performance. The influences of geometric parameters of the ridged ground plane on the impedance bandwidth are also studied extensively.

A CPW-fed printed monopole antenna consisting of a rectangular monopole and a trapeziform ground plane introduced in [38] achieved an impedance bandwidth ratio of 3.7:1 (0.76 to 2.86 GHz). This structure can be considered as a printed version of the discone antenna where the rectangular patch is used to replace the disc, the trapeziform ground plane is used to replace the cone, and the CPW is used to replace the coaxial feed. To enhance the bandwidth further, a linearly tapered central strip line is used as an impedance transformer [39] and an impedance bandwidth ratio of 10.7:1; covering frequencies from 0.76 to 8.15 GHz. By using the tapered CPW feeder, the impedance

bandwidth of the antenna is enhanced by a factor of about 2.8 times compared with a 50 Ω CPW feeder. Later different monopole geometries such as circular [40], annular ring [41] and elliptical [42] are adopted to enhance the bandwidth. Among these the elliptical monopole exhibits largest impedance bandwidth ratio of 21.6:1, covering frequencies from 0.41 to 8.86 GHz. A modified version of [42] is presented [43] in which the elliptical monopole is hollowed by cutting a circular slot at its centre. The hollowed elliptical monopole antenna achieved a bandwidth ratio of 25.1:1 (0.4 to 10.6 GHz) for VSWR < 2 and exhibited a nearly omnidirectional radiation pattern. In these designs, three techniques which help to broaden the bandwidth are geometry of the monopole, trapeziform ground plane and tapered CPW feeder.

A CPW-fed rectangular monopole antenna with a bandwidth of about 2.3 times of the conventional one (164%) is proposed and designed [44]. The enhancement of the bandwidth is achieved by an M-shaped notch at the patch bottom a with a tapered CPW ground plane.

A printed rectangular monopole antenna with impedance bandwidth enhancement techniques is presented [45]. The bandwidth is enhanced by including the following modifications in the monopole and the ground plane; notched semi-elliptical ground plane, cutting two staircase steps at the lower corners of the monopole and slits on the monopole. The proposed antenna has an omnidirectional pattern for all the measured frequencies (2.9 - 10.8 GHz), which covers the commercial UWB band.

Printed antenna designed with square slots of equal size on the square (check-shaped) patch and a pair of L-shaped notches in the corners of the ground plane is proposed [46]. By increasing the numbers of slots inside the square patch, the upper and lower frequencies of the band can be controlled. The effect of the ground plane notch on the optimization of the return loss is discussed.

A modified square monopole antenna having multi-resonance performance is proposed [47]. The proposed antenna consists of a radiating square patch with a pair of T-shaped slots, ground plane with a pair of rectangular sleeve and a T-shaped resonator. The antenna provides a wide usable fractional bandwidth of more than 125% (3.05 - 13.57 GHz). By optimizing dimension of rectangular sleeves, T-shaped slots and resonator, the total bandwidth of the antenna is greatly improved.

A planar microstrip-fed super wideband monopole antenna is developed [48]. By embedding a fractal-complementary slot into the asymmetrical ground plane, the proposed antenna is able to operate from 1.44 to 18.8 GHz with bandwidth ratio up to 13.06: 1. The design and effects of this fractal-complementary slot are discussed.

A technique to enhance the bandwidth of a double sided rectangular printed antenna is presented [49]. Improvement in bandwidth is obtained by cutting triangular shaped slots on the top edge of the truncated ground plane.

A triple-band antenna with L and T-shaped stubs for PCS/WLAN/ UWB applications is proposed [50]. The proposed antenna consists of

two symmetrical strips with two steps, L and T-shaped stubs which help to produce the resonances at each frequency bands. The antenna offers low dispersion and good impedance matching.

A novel CPW-fed UWB antenna without slot on the patch or ground plane is proposed [51] to enhance the bandwidth of the antenna. By using a pair of ellipse shape- combined design on the patch, a proper control on the upper and lower frequencies of the band can be achieved. In addition, a pair of ESC form is placed on the ground plane for improving the impedance match.

A planar monopole UWB antenna with rounded patch and rounded truncated ground plane for ultra-wideband applications is investigated [52]. The geometry of the antenna is optimized to obtain improved impedance bandwidth performance.

Later several CPW fed and microstrip fed monopole structures such as folded monopole with asymmetric ground plane [53], fan-shaped structure [54], circular disc with tapered feed line and trapezoidal ground [55], rectangular patch with a pair of modified L-shaped notches inserted on the patch [56], elliptical radiator with three-step staircase on both sides of the feed line and a notched ground [57], palmate leaf-shaped radiator with a modified shaped ground plane [58], triangular radiating patch with a round-corner ground and a step in the feed line [59], slot cut elliptical printed monopole [60] etc are reported to realise UWB response.

First part of Chapter 4 proposes a CPW fed truncated circular disc monopole antenna for UWB application. This structure is derived from [17] by removing the upper portion of the circular disc without disturbing its radiation properties. The upper portion of the ground plane is semi-elliptical in shape instead of rectangular. This antenna provides a wide impedance bandwidth ratio of 5.8:1 (3.4 - 20 GHz) with reduced overall size (25mm × 20mm) without employing any additional bandwidth enhancement techniques.

2.2 Printed UWB Slot Antennas

The wide slot antennas are one of the most suitable candidates for UWB applications because of its ability to provide impedance match over wide bandwidth and negligible radiation from feed network [61]. This type of antenna consists of a wide-slot and a tuning stub connected with a microstrip or CPW feed line. In conventional slot antennas, the slot is fed by an open-ended microstrip line. Microstrip line fed printed wide- slot antennas have received much attention and are useful for a variety of radar and satellite communication applications. Characteristics of printed wide-slot antennas excited by a microstrip line are extensively studied [62], [63].

The bandwidth of the slot antennas are affected by the parameters of the slot and the feed network. It is observed that for a rectangular slot antenna, as the slot width increases the bandwidth increases. This property continues up to a certain range of slot width and after that the bandwidth decreases [64]. This is because the radiation resistance of the slot increases as the width of the slot increases, which leads to

impedance mismatch between the slot and microstrip line. This in turn reduces the impedance bandwidth of the antenna [62].

Various methods for enhancing the impedance bandwidth of the conventional slot antennas are reported. One of the techniques is to modify the shape of the slot; design of a microstrip-line-fed printed wide-slot antenna with a semi-circular slot incorporating a protruding small rectangular slot for achieving a larger operating bandwidth (1.7 – 2.734 GHz) is proposed [65]. Another technique for increasing the bandwidth of the wide rectangular slot antenna is to excite the slot with a T-shaped microstrip tuning stub; an improvement in bandwidth (1.5 - 3.2 GHz) is obtained [66]

Study of microstrip-line-fed printed wide square slot antennas with a fork-like tuning stub for bandwidth enhancement is presented [67]. From experiments, the obtained impedance bandwidth ratio is 1.6:1 (1.821-2.912 GHz) which is much higher than that of a conventional microstrip-line-fed printed wide-slot (1.61-1.725 GHz) antenna with a simple tuning stub [62]. This bandwidth enhancement is obtained mainly through the enhanced coupling between the microstrip feed line and the printed square slot by the fork-like tuning stub. When dimensions of the fork-like tuning stub vary, the coupling changes and the input impedance curve can have different resonant loops on the Smith chart.

A few attempts have been made to increase the bandwidth of CPW-fed slot antennas, including the use of a wide rectangular slot [68], [69] or a bow-tie slot [70], [71]. However, for these published

CPW-fed broadband designs, their impedance bandwidth ratio is less than 1.5:1. An alternative method for enhancing the impedance bandwidth of CPW-fed square slot antenna is proposed [72]. For this design, a widened tuning stub is used. The location and size of the tuning stub can control the coupling between the CPW feed line and the radiating slot, which facilitates the impedance matching of the antenna. This leads to an increased bandwidth ratio of 1.8:1 (1.56 -2.88 GHz).

A coplanar waveguide fed rectangular slot antenna excited using U-shaped tuning stub is proposed [73] for enhancing the antenna band width. The antenna operates over a frequency range of 2.79–9.48 GHz, which corresponds to an impedance bandwidth of 110%. The wide bandwidths are due to the multiple resonances introduced by the combination of the rectangular slot and the U-shaped stub. The resonant frequency and bandwidth are controlled by the size of the rectangular slot and tuning stub.

Through proper selection of the parameters of the stub and slot shape, the coupling between the feed line and the printed wide slot can be controlled more effectively, which in turn provide significant bandwidth enhancement for the printed wide-slot antenna [72]. Many wide-slot antennas, with different slot shapes such as rectangular [74]-[78], triangular [79], semi-circular [80] [81], square [82], rhombus [83], hexagonal [84], [85], tapered [86], circular [87], [88], elliptical [89] [90] etc. are studied.

Rectangular wide-slot antennas with different shapes of the tuning stub are studied for which the bandwidth ratios vary from 1.8:1 to 11.9:1. Rectangular wide-slot antennas fed by the microstrip line with cross-shaped stub, π-shaped stub and fan shaped stub with horizontal strip are presented [74] - [76] respectively. These slot antennas achieve the impedance bandwidth ratios of 2.8:1 (1.7 - 4.9 GHz), 3.5:1 (1.7 - 6.0 GHz) and 3.6:1 (0.5 - 5.7 GHz) respectively. Later, rectangular slot antenna with CPW fed novel radiator consists of two semicircles with difference radii is proposed [77], which contributes a bandwidth ratio of 11.9:1 (2.8 – 33.4 GHz), much greater than the other rectangular slots reported.

Antenna employs a near-rectangular slot along with a tapered tuning stub exhibits a wide impedance bandwidth ratio of 3.9:1 (2.9 - 11 GHz) is proposed [78]. The antenna performance is observed to be unaffected by ground length, making the proposed design an ideal candidate for Wireless Universal Serial Bus (WUSB) dongle antenna.

Microstrip fed semi-circular slot with square stub and triangular slot with triangular stub are presented [79] to achieve an impedance band width ratio of 3.9:1 (1.82 to 7.23 GHz) and 3.5:1 (2.42 to 8.48 GHz) respectively. An increased band width ratio of 7:1 (1.5 – 10.6 GHz) is obtained with semi-circular slot when the square stub is replaced by a circular stub [80]. An antenna with semi-circle like slot fed with modified circular radiating patch providing an impedance bandwidth ratio of 5.24:1 (3.07 - 16.26 GHz) is discussed [81]. By choosing suitable combinations of feed and slot shapes with proper dimensions,

large impedance bandwidth with stable radiation patterns can be obtained

A new design of microstrip-line-fed printed wide square slot antennas with a rotated slot for bandwidth enhancement is proposed and investigated [82]. The impedance bandwidth ratio of the printed wide slot antenna can significantly be improved to 1.6:1 (3.4 – 5.6 GHz) by simply rotating the square wide slot through a suitable angle. Also, the antenna gain within the operating band is measured and studied. An impedance bandwidth ratio of 2.2:1 (2.68 - 5.91 GHz) which is larger than that of [82] is achieved by using an offset microstrip-fed line for a rhombus-like slot antenna [83].

A forklike tuning stub and a polygon like wide slot are employed in order to enhance the bandwidth of the slot antenna [84]. An impedance bandwidth of about 3.2:1 (2.89 to 9.19 GHz) is achieved. The characteristics of the antenna's radiation patterns and gain over the entire operation frequency range are also discussed.

A hexagonal slot excited by microstrip fed trapezoid patch with rounded corners producing a band width ratio of 6.2:1 (2.9 - 18 GHz) is studied [85].

Combination of rectangular tuning stub to excite the slots of different shapes such as circular, elliptical, square and tapered are studied [86]. Among theses the tapered slot excited by a rectangular tuning stub achieves an impedance bandwidth ratio of 3.1:1 (3 - 11.2 GHz) with a stable gain and radiation over the bandwidth.

A comparative study on the impedance bandwidth and radiation property of CPW fed circular slot antenna with different stub shapes such as rectangular, hexagonal and elliptical are presented [87]. The use of hexagonal stub allows broadening of the band up to 4.3:1 (2.7-11.84 GHz), but larger broadening of 19:1 (1.55-30 GHz) is achieved for elliptical shaped stubs. All these antennas exhibit almost similar radiation patterns.

A bandwidth ratio of 6.1:1 (2.3 - 13.9 GHz) is obtained [88] when a circular slot is excited by CPW fed circular patch. The slot diameter controls the lowest edge frequency of the antenna bandwidth and the patch radius ensures the impedance matching between the line and the slot across the operating frequency band.

Printed elliptical/circular slot antenna using tapered microstrip or CPW feeding line with U-shaped tuning stub proposed [89] produces a band width ratio of greater than 3.2:1 and 2.7:1 for elliptical and circular slot respectively. In both designs, U-shaped tuning stubs broaden the operating bandwidth of the antenna by enhancing the coupling between the slot and the feed line. Further, the tapered feed lines provide an additional bandwidth enhancement.

The antennas comprised of elliptical or circular stubs that excite similar-shaped slot apertures are studied [90]. Elliptical slot with an elliptical tuning stub and circular slot with circular tuning stub has achieved an impedance bandwidth ratio of 7.5:1 (2.65 - 20 GHz) and 6.7:1 (2.95 - 20 GHz) respectively. It is concluded that for optimum

impedance matching, the antenna feed and slot should be of almost similar shapes.

Different from above regular shapes of the slot or tuning stub, several special geometries of printed slot antennas are also introduced for UWB applications,

Broad-band operation of a CPW capacitive coupled square slot antenna with metallic strips loaded at the four corners of the square slot is demonstrated [91]. The proposed antenna has a simple structure, and impedance matching can easily be achieved by tuning the lengths of the CPWs signal strip in the slot and the loading metallic strips. An impedance bandwidth of 1.5 - 2.5 GHz can be obtained by choosing suitable length ratio.

Investigations of a printed microstrip slot antenna which consists of a quarter wavelength monopole slot cut in the finite ground plane with electromagnetically fed microstrip line is proposed [92]. It provides a wide impedance bandwidth adjustable by variation of its parameters, such as the relative permittivity and thickness of the substrate, width and location of the slot in the ground plane and ground plane dimensions. An impedance bandwidth up to about 60% (2.3 - 4.25 GHz) is achieved by individually optimizing its parameters. Further investigation of monopole slots with different slot shapes straight, L and inverted T placed on a small ground plane are discussed [93]. It is shown that, the variation in the slot shape, from straight to L and T shapes, helps in generating additional resonances, which when

coupled to the original resonances of the slot, further increases impedance bandwidths. The measured impedance bandwidths of up to 60% (2.42 - 4.31 GHz), 82% (2.42 - 5.78 GHz) , and 80% (2.74 - 6.4 GHz) are achieved for these straight, L and inverted T slots respectively, by suitably selecting their design parameters.

A planar annular slot antenna utilizes a unique tapered-slot feeding structure is proposed [94]. The radiating annular slot and its tapered-slot feeding structure are on the top layer of the substrate whereas the microstrip line and its open stub are printed on the bottom layer of it. The tapered-slot feeding structure serves as an impedance transformer and guides the wave propagating from the slot line to the radiating slot without causing reflection. The radiating slot is curved to distribute part of the energy to the reverse side of the feeding aperture. This antenna achieves an impedance bandwidth ratio of 3.7:1 (2.95 - 11 GHz). By means of a normalized antenna transfer function, both frequency domain and time domain characteristics of the antenna are carefully investigated.

A coplanar waveguide- fed tapered ring slot antenna consists of coplanar waveguide (CPW), a wideband coplanar waveguide-to-slotline transition and a pair of curved radiating slots is considered [95]. In designing UWB antenna, there is a need for an impedance transformer so that the wideband impedance matching between the transmission line and free space can be accomplished. At the end of the CPW feeding line, a pair of 100 Ω slot lines is connected in parallel to ensure impedance matching. By gradually changing the width of the radiating

slots, impedance matching between the transmission line and free space is achieved over a wide bandwidth of 3.1 GHz to more than 12 GHz.

T-shaped open-ended slot in the ground plane excited by a microstrip feed line is presented [96]. To improve the impedance matching around the lower resonant frequencies a small notch is inserted into the slot while the impedance matching for the middle and upper resonant frequencies are achieved by extending a small section to the feed line. Thus multiple resonant frequencies are excited and merged to form a large bandwidth from 3.1 - 11.45 GHz.

Linear tapered slot antenna excited using a microstrip line is discussed [97]. A rectangular cut is optimised in the 50 Ω feed line to match multiple resonances in the antenna, resulting in wide impedance bandwidth covering the 3.1–10.6 GHz. The antenna provides omnidirectional coverage with appreciable gain throughout the band.

The antenna features a coplanar waveguide signal strip terminated with a semi-elliptic stub and a ground plane shaped as a semi-ellipse near the patch to achieve wide bandwidth from 2.85–20 GHz is investigated [98]. The proposed antenna introduces only two resonances within the operating band, each due to the modified ground and the semi elliptic patch respectively. An exhaustive study of the radiation characteristics of this antenna in the frequency and time domains are presented.

Bandwidth enhancement of open slot antenna by varying the shape of the open slot is presented [99]. By cutting two notches along

the inverted-L shaped open slot in the ground plane, band width extending from 3 to 10.9 GHz is obtained.

A special square slot antenna for circular polarization, which is composed of a square ground plane embedded with two unequal-size inverted-L strips around two opposite corners of the square slot [100], is presented. The antenna owns an impedance bandwidth ratio of 4.7:1 (2.67 - 13 GHz) and a circular polarization bandwidth ratio of 1.5:1 (4.9 - 6.9 GHz).

Slot antenna comprised of an open-ended semi-circular slot and a narrow rectangular slot is proposed [101]. To achieve good impedance match within the band of 3.09 - 11.0 GHz, the 50 Ω microstrip feed-line is loaded with an elliptical slot, while an extended substrate is protruded above the upper edge of the antenna.

Study on printed binomial-curved slot antennas, where the slot and the tuning stub both formed by a binomial curve function is discussed [102]. To achieve an efficient excitation and wide impedance matching, the signal strip is terminated to a tuning stub with the same shape as the slot but with a smaller size, which has an offset from the bottom edge of slot. As N (order of binomial curve function) equals to 1, both the slot and the tuning stub are the triangular shape. As N increases, the bottom widths of the slot and the tuning stub expand gradually, and their shapes look like bowls. It is found that the larger order N is selected, the wider bandwidth may be obtained which allows the antenna designers to find a suitable slot antenna structure according to the required operation bandwidth.

First part of Chapter 5 presents the design, study and experimental results of the proposed CPW fed UWB slot antenna which covers a frequency band from 2.5 GHz -12 GHz. The antenna consists of a bevelled rectangular monopole and a ground plane extended to surround the monopole to form a slot-like structure. In this design, certain modifications are introduced in the extended ground plane to enhance the impedance bandwidth of the antenna. Pair of rectangular slits inserted in the ground plane extends the lower edge of the band without increasing the overall size of the antenna. The upper edge of the band is enhanced by bevelling the ground plane corners near the feed point.

2.3 Band-notched UWB Antennas

Some existing narrowband wireless services such as wireless local area network (WLAN) IEEE802.11a and HIPERLAN/2 WLAN occupy 5.15 - 5.35 GHz and 5.725 - 5.825 GHz frequency bands respectively in the UWB band. World interoperability for microwave access (WiMAX) service from 3.3 to 3.6 GHz also shares spectrum with the UWB. This may cause interference with the UWB system. One of the methods to overcome this problem is to use filters to remove these interfering bands. However, the use of an additional filter will make the UWB system complex and bulkier. Therefore, various printed UWB antennas with notched functions are introduced to overcome this electromagnetic interference. This section deals with various band notched techniques reported so far such as inserting slots, placing parasitic elements, adding stubs and using different combination of these notch structures (hybrid techniques) etc..

Among the various band notched techniques one of the simplest and common methods is etching slots of different shape on the patch or on the ground plane. The band-reject operation is achieved when the length of the embedded slot is approximately one-half wave length of the desired notch frequency. In this case, a destructive interference for the excited surface currents in the antenna will occur, which prevents the antenna from radiating at that frequency [103].

A CPW-fed planar ultra-wideband antenna with hexagonal radiating elements having a frequency band notch feature at the WLAN frequency band is presented [104]. By inserting a V-shaped thin slot on the hexagonal radiating element, the narrow frequency band notch is created very close to the desired frequency. The notched frequency band is adjustable by varying the length of the V-shaped slot.

Wideband monopole antenna with a narrow slit having frequency band-notch characteristic is presented [105]. Band-notch characteristic is achieved by inserting a modified inverted U-slot on the main patch. Narrow slit is used to improve the VSWR performance of the monopole antenna.

A microstrip line fed triangular monopole antenna with a staircase shape to achieve wide bandwidth is presented [106]. By etching a U-shaped slot in the radiating element, the antenna can relax the requirements imposed upon the filtering electronics within the wireless device and also prevents interference with WLAN systems. The resonant frequency of a notched band is determined by the total

length of the slot; the shorter the total length of the U-shaped slot, the higher the resonant frequency.

A coplanar waveguide fed rectangular aperture antenna with a T-shaped exciting stub is proposed [107]. The proposed antenna is further extended to the band-notched function and two different band-notched designs are provided. The design concept of the band-rejection function is to make the input impedance resistive at the notch frequency. To implement it, a narrow-band resonant structure is added to the original wide-band antenna area. The first design embeds an isolated slit of total length equal to half a wavelength for the frequency at 5.5 GHz inside the T-stub. The second design employs two open-end slits at the top edge of the T-stub where the effective length of each slit is around quarter wavelength for the 5.5 GHz resonance.

The configuration of a planar UWB antenna with the capability of rejecting frequencies within the 4.0 - 6.0 GHz band is illustrated [108]. The radiating slot is the result of intersecting of two circles in a conductive layer on top of the substrate. The antenna is fed with a coplanar waveguide. An arc shaped tuning slot to reject a signal within the 4–6 GHz band is introduced in the second circle.

The antenna consists of a bevelled rectangular metal patch and a 50 Ω coplanar waveguide (CPW) transmission line is presented [109]. By etching two nested C-shaped slots in the patch, band-rejected filtering properties in the WiMAX/WLAN bands are achieved. An equivalent circuit model of the proposed antenna is presented to discuss the mechanism of the dual band-notched UWB antenna.

The proposed multiple band notched antenna consist of a planar circular patch monopole UWB antenna and multiple etched slots on the patch [110]. Two split ring slots and two arc slots have been etched on the patch to generate triple notched bands. Two split ring slots are used to generate notched bands with central frequency of 2.4 and 3.5 GHz, respectively, while the couple arc slots with the same radius are corresponding to the notched band centred on 5.8 GHz.

Planar ultra wideband (UWB) antennas with on-ground band-notched structures are studied [111]. Two different slot resonators, which feature quarter-wavelength and half-wavelength configurations, are embedded into the arc shaped ground plane of the circular disk patch antenna in order to obtain the desired band-rejection around 5.8 GHz. This antenna retains a super wide working band which spans from 1.62 GHz - 17.43 GHz. Performance in both the frequency domain and time domain for this antenna has been investigated carefully.

Analysis and the operational principles of the embedded slots, both half-wavelength and quarter-wavelength types, in getting the notched band function is discussed [112]. A straight, open-ended quarter-wavelength slot is etched in the radiating patch to create the first notched band in 3.3 - 3.7 GHz for the WiMAX system. In addition, three semi-circular half-wavelength slots are cut in the radiating patch to generate the second and third notched bands at 5.15 - 5.825 GHz for WLAN and 7.25 - 7.75 GHz for downlink of C-band satellite communication systems. Surface current distributions and transmission line models are used to analyse the effect of these slots.

The antenna consists of a circular monopole and two W-shaped slots etched into the monopole and the truncated ground plane, which lead to the desired high attenuation at the two notch frequencies: WiMAX (3.4 - 3.8 GHz), WLAN (4.8 - 6.2 GHz) is presented [113]. The circular monopole antenna is fed by a 50 Ω microstrip line with a double-fed structure which prevents the excitation of horizontal currents and ensures that only the dominant vertical current mode is present in the structure.

Similar to the inserting slot structure in the UWB antenna design, another commonly used technique is attaching stubs to the patch, ground or feed line. When the length of the open circuited stubs approximately equal to one quarter of wavelength of the desired notch frequency, a destructive interference of the current distribution takes place and makes the antenna non-radiating at that frequency.

Band-notched printed monopole antenna with constant gain over a wide bandwidth is presented [114]. By using a pair of coupled T-shaped strip and by inserting a protruded rectangular strip in the ground plane, the gain of the square antenna is enhanced, and also much wider impedance bandwidth can be produced, especially at the higher band. The notched band, covering the 5.05 - 5.95GHz WLAN band, is obtained by electromagnetically adjusting the coupling between a pair of T-shaped stubs protruded inside the square ring.

Microstrip slot antenna with very sharp frequency notched function is proposed and investigated [115]. The antenna consists of an

octagonal wide slot etched on the ground plane used as it radiator with a rectangular tuning stub on the other side. Two small notches are used to finely tune the impedance matching characteristic. By simply introducing an embedded square ring resonator in the tuning stub of the slot antenna, high, sharp gain reduction performance at WLAN band can be achieved.

Technique for simultaneously adding an extra frequency band at 2.4 GHz (Bluetooth band) without increasing the size of the antenna and two frequency notched bands centred at 3.5 GHz (WiMAX band) and 5.8 GHz (WLAN band) to an octagonal shaped UWB slot antenna are proposed [116]. The extra band and dual band notches, which are independent of each other, are created by attaching the L-shaped stubs of a quarter-wavelength to the ground plane near the feed line. The centre frequency of the notched bands can be finely tuned by changing the length of the stubs. The stubs act independently and their addition to the slot antenna does not change the behaviour of the original UWB slot antenna.

Double trapezoid slot monopole antenna with dual band-notched performance at 3.5/5.5 GHz is discussed [117]. A U-shaped stub and a T-shaped stub in the radiation patch are embedded in upper and lower trapezoid slots of the radiation patch respectively to realise the dual band-notched characteristics.

UWB monopole antenna with notched band at 3.3 - 3.7 GHz (WiMAX) and 5.15 - 5.825 GHz (WLAN) is developed [118]. The

original UWB antenna is mainly composed of a hexagon radiation patch and a circular slotted ground plane. In order to obtain band-notched characteristics at 3.3 - 3.7 GHz and 5.1 - 5.8 GHz, a pair of bended dual-L-shape branches are added to the slotted ground symmetrically. Also, one branch consists of two strips of different length, but these two strips share a common circle centre. The different strips control different notch-band, the longer strip for the lower notch-band and the shorter one for the upper notch-band.

Another band rejection technique is parasitic strip method, in which a certain piece of conducting strip is placed in the radiating aperture or adjacent to the radiating element. This element is called "Parasitic" since it is not directly fed to the radiating element. When the parasitic element resonates at the desired notch frequency, the current distribution across the radiating element is disturbed and leads to reduced radiation.

The antenna composed of a rounded ground with a slit, a planar half ellipse-shaped radiation patch with an ellipse-shaped slot is designed to reject the limited band (5.15 - 5.825 GHz) by attaching the parasitic strip to the bottom layer of the antenna [119]. The notched frequency band is adjustable by varying the length and location of the parasitic strip.

A segmented circular planar monopole antenna with a notched band centred at 5.7 GHz is proposed [120]. Band-notched characteristic at 5.7 GHz band is obtained by segmenting a circular monopole patch

into three parts. Through cutting apart a circular monopole patch with a pair of symmetrical slots, the patch is divided into three segments: the centre patch and two side patches. Practically, the side patches function as two parasitic elements and work as band stop filters. The segmenting method that brings on band notched function could be regarded as a hybrid between the methods of cutting slots and attaching parasitic elements.

Microstrip-fed antenna, consisting of a square slot patch with a vertical coupling strip is discussed [121]. The vertical coupling strip at the centre of the slot patch controls the WLAN rejection frequency band for UWB system operation. This coupling strip acts as a quarter-guid-wavelength resonator.

Method for the design of a UWB planar antenna with band-notch characteristics is proposed [122]. In this method, parasitic elements in the form of printed strips placed in the radiating aperture of the planar antenna at the top and bottom layer are employed to suppress the radiation at certain frequencies within an ultra wide frequency band. The parasitic elements have dimensions which are chosen according to a certain formula. They can be used to reject a single narrow band, a wide band, or three narrow bands, while the normal performance of the antenna is maintained at the remaining pass band.

Dual band-notched monopole antenna with increased bandwidth is proposed [123]. To improve the bandwidth a pair of L-shaped slots is inserted on the ground plane. Dual band-notched characteristic is

obtained by using one single element with fork-like shape, which is electromagnetically coupled to the radiation patch. Moreover, single band-rejected function is provided by using an inverted U-shaped parasitic element instead of fork-shaped element.

The split-ring resonator (SRR) and complementary split-ring resonator (CSRR) structures can also be applied in UWB antennas for the notched band design. A SRR consists of a pair of concentric annular or rectangular rings with splits at the opposite ends. The length and width of the rings determine the centre frequency and bandwidth of the notched band.

Realisation of dual band-notched characteristics using CSRR is presented [124]. By adjusting the size of the CSRR inserted in the radiating patch of a UWB monopole antenna, dual stop bands can be obtained. This design uses a single CSRR instead of two separate notch structures to produce notched bands at 3.40 - 3.48 GHz and 5.40 - 5.98 GHz.

Microstrip-fed half-elliptic monopole antenna with band-notched characteristics is studied [125]. Two elliptic single complementary split-ring resonators (ESCSRRs) are embedded in the radiating patch to cancel interferences due to WiMAX (3.3 - 3.7 GHz) and upper WLAN frequencies (5.15 - 5.85 GHz). Furthermore, rectangular split-ring resonators are placed as parasitic elements near the junction of feed line and radiating element to reject the ITU-specified X-band communication frequencies (7.9 - 8.4 GHz).

Recently, electromagnetic band-gap (EBG) structures have been introduced in the design of UWB antennas with a stop band characteristic because of its filtering behaviour. An EBG consists of metallic patches and short pins named vias that connect patches into the ground plane. The operation of EBGs is similar to a LC filter array [126].

Ultra wide band circular monopole antenna which employs EBG structure to realise band-rejection characteristic is investigated [126]. Mushroom-like EBG structure is located near the feed line to achieve this goal. The amount of coupling between the EBG and the proposed antenna depends on the distance between the feed line and the EBG structure. As the EBG nears the feed line, coupling is increased and stronger rejection is achieved. The stop band can be adjusted by changing the gap distance between EBG cells.

UWB antenna consists of a microstrip line fed bevelled rectangular metal patch with a defective ground plane utilizing two electromagnetic band-gap (EBG) structures to produce dual notched band response is studied [127]. The corner-located vias mushroom-type EBG (CLV-EBG) structure is utilized for frequency-rejected function design as it is more compact than the edge-located vias mushroom-type EBG (ELV-EBG) structure by moving via from edge to corner. Then, by placing one or two CLV-EBG structures coupling to the microstrip feeding line of the UWB antenna, single or dual notches are obtained as desired. The time- domain characteristics of the antennas are also investigated with good performances.

Folded strip monopole ultra wideband antenna with band-notched characteristics at WLAN is proposed [128]. This antenna is composed of a forked-shape radiator and a 50 Ω microstrip line. To achieve band-rejected filtering property at the WLAN bands, the forked-shape strips are folded back and result in a pair of coupled lines on the radiator. The length and gap width of the coupled lines primarily determine the notched frequency of the antenna.

A band-rejected circle-like slot antenna with a folded fork-shaped tuning stub is proposed [129]. To achieve band-rejected filtering property at 5 GHz WLAN bands, the forked-shaped strips are folded back and result in a pair of coupled lines on the tuning stub. These coupled line sections act as parallel resonators and prevent the antenna from radiating at the targeted rejection band from 5.1 - 5.9 GHz.

UWB antennas structure which use various notched-band techniques together (hybrid techniques) i.e., combinations of slot, stub and parasitic element, to realise multiple band notched are common in literature.

The antenna consists of a U-shaped slot excited by microstrip fed circular stub is proposed [130]. The band-notched characteristics are realised by attaching a slot and a parasitic strip to the antenna. The parasitic strip on the bottom layer deals with the WiMAX notched band while the C-shaped slot inserted in the circular feeding stub aims at the WLAN band.

Antenna consists of annular patch producing dual band notched characteristics is presented [131]. The dual band-notched response in

both 3.4 - 3.7 GHz and 5 - 6 GHz can be achieved by etching a C-shaped slot in the annular patch and CSRR in the ground, respectively. A rectangular notch on the top of the ground is proposed to improve impedance bandwidth of the presented antenna. CSRR in the ground plane, together with the open stub extended from feed line, can obtain band-stop filtering property at 5.5 GHz with good out-off-band flatness.

Printed monopole antenna with dual band notched characteristics used for UWB applications is presented and investigated [132]. By inserting two I-shaped notches in both sides of the microstrip feed line on the ground plane with proper dimensions, a wide impedance bandwidth is achieved. Dual band-notched characteristic is achieved using a G-slot defected ground structure (DGS) in the ground opposite to the feeding line and a pair of Γ-shaped stubs in the radiating patch.

The antenna consists of a spade-shaped radiation patch with truncated ground is presented [133]. By employing three crescent-shaped parasitic resonators on the back side and etching an inverted U-slot in the ground plane, four efficient notched bands centred on 5.2 GHz, 5.8 GHz, 7.5 GHz and 8.2 GHz are achieved.

Ultra-wideband (UWB) antenna with dual-band notched characteristics is presented [134]. To realise the narrow band of WiMAX centred at 3.5 GHz, the circular patch is first cut to an annular ring, and then a pair of Y-shaped strips are connected to the annular ring. Then by etching an inverted Ω-shaped slot on the patch, a notched band of 5.2 - 5.98 GHz for WLAN band is achieved.

Dual band-notched slot antenna with enhanced bandwidth from 2.1 - 20 GHz is proposed [135]. By embedding two L-shaped stubs on the rear of the substrate, the total bandwidth of the antenna is greatly improved. In addition, by inserting two parasitic strips inside the circle-like slot and etching two L-shaped slots in the ground plane, dual band-notched characteristics are obtained.

Open slot antenna with dual band notched characteristics is investigated [136]. To achieve the UWB operating characteristic, a L-shaped open slot is etched on the ground plane. The desired 5.2 GHz and 5.8 GHz WLAN band-notched characteristics are achieved by placing a slot resonator on the ground plane and a slot-type SRR inside a circular exciting stub on the front side, respectively.

The antenna consists of a square patch and a modified ground plane producing band-notched response is studied [137]. A T-shaped stub on the radiating patch and a pair of U-shaped stubs near the feeding line are adopted to generate notched bands with central frequencies of 3.6 GHz and 5.5 GHz, respectively.

A step-by-step design procedure aimed at achieving the required UWB response with dual notched bands is presented [138]. The radiator of the antenna is a slotted square patch. The ground plane is located at the bottom layer, which also includes a π-shaped conductor-backed plane to widen the impedance bandwidth. The first notched frequency band is achieved by using a pair of mirror inverted L-shaped slots embedded in the radiator, whereas the second notched band is realised by an inverted T-shaped strip inside the radiator.

Design of multiple band notches for compact UWB antenna is proposed [139]. The antenna consists of an elliptical radiator, a microstrip-feed line and a ground plane. Four pairs of meander lines (MLs), working as resonators, are added to the antenna to produce a quadruple band notch characteristic, without increasing the overall antenna size. Two types of feeding techniques, direct-connected feed and parallel-coupled feed, are used in the resonators. The centre frequencies and bandwidths of the individual notches can be adjusted independently using the dimensions of the corresponding MLs.

Microstrip-fed U-shaped monopole ultra-wideband antenna with dual band-notched characteristics is proposed and investigated [140]. The dual band- notched operations are achieved by introducing a spiral shaped quarter wavelength stub in the microstrip feed line and a pair of symmetrical L shaped slots on the ground patch. The spiral stub in the radiating patch is used to reject the frequency band limited by WiMAX systems while the symmetrical L-shaped slot on the DGS is used to reject the frequency band limited by WLAN systems. The dual band rejections are thus mutually uncorrelated due to the placement of structure in different places ie., in the radiating plane and the ground plane.

Circular ultra-wideband planar monopole antenna designed to obtain dual band-notched characteristics is presented [141]. The antenna consists of a pair of arc-shaped strips near the patch and a pair of two slots in the ground plane to realize the band-notched

characteristics. The parasitic strips reject the upper band while the slots in the ground plane deals with the lower one.

Dual band-notched monopole antenna with multi resonance performance is presented [142]. The antenna consists of a square radiating patch with an inverted T-shaped ring slot, surrounded by a C-shaped slot, which provides a wide usable fractional bandwidth of more than 125% (2.71 - 12.06 GHz). In the proposed structure, single band-notched function is provided by cutting an inverted T-shaped slot, surrounded by a C-shaped slot, in the radiating patch, and dual band-notch characteristic is obtained by adding an inverted T-shaped parasitic structure inside the slot in the radiating patch. By inserting this parasitic structure, additional resonance is excited, the bandwidth is improved and leads to a fractional bandwidth of more than 125%, with respect to the multi resonance performance.

Microstrip-fed UWB antenna with dual notch-band, including 3.3 - 3.7 GHz (WiMAX) and 5.15 - 5.825 GHz (WLAN) is proposed [143]. In order to get notch-band at 3.3 - 3.7 GHz, a meandering slot is embedded into the junction of feed-line and radiation patch. The notch-band at 5.15 - 5.825 GHz is achieved by symmetrically adding two C-shaped strips to the feed-line. Both the slot and the symmetrical strips are analysed and discussed.

A dual band-notched inverted U-shaped wide-slot UWB antenna with a radiation patch similar to the slot shape is proposed [144]. The rejection of the WLAN band is obtained by etching a C-shaped slot on

the radiation patch. To achieve the band-notched function at the WiMAX band, an L-shaped stub is extruded from the ground plane. By putting the two band-notched structures in the right position and choosing the appropriate length for both structures, a dual band-notched UWB antenna with high performance can be acquired.

UWB antenna with 3.5/5.5 GHz dual notch-band characteristics is presented [145]. Firstly, a modified UWB rotated cross monopole antenna is obtained. Then by inserting a quarter wavelength stub and etching two symmetrical half-wavelength L-shaped slots on the UWB antenna, a dual band-notched ultra-wideband antenna is obtained.

CPW fed rectangular slot antenna with stepped impedance resonator-defected ground structure (SIR-DGS) and fork-shaped stubs to achieve sharp notches at frequencies of 3.5 GHz, 5.68 GHz and 7.48 GHz is proposed [146]. The proposed antenna operates from 2.8 to 11.3 GHz except for the selected notched bands. The main advantage of the antenna is that the frequency of the notched band can be tuned easily over a wide frequency range.

UWB antenna designed for rejecting the potential interference from WLAN band (5.15 - 5.825 GHz) as well as X-band (7.25 - 7.75 GHz and 7.9 - 8.4 GHz) is presented [147]. Two frequency rejection bands are realized in the proposed design by using a stepped impedance stub (SIS) and an arc-shaped parasitic element (ASPE). In addition, the design enables one to tune the centre frequencies of these two rejection bands by adjusting the dimensions of the SIS and the ASPE.

CPW-fed ultra wideband antenna with 3.9/5.5 GHz dual band-notched characteristics is presented [148]. The antenna consists of a cup-like radiating patch and a 50 Ω coplanar waveguide transmission line. The dual band-notched characteristics are obtained by etching a pair of L-shaped slots on the edge of ground plane and introducing two symmetrical L-shaped stubs on the radiating patch.

This thesis deals with CPW-fed UWB antennas designed to reject WiMAX and WLAN bands. Chapter 4 presents a truncated circular disc UWB monopole antenna with dual band notched characteristics. To realise the WiMAX notched band, a folded U-slot is etched near the upper edge of the radiating patch. WLAN rejection band is realised by inserting a U-slot in the radiating patch near the feed point. Chapter 5 proposes a dual band notched UWB slot antenna, where the multiple notched functions are achieved by using hybrid techniques. It employs a combination of parasitic element and stub to realise the dual band rejection. Parasitic element placed within the radiating aperture of the antenna produces notch characteristics at WiMAX band while the stub connected to the upper edge of the ground provides the notch function at WLAN band.

References

[1]   M. J. Ammann and Z. N. Chen, "Wideband monopole antennas for multi-band wireless systems," IEEE Antennas and Propagation Magazine, vol. 45, no. 2, pp. 146-150, 2003.

[2]   H.G. Schantz, "A brief history of UWB antennas". IEEE Aerospace and Electronic Systems Magazine, vol. 19, no. 4, pp. 22-26, 2000

[3]   M. J. Amman, "Control of the impedance bandwidth of wideband planar monopole antennas using a bevelling technique", Microwave and Optical Technology Letters, vol. 30, no. 4, pp. 229–232, 2001.

[4]   E. Lee, P. S. Hall and P. Gardener, " Compact wideband planar monopole antenna", Electronics Letters, vol. 35, no. 35, pp. 2157–2158, 1999.

[5]   M.J. Ammann and Z.N. Chen, "A wide-band shorted planar monopole with bevel", IEEE Transactions on Antennas and Propagation, vol. 51, no.4, pp. 901- 903, 2003.

[6]   P. V. Anob, K. P. Ray, and G. Kumar, "Wideband orthogonal square monopole antennas with semi-circular base", IEEE Antennas Propagation Symposium, Boston, vol.3, pp.294-297, 2001.

[7]   D.E. Antonino, F.M. Cabedo, B.M. Ferrando and N.A. Valero, "Wideband double-fed planar monopole antennas", Electronics Letters, vol. 39, no. 23, pp. 1635-1636, 2003.

[8]   K.L. Wong, C.H. Wu and S.W. Su, "Ultra wide-band square planar metal-plate monopole antenna with a trident-shaped feeding strip", IEEE Transactions on Antennas and Propagation, vol. 53, no. 4, pp. 1262-1269, 2005.

[9]   S.Su, K.Wong and C.Tang, "Ultra-wideband square planar antenna for IEEE 802.16a operating in the 2–11 GHz band", Microwave and Optical Technology Letters, vol. 42, no. 6, pp. 463-466, 2004.

[10]   Z. N. Chen, X. H. Wu, N. Yang, and M. Y. W. Chia, "Design considerations for antennas in UWB wireless communication systems", IEEE Antennas and Propagation Society International Symposium, pp. 822-825, 2003.

[11]   Z. N. Chen, X. H. Wu, H. F. Li, N. Yang, and M. Y. W. Chia, "Considerations for source pulses and antennas in UWB radio systems", IEEE Transactions on Antennas and Propagation, vol. 52, no. 7, pp. 1739-1748, 2004.

[12] K.W. Loi, S. Uysal, and M. S. Leong, "Design of a wideband microstrip bowtie patch antenna", Proc. Inst. Elect. Eng. Microwave Antennas Propagation, vol. 145, 1998.

[13] K. Kiminami, A. Hirata, and T. Shiozawa, "Double-sided printed bow-tie antenna for UWB communications", IEEE Antennas Wireless Propagation Letters, vol. 3, pp.152-153, 2004.

[14] S.H. Choi , J.K. Park , S.K.Kim and J.Y. Park , "A new ultra-wideband antenna for UWB applications", Microwave and Optical Technology Letters, vol. 40, no. 5, pp. 399 – 401, 2004.

[15] J. Liang, C.C. Chiau, X. Chen and C.G. Parini, "Printed circular disc monopole antenna for ultra-wideband applications", Electronics Letters, vol. 40, no. 20, 2004

[16] J.X. Liang, C.C. Chiau , X.D. Chen and C.G. Parini, "Study of a printed circular disc monopole antenna for UWB systems", IEEE Transactions on Antennas and Propagation, vol. 53, no. 11, pp. 3500-3504, 2005.

[17] J. Liang, L. Guo, C.C. Chiau, X. Chen and C.G. Parini, "Study of CPW-fed circular disc monopole antenna for ultra wideband applications", IEE Proc.-Microwave Antennas Propagation, vol. 152, no. 6, pp. 520-526, 2005.

[18] Z. N. Low, J. H. Cheong and C. L. Law, "Low-cost PCB antenna for UWB applications", IEEE Antennas and Wireless Propagation Letters vol. 4, pp. 237-239, 2005.

[19] J. Jung, W. Choi and J. Choi, "A small wideband microstrip-fed monopole antenna", IEEE Microwave and Wireless Components Letters, vol. 15, no. 10, pp. 703-705, 2005.

[20] C.-C. Lin, Y.-C. Kan, L.-C. Kuo and H.-R. Chuang, "A planar triangular monopole antenna for UWB communication", IEEE Microwave and Wireless Components Letters, vol. 15, no. 10, pp. 624-626, 2005.

[21] J. Kim, T. Yoon, J. Kim and J. Choi, "Design of an ultra wide-band printed monopole antenna using FDTD and genetic algorithm", IEEE Microwave and Wireless Components Letters, vol. 15, no. 6, pp. 395-397, 2005.

[22] C.Y. Huang and W.C. Hsia, "Planar elliptical antenna for Ultra-wideband communications", Electronics Letters, vol. 41, no.6, pp. 296-297, 2005.

[23] X. L. Bao and M. J. Ammann, "Investigation on UWB printed monopole antenna with rectangular slitted groundplane", Microwave and Optical Technology Letters, vol. 49, no. 7, pp. 1585-1587, 2007.

[24] K. Chung, H. Park, and J. Choi, "Wideband microstrip-fed monopole antenna with a narrow slit", Microwave and Optical Technology Letters, vol. 47, no. 4, pp. 400-402, 2005.

[25] H.M. Chen, "Microstrip-fed dual-frequency printed triangular monopole", Electronics Letters, vol. 38, pp. 619–620, 2002.

[26] K. Rambabu, H. A. Thiart, J. Bornemann and S. Y. Yu, "Ultra wideband printed-circuit antenna", IEEE Transactions on Antennas and Propagation, vol. 54, no. 12, pp. 3908-3911, 2006.

[27] A. A. Eldek, "A small ultra-wideband planar tap monopole antenna with slit, tapered transition, and notched ground plane", Microwave and Optical Technology Letters, vol. 48, no. 8, pp. 1650-1654, 2006.

[28] J. Kim and Y. Jee, "Design of ultra wideband coplanar waveguide-fed li-shape planar monopole antennas", IEEE Antennas and Wireless Propagation Letters, vol. 6, pp. 383-387, 2007.

[29] K. P. Ray and Y. Ranga, "Ultra wideband printed elliptical monopole antennas", IEEE Transactions on Antennas and Propagation, vol. 55, no. 4, pp. 1189-1192, 2007.

[30] Y. Zhang, Z. N. Chen, and M. Y. W. Chia, "Effects of finite ground plane and dielectric substrate on planar dipoles for UWB applications," Proc. IEEE International Symposium on Antennas Propagation, pp. 2512–2515, 2004.

[31] Z. N. Chen, N. Yang, Y. X. Guo, and M. Y. W. Chia, "An investigation into measurement of handset antennas", IEEE Trans. Instrum. Meas., vol. 54, no. 3, pp. 1100–1110, 2005.

[32] Z. N. Chen, T. S. P. See and X. Qing, "Small printed ultra-wideband antenna with reduced ground plane effect", IEEE Transactions on Antennas and Propagation, vol. 55, no. 2, pp. 383-388, 2007.

[33] C.W. Ling, W.H. Lo, R.H. Yan and S.J. Chung, "planar binomial curved monopole antennas for ultra wideband communication", IEEE Transactions on Antennas and Propagation, vol. 55, no. 9, pp. 2622-2624, 2007.

[34] A. M. Abbosh and M. E. Bialkowski, "Design of ultra wideband planar monopole antennas of circular and elliptical shape", IEEE Transactions on Antennas and Propagation, vol. 56, no. 1, pp. 17-33, 2008.

[35] M.E. Chen and J.H. Wang, "CPW-fed crescent patch antenna for UWB applications", Electronics Letters, vol. 44, no. 10, 2008.

[36] K.S. Lim, M. Nagalingam and C.P. Tan, "Design and construction of microstrip UWB antenna with time domain analysis", Progress In Electromagnetics Research M, vol. 3, pp. 153–164, 2008.

[37] C.C. Lin, H.R. Chuang and Y.C. Kan, "A 3–12GHz UWB planar triangular monopole antenna with ridged ground-plane", Progress In Electromagnetics Research, vol. 83, pp. 307–321, 2008.

[38] X.L. Liang, S.S. Zhong and W. Wang, "Tapered CPW-fed printed monopole antenna", Microwave and Optical Technology Letters, vol. 48, no. 7, pp. 1242-1244, 2006.

[39] X.L. Liang, S.S. Zhong and W. Wang, "UWB printed circular monopole antenna", Microwave and Optical Technology Letters, vol. 48, no. 8, pp. 1532-1534, 2006.

[40] X.L. Liang, S.S. Zhong, W. Wang and F.-W. Yao, "Printed annular monopole antenna for ultra-wideband applications", Electronics Letters, vol. 42, no. 2, 2006.

[41] X.L. Liang, S.S. Zhong and W. Wang, "Elliptical planar monopole antenna with extremely wide bandwidth", Electronics Letters, vol. 42, no. 8, 2006.

[42] S.S. Zhong, X.L. Liang and W. Wang, "Compact elliptical monopole antenna with impedance bandwidth in excess of 21:1", IEEE Transactions on Antennas and Propagation, vol. 55, no. 11, pp. 3082-3085, 2007.

[43] X.R. Yan, S.S. Zhong and G.Y. Wang, "Compact printed monopole antenna with 24:1 impedance bandwidth", Electronics Letters, vol. 44, no. 2, 2008.

[44] C. Deng, Y.J. Xie and P. Li, "CPW-fed planar printed monopole antenna with impedance bandwidth enhanced", IEEE Antennas and Wireless Propagation Letters, vol. 8, pp. 1394-1393, 2009.

[45] H. Kimouche, D. Abed, B. Atrouz, and R. Aksas, "Bandwidth enhancement of rectangular monopole antenna using modified semi-elliptical ground plane and slots", Microwave and Optical Technology Letters, vol. 52, no. 1, pp. 54-58, 2010.

[46] M. Moosazadeh, C. Ghobadi and M. Dousti, "Small monopole antenna with checkered-shaped patch for UWB application", IEEE Antennas and Wireless Propagation Letters,   vol. 9, pp. 1014-1013, 2010.

[47] A. Ghazi, M. N. Azarmanesh and M. Ojaroudi, "Multi-resonance square monopole antenna for ultra-wideband applications", Progress In Electromagnetics Research C, vol. 14, pp. 103 -113, 2010.

[48] K.R. Chen, C.Y.D. Sim and J.S. Row, "A compact monopole antenna for super wideband applications", IEEE Antennas and Wireless Propagation Letters, vol. 10, pp. 488-491, 2011.

[49] R. Azim, M.T. Islam and N. Misran, "Ground modified double-sided printed compact UWB antenna", Electronics Letters, vol. 47, no. 1, 2011.

[50] S. Y. Park and J. K. Park, "Design of triple-band antenna for PCS/WLAN/UWB applications", Microwave and Optical Technology Letters, vol. 53, no. 1, pp. 235-238, 2011.

[51] M. Moosazadeh and Z. Esmati, "A novel coplanar waveguide-fed elliptical-shaped printed monopole antenna for ultra wideband applications", Microwave and Optical Technology Letters, vol. 54, no. 3, pp. 675-677, 2012.

[52] D. R. Melo, M. N. Kawakatsu, D. C. Nascimento and V. Dmitriev, "A planar monopole UWB antennas with rounded patch and ground plane possessing improved impedance matching", Microwave and Optical Technology Letters vol. 54, no. 2, pp. 335-338, 2012.

[53] S. Sreenath, P. Ashkarali, P. Thomas, R. Dinesh, and C. K Anandan, "CPW-fed compact bent monopole antenna for UWB applications", Microwave and Optical Technology Letters, vol. 55, no. 1, pp. 56-58, 2013.

[54] C. Wang, Z.H. Yan, B. Li and S. Li, "An ultra-wideband CPW-fed monopole antenna with fan shaped structure" ,Microwave and Optical Technology Letters, vol. 54, no. 12, pp. 2878-2880, 2012.

[55] Y. Zhang and M. Hara, "Miniaturized planar ultra wideband antenna on a trapezoidal ground fed with a tapered microstrip line", Microwave and Optical Technology Letters,   vol. 54, no. 11, pp. 2468-2471, 2012.

[56] M. Sefidi, Y. Zehforoosh and S. Moradi, "A novel monopole antenna for wireless communication systems and UWB application", Microwave and Optical Technology Letters, vol. 55, no. 8, pp. 1856-1860, 2013.

[57] Y. Y. Sun, S. W. Cheung and T. I. Yuk, "Design of a very compact UWB monopole antenna with microstrip-fed", Microwave and Optical Technology Letters, vol. 55, no. 9, pp. 2232-2234, 2013.

[58] M. M. Fakharian and P. Rezaei, "Very compact palmate leaf shaped CPW-fed monopole antenna for UWB applications", Microwave and Optical Technology Letters, vol. 56, no. 7, pp. 1612-1616, 2014.

[59] M. Manohar, R. S. Kshetrimayum and A.K. Gogoi, "A compact printed triangular monopole antenna for ultra wideband applications", Microwave and Optical Technology Letters, vol. 56, no. 5, pp. 1155-1160, 2014.

[60] K. P. Ray, S. S. Thakur and A. A. Deshmukh, "Slot cut printed elliptical UWB monopole antenna", Microwave and Optical Technology Letters, vol. 56, no. 3, pp. 631-635, 2014.

[61] Y. Yoshimura, "A microstrip slot antenna", IEEE Transactions on Microwave Theory and Techniques, vol. 20, pp. 760-762, 1972.

[62] M. Kahrizi, T. K. Sarkar, and Z. A. Maricevic, "Analysis of a wide radiating slot in the ground plane of a microstrip line", IEEE Transactions on Microwave Theory and Techniques, vol. 41, no.1, pp. 29 -37, 1993.

[63] S. M. Shum, K. F. Tong, X. Zhang, and K. M. Luk, "FDTD modeling of microstrip-line-fed wide-slot antenna", Microwave and Optical Technology Letters, vol. 10, pp. 118–120, 1995.

[64] N. Behdad and K. Sarabandi, "Dual resonant slot antennas for wireless applications", Proc. IEEE AP-S International Symposium, pp. 1931–1934, 2004.

[65] W.S. Chen, C. C. Huang and K. L. Wong, "A novel microstrip line fed printed semi-circular slot antenna for broad band application", Microwave and Optical Technology Letters, vol. 26, no. 4, pp. 237–239, 2000.

[66] M. K. Kim, K. Kim, Y. H. Suh and I. Park, "A T-shaped microstrip-line-fed wide slot antenna', Proc. IEEE AP-S International Symposium, pp. 1500–1503, 2000.

[67] J.Y. Sze and K.L. Wong, "Bandwidth enhancement of a microstrip-line-fed printed wide-slot antenna", IEEE Transactions on Antennas and Propagation, vol. 49, no. 7, pp. 1020-1024, 2001.

[68] X. Ding and A. F. Jacob, "CPW-fed slot antenna with wide radiating apertures", Proc. Inst. Elect. Eng/ Microwave Antennas Propagation, vol. 145, pp. 104–108, 1998.

[69] J. F. Huang and C. W. Kuo, "CPW-fed slot antenna with CPW tuning stub loading," Microwave and Optical Technology Letters, vol. 19, pp. 257–258, 1998.

[70] E. A. Soliman, S. Brebels, P. Delmotte, G. A. E. Vandenbosch, and E.Beyne, "Bow-tie slot antenna fed by CPW," Electronic Letters, vol. 35, pp. 514–515, 1999.

[71] M. Miao, B. L. Ooi, and P. S. Kooi, "Broadband CPW-fed wide slot antenna," Microwave and Optical Technology Letters, vol. 25, pp. 206–211, 2000.

[72] H.D. Chen, "Broadband CPW-fed square slot antennas with a widened tuning stub", IEEE Transactions on Antennas and Propagation, vol. 51, no. 8, pp. 1982-1986, 2003.

[73] R. Chair, A. A. Kishk and K. F. Lee, "Ultra wide-band coplanar waveguide-fed rectangular slot antenna", IEEE Antennas and Wireless Propagation Letters, vol. 3, pp. 227-229, 2004.

[74] Y.W. Jang, "Broadband cross-shaped microstrip-fed slot antenna", Electronics Letters, vol. 36, no. 25, pp. 2056-2057, 2000.

[75] Y.W. Jang, "Experimental study of large bandwidth three-offset microstrip line-fed slot antenna", IEEE Microwave and Wireless Components Letters, vol. 11, no. 10, pp. 425-427, 2011.

[76] F.W. Yao, S.S. Zhong and X.L. Liang, "Wideband slot antenna with a novel microstrip feed", Microwave and Optical Technology Letters, vol. 46, no.3, pp. 275-278, 2005.

[77] M. Koohestani and M. Golpour, "Very ultra-wideband printed CPW-fed slot antenna", Electronics Letters, vol. 45, no. 21, 2009.

[78] D.D. Krishna, M. Gopikrishna, C.K. Aanandan, P. Mohanan and K. Vasudevan, "Ultra-wideband slot antenna for wireless USB dongle applications" Electronics Letters, vol. 44, no. 18, 2008.

[79] Y. F. Liu, K. L. Lau, Q. Xue and C. H. Chan, "Experimental studies of printed wide-slot antenna for wide-band applications", IEEE Antennas and Wireless Propagation Letters, vol. 3, pp. 273–275, 2004.

[80] D. Chen and C. H. Cheng, "A novel ultra-wideband microstrip-line fed wide-slot antenna", Microwave and Optical Technology Letters, vol. 48, no. 4, pp. 776-777, 2006.

[81] F. Amini, M. N. Azarmanesh and M. Ojaroudi, "Small semi-circle-like slot antenna for ultra-wideband applications", Progress In Electromagnetics Research C, vol. 13, pp. 149-158, 2010.

[82] J.Y. Jan and J.W. Su, "Bandwidth enhancement of a printed wide-slot antenna with a rotated slot", IEEE Transactions on Antennas and Propagation, vol. 53, no. 6, pp. 2111-2114, 2005.

[83] J. Y. Jan and J. C. Kao, "Novel printed wideband rhombus like slot antenna with an offset microstrip fed line", IEEE Antennas and Wireless Propagation Letters, vol. 6, pp. 249–251, 2007.

[84] W. J. Lui, C. H. Cheng, Y. Cheng, and H. B. Zhu, "A compact ultra-wideband CPW-fed slot antenna with a forklike stub", Microwave and Optical Technology Letters, vol. 46, no. 6, pp. 548-550, 2005.

[85] M.R. Ghaderi and F. Mohajeri, "A compact hexagonal wide-slot antenna with microstrip -fed monopole for UWB application", IEEE Antennas and Wireless Propagation Letters, vol. 10, pp. 682-685, 2011.

[86] R. Azim, M.T. Islam and N. Misran, "Compact tapered-shape slot antenna for UWB applications", IEEE Antennas and Wireless Propagation Letters, vol. 10, pp. 1190-1193, 2011.

[87] S. Barbarino and F. Consoli, "Study on UWB and SWB planar slot antennas with different stub shapes", Microwave and Optical Technology Letters, vol. 53, no. 7, pp. 1528-1532, 2011.

[88] T.A. Denidni and M.A. Habib, "Broadband printed CPW-fed circular slot antenna", Electronics Letters, vol. 42, no.3, pp. 135-136, 2006.

[89] P. Li, J. Liang and X. Chen, "Study of printed elliptical/circular slot antennas for ultra wideband applications", IEEE Transactions on Antennas and Propagation, vol. 54, no. 6,   pp. 1670–1675, 2006.

[90] E. S. Angelopoulos, A. Z. Anastopoulos, D. I. Kaklamani,   A. A. Alexandridis, F. Lazarakis, and K. Dangakis, "Circular and elliptical CPW-fed slot and microstrip-fed antennas for ultra wideband applications", IEEE Antennas and Wireless Propagation Letters, vol. 5, pp. 294-297, 2006.

[91] J.Y. Chiou, J.Y. Sze and K.L. Wong, "A broad-band CPW-fed strip-loaded square slot antenna",   IEEE Transactions on Antennas and Propagation, vol. 51, no. 4, pp. 719-801, 2003.

[92] S. K. Sharma, L. Shafai, and N. Jacob, "Investigation of wide-band microstrip slot antenna", IEEE Transactions on Antennas and Propagation, vol. 52, no. 3, pp. 865-882, 2004.

[93] S.I. Latif, L. Shafai and S. K. Sharma, "Bandwidth enhancement and size reduction of microstrip slot antennas", IEEE Transactions on Antennas and Propagation, vol. 53, no. 3,   pp. 994-1003, 2005.

[94] T.G. Ma and S.K. Jeng, "Planar miniature tapered-slot-fed annular slot antennas for ultra wide-band radios", IEEE Transactions on Antennas and Propagation, vol. 53, no. 3, pp. 1194-1202, 2005,

[95] T.G. Ma and C.H. Tseng, "An ultra wideband coplanar waveguide-fed tapered ring slot antenna", IEEE Transactions on Antennas and Propagation, vol. 54, no. 4, pp. 1105-1110, 2006.

[96] C.Y.D. Sim, W.T. Chung and C.H. Lee, "Compact slot antenna for UWB applications", IEEE Antennas and Wireless Propagation Letters, vol. 9, pp. 63-66, 2010.

[97] M. Gopikrishna, D.D. Krishna, C.K. Aanandan, P. Mohanan and K. Vasudevan, "Compact linear tapered slot antenna for UWB applications", Electronics Letters vol. 44, no. 20, 2008.

[98] M. Gopikrishna, D. D. Krishna, C. K. Anandan, P. Mohanan and K. Vasudevan, "Design of a compact semi-elliptic monopole slot antenna for UWB systems", IEEE Transactions on Antennas and Propagation , vol. 57, no. 6, pp. 1834-1837, 2009.

[99] W.S. Chen and K.Y. Ku, "Bandwidth enhancement of open slot antenna for UWB applications", Microwave and Optical Technology Letters, vol. 50, no. 2, pp. 438-439, 2008.

[100] J. Pourahmadazar, C. Ghobadi , J. Nourinia , N. Felegari and H. Shirzad, "Broadband CPW-fed circularly polarized square slot antenna with inverted-L strips for UWB applications", IEEE Antennas and Wireless Propagation Letters vol. 10, pp. 369-372, 2011.

[101] C.Y. D. Sim, C.W. Tseng and W.C. Weng, "A compact open-ended slot antenna design for ultra wideband applications", Microwave and Optical Technology Letters, vol. 54, no. 1 pp. 86-71, 2012.

[102] X.L. Liang, T.A. Denidni and L.N. Zhang, "Printed binomial- curved slot antennas for various wideband applications", IEEE Transactions on Microwave Theory and Techniques, vol. 59, no.4, pp. 1058-1065, 2011.

[103] W.S. Lee, D.Z. Kim, K.J. Kim and J.W. Yu, "Wideband planar monopole antennas with dual band-notched characteristics", IEEE Transactions on Microwave Theory and Techniques, vol. 54, no. 6, pp. 2800-2806, 2006.

[104] Y. Kim and D.H. Kwon, "CPW-fed planar ultra wideband antenna having a frequency band notch function", Electronics Letters, vol. 40, no. 7, 2004.

[105] K. Chung, J. Kim and J. Choi, "Wideband microstrip-fed monopole antenna having frequency band-notch function", IEEE Microwave and Wireless Components Letters, vol. 15, no. 11, pp. 766-770, 2005.

[106] Y. J. Cho, K. H. Kim, D. H. Choi, S. S. Lee and S.O. Park, "A Miniature UWB planar monopole antenna with 5 – 6 GHz band-rejection filter and the time-domain characteristics", IEEE Transactions on Antennas and Propagation, vol. 54, no. 5, pp. 1453-1460, 2006.

[107] Y.C. Lin and K.J. Hung, "Compact ultra wideband rectangular aperture antenna and band-notched designs" IEEE Transactions on Antennas and Propagation, vol. 54, no. 11, pp. 3075-3081, 2006.

[108] A. M. Abbosh, M. E. Bialkowski, J. Mazierska, and M. V. Jacob, "A planar UWB antenna with signal rejection capability in the 4 – 6 GHz band", IEEE Microwave and Wireless Components Letters, vol. 16, no. 5, pp.278-281, 2006.

[109] Q.X. Chu and Y.Y. Yang, "A Compact ultra wideband antenna with 3.4/5.5 GHz dual band-notched characteristics", IEEE Transactions on Antennas and Propagation, vol. 56, no. 12, pp. 3637-3644, 2008

[110] Y. Zhang, W. Hong, C. Yu, Z.Q. Kuai, Y.D. Don and J.Y. Zhou, "Planar Ultra wideband antennas with multiple notched bands based on etched slots on the patch and/or split ring resonators on the feed line", IEEE Transactions on Antennas and Propagation, vol. 56, no. 9, pp. 3063-3068, 2008.

[111] Y. D. Dong, W. Hong, Z. Q. Kuai and J. X. Chen, "Analysis of planar ultra wideband antennas with on-ground slot band-notched structures", IEEE Transactions on Antennas and Propagation, vol. 57, no. 7, pp. 1886-1895, 2009.

[112] T. D. Nguyen, D. H. Lee and H. C. Park, "Design and analysis of compact printed triple band-notched UWB antenna", IEEE Antennas and Wireless Propagation Letters, vol. 10, pp. 403-406, 2011.

[113] L.Y. Cai, Y. Li, G. Zeng and H.C. Yang, "Compact wideband antenna with double-fed structure having band-notched characteristics", Electronics Letters, vol. 46, no. 23, 2010.

[114] M. Ojaroudi, Sh. Yazdanifard, N. Ojaroudi, and R. A. Sadeghzadeh, " Band-notched small square-ring antenna with a pair of T-shaped strips protruded inside the square ring for UWB applications", IEEE Antennas and Wireless Propagation Letters, vol. 10, pp. 227-230, 2011.

[115] W.J. Lui, C.H. Cheng and H.B. Zhu, "Improved frequency notched ultra wideband slot antenna using square ring resonator", IEEE Transactions on Antennas and Propagation, vol. 55, no. 9, pp. 2445-2450, 2007.

[116] M. M. S. Taheri, H. R. Hassani and S. M. A. Nezhad, "UWB printed slot antenna with bluetooth and dual notch bands", IEEE Antennas and Wireless Propagation Letters, vol. 10, pp. 255-258, 2011.

[117] J. Wang, Y. Yin, X. Liu and T. Wang, "Trapezoid UWB antenna with dual band notched characteristics for WiMAX/WLAN bands", Electronics Letters, vol. 49, no. 11, 2013.

[118] X. Liu, Y. Yin, P. Liu, J. Wang and B. Xu, "A CPW-fed dual band-notched UWB antenna with a pair of bended dual-L-shape parasitic branches", Progress In Electromagnetics Research, vol. 136, pp. 623 - 634, 2013.

[119] K.H. Kim and S.O. Park, "Analysis of the small band-rejected antenna with the parasitic strip for UWB", IEEE Transactions on Antennas and Propagation, vol. 54, no. 6, pp. 1688-1692, 2006.

[120] K. Zhang, Y. Li and Y. Long, "Band-notched UWB printed monopole antenna with a novel segmented circular patch", IEEE Antennas and Wireless Propagation Letters, vol. 9, pp. 1209-1212, 2010.

[121] H.W. Liu, C.H. Ku, T.S. Wang and C.F. Yang, "Compact monopole antenna with band-notched characteristic for UWB applications", IEEE Antennas and Wireless Propagation Letters, vol. 9, pp. 397-400, 2010.

[122] A. M. Abbosh and M. E. Bialkowski , "Design of UWB planar band-notched antenna using parasitic elements", IEEE Transactions on Antennas and Propagation, vol. 57, no. 3, pp. 796-799, 2009.

[123] R. Zaker, C. Ghobadi and J. Nourinia, "Bandwidth enhancement of novel compact single and dual band-notched printed monopole antenna with a pair of L-shaped slots", IEEE Transactions on Antennas and Propagation, vol. 57, no. 12, pp. 3978-3983, 2009.

[124] J. Liu, S. Gong, Y. Xu, X. Zhang, C. Feng and N. Qi, "Compact printed ultra-wideband monopole antenna with dual band-notched characteristics", Electronics Letters, vol. 44, no. 12, 2008.

[125] D. Sarkar, K.V. Srivastava, and K. Saurav, "A compact microstrip-fed triple band-notched UWB monopole antenna, IEEE Antennas and Wireless Propagation Letters, vol. 13, pp. 396-399, 2014.

[126] M. Yazdi and N. Komjani, "Design of a band-notched UWB monopole antenna by means of an EBG structure", IEEE Antennas and Wireless Propagation Letters, vol. 10, pp. 170-173, 2011.

[127] L. Peng and C. Ruan, "Design and time-domain analysis of compact multi-band-notched UWB antennas with EBG structures", Progress In Electromagnetics Research B,   vol. 47, pp. 339 - 357, 2013.

[128] T.G. Ma and S.J. Wu, "Ultra wideband band-notched folded strip monopole antenna", IEEE Transactions on Antennas and Propagation, vol. 55, no. 9, pp. 2473-2480, 2007.

[129] V. Sadeghi, C. Ghobadi and J. Nourinia, "Design of UWB semi-circle-like slot antenna with controllable band-notch function", Electronics Letters, vol. 45, no. 25, 2009.

[130] H.J. Zhou, B.H. Sun, Q.Z. Liu and J.Y. Deng, "Implementation and investigation of U-shaped aperture UWB antenna with dual band-notched characteristics", Electronics Letters, vol. 44, no. 24, 2008.

[131] M. Zhang, X. Zhou, J. Guo and W. Yin, "A novel ultra wideband planar antenna with dual band-notched performance", Microwave and Optical Technology Letters, vol. 52, no. 1, pp. 90-92, 2010.

[132] M. Abdollahvand, G. Dadashzade and D. Mostafa, "Compact dual band-notched printed monopole antenna for UWB application", IEEE Antennas and Wireless Propagation Letters, vol. 9, pp. 1148-1151, 2010.

[133] L. Li, Z.L. Zhou and J.S. Hong, "Compact UWB antenna with four band-notches for UWB applications", Electronics Letters, vol. 47, no. 22, 2011.

[134] Z.L. Zhou, L. Li and J.S. Hong, "Compact UWB printed monopole antenna with dual narrow band notches for WiMAX/ WLAN bands", Electronics Letters, vol. 47, no. 20, 2011.

[135] R. Emadian, M. Mirmozafari, C. Ghobadi and J. Nourinia, "Bandwidth enhancement of dual band-notched circle-like slot antenna", Electronics Letters, vol. 48, no. 7, 2012.

[136] A.F. Sun, Y.Z. Yin, and Y. Yang, "Novel design of compact open-slot antenna for UWB application with dual band-notched characteristics", Microwave and Optical Technology Letters, vol. 54, no. 5, pp. 1159-1163, 2012.

[137] W. Jiang and W. Che, "A Novel UWB Antenna With Dual Notched Bands for WiMAX and WLAN Applications, IEEE Antennas and Wireless Propagation Letters, vol. 11, pp. 293-297, 2012.

[138] M. Moosazadeh, A.M. Abbosh, Z. Esmati, "Design of compact planar ultra wideband antenna with dual-notched bands using slotted square patch and π-shaped conductor-backed plane", IET Microwave and Antennas Propagation, vol. 3, pp. 290–294, 2012.

[139] Y.F. Weng S.W. Cheung T.I. Yuk, "Design of multiple band-notch using meander lines for compact ultra-wide band antennas", IET Microwave and Antennas Propagation, vol. 6, no. 8, pp. 908–914, 2012.

[140] K. Mishra and J. Mukherjee, "Compact printed dual band-notched U-shape UWB antennas", Progress In Electromagnetics Research C, vol. 27, pp. 169 -181, 2012.

[141] M. Yazdi and N. Komjani, "Planar UWB monopole antenna with dual band-notched characteristics for UWB applications", Microwave and Optical Technology Letters, vol. 55, no. 2, pp. 241-245, 2013.

[142] N. Ojaroudi and M. Ojaroudi, "Novel design of dual band-notched monopole antenna with bandwidth enhancement for UWB applications", IEEE Antennas and Wireless Propagation Letters, vol. 12, pp. 698-701, 2013.

[143] X.L. Liu, Y.Z. Yin and J.H. Wang, "A compact dual band-notched UWB antenna with meandering slot and C-shape strips", Microwave and Optical Technology Letters, vol. 55, no. 11, pp. 2631-2636, 2013.

[144] P. Gao, L. Xiong, J. Dai, S. He and Y. Zheng, "Compact printed wide-slot UWB antenna with 3.5/5.5-GHz dual band-notched characteristics", IEEE Antennas and Wireless Propagation Letters, vol. 12, pp. 983-987, 2013.

[145] J. Ren and Y. Yin," A Compact dual band-notched ultra wideband antenna with $\lambda/4$ stub and open slots", Progress In Electromagnetics Research C, vol. 49, 133 -139, 2014.

[146] C. Zhang, J. Zhang and L. Li, "Triple band-notched UWB antenna based on SIR-DGS and fork-shaped stubs", Electronics Letters, vol. 50, no. 2, pp. 67–69, 2014.

[147] Y. Li, W. Li and R. Mittra, "Miniaturized CPW-fed UWB antenna with dual frequency rejection bands using stepped impedance stub and arc-shaped parasitic element", Microwave and Optical Technology Letters, vol. 56, no. 4, pp. 783-787, 2014.

[148] X. Wang, L. Wang, H. Zhou and W.Lu, "A compact CPW-fed antenna with dual band-notched characteristics for UWB applications", Microwave and Optical Technology Letters, vol. 56, no. 5, pp. 1047-1049, 2014.

.....&൦ര.....

Chapter **3**

METHODOLOGY

Contents

This chapter highlights the fabrication, experimental methodology employed to characterise the antenna and simulation tools used for the analysis of the UWB antenna. The simulation, optimisation and analysis of these antennas are done using CST Microwave Studio. A detailed account on theoretical approach to analyse the transfer characteristics of the antenna is discussed. The antennas are fabricated on microwave substrates using photolithography facility available in the department. This chapter concludes with a brief description of experimental setup and measurement techniques for electrical properties and transfer characterisation of UWB antennas.

3.1 Antenna Simulation

CST Microwave Studio (CST MWS) facilitates fast and accurate analysis of high frequency (HF) devices such as antennas, filters, couplers, planar/multi-layer structures and EMI/EMC effects. The simulation models of the investigated antennas are developed in CST Microwave Studio. Among the different simulation methods in CST, the transient solver could be best for wideband or planar antennas [1].

Using the built-in Graphical User Interface (GUI), antenna structure is drawn. Once the antenna structure is modelled as in Fig. 3.1, the waveguide ports are assigned to excite the antennas. Then the desired frequency range is selected before the transient solver starts. The transient solver is executed to start the simulation. From the simulated results, electrical properties/frequency domain parameters of the antenna such as input impedance, return loss, VSWR, radiation patterns, gain etc. can be conveniently displayed/ stored/ printed. The parameterisation and optimization tools in CST can optimise any parameter such as the dimensions or position of a component, the materials properties, and the values of circuit elements connected to it. The antenna geometry can then be appropriately optimised for the desired impedance response. Transient response can be analysed by inserting virtual probes at the desired positions on a spherical surface surrounding the antenna as described in section 3.2.2.
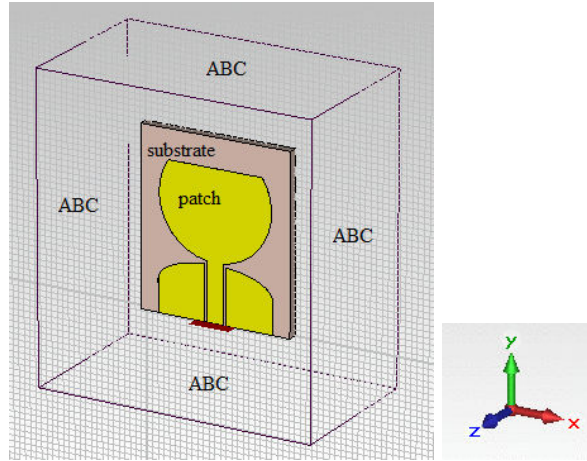
Fig. 3.1: CAD model of the antenna in CST

3.2 Time/Frequency model of UWB Antenna

Since the UWB systems are often employed in an impulse-based technology, evaluation of the conventional parameters such as reflection coefficient, efficiency, radiation pattern, gain, polarisation etc. as functions of frequency is inadequate for the characterisation of the transient radiation behaviour. So the transient properties have to be considered in addition to the frequency domain characteristics of the antennas [2].

3.2.1 Transient Transmission Model

In order to take transient properties into account, the antenna is considered as a Linear Time Invariant (LTI) system [3]. Fig. 3.2 presents an approach to characterise the UWB radio link [4] which consists of three blocks: the TX antenna, the free space channel and the RX antenna. In frequency domain, each block is characterised by transfer functions $\vec{H}_{TX}(\omega, \theta, \varphi)$, $H_{CH}(\omega)$ and $\vec{H}_{RX}(\omega, \theta, \varphi)$ under the approximation of far

field and line-of-sight propagation. The associated transient responses are $\vec{h}_{Tx}(t,\theta,\varphi)$, $h_{CH}(t)$ and $\vec{h}_{Rx}(t,\theta,\varphi)$ respectively.
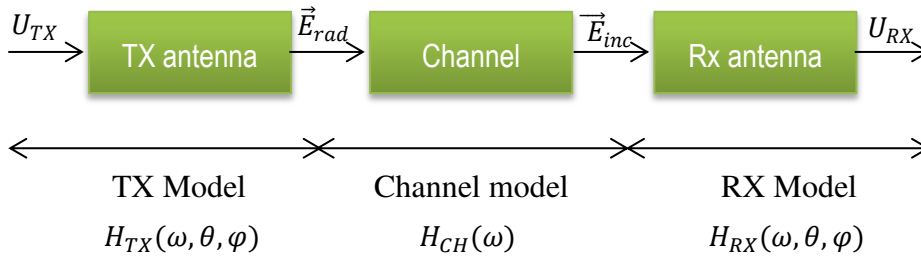
Fig. 3.2: UWB radio link model [4]

For a free space channel, the transient transmission can be written in the frequency domain and the time domain, respectively, as

$$\frac{U_{RX}(\omega,\theta,\varphi)}{U_{TX}(\omega,\theta,\varphi)} = S_{21} = \vec{H}_{TX}(\omega,\theta,\varphi)H_{CH}(\omega)\vec{H}_{RX}(\omega,\theta,\varphi)........(3.1)$$

$$u_{RX}(t) = \vec{h}_{TX}(t,\theta,\varphi) * h_{CH} * \vec{h}_{RX}(t,\theta,\varphi) * u_{TX}(t) ....(3.2)$$

where the free space channel transfer function is given by

$$H_{CH}(\omega) = \frac{c}{2r\omega} \, exp\left(-j\omega\frac{r}{c}\right) ....(3.3)$$

$\vec{H}_{TX}(\omega,\theta,\varphi)$ is the transfer function that relates the transmit signal U_{TX} (ω) to the radiated field strength $\vec{E}_{rad}(\omega,r,\theta,\varphi)$ at a certain distance r from an antenna in the transmit mode as in (3.4) whereas $\vec{H}_{RX}$ *(ω, θ, φ)* is the transfer function that relates the received signal amplitude $U_{RX}(\omega,)$ to the incident field strength $\vec{E}_{inc}$ *(ω, θ, φ)* for an antenna in the receive mode (3.5) [2].

$$\frac{\vec{E}_{rad}(\omega,r,\theta,\varphi)}{\sqrt{Z_o}} = \frac{e^{-j\omega r/c}}{r} \ \vec{H}_{TX}(\omega,\theta,\varphi) \ \frac{U_{TX}(\omega)}{\sqrt{Z_c}} \dots\dots\dots\dots\dots(3.4)$$

$$\frac{\vec{U}_{RX}(\omega,r,\theta,\varphi)}{\sqrt{Z_c}} = \vec{H}_{RX}(\omega,\theta,\varphi) \ \frac{\vec{E}_{inc}(\omega,\theta,\varphi)}{\sqrt{Z_o}} \dots\dots\dots\dots\dots(3.5)$$

Z_c and Z_o are the characteristic impedance of the antenna port and free space respectively.

For the transient response description, it is assumed that the transmit antenna is excited with an impulse. In this case, the antenna's transient response $h(t,\theta,\varphi)$ becomes more adequate for the description of impulse systems. The impulse responses of the antenna in transmission and reception are calculated by taking the inverse Fourier transform of (3.4) and (3.5) respectively.

$$\frac{\vec{e}_{rad}(t,r,\theta,\varphi)}{\sqrt{Z_o}} = \frac{1}{r} \ \delta\left(t - \frac{r}{c}\right) * \ \vec{h}_{TX}(t,\theta,\varphi) * \frac{u_{TX}(t)}{\sqrt{Z_c}} \dots\dots\dots(3.6)$$

$$\frac{\vec{u}_{Rx}(t,r,\theta,\varphi)}{\sqrt{Z_c}} = \vec{h}_{RX}(t,\theta,\varphi) * \frac{\vec{e}_{inc}(t,\theta,\varphi)}{\sqrt{Z_o}} \dots\dots\dots\dots\dots(3.7)$$

Here, the mathematical operation multiplication in the frequency domain is substituted by convolution in the time domain. The convolution with the Dirac function $\delta\left(t - \frac{r}{c}\right)$ represents the time retardation due to the finite transit time r/c. As the antenna characteristics also depend on the signal propagation direction (i.e., are spatial dependent), the transfer functions and the transient responses modelling the UWB antennas are spatial vectors [2]. As a consequence, the antennas do not radiate the same pulse in all the directions.

The application of the reciprocity theorem [5] yields the relation between the receiving and transmitting mode transfer functions in the frequency and in the time domain are as in (3.8) and (3.9).

$$H_{TX}(\omega, \theta, \varphi) = \frac{j\omega}{2\pi c} H_{RX}(\omega, \theta, \varphi) = \frac{j}{\lambda} H_{RX}(\omega, \theta, \varphi) \,\ldots\ldots\ldots(3.8)$$

$$h_{TX}(t, \theta, \varphi) = \frac{1}{2\pi c} \frac{\partial}{\partial t} h_{RX}(t, \theta, \varphi) \,\ldots\ldots\ldots\ldots\ldots\ldots\ldots\ldots(3.9)$$

From (3.9) it is observed that the transmit impulse response $h_{TX}(t, \theta, \varphi)$ is directly proportional to the time derivative of the receive impulse response $h_{RX}(t, \theta, \varphi)$. Substituting (3.9), the transient radiation in time domain (3.6) can be rewritten as (3.10), after exchanging the derivative ($\frac{\partial}{\partial t}$) and the convolution($*$).

$$\frac{\vec{e}_{rad}(t, r, \theta, \varphi)}{\sqrt{Z_o}} = \frac{1}{2\pi rc} \delta\left(t - \frac{r}{c}\right) * \vec{h}_{RX}(t, \theta, \varphi) * \frac{\partial}{\partial t} \frac{u_{TX}(t)}{\sqrt{Z_c}} \ldots(3.10)$$

The expression (3.10) is similar to the known formulation for the radiated fields of impulse radiating antennas (IRAs) [6] and it indicates that an ideal antenna with $h_{RX}(t, \theta, \varphi) = \pm\delta(t)$ will radiate an electric field pulse that is proportional to the time derivative of the input voltage pulse. i.e., ideal Dirac pulse would characterise the transmitting antenna as a mere differentiator in time [2].

3.2.2 Transient Analysis in CST

Fig. 3.3 shows the setup in CST for transient analysis. The radial distance and the separation between probes are selected according the far field criterion and resolution required respectively. The orientations

of the probes are parallel to the polarisation of the test antenna. The antenna is excited with a pulse $u_{TX}(t)$ whose frequency bandwidth covers the FCC specified UWB spectrum and its radiated field pulses $\vec{e}_{rad}(t, r, \theta, \varphi)$ are detected on the surface of a sphere with radius r satisfies the far field range criterion. Virtual probes inserted in the two principal planes as shown in Fig. 3.3 detect both the radiated pulses and the corresponding transfer functions. For antennas with nearly omni-directional radiation patterns, the transient parameters are usually investigated in azimuth plane (H-plane).
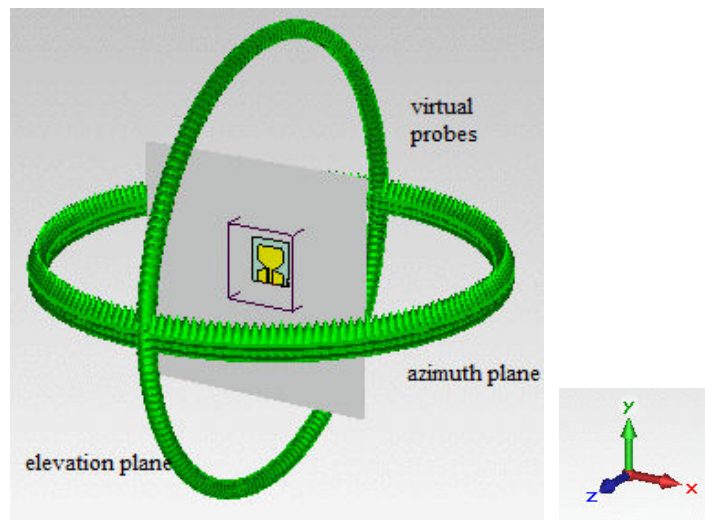
Fig. 3.3: Transient analysis setup in CST

Here, fourth order Rayleigh pulse (4th derivative of the Gaussian pulse) is chosen as the input pulse as discussed in Chapter 1, section 1.2.3 and its expression is given [7] by (3.11)

$$u_{TX}(t) = s_i(t) = \left[\frac{16}{\tau^8}(t-1)^4 - \frac{48}{\tau^6}(t-1)^2 + \frac{12}{\tau^2}\right] exp\left(-\left(\frac{t-1}{\tau}\right)^2\right) \dots (3.11)$$

where t represents time and τ is the pulse width.

To avoid possible interference between the UWB communication systems and co-existing narrow band wireless systems, the FCC has regulated emission mask which defines the maximum allowable radiated power for UWB systems. Fig. 3.4 shows the fourth order Rayleigh pulse and its corresponding power spectral density (dBm/MHz) which comply with the FCC indoor emission mask when $\tau = 67$ ps [7].

(a)

(b)
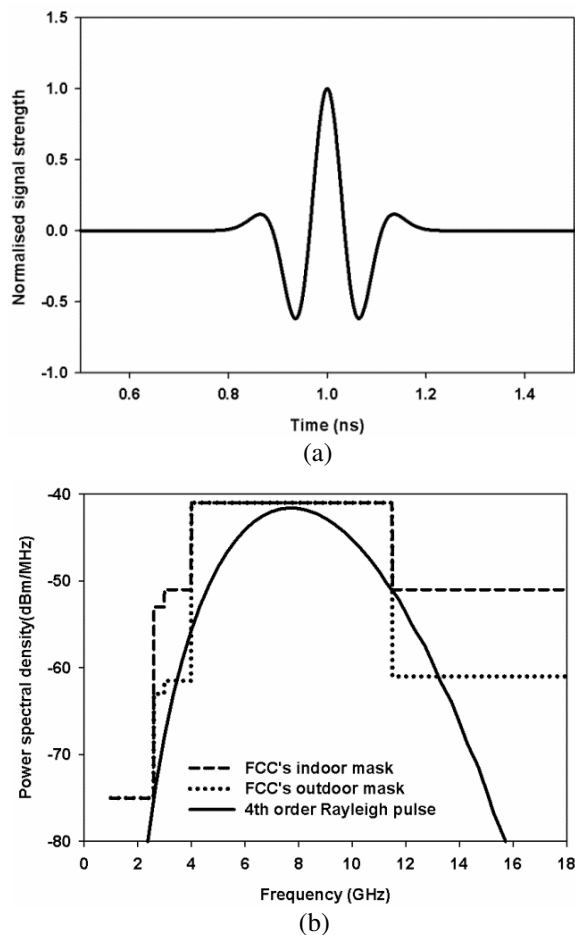
Fig. 3.4: (a) Fourth order Rayleigh pulse and (b) power spectral density normalised to FCC emission mask

3.3 Fabrication

The prototypes of the antennas are fabricated on microwave substrate using photolithography. This technique is employed where high accuracy in dimensions is required. First a negative mask of the antenna geometry is printed on a butter paper by Laser printer. Copper clad sheet of suitable size is cleaned using acetone to remove the oxide coating on its surface. Using a high speed spinner, thin layer of photo resist material is applied on the copper clad and dried. Then the copper clad is exposed to UV rays with the prepared negative mask just on the substrate. The layer of photo resist material in the exposed portion hardens while in the unexposed region remains unaffected and can be removed by dipping in developer solution. It is then rinsed in water. The unwanted copper is now etched using Ferric Chloride ($FeCl_3$) solution. Finally, the board is cleaned to remove the hardened negative photo resist.

3.4 Antenna Measurement Facilities

The antenna measurements are carried out using the antenna research facility which includes Vector Network Analysers (HP 8510C, R&S ZVB 20, Agilent PNA E8362B), automated antenna positioner and anechoic chamber.

The network analyser is a versatile instrument which can evaluate the characteristics of the antenna under test (AUT) with a high level of precision through the use of scattering parameters. S-parameters have long been the chosen method because they are relatively easy to derive at high frequencies and are directly related to the measurement parameters

of interest to microwave designers such as gain, return loss and reflection coefficient [8]. To measure the S-parameters accurately, the Network Analyser is first calibrated using the calibration standards over the desired frequency range. This is done in order to eliminate the losses associated with the cables and connectors used in the measurements.

Anechoic chambers are indoor free space antenna ranges designed to simulate measurements that would be performed in free space. That is, all reflected waves from nearby objects and the ground (which are undesirable) are suppressed as much as possible. The walls, ceilings and floor are covered with special electromagnetic wave absorbing material. The tapered shapes of the absorber provide good impedance match for the microwave power impinging upon it. Aluminium sheets are used to shield the chamber from surrounding electromagnetic interference [9].

An automated antenna positioner is employed for the radiation pattern measurement. It consists of a microcontroller based antenna positioner, interfaced with the PC. The PC synchronises the movement of the antenna and the network analyser measurements. The antenna under test (AUT) is mounted over the antenna positioner and a wideband standard horn antenna is used as the transmitter for the radiation pattern measurement.

3.5   UWB Antenna Characterisation and Measurements

3.5.1 Electrical Properties

In general, the electrical properties of antennas are described in frequency domain and are characterised by return loss, VSWR, efficiency,

radiation pattern, gain and polarisation properties [9]. Theory and measurement procedures are discussed in the following sections.

Reflection coefficient and VSWR:

Antenna is considered as an impedance matching device between the transmission line connected to source and free space. When there is an impedance mismatch between the antenna and the transmission line, a part of the incident power is reflected back to the source. The ratio of reflected voltage (or current) to the incident voltage (or current) is called as the voltage reflection coefficient (Γ). Reflection coefficient expressed in dB is termed as S_{11} or Return loss. Return loss (RL) is defined as the ratio of the reflected power to the incident power, its expression is

$$RL = -20\log(\Gamma) = -(S_{11}) \quad ....(3.12)$$

Voltage standing wave ratio (VSWR) is another term used to represent the amount of impedance mismatch and is the ratio of maximum voltage to minimum voltage of the standing wave formed on the transmission line. VSWR ≤ 2 is considered as the tolerable limits for a matched antenna which gives $S_{11} \leq -10\ dB$.

$$VSWR = \frac{v_{max}}{v_{min}} = \frac{1+|\Gamma|}{1-|\Gamma|} \quad ....(3.13)$$

Firstly, the input port of the network analyser is calibrated using standards such as short, open and matched loads in S_{11} trace mode over the desired frequency range. When AUT is connected to the input port, the display gives the S_{11} as a function of frequency. Using markers resonant frequencies, bandwidth etc. can be easily displayed. The

range of frequencies for which the S_{11} is within the -10dB points is usually treated as the band width of the antenna. Plots of VSWR, real and imaginary components of the input impedance etc. can also be obtained by selecting the respective parameters from the format menu.

Efficiency:

According to IEEE standard test procedure [IEEE std. 149™-1979], the radiation efficiency of an antenna is defined as the ratio of the total power radiated by the antenna to the net power accepted by the antenna at its input terminals during the radiation process. After considering the reflected power loss due to impedance mismatch, a more reasonable definition for antenna efficiency is given as the ratio of the total power radiated by the antenna to the net power applied/ input at the antenna terminals [10].

$$\eta_{UWB} = \frac{P_{rad}}{P_{applied}}$$ ....(3.14)

For evaluating UWB antenna efficiency, "UWB Wheeler Cap" method has been developed which uses a much larger spherical shell instead of a closed spherical shell of radius $r = \frac{\lambda}{2\pi}$ at the frequency of interest as for narrow band antennas. This allows the antenna to radiate freely, and then receive its own transmitted, reflected signal. Fig. 3.5 shows the experimental arrangement using large 'Wheeler cap'.
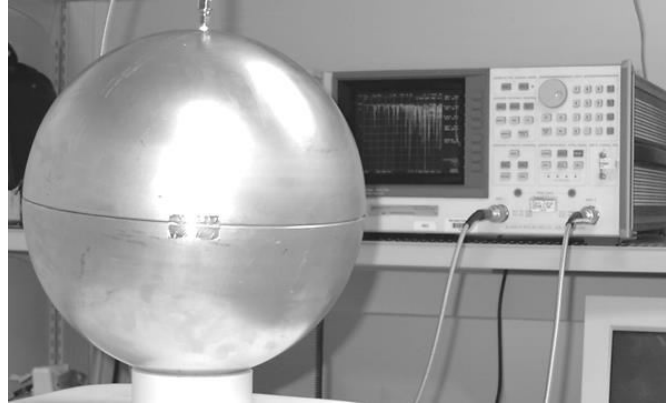
Fig. 3.5: Antenna efficiency measurement setup [10]

The power applied to the transmit antenna can be expressed as the sum of dissipation loss, mismatch loss and radiated power. All these can be expressed in terms of power fractions, i.e., fraction of the input power dissipated in losses $\left(l = \frac{P_{loss}}{P_{in}}\right)$, a fraction of reflected power due to mismatch $\left(m = \frac{P_{reflected}}{P_{in}}\right)$ and a fraction of power radiated $\left(n = \frac{P_{rad}}{P_{in}}\right)$ so that

$$l + m + n = 1 \quad \text{..(3.15)}$$

The scattering parameter of the antenna obtained under free space condition is the mismatch fraction $(m = |S_{11-FS}|^2)$ in free space. The receive and transmit efficiencies (η) are identical by reciprocity. The scattering coefficient inside the UWB Wheeler Cap becomes [10]:

$$|S_{11-WC}|^2 = m + \eta^2 + \eta^2 m^1 + \eta^2 m^2 + \eta^2 m^3 + \ldots \ldots \ldots$$

$$= |S_{11-FS}|^2 + \eta^2 \frac{1}{1-|S_{11-FS}|^2} \quad \text{..(3.16)}$$

which solves to yield the following result for the radiation efficiency:

$$\eta = \sqrt{(1 - |S_{11-FS}|^2)(|S_{11-WC}|^2 - |S_{11-FS}|^2)} \ldots\ldots\ldots\ldots(3.17)$$

For measurements, a nearly spherical metallic chamber with diameter 50 cm is used. First, S_{11-FS} of the AUT is measured in free space condition. Then the AUT is placed at the centre of the closed metallic chamber and S_{11-WC} is measured. The radiation efficiency is calculated using (3.17). The raw data thus obtained is smoothed by taking the peak value over small frequency intervals [10].

Radiation pattern:

The radiation pattern of an antenna is graphical representation of its radiation properties as a function of the space coordinates. In general, the radiation pattern of an antenna is three dimensional in nature. Because it is impractical to measure a three dimensional pattern, a number of two dimensional patterns are measured which are used to construct a three dimensional pattern. Usually the patterns are measured in two orthogonal principal planes, E-plane and H-plane (both co-polar and cross-polar). The far field radiation patterns are measured on the surface of a sphere with radius $r \geq \dfrac{2D^2}{\lambda}$ where D is the largest dimension of the antenna and λ is the smallest operating wavelength.

The patterns of antenna can be measured by using test antenna in the receiving mode. As shown in Fig. 3.6, the standard ridge horn covering 1 GHz to 18 GHz band is connected to port 1(transmitter) and

the AUT is connected to port 2 (receiving mode) of the network analyser and the frequency range for which $S_{11} <$ -10 dB is selected. To obtain two-dimensional patterns in the desired plane the AUT is mounted on an automated antenna positioner, and then the height and polarisation of both antennas are aligned for maximum reception ($|S_{21}|$) between them. A THRU calibration is performed along the bore sight direction over a selected frequency range. The radiation patterns of the antenna at multiple frequencies are measured over a single rotation of the antenna positioner in steps of fixed angle by using CREMA soft. The positioner stops at each step angle and records S_{21} data till it reaches the final stop angle. The entire measured data are stored in ASCII format and can be used for further processing like pattern analysis and plotting.
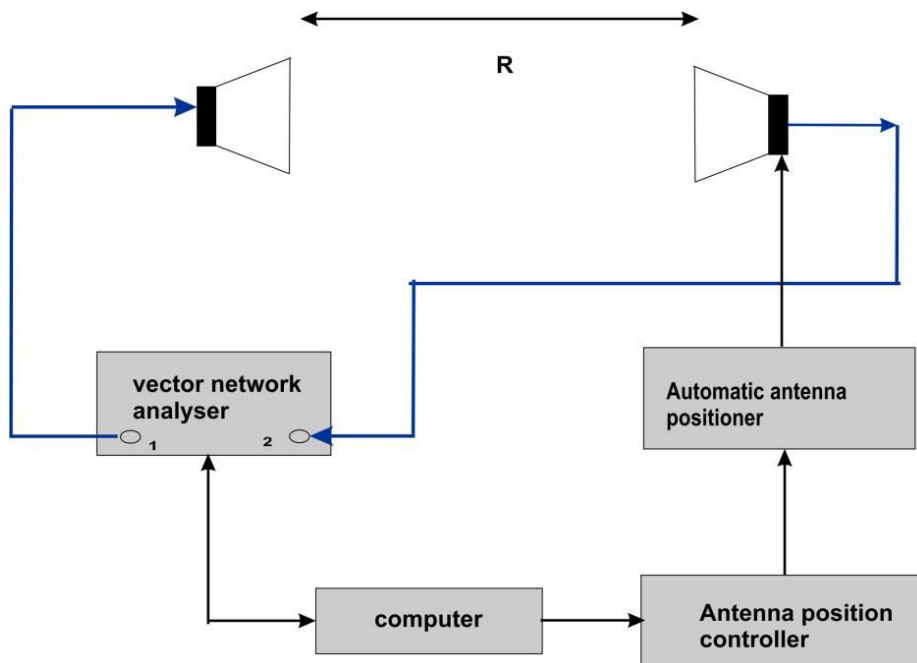
Fig. 3.6: Antenna pattern measurement setup

Gain:

Gain is the ratio of radiation intensity, in a given direction, to the radiation intensity that would be obtained if the power accepted by the antenna were radiated isotropically [9]. Gain transfer/ Gain comparison is the most commonly used method to measure the gain of an antenna. This method uses a standard gain antenna to determine the absolute gain. Initially relative gain measurements are performed, which when compared with the known gain of the standard antenna yield absolute values.

The measurement setup used for the radiation pattern can be used for the gain measurement also. Here, a wide band ridged horn antenna is used as the standard gain antenna. Initially an arbitrary antenna is connected to port 1 and a standard antenna is connected to port 2 of network analyser and aligned for maximum reception. THRU calibration is performed and is the reference for AUT gain. Now the standard antenna at the receiving end is replaced by the AUT and S_{21} is recorded which gives the relative gain. The absolute gain can be calculated as

$$G \ (dBi) = G_{ref}(dB) \ \pm \ |S_{21}|_{AUT(dB)} \dots\dots\dots\dots\dots\dots\dots\dots\dots(3.18)$$

3.5.2 Transfer Characterisation (Transient) Parameters

The transient parameters of a dispersive UWB antenna under test (AUT) can be derived directly from either the antenna time-domain impulse response $\vec{h}_{Rx}(t,\theta,\varphi))$ or frequency domain transfer function $\vec{H}_{Rx}(\omega,\theta,\varphi)$ as both of them contain the full information on the

antenna radiation [11]. Here, two important effects of the antenna are considered, the ability of the antenna to transmit and receive power effectively and then the distorting effects of antenna on the waveform to be transmitted or received [2], [12]-[13].

3.5.2.1 Frequency Domain Parameters

Gain:

The gain in frequency domain can be calculated from the antenna transfer function

$$G(f, \theta, \varphi) = \frac{4\pi f^2}{c^2} |H(f, \theta, \varphi)|^2 \dots\dots\dots\dots\dots\dots\dots(3.19)$$

It is important that the transfer function is multiplied by f^2.

Group delay:

The group delay $\tau_g(\omega)$ of an antenna characterizes the frequency dependence of the time delay. It is defined in frequency domain

$$\tau_g(\omega) = -\frac{d\phi(\omega)}{d\omega} = -\frac{d\phi(f)}{2\pi df}) \dots\dots\dots\dots\dots\dots(3.20)$$

where $\phi(f)$ is the frequency-dependent phase of the received signal. For minimum distortion, the group delay should be constant within the frequency band of interest, i.e. the phase increases linearly with frequency.

3.5.2.2 Time Domain Parameters

The effects of antenna on pulse distortion are also to be investigated in time domain. For the sake of simplification, all the

formulations are given for the co-polarisation. The dispersion of the antenna can be analysed by considering the envelope of the pulse response shown in Fig. 3.7, which is calculated by the Hilbert transform H, commonly used in signal processing. The envelope $|h^+(t,\theta,\varphi)|$ of the analytic pulse response shows the distribution of energy versus time and hence is a measure of dispersion due to an antenna [2], [12]-[13].

Pulse responses of the antenna $h(t)$ and $h^+(t)$ are shown in Fig. 3.7 for a given polarisation and direction (θ,φ) of radiation with characteristic parameters like peak value, full-width at half-maximum (FWHM) and the ringing duration τ_r. The parameters are dependent on polarisation and spatial co-ordinates (θ,φ).
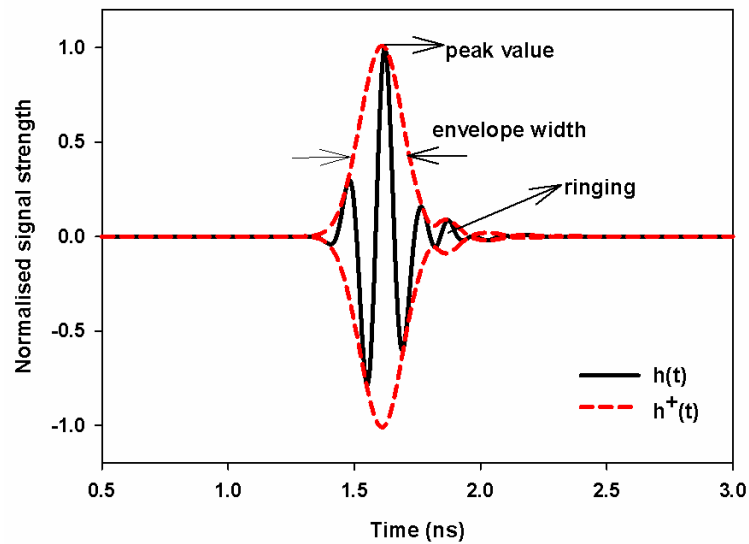
Fig. 3.7: Characterisation of antenna transient response

Peak value of the envelope:

The peak value $p(\theta, \varphi)$ of the analytic envelope $|h^+(t, \theta, \varphi)|$ is a measure for the maximal value of the strongest peak of the antenna's transient response. It is mathematically defined as

$$p(\theta, \varphi) = \max_t |h^+(t, \theta, \varphi)| \quad \dots\dots\dots\dots\dots\dots\dots\dots\dots\dots\dots (3.21)$$

Envelope width:

The envelope width describes the broadening of the received pulse and is defined as the full width of the analytic envelope $|h^+(t)|$ magnitude at full width half maximum (FWHM). Analytically, it is defined as

$$\tau_{FWHM} = t_{2|h^+(t2)|=p/2} - t_{1|h^+(t1)|=\frac{p}{2}, \ t_2 > t_1} \ ns \dots\dots\dots\dots (3.22)$$

Ringing duration:

The ringing τ_r of a UWB antenna is undesired and usually caused by resonances due to energy storage or multiple reflections within the antenna. It results in oscillations of the received pulse. The duration of the ringing τ_r, which is defined as the time required for the envelope to fall from the peak value $p(\theta, \varphi)$ to below a certain lower bound $\alpha. p(\theta, \varphi)$, and is measured as follows

$$\tau_r = t_{2|h^+(t2)|=\alpha p} - t_{1|h^+(t1)|=p, \ t_2 > t_1} \ ns \ \dots\dots\dots\dots\dots (3.23)$$

The lower bound for α is chosen according to the noise floor of the antenna measurement. In order to compare the ringing of antennas

having different gains under the restriction of constant noise floor, the fraction α is chosen to be 0.22 [2], [13].

3.5.2.3 Transient response Measurement

The antenna's transient response measurements can be performed either in time domain or in frequency domain. The results of both the measurements match perfectly well. Usually, the measurement in frequency domain is preferred because of standardised easy calibration methods and high dynamic range of network analysers [11]. In this thesis, the transient response of the antenna is derived from the measured S_{21}.
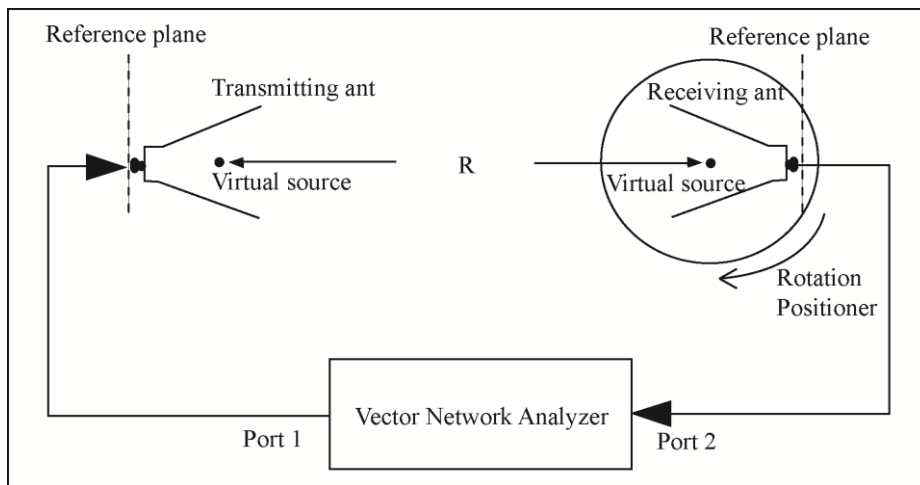
Fig. 3.8: Antenna transfer function S_{21} measurement setup [14]

The antenna measurement system includes two identical UWB antennas with one as transmitting and the other as receiving antenna, connected to port 1 and port 2 of the network analyser respectively as in shown in Fig. 3.8. The antennas are separated by a distance of 15 cm

so that they are in the far field. Before connecting the antennas, a THRU calibration is done in S_{21} trace mode in order to eliminate dispersive effects of the connecting cables. The transmission coefficient S_{21} between the transmitting and receiving antennas, which is given by (3.1), is measured for different orientations of the receiving antenna. With the same orientations of antennas the group delay is measured by selecting delay option from the format menu. Fig. 3.9 shows the orientations of the antennas for two extreme cases, face to face and face to side.

15 cm   15 cm

(a)   (b)
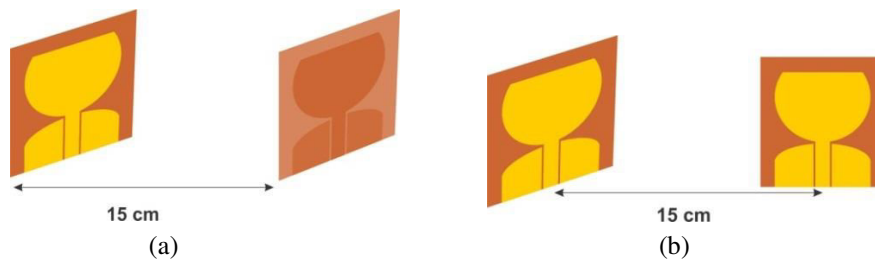
Fig. 3.9: Antenna orientations for S_{21} measurement (a) face to face and (b) face to side

From the measured scattering parameter S_{21} in the frequency domain, the transmitting and receiving antenna transfer functions can be deduced. Using two identical antennas, the following relation is obtained by substituting $H_{TX} = \frac{j}{\lambda} H_{RX}$ in (3.1), [4]. In order to obtain physical results, the phase of the transmission coefficient S_{21} has to be unwrapped correctly.

$$H_{RX}(\omega, \theta, \varphi) = \left(\frac{S_{21}(\omega,\theta,\varphi)}{H_{CH}(\omega)} \frac{\lambda}{j} \right)^{\frac{1}{2}} \text{...(3.24)}$$

Then, the impulse response $\vec{h}_n(t, \theta, \varphi)$ can be easily deduced from the transfer function by taking Inverse Fast Fourier Transform (IFFT).

Fidelity - pulse distortion analysis:

For UWB systems, receivers are based on correlation of the received pulse with a template waveform already stored in the receiver. The received pulse can be obtained by convolving input pulse $s_i(t)$ with the impulse response of the antenna $\vec{h}_n(t, \theta, \varphi)$.

$$s_o(t) = s_i(t) * h_n(t, \theta, \varphi) \dots\dots\dots\dots\dots\dots\dots(3.25)$$

A well-defined parameter named fidelity is then proposed to evaluate the pulse handling capability of an antenna [14].

$$F(\theta, \varphi) = \max_\tau \left[\frac{\int_{-\infty}^{+\infty} s_i(t)s_o(t+\tau, \theta, \varphi)dt}{\sqrt{\int_{-\infty}^{+\infty} s_i^2(t)dt \int_{-\infty}^{+\infty} s_o^2(t, \theta, \varphi)dt}} \right] \dots\dots\dots\dots(3.26)$$

where τ is the delay which is varied to maximize the numerator. The fidelity is the maximum of the correlation coefficient of the template and received pulses. It compares only shapes of the waveforms, not amplitudes. The fidelity reaches unity as the two pulses are exactly the same in shape, which means the antenna does not distort the incident pulse at all. This measurement is performed for different spatial orientations of the test antenna.

3.6 Conclusion

Methodology adopted to simulate, analyse, fabricate and measure characteristics of antennas in the following chapters are discussed. Antenna structure simulation, optimisation and transient analysis using CST are described. Detailed studies on transient transmission model with supporting mathematical analysis are carried out. Theory and measurement techniques of various parameters including electrical properties such as reflection coefficient, efficiency, radiation pattern and gain as well as transient characteristics such as peak value, FWHM, ringing and group delay are explained to evaluate the performance of the UWB antennas.

References

[1]   Antenna design and simulation – CST, https://www.cst.com/Applications/

[2]   W. Sorgel and W. Wiesbeck, "Influence of the Antennas on the Ultra-Wideband Transmission", EURASIP Journal on Applied Signal Processing, pp. 296–305, 2005.

[3]   A. H. Mohammadian, A. Rajkotia, and S. S. Soliman, "Characterization of UWB transmit-receive antenna system," IEEE Conf. Ultra Wideband Systems and Technology, pp. 157–161, 2003.

[4]   Y. Duroc, T. P. Vuong, and S. Tedjini, "A Time/Frequency Model of Ultra wide band Antennas", IEEE Transactions on Antennas and Propagation, vol. 55, no. 8, pp. 2342—2351, 2007.

[5]   J. Kunisch and J. Pamp, "UWB radio channel modelling considerations," Proc. International Conference on Electromagnetics in Advanced Applications (ICEAA '03), pp. 277–284, 2003.

[6] C. E. Baum, E. G. Farr, and D. V. Giri, "Review of Impulse-Radiating Antennas", Sensor and Simulation Notes, Air Force Research Laboratory, USA, 1998.

[7] J. Liang, Thesis on "Antenna Study and Design for Ultra Wideband Communication Applications" 2006.

[8] M. Hiebel, Vector Network Analyser (VNA) Calibration: The Basics, ROHDE & SCHWARZ.

[9] C. A. Balanis, Antenna Theory: Analysis and Design, Wiley & Sons, 1996.

[10] H.G. Schantz, "Radiation efficiency of UWB antennas". Proceedings of the IEEE UWBST Conference, 2002.

[11] W. Sorgel, F. Pivit, and W. Wiesbeck, "Comparison of frequency domain and time domain measurement procedures for ultra-wide band antennas," Proc. 25th Annual Meeting and Symposium of the Antenna and Measurement Techniques Association (AMTA'03), pp. 72–76, 2003.

[12] W. Wiesbeck, G. Adamiuk and C. Sturm, "Basic Properties and Design Principles of UWB Antennas", Proceedings of the IEEE, vol. 97, no. 2, pp. 372- 386, 2009.

[13] W. Sorgel, S. Knorzer and W. Wiesbeck, "Measurement and Evaluation of Ultra Wideband Antennas for Communications", International ITG Conference on Antennas – INICA, pp. 377- 380, 2003

[14] T. G. Ma and S. K. Jeng, "Planar Miniature Tapered-Slot-Fed Annular Slot Antennas for Ultra wide-Band Radios', IEEE Transactions on Antennas and Propagation, vol. 53, no. 3, pp. 1194 - 1202, 2005.

.....ಬಾಇ.....

Chapter 4

DUAL BAND-NOTCHED TRUNCATED CIRCULAR DISC ANTENNA

A truncated circular disc monopole with improved radiation pattern for ultra wide band applications is proposed in this chapter. The structure is actually derived from a conventional CPW-fed circular disc by removing the upper portion of the disc and reducing the width of the ground. Planar circular monopole antenna is considered because it offers large bandwidth compared to any other regular structures. The antenna presented is having simple structure with compact size of 25 mm × 20 mm. To avoid the interferences with co-existing narrow band wireless services like WLAN and WiMAX, band-notched design is included. The effects of various geometric parameters on impedance bandwidth and resonant frequencies are discussed. Experimental studies on radiation properties and transient characteristics are performed in frequency domain.

4.1 Truncated Circular Disc Monopole Antenna

4.1.1 Evolution and Geometry of the antenna

A truncated circular disc monopole antenna covering UWB spectrum is presented. The proposed antenna is derived from a circular disc monopole [1] of size $1.315\lambda_{gc} \times 1.766\lambda_{gc}$ fabricated on a substrate with relative permittivity $\varepsilon_r = 3$ and height $h = 1.6\ mm$ as shown in Fig. 4.1 (a). λ_{gc} is the guide wavelength corresponding to the centre frequency of UWB bandwidth.

(a)   (b)

(c)
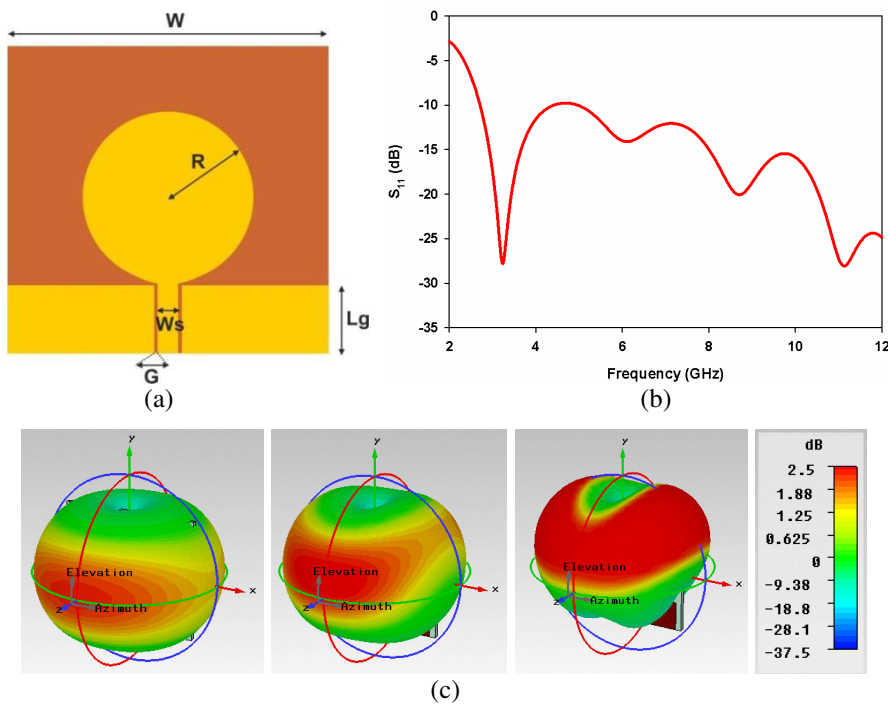
Fig. 4.1: (a) Structure of circular disc monopole [1], (b) S_{11} of the antenna and (c) radiation patterns at 3.1 GHz, 4.5 GHz and 5.5 GHz. (W = 1.766λ_{gc}, R = 0.469λ_{gc}, L$_g$ = 0.375λ_{gc}, W$_s$ = 4mm, G = 0.35 mm, ε_r = 3, h = 1.6 mm)

A 50 Ω CPW feed line, which has a signal strip of width W_s and a gap G between the strip and the coplanar ground plane, is used to excite the antenna. The antenna consists of a circular disc with radius R and a rectangular ground of size $L_g \times W$.

The work on ref [1] antenna is mainly concentrated on widening the impedance bandwidth by increasing the ground width W. The reflection coefficient characteristics S_{11} is shown in Fig. 4.1 (b) and exhibits a wide bandwidth extends from 2.7 GHz to more than 12 GHz. But from Fig. 4.1 (c), it is observed that at 5.5 GHz the radiation pattern of the ref [1] antenna starts to lose its omni-directionality, i.e., the direction of maximum radiation starts to deviate from the xz-plane. This is due to the presence of immediate second resonance which is a higher harmonic of the fundamental mode [1]. i.e., its pattern bandwidth doesn't cover the entire spectrum, limited to 4.5 GHz make it less efficient in UWB communication applications.

4.1.1.1 Evolution of the proposed antenna

In ref [1] antenna, the induced current on the ground plane concentrates mainly along its upper edge. It is observed that the radiation patterns of the ref [1] antenna can be improved to a certain extent without sacrificing the impedance match by decreasing the ground width and changing the relative permittivity to 4.4 (modifying the dimensions of the signal strip W_s and gap G). Thus a compact circular disc antenna (antenna 1) similar to the ref [1] antenna structure

with improved pattern bandwidth is derived using a substrate with relative permittivity $\varepsilon_r = 4.4$ and height $h = 1.6\ mm$. The radius of the circular disc is reduced compared to ref [1] antenna so that the impedance bandwidth of the antenna starts nearly from the lower edge of the UWB spectrum.

(a)

(b)

(c)
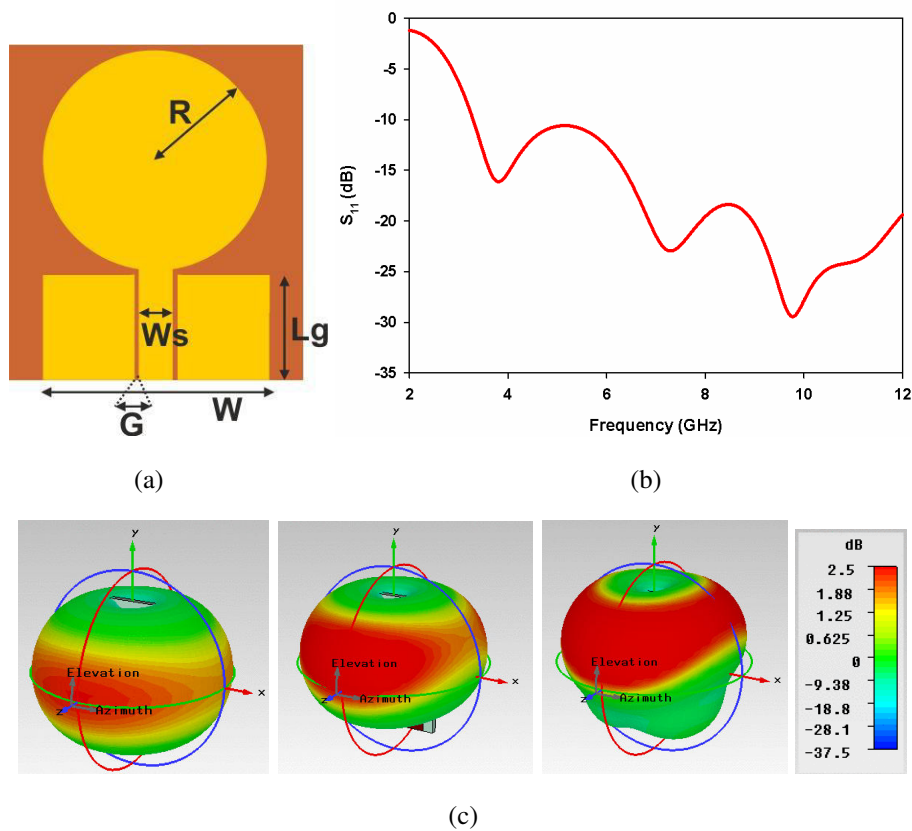
Fig. 4.2: (a) Structure of antenna 1, (b) S_{11} of antenna 1 and (c) radiation patterns at 3.3 GHz, 5.5 GHz and 7.0 GHz. (W = 0.751λ_{gc}, R = 0.368λ_{gc}, L$_g$ = 0.356λ_{gc}, W$_s$ = 3mm, G =0.4 mm, ε_r = 4.4, h = 1.6 mm)

The antenna 1 structure, reflection coefficient and radiation patterns of the compact circular disc antenna are shown in Fig. 4.2 (a) - (c). The antenna 1 operates from 3.29 GHz to more than 12 GHz with first and second resonances at 3.8 GHz and 7.3 GHz respectively as shown in Fig. 4.2 (b). The resonant frequencies are increased because the size of the circular disc is decreased. Compared to Fig. 4.1 (c), the pattern maximum of antenna 1 remains in the azimuth plane (xz-plane) even at 5.5 GHz as in Fig. 4.2 (c), because its second resonance is far away from that of the ref [1] antenna. It is also noted that pattern response obtained at 7.0 GHz is comparable to the response of ref [1] antenna at 5.5 GHz.

For circular disc monopole, the current is concentrated mainly on the lower edge of the disc for the fundamental mode [1]. So the size of the antenna can further be reduced by truncating the upper portion of the circular disc as in Fig. 4.3 (a) and is referred as antenna 2. The circular disc is truncated at a point L_t below the topmost point on its circumference. The overall size of the antenna 2 is reduced to $0.939\lambda_{gc} \times 0.751\lambda_{gc}$. Fig. 4.3 (b) shows the reflection coefficient characteristics of antenna 2 with first and second resonances at 4.2 GHz and 7.8 GHz respectively.

(a)   (b)

(c)
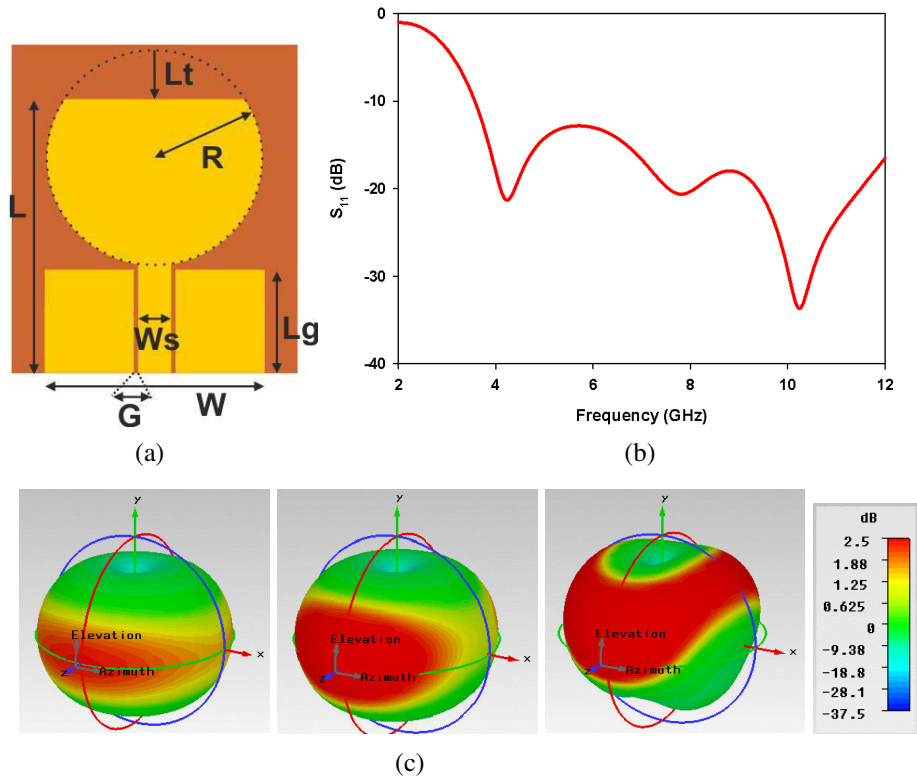
Fig. 4.3: (a) Structure of antenna 2, (b) S_{11} of antenna 2 and (c) radiation patterns at 4 GHz, 5.5 GHz and 8 GHz. (L = $0.939\lambda_{gc}$, W = $0.751\lambda_{gc}$, R = $0.368\lambda_{gc}$, L_t = $0.165\lambda_{gc}$, L_g = $0.356\lambda_{gc}$, W_s = 3mm, G =0.4 mm, ε_r = 4.4, h = 1.6 mm)

Fig. 4.3 (c) shows a slight improvement in the direction of pattern maximum (nearing xz-plane, $\theta = 0^o$) at 8 GHz compared to Fig. 4.2 (c). i.e., truncation of the circular disc improves the radiation pattern bandwidth with added advantage of size reduction. But the truncation increases the lower cut-off frequency of the antenna, thus reduces the impedance bandwidth slightly.

The current is mainly distributed along its upper edge of the ground plane, so the impedance characteristics can be tuned by optimizing the shape and dimensions of the ground plane [2]. It is known that smooth transition between the ground plane and the patch near the feed point enhances the impedance bandwidth of the antenna (eg. tapered feed bi-conical antenna & volcano smoke antenna) [3]-[4]. For enhancing the bandwidth, the ground plane is modified by adopting semi-elliptical shape for its upper edge and results in the proposed antenna structure.

4.1.1.2 Geometry of the antenna

The proposed antenna consists of a truncated circular disc and a rectangular ground plane with semi-elliptically shaped upper edge. A 50 Ω CPW feed line, which has a signal strip of width W_s, a gap G between the strip and the coplanar ground plane, is used to excite the antenna. R is the radius of the circular disc which is truncated at a point L_t below the topmost point on its circumference. The upper edge of the ground plane is made semi-elliptical in shape by placing an ellipse on a rectangular ground plane of size $L_g \times W$ so that the lower half of the ellipse is overlapped with the rectangular ground. Here, R_M and R_m are semi-major and semi-minor axes of the embedded ellipse respectively.
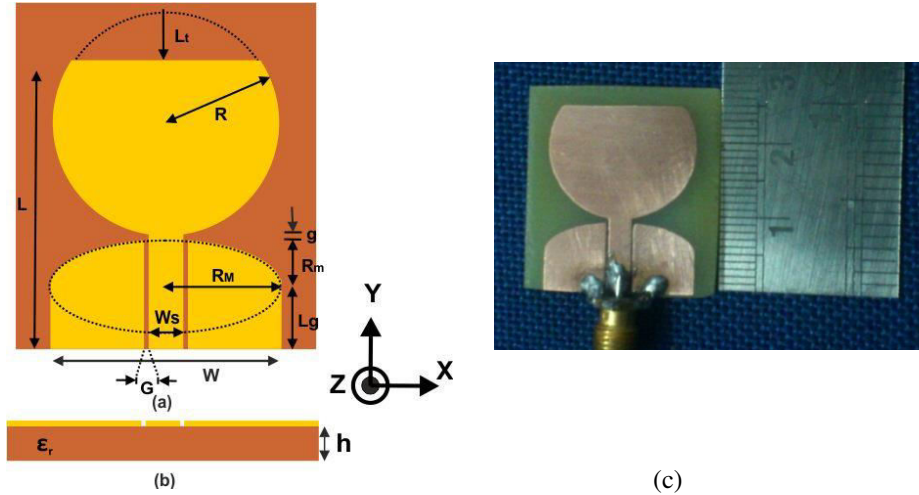
Fig. 4.4: Geometry of truncated circular disc UWB antenna (a) top view (b) side view and (c) photograph of the fabricated antenna (L = 0.939λ_{gc}, W = 0.751λ_{gc}, R = 0.368λ_{gc}, L$_t$ = 0.165λ_{gc}, L$_g$ = 0.206λ_{gc}, R$_M$ = 0.375λ_{gc}, R$_m$ = 0.15λ_{gc}, W$_s$ = 3 mm, G = 0.4 mm, g = 0.3 mm, h =1.6 mm, ε$_r$ = 4.4)

Fig. 4.4 shows the geometry and photograph of the proposed UWB antenna having a size of 25 mm × 20 mm, fabricated on a substrate of relative permittivity $\varepsilon_r = 4.4$, $tan\delta = 0.02$ and thickness $h = 1.6\ mm$.

4.1.2 Simulation, Parametric Analysis and Design
4.1.2.1 Simulation

Reflection coefficient:

Fig. 4.5 demonstrates the simulated reflection coefficient (S_{11}) of UWB antenna shown in Fig. 4.4. The antenna operates from 3.4 GHz to more than 12 GHz and resonates at 4.04 GHz, 7.93 GHz and

11.84 GHz. The overlapping of these resonant modes results in UWB characteristics.
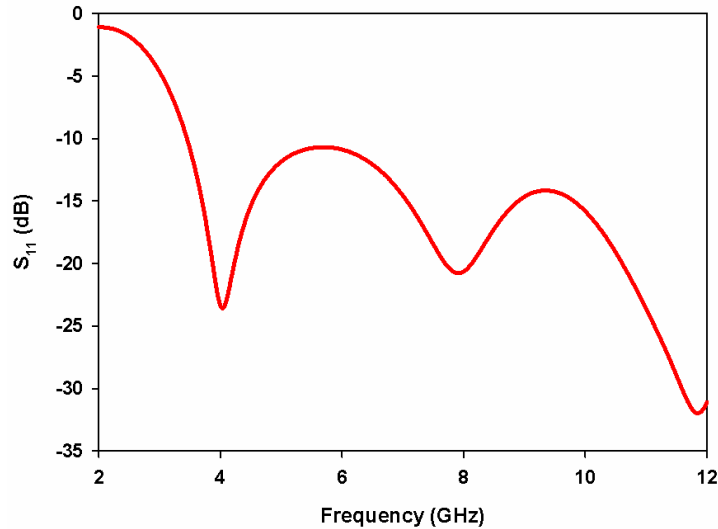
Fig. 4.5: Simulated S_{11} of truncated circular disc antenna (L = 0.939λ_{gc}, W = 0.751λ_{gc}, R = 0.368λ_{gc}, L$_t$ = 0.165λ_{gc}, L$_g$ = 0.206λ_{gc}, R$_M$ = 0.375λ_{gc}, R$_m$ = 0.15λ_{gc}, W$_s$ = 3 mm, G = 0.4 mm, g = 0.3 mm, h =1.6 mm, ε_r = 4.4)

Surface current distribution and radiation pattern:

By observing the surface current distribution at resonances, polarisation and radiation properties of the antenna can be studied. Surface current distribution and radiation pattern at three resonant frequencies are plotted in Fig. 4.6. From the Fig. 4.6 (a), it is clear that the first resonance (4.04 GHz) is due to the quarter wavelength current variation along the edge of the radiator. Here, the current on the radiator edges produces resultant electric field along Y-direction i.e., vertical polarisation. The radiation pattern observed at this frequency

satisfies the polarisation condition and is nearly omni-directional similar to that of a vertically polarised monopole antenna.

(a)

(b)

(c)
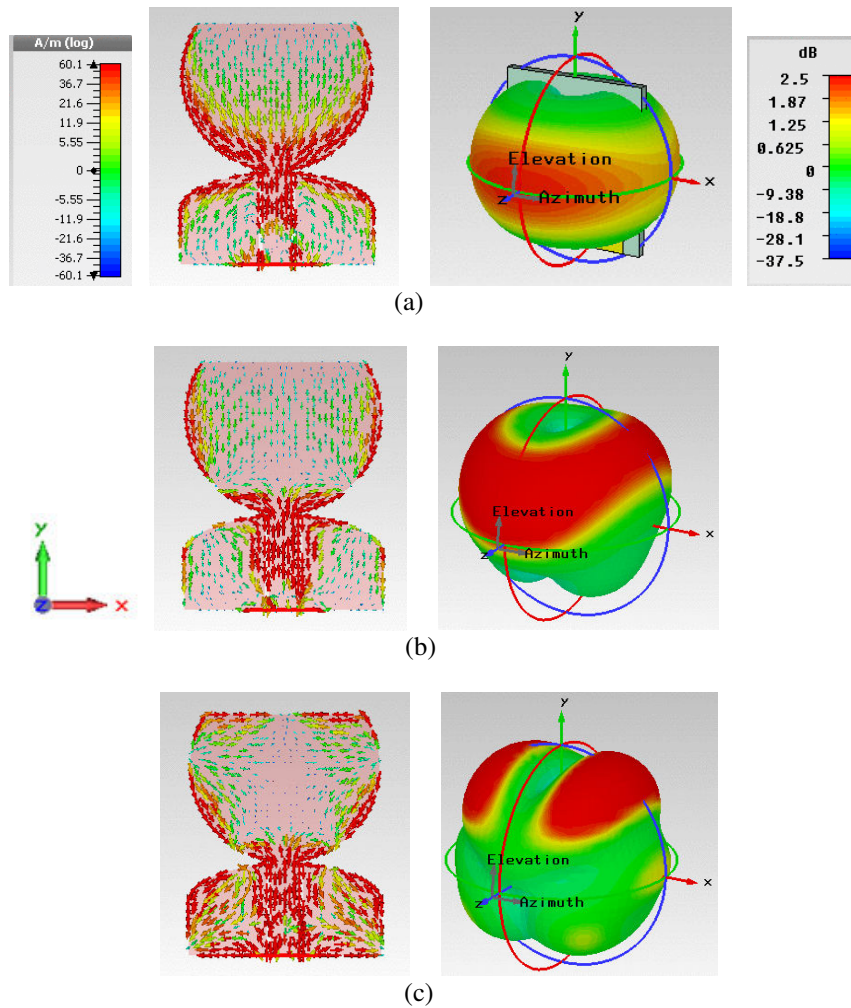
Fig. 4.6: Simulated surface current distribution and 3D radiation patterns at frequencies (a) 4.0 GHz (b) 7.93 GHz and (c) 10.5 GHz. (L = 0.939λ_{gc}, W = 0.751λ_{gc}, R = 0.368λ_{gc}, L$_t$ = 0.165λ_{gc}, L$_g$ = 0.206λ_{gc}, R$_M$ = 0.375λ_{gc}, R$_m$ = 0.15λ_{gc}, W$_s$ = 3 mm, G = 0.4 mm, g = 0.3 mm, h =1.6 mm, ε_r = 4.4)

As the frequency increases, the current remains along the radiator edge with nulls at which the currents are in opposite directions. The current pattern corresponding to the second resonance is shown in Fig. 4.6 (b). By observing the current pattern it is clear that this resonance corresponds to second harmonic of the fundamental mode. Fig. 4.6 (b) shows the radiation pattern at second harmonic (7.94 GHz) and maintains its omni-directionality to a certain extent with maximum radiation along $\phi = 0^0 \ and \ \theta = 40^0$. After 10 GHz, the antenna exhibits multiple lobe radiation patterns with maximum radiation in xy-plane as shown in Fig. 4.6 (c). It is observed that this antenna is capable of maintaining its omni-directionality over a large frequency range of 3.4 GHz to 7.9 GHz compared to the ref [1] antenna in Fig. 4.1(a). Since the current present on the edges of the truncated disc for all the modes, the resonant frequencies are related to the circumference of the structure, i.e., truncated circular disc supports multiple resonant modes which are the harmonics of the fundamental mode like in circular disc antenna.

4.1.2.2 Parametric analysis

In this work, the radiating patch is a truncated circular disc monopole antenna (TCDMA). With the truncation overall size of the structure is slightly less compared to the one which uses a complete circular disc. In section 4.1.1.1 it is seen that the truncation improves the radiation pattern of the antenna slightly.
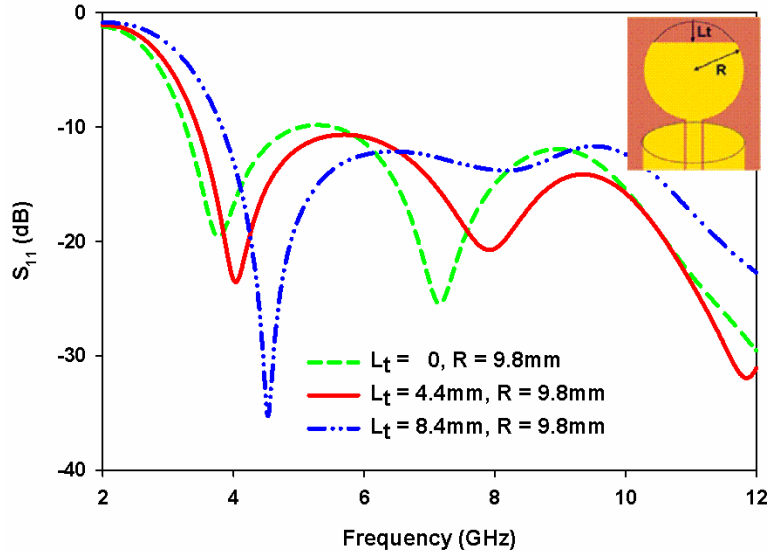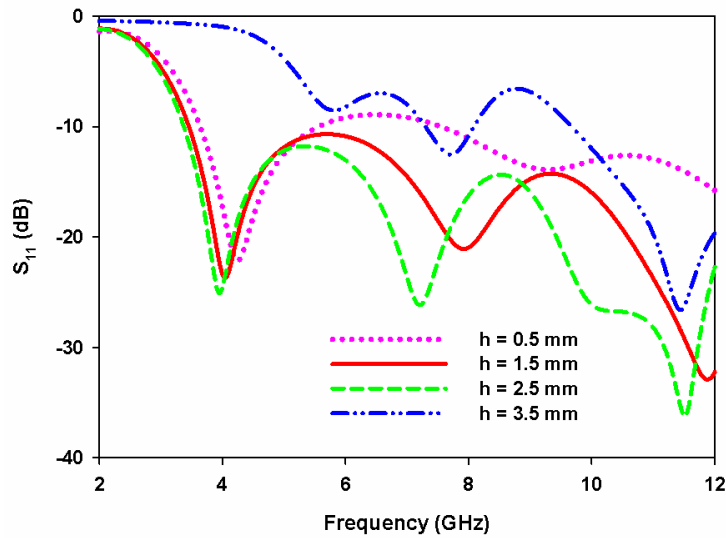
Fig. 4.7: Effect of truncation length L_t on S_{11} (L = $0.939\lambda_{gc}$, W = $0.751\lambda_{gc}$, R = $0.368\lambda_{gc}$, L_t = $0.165\lambda_{gc}$, L_g = $0.206\lambda_{gc}$, R_M = $0.375\lambda_{gc}$, R_m = $0.15\lambda_{gc}$, W_s = 3 mm, G = 0.4 mm, g = 0.3 mm, h =1.6 mm, ε_r = 4.4)

Fig. 4.7 illustrates the effect of truncation L_t on the reflection characteristics S_{11} of the antenna. From Fig. 4.7, it is observed that for $L_t = 4.4\ mm$, the S_{11} response obtained is comparable to that of circular disc. It is found that as the truncation length increases the first and second resonant frequencies increase even though the radius R is kept constant. This is because the circumference of the TCDMA decreases with increase in truncation length.

On the ground plane, the current is mainly distributed along the upper edge which indicates that the portion of the ground plane close to the disc acts as a part of the radiating structure [2], [5]. In this structure, the analysis is done by increasing the semi-minor axis R_m which is

accompanied with decrease in length L_g of rectangular portion of the ground plane by the same quantity as in Fig. 4.8 so that the feed gap g remains constant. i.e., sum of R_m and L_g remains constant (= 9.5 mm).
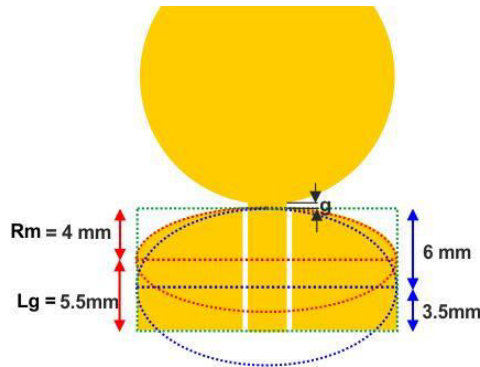
Fig. 4.8: Variations in semi-minor axis R_m and ground length L_g
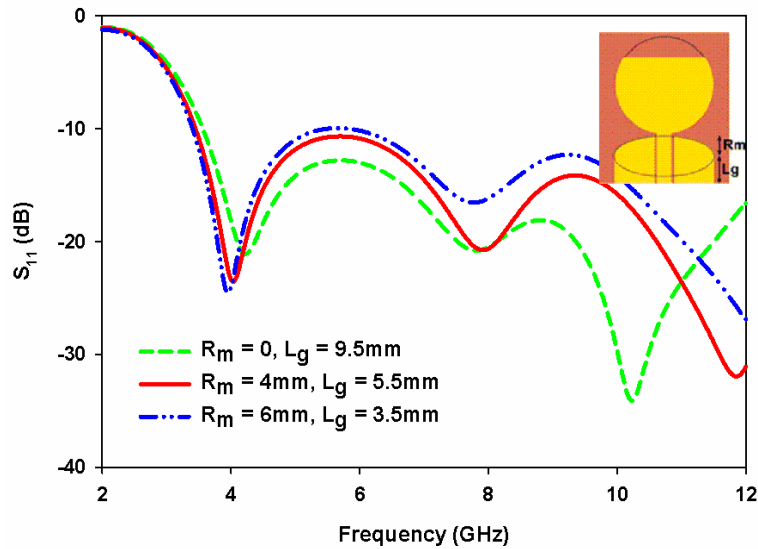
Fig. 4.9: Effect of semi-minor axis R_m on S_{11}. (L = 0.939λ_{gc}, W = 0.751λ_{gc}, R = 0.368λ_{gc}, L$_t$ = 0.165λ_{gc}, R$_M$ = 0.375λ_{gc}, R$_m$ = 0.15λ_{gc}, L$_g$ = 0.206λ_{gc}, W$_s$ = 3 mm, G = 0.4 mm, g = 0.3 mm, h = 1.6 mm, ε_r = 4.4)

In Fig. 4.9, the plot with $L_g = 9.5\ mm$ corresponds to a structure with rectangular ground plane whereas the plots with $L_g < 9.5\ mm$ correspond to a structure with semi-elliptical ground with different dimensions of semi-minor axis. It is found that as the shape of the upper edge of the ground plane changes from rectangular to elliptical, the lower resonance frequency decreases slightly and thus the lower cut-off frequency of the S_{11} bandwidth. This is because of gradual tapering between the radiating patch and the ground plane near the feed point tends to improve the impedance bandwidth.
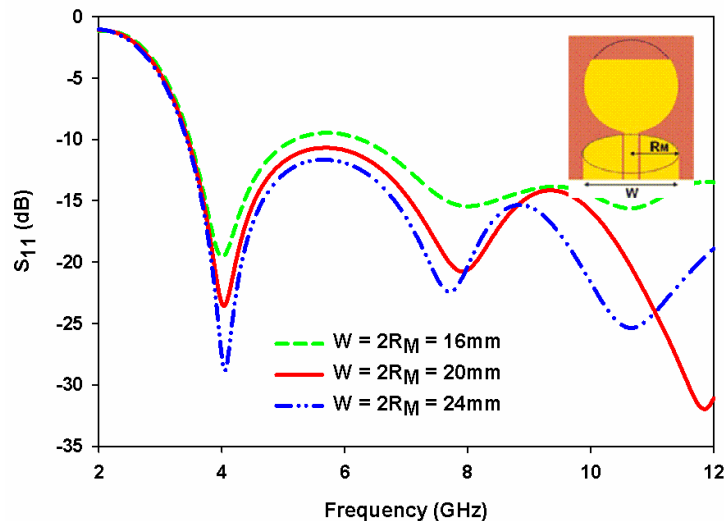
Fig. 4.10: Effect of ground plane width W on S_{11}. (L = $0.939\lambda_{gc}$, W = $0.751\lambda_{gc}$, R = $0.368\lambda_{gc}$, L$_t$ = $0.165\lambda_{gc}$, L$_g$ = $0.206\lambda_{gc}$, R$_M$ = $0.375\lambda_{gc}$, R$_m$ = $0.15\lambda_{gc}$, W$_s$ = 3 mm, G = 0.4 mm, g = 0.3 mm, h =1.6 mm, ε$_r$ =4.4)

In this structure, dimension of the semi-major axis R_M determines the width of the ground plane W, i.e., $W = 2R_M$. Fig. 4.10, shows the

variations in the S_{11} characteristics of the antenna when the width of the ground plane changes. It is observed that the S_{11} curve start to drop its matching at lower operating band when the width is reduced to $W = 16mm$.
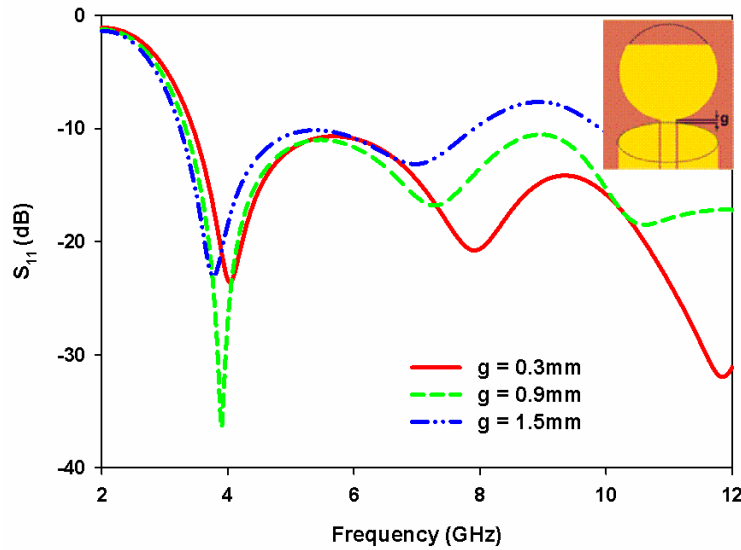
Fig. 4.11: Effect of feed gap g on S_{11}. (L = 0.939λ_{gc}, W = 0.751λ_{gc}, R = 0.368λ_{gc}, L$_t$ = 0.165λ_{gc}, L$_g$ = 0.206λ_{gc}, R$_M$ = 0.375λ_{gc}, R$_m$ = 0.15λ_{gc},W$_s$ = 3 mm, G = 0.4 mm, g = 0.3 mm, h =1.6 mm, ε$_r$ = 4.4)

Fig. 4.11 illustrates the S_{11} curves with variations in feed gap g. From Fig. 4.11, it is learnt that as the feed gap increases from 0.3 to 1.5 mm, the lower resonant frequency decreases, thus tends to increase the bandwidth. It indicates that the ground plane act as an impedance matching circuit and controls the operating bandwidth as the feed gap varies [6]. For feed gap variations from 0.3 to 0.9 mm, the antenna

continues to be impedance matched over the whole band. Further increment in g to 1.5 mm drops the impedance match of the S_{11} curve.

Fig. 4.12: Effect of substrate height h on S_{11} (L = 0.939λ_{gc}, W = 0.751λ_{gc}, R = 0.368λ_{gc}, L$_t$ = 0.165λ_{gc}, L$_g$ = 0.206λ_{gc}, R$_M$ = 0.375λ_{gc}, R$_m$ = 0.15λ_{gc}, W$_s$ = 3 mm, G = 0.4 mm, g = 0.3 mm, h = 1.6 mm, ε$_r$ = 4.4)

From Fig. 4.12 it is seen that as the substrate height h increases the resonant frequency decreases slightly, thus increases the operating bandwidth. For large variation in substrate height from 0.5 to 2.5 mm, the structure covers the entire UWB bandwidth. When $h \geq 3.5\ mm$, impedance match of the structure falls.

For a CPW structure the effective relative permittivity is the average of relative permittivity of air and the substrate ($\varepsilon_{re} = \frac{\varepsilon_r + 1}{2}$). From Fig. 4.13 it is observed that as the relative permittivity increases

both the first and second the resonant frequencies decrease, satisfying the relation $f_r \propto \frac{1}{\sqrt{\varepsilon_{re}}}$. An improvement in bandwidth is observed on increasing the relative permittivity of the substrate. It is also seen that for a wide variation in ε_r from 2 to 8 the antenna covers the entire UWB spectrum.
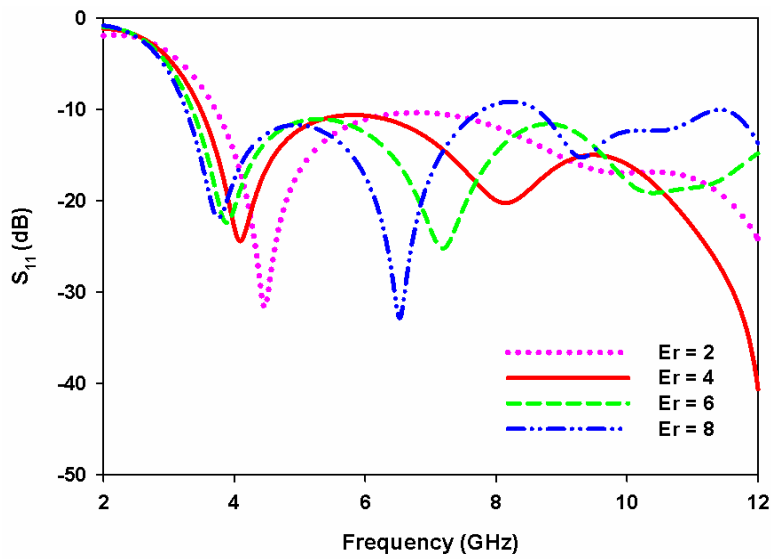
Fig. 4.13: Effect of substrate permittivity ε_r on S_{11} (L = 0.939λ_{gc}, W = 0.751λ_{gc}, R = 0.368λ_{gc}, L$_t$ = 0.165λ_{gc}, L$_g$ = 0.206λ_{gc}, R$_M$ = 0.375λ_{gc}, R$_m$ = 0.15λ_{gc}, W$_s$ = 3 mm, G = 0.4 mm, g = 0.3 mm, h =1.6 mm, ε_r = 4.4)

4.1.2.3 Design

Design procedures for the truncated circular disc UWB antenna on any substrates are outlined. For deriving the design equations, the centre frequency f_c of the UWB operating bandwidth is considered.

- Design a 50-Ω CPW line on a substrate with permittivity ε_r and thickness h.

- Calculate the effective relative permittivity for CPW line using $\varepsilon_{re} = \frac{\varepsilon_r + 1}{2}$.

- Calculate the guide wavelength λ_{gc} corresponding to the centre frequency f_c

$$\lambda_{gc} = \frac{c}{f_c \sqrt{\varepsilon_{re}}}$$ ....(4.1)

- Calculate the radius R and truncation L_t using

$$R = 0.368\,\lambda_{gc}$$ ....(4.1)

$$L_t = 0.165\,\lambda_{gc}$$ ....(4.2)

- Calculate semi-major R_M and semi-minor R_m axes of elliptical curve placed at the upper portion of ground plane and length L_g of the ground plane using

$$R_M = 0.3751\lambda_{gc}$$ ....(4.3)

$$R_m = 0.15\,\lambda_{gc}$$ ....(4.4)

$$L_g = 0.206\,\lambda_{gc}$$ ....(4.5)

The geometrical parameters are calculated for different substrates in Table 4.1 to validate the design equations and the S_{11} characteristics obtained with computed values are shown in Fig. 4.14.

Table 4.1: Description of substrates

Parameters	Rogers 5880	FR4 Epoxy	Rogers RO3006	Rogers 6010LM
h (mm)	1.57	1.6	1.28	0.635
ε_r	2.2	4.4	6.15	10.2
ε_{eff}	1.6	2.7	3.575	5.6
W_s(mm)	4	3	2.58	2.05
G(mm)	0.17	0.35	0.45	0.5
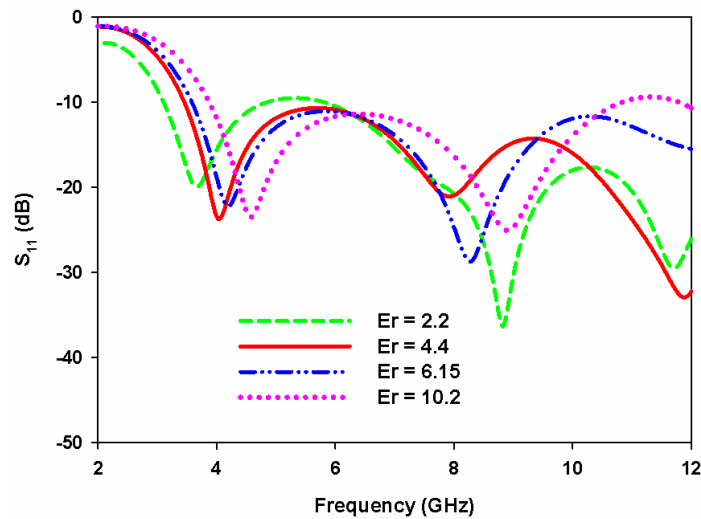
Fig. 4.14: Simulated S_{11} of truncated circular disc using different substrates

Fig. 4.14 shows that a wide impedance bandwidth with slight variations in the resonant frequencies is obtained for all substrates and hence satisfies the design equations.

Radiation patterns at resonant frequencies of the antenna on different substrates are shown in Fig. 4.15 (a) – (c). At first resonant frequency all the three antennas exhibit omni-directional patterns with

maximum radiation along xz-plane ($\theta = 0^o$). Radiation patterns at the second resonance are almost similar for all the three antennas with the direction of maximum radiation slightly tilted from the xz-plane. From the Fig. 4.15 it is learnt that the antenna is characterised by wide pattern bandwidth which make it suitable for UWB communication applications.
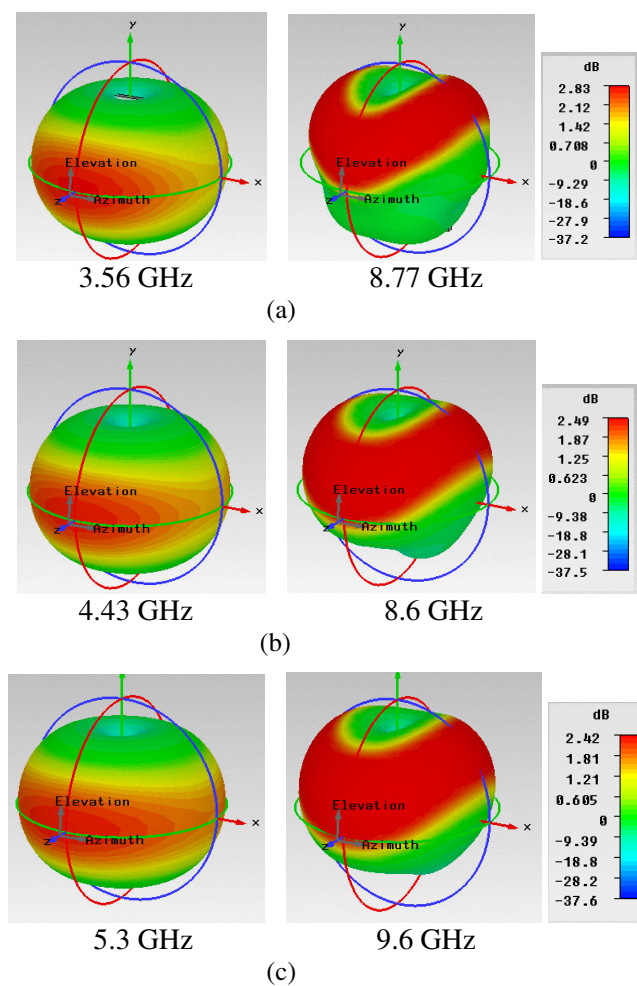
Fig. 4.15: Radiation patterns at resonant frequencies of the antenna on different substrates with relative permittivity (a) 2.2 (b) 6.15 and (c) 10.2

4.2 Dual Band-notched Truncated Circular Disc Monopole Antenna

To realise the dual band-notched characteristics, two resonant slots are etched on the radiating patch as shown in Fig. 4.16. A folded U-slot (slot 1) near the truncated edge of the disc and a U-slot (slot 2) near the feed point which produce a rejection band at WiMAX (3.30 –3.6 GHz) and at WLAN (5.5 – 5.9 GHz) respectively.
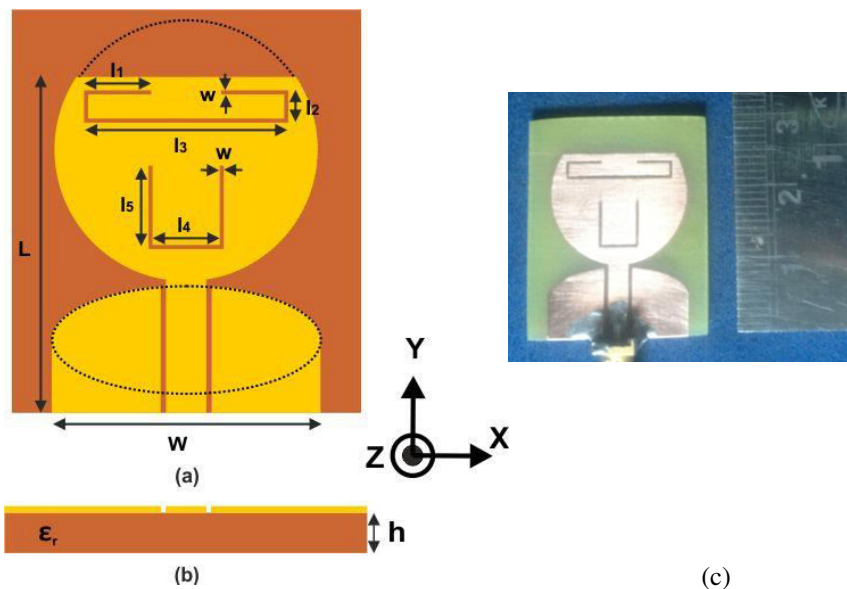
Fig. 4.16: **Geometry of dual band-notched UWB antenna (a) top view (b) side view and (c) photograph of the fabricated antenna. (L = 0.939λ_{gc}, W = 0.751λ_{gc}. Folded U-slot: l$_1$ = 0.098λ_{n1}, l$_2$ = 0.045λ_{n1}, l$_3$ = 0.278λ_{n1}, w = 0.4 mm. U-slot: l$_4$ = 0.177λ_{n2}, l$_5$ = 0.195λ_{n2}, w = 0.4 mm; where λ_{n1} and λ_{n2} are the guide wavelength corresponding to the notch frequencies)**

4.2.1 Simulation and Parametric Analysis

4.2.1.1 Simulation

Reflection coefficient:

The reflection coefficient characteristic S_{11} of the dual band notched antenna is shown in Fig. 4.17. The antenna covers frequencies from 3.1 GHz to 12 GHz with resonant frequencies at 4.1 GHz, 7.93 GHz and 11.8 GHz. From the Fig. 4.17, it is seen that the slots incorporated within the radiating patch of the antenna notch out the WiMAX and WLAN bands effectively without distorting the S_{11} characteristics of the truncated circular disc antenna.
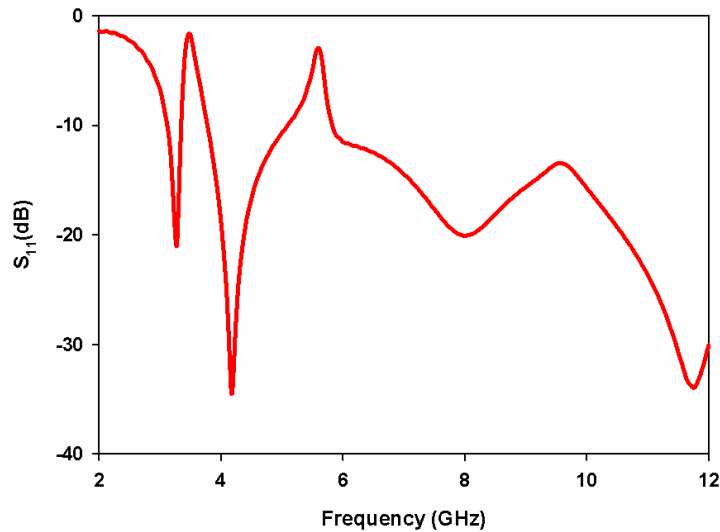
Fig. 4.17: **Simulated S_{11} of dual band-notched truncated circular disc antenna. (Folded U-slot: $l_1 = 0.098\lambda_{n1}$, $l_2 = 0.045\lambda_{n1}$, $l_3 = 0.278\lambda_{n1}$, w = 0.4 mm. U-slot: $l_4 = 0.177\lambda_{n2}$, $l_5 = 0.195\lambda_{n2}$, w = 0.4 mm)**

Radiation pattern, Surface current distribution and Design:

The 3D radiation pattern of dual band-notched antenna at 4.04 GHz, 7.95 GHz and 10.5 GHz shown in Fig. 4.18 (a) - (c) are similar to the corresponding plots of the antenna without notch structures. From Fig. 4.18 (d) & (e) which corresponds to 3.45 GHz (f_{n1}) and 5.65 GHz (f_{n2}) respectively, it is observed that the radiations in all the directions are much reduced compared to that at the resonant frequencies. This indicates that the antenna rejects these frequencies efficiently. For analysing the frequency rejection mechanism involved, surface current distribution at the centre frequencies of the notched bands, 3.45 GHz and 5.65 GHz, are presented in Fig. 4.19 (a) & (b). It is observed that at the centre frequency of the rejection bands, the current distribution is more in the respective slots than any other portion of the antenna. At the WiMAX band, the surface current distributes mainly around the edge of the slot 1 as shown in Fig. 4.19 (a) and at the second notch band of WLAN, current concentrates around the edges of the slot 2 as in Fig. 4.19 (b). This indicates that the slot 1 and slot 2 controls the notch properties at 3.45 GHz and 5.65 GHz respectively.
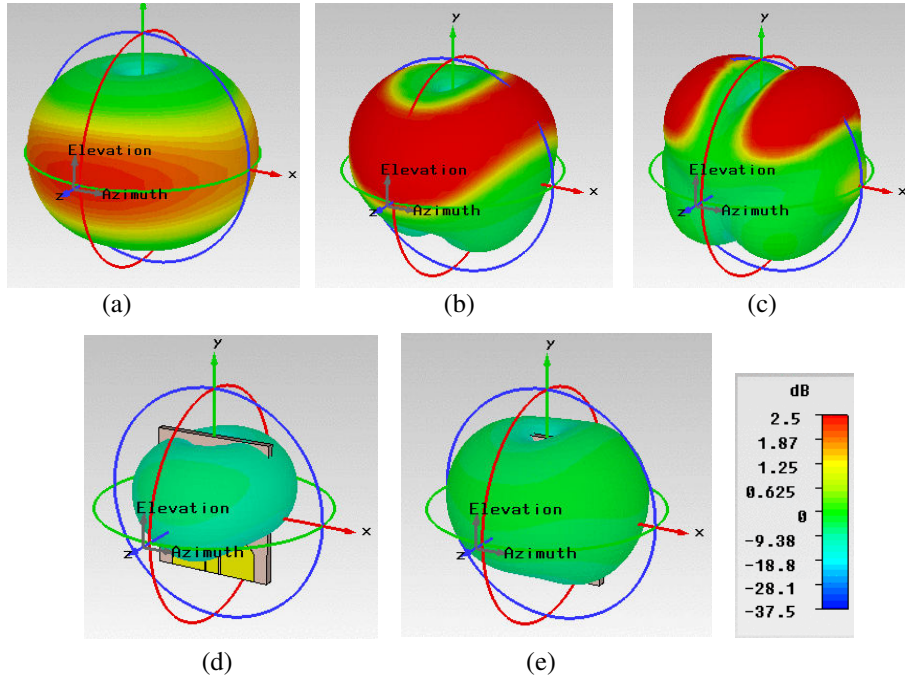
Fig. 4.18: Simulated 3D radiation patterns at frequencies (a) 4.0 GHz (b) 7.93 GHz (c) 10.5 GHz (d) 3.45 GHz and (e) 5.65 GHz
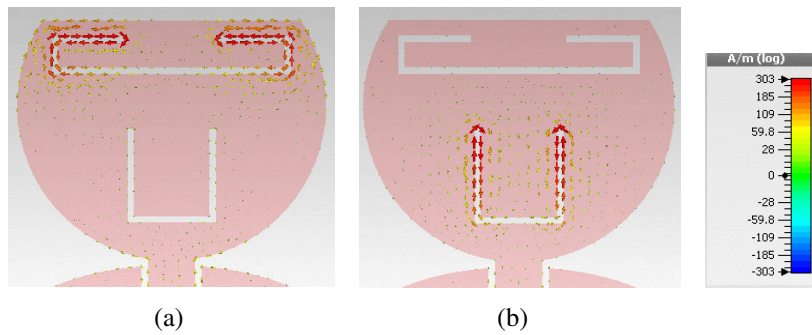
Fig. 4.19: Simulated current distribution at notch frequencies (a) 3.45 GHz and (b) 5.65 GHz

Since the current distribution in these slot structures are symmetrical and in opposite directions, the radiation fields so generated cancel each other [7] − [8]. Performance of the notch structures are further confirmed from the radiation patterns at these frequencies in Fig. 4.18 (d) and (e) which show a considerable reduction in the radiation in all the directions. At notch frequency the current distribution on the slot structure presents a half wavelength variation, reveals that it acts as a half wavelength resonator. So to reject a particular frequency the total length of the slot is to be approximately half the guide wavelength at that frequency. The guide wavelength is defined as

$$\lambda_{nk} = \frac{c}{f_{nk}\sqrt{\varepsilon_{re}}} \dots\dots\dots\dots\dots\dots\dots\dots\dots\dots\dots\dots\dots\dots\dots\dots\dots\dots(4.6)$$

$$l_{slot1} = 2l_1 + 2l_2 + l_3 = \frac{\lambda_{n1}}{2}\dots\dots\dots\dots\dots\dots\dots\dots\dots\dots\dots\dots\dots(4.7)$$

$$l_{slot2} = l_4 + 2l_5 = \frac{\lambda_{n2}}{2} \dots\dots\dots\dots\dots\dots\dots\dots\dots\dots\dots\dots\dots\dots(4.8)$$

where c is the velocity of light, f_{nk} is the kth notch frequency and ε_{re} is the effective relative permittivity.

4.2.1.2 Parametric Analysis:

Fig. 4.20 (a) - (e) illustrates the effects of various parameters of the slot structures on the notch characteristics with all the other dimensions of the truncated disc same as in Fig. 4.4.

(a)

(b)
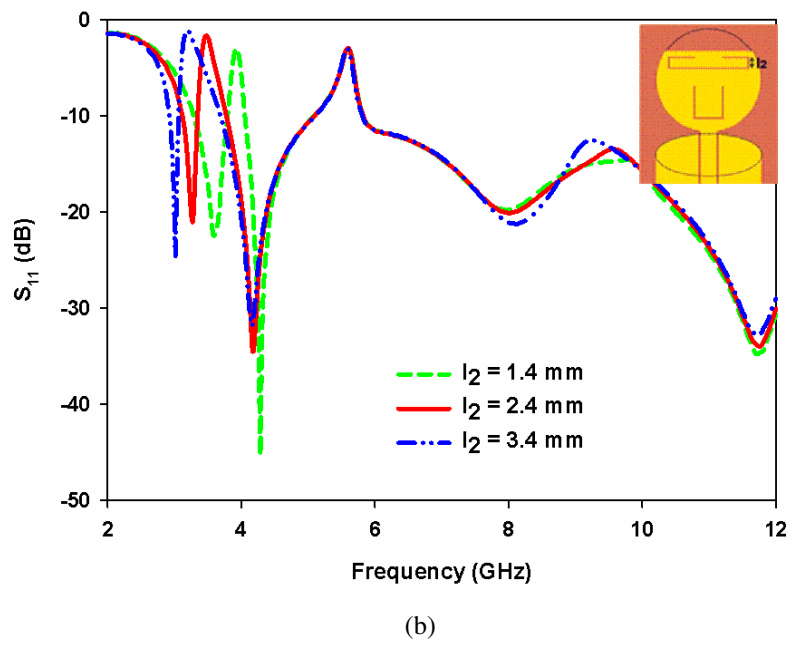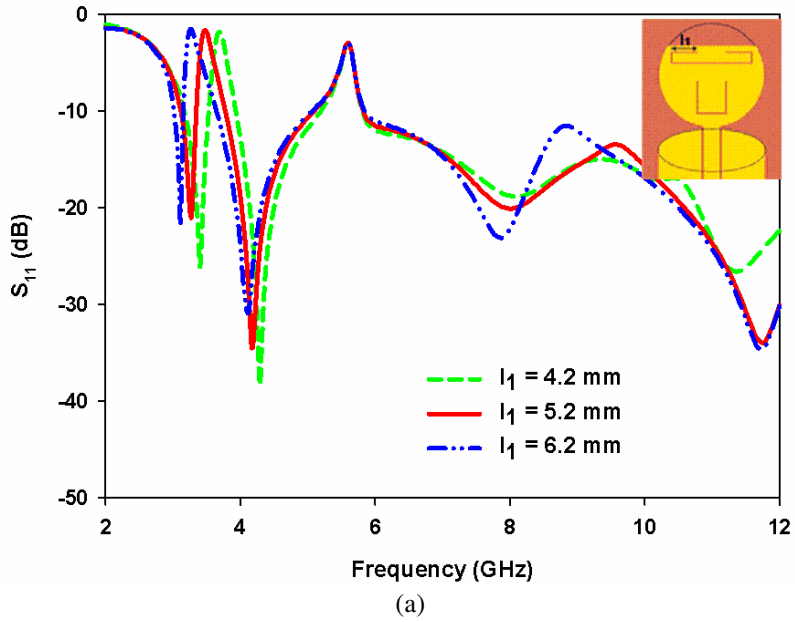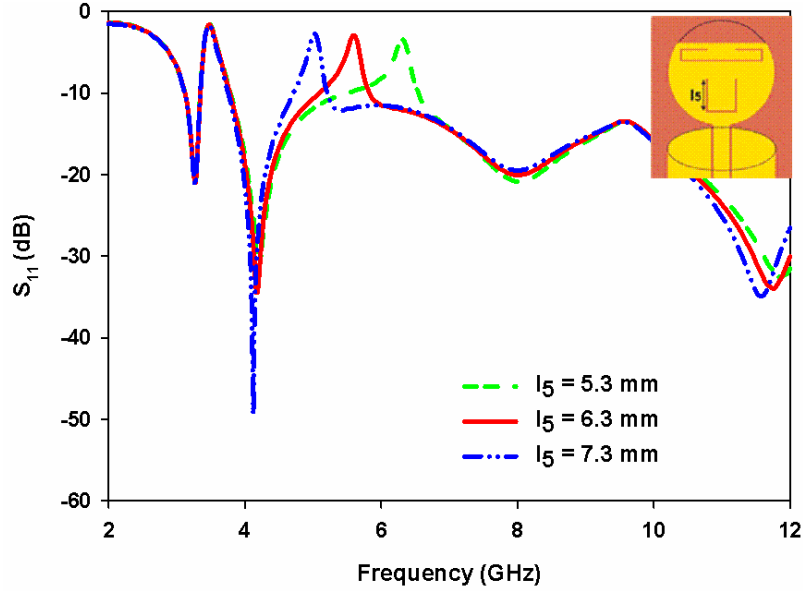
(c)
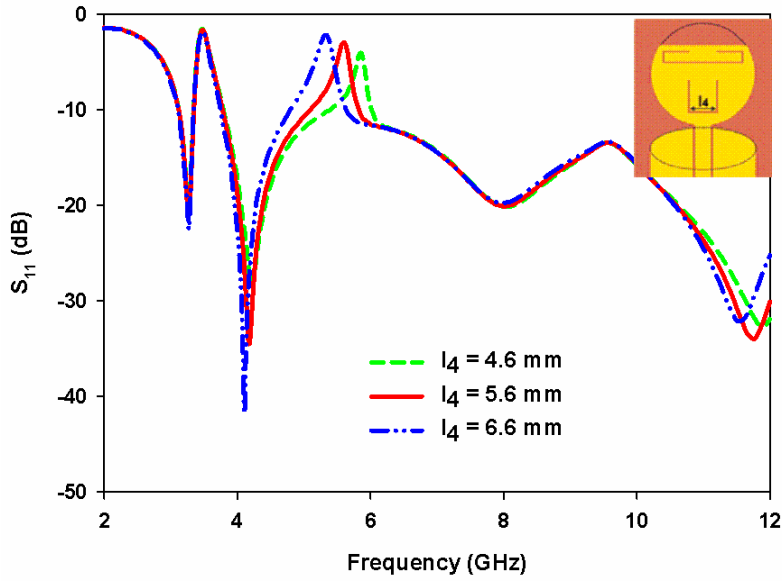
(d)

Fig. 4.20: **Effect of (a) length l_1 and (b) length l_2 of the folded U-slot (c) length l_5 and (d) length l_4 of the U-slot on S_{11} of the dual band-notched antenna. (Folded U-slot: $l_1 = 0.098\lambda_{n1}$, $l_2 = 0.045\lambda_{n1}$, $l_3 = 0.278\lambda_{n1}$, w = 0.4 mm. U-slot: $l_4 = 0.177\lambda_{n2}$, $l_5 = 0.195\lambda_{n2}$, w = 0.4 mm)**

As the length of the slots increases, l_1 of slot 1 and l_5 of slot 2, the centre frequencies of the notch bands decrease as expected and are shown in Fig. 4.20 (a) & (c). From Fig. 4.20 (b) & (d) an increase in l_2 in slot 1 and l_4 in slot 2 not only decrease the notch frequencies but also increase the notch bandwidth. This is because the variations in l_2 & l_4 change the spacing between the parallel arms of the slots along with its total length, thus changes the effective capacitance which in turn controls the notch bandwidth. Here, it is also seen that as the rejection band becomes narrower the signal rejection level tends to reduce slightly. Widths of the slot w make slight variation in the centre frequency and notch bandwidth as seen in Fig. 4.20 (e).
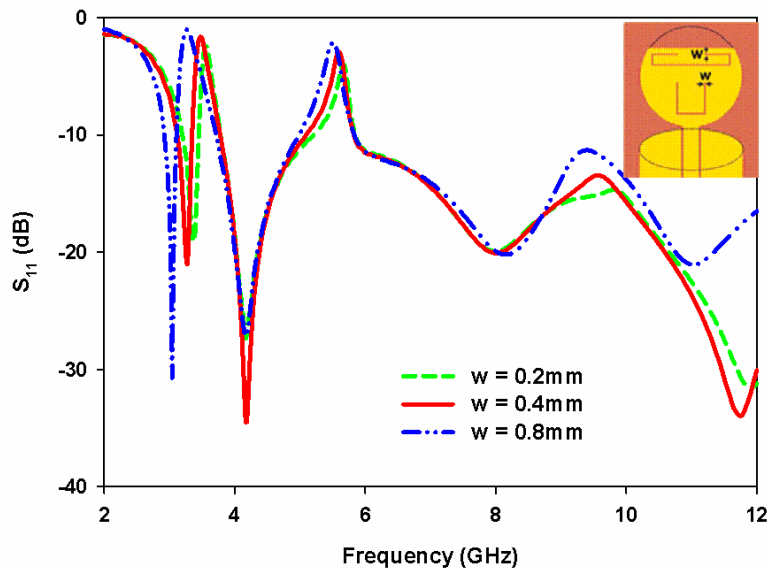
Fig. 4.20: **(e) Effect of width w of the slots on S_{11} of the dual band-notched antenna. (Folded U-slot: $l_1 = 0.098\lambda_{n1}$, $l_2 = 0.045\lambda_{n1}$, $l_3 = 0.278\lambda_{n1}$, $w = 0.4$ mm. U-slot: $l_4 = 0.177\lambda_{n2}$, $l_5 = 0.195\lambda_{n2}$, $w = 0.4$ mm)**

From the parametric analysis, the best result is obtained at WiMAX band for the dimensions of $l_1 = 5.2\ mm$, $l_2 = 2.4\ mm$, $l_3 = 14.8\ mm\ and\ w = 0.4\ mm$ of slot 1 (folded U-slot). Similarly at WLAN band, the dimensions are $l_4 = 5.6\ mm$, $l_5 = 6.3\ mm\ and$ $w = 0.4\ mm$ for slot 2 (U-slot). The simulated reflection coefficients with and without the slots are plotted in Fig. 4.21. From Fig. 4.21, it is seen that the insertion of slot 1 results in the rejection of WiMAX band. Then with the insertion of slot 2, antenna response remains unchanged except over the desired rejection band 5 GHz to 6 GHz.
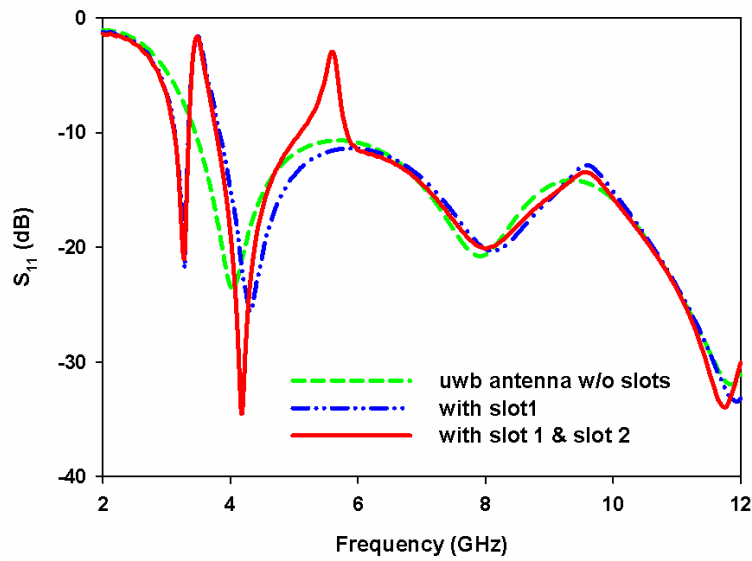
Fig. 4.21: **Simulated S_{11} of truncated circular disc with and without slots. (L = 0.939λ_{gc}, W = 0.751λ_{gc}, R = 0.368λ_{gc}, Lt = 0.165λ_{gc}, Lg = 0.206 λ_{gc}, R_M = 0.375λ_{gc}, R_m = 0.15λ_{gc}, W_s = 3mm, G = 0.4 mm, g = 0.3 mm, h = 1.6 mm, $\varepsilon_{r=}$4.4, Folded U-slot: l_1 = 0.098λ_{n1}, l_2 = 0.045λ_{n1}, l_3 = 0.278λ_{n1}, w = 0.4 mm, U-slot: l_4 = 0.177λ_{n2}, l_5 = 0.195λ_{n2}, w = 0.4 mm)**

4.3 Transient Analysis

In this section, the antenna transfer functions $H(j\omega)$ obtained from CST simulation are discussed. The transfer function for two different orientations of the virtual probes in CST as described in Chapter 3, section 3.2.2, i) azimuth plane ($\phi = 0^o - 360^o \ for \ \theta = 0^o$) & ii) elevation plane ($\theta = 0^o - 360^o \ for \ \phi = 0^o$) are shown in Fig. 4.22 and Fig. 4.23 respectively. These are actually field intensity image plots with angles along x-axis, and frequency along y-axis. So these plots gives a two dimensional view of antenna field pattern over a spherical surface for the entire operating frequency range.

Antenna transfer function H(jω):

From Fig. 4.22 (a) it is clear that the antenna exhibits nearly omni-directional field pattern for all the frequencies in the azimuth plane. Reduced intensity in transfer function observed at frequencies above 7.9 GHz matches well with the radiation patterns shown in Fig. 4.6 (b) & (c). Sharp reduction in intensity at 3.45 GHz and 5.65 GHz band observed in Fig. 4.22 (b) for all the angles confirm the band rejection capability of the band-notched antenna design.
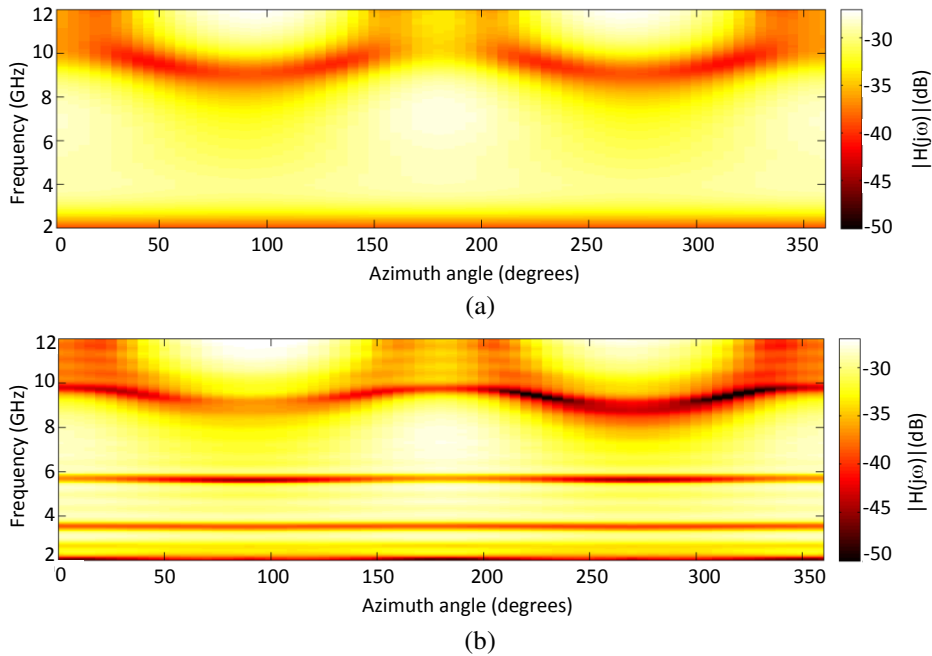
Fig. 4.22: Magnitude of simulated antenna transfer function H($j\omega$) in the azimuth plane (a) UWB antenna and (b) dual band-notched UWB antenna.

The elevation plots shown in Fig. 4.23 follow 'figure of eight' radiation pattern with nulls at 90° and 270°. Null at 270° spreads over a larger portion at frequencies around 7.9 GHz compared to null at 0°. From the simulated radiation patterns in Fig. 4.6 and Fig. 4.18, the antenna produces less radiation in the lower hemi-sphere for frequencies greater than 7.9 GHz. This results in reduced intensity spread over a wide angle around 270° in the elevation plane as in Fig. 4.23 (a) and (b). Two narrow, reduced intensity bands at 3.45 GHz and 5.65 GHz in Fig. 4.23 (b) correspond to the rejection bands of the dual band-notched antenna.

(a)

(b)
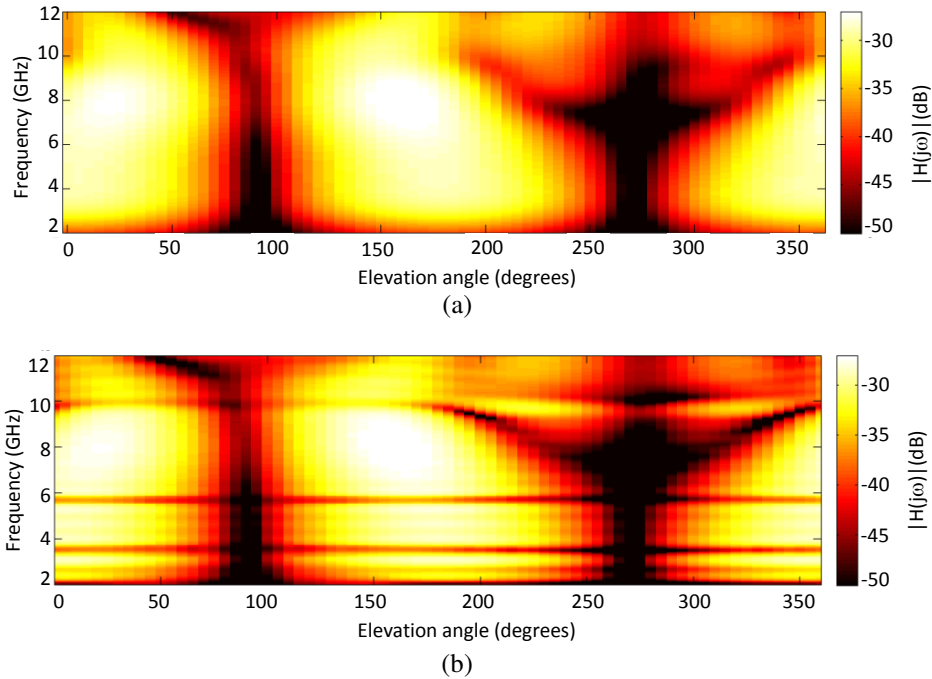
Fig. 4.23: Magnitude of simulated antenna transfer function H($j\omega$) in the elevation plane (a) UWB antenna and (b) dual band-notched UWB antenna.

Gain response:

Gain of the antenna can be deduced from the transfer function using the equation (3.19) as described in Chapter 3, section 3.5.2.1 and are plotted in Fig. 4.24 and Fig. 4.25. From Fig. 4.24 (a) and (b) it is found that the antenna exhibits fairly flat gain response in the azimuth plane for all the angles. A considerable reduction in antenna gain observed in the frequency bands of 3.45 GHz and 5.65 GHz in Fig. 4.24 (b) ensures the reasonable rejection of these bands.

(a)

(b)
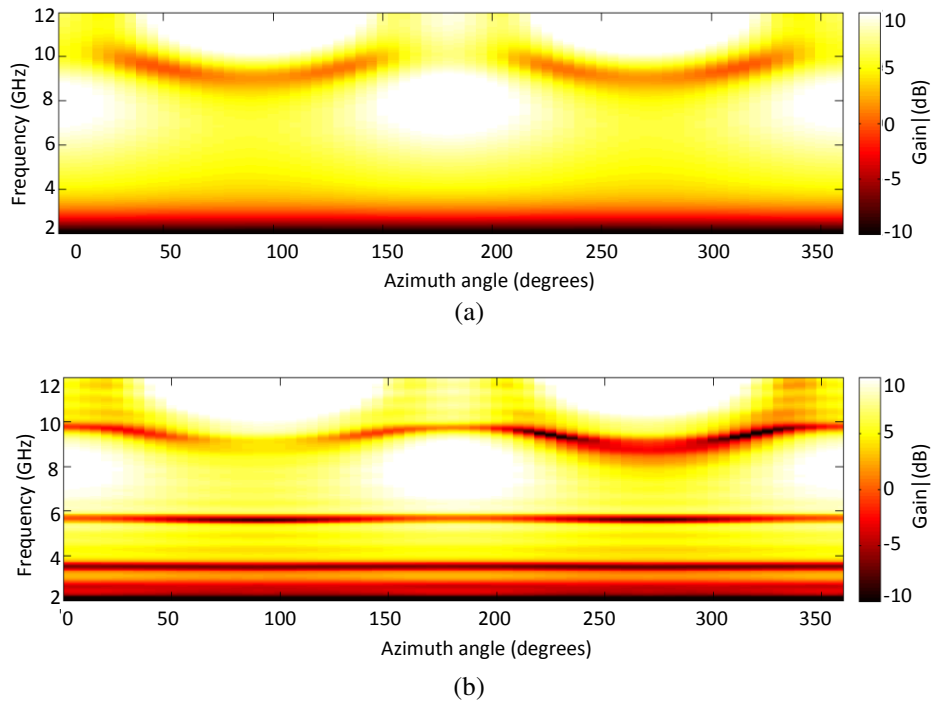
Fig. 4.24: Simulated gain in azimuth plane (a) UWB antenna and (b) dual band-notched UWB antenna.

Gain pattern in the elevation plane Fig. 4.25 (a) and (b) are more distorted compared to that in azimuth plane, especially around 90° and 270° which corresponds to the nulls of 'figure of eight' pattern in that plane. In the elevation plane, flat gain response is obtained at angles around 0° and 180° only. The reduced intensity bands at 3.45 GHz and 5.65 GHz in Fig. 4.25 (b) indicates the rejection of these bands.

(a)

(b)
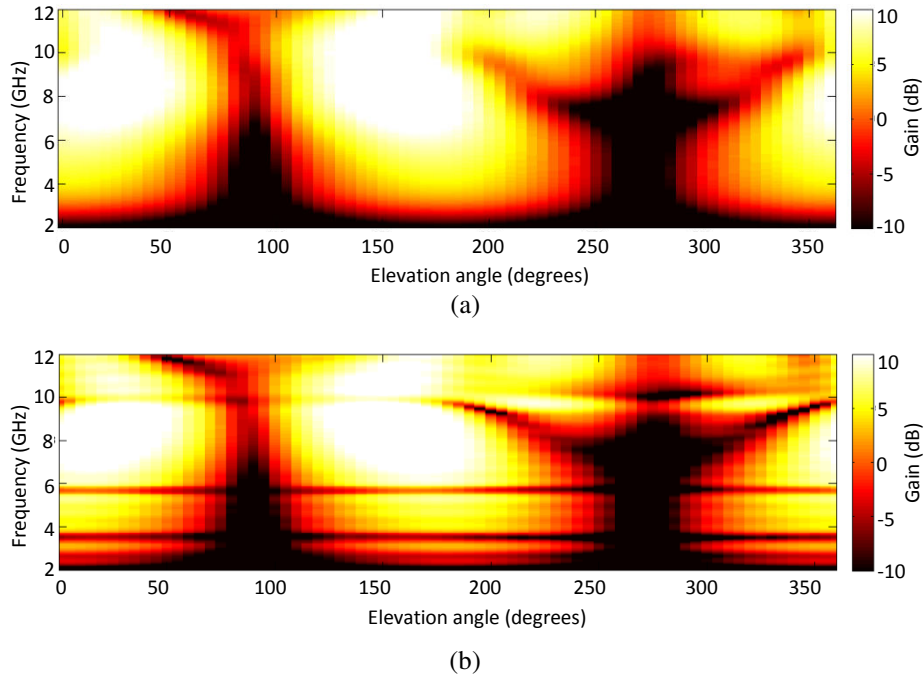
Fig. 4.25: Simulated gain in elevation plane (a) UWB antenna and (b) dual band- notched UWB antenna

Received pulses:

Normalised signal strength of the pulses received by virtual probes oriented around the antenna in CST simulation is shown in Fig. 4.26 and Fig. 4.27. It is observed that the received pulse retains the shape of the excitation pulse (4th order Rayleigh pulse) for all the orientations in the azimuth plane. Fig. 4.26 (b) displays the received pulses of the band notched structures in azimuth and have more ringing compared to Fig. 4.26 (a). Ringing durations of these pulses are plotted in Fig. 4.28 and are within the tolerable limits of few hundreds of picoseconds [9].

(a)

(b)
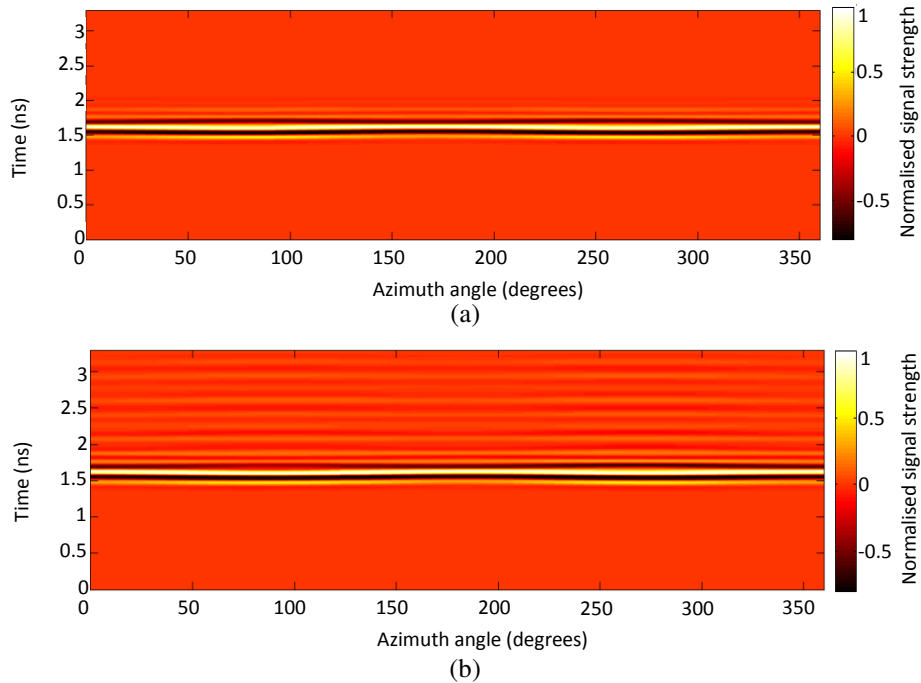
Fig. 4.26: Normalised received pulses in azimuth plane (a) UWB antenna and (b) dual band- notched UWB antenna

Received pulses in the elevation plane shown in Fig. 4.27 are found to be distorted more compared to that in azimuth plane. The discontinuities/distortions seen around 90° and 270° in the elevation plane correspond to the 'figure of eight' shape of the antenna transfer function. Moreover, the pulses are inverted over the angles from 90° to 270°. From Fig. 4.27 (b), it is also observed that the band-notched structure possesses more ringing compared to the one without notch functions.

(a)

(b)
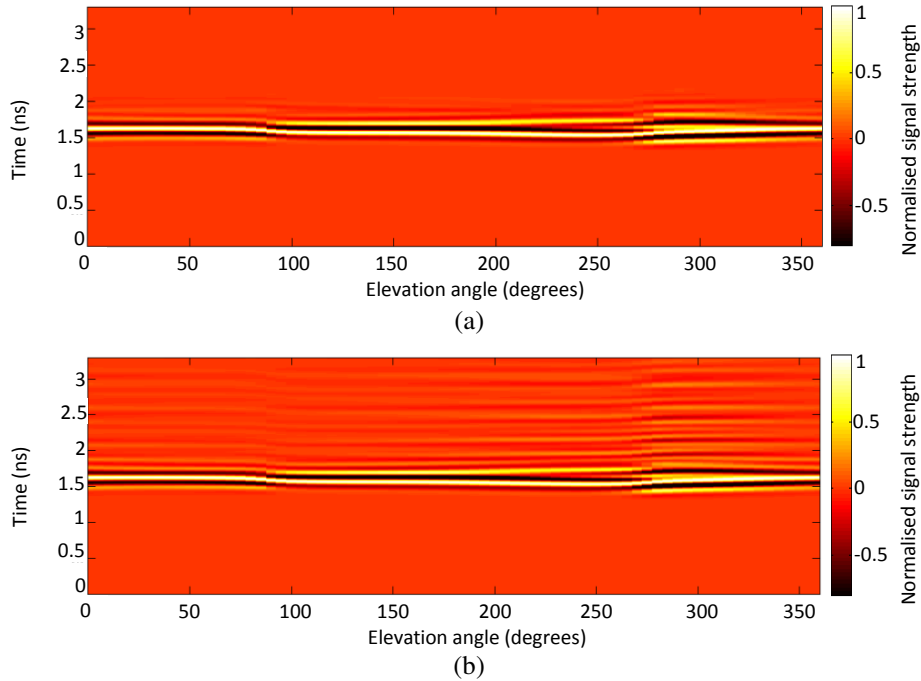
Fig. 4.27: Normalised received pulses in elevation plane (a) UWB antenna and (b) dual band- notched UWB antenna

Parameters of received pulse:

Envelope width (FWHM) and ringing duration are two important parameters of the received pulses which are mentioned in Chapter 3, section 3.5.2.2. For high data rate communication FWHM should not exceed few hundreds of picoseconds. Ringing is not desirable in UWB applications and its duration should be less than few envelope widths [9] – [10]. The FWHM and duration of ringing are calculated using equation (3.22) and (3.23) respectively given in Chapter 3. Fig. 4.28 (a) and (b) describes the FWHM and ringing of the radiated pulses in the azimuth and elevation planes respectively. The envelope width varies from 150 – 250 ps (picoseconds) in both the planes. In the azimuth

plane, the ringing duration has an average value of 280 ps for UWB antenna and 540 ps for band-notched antenna. In the elevation plane, plot of ringing duration shows more variations around 270°, but limited to tolerable range.
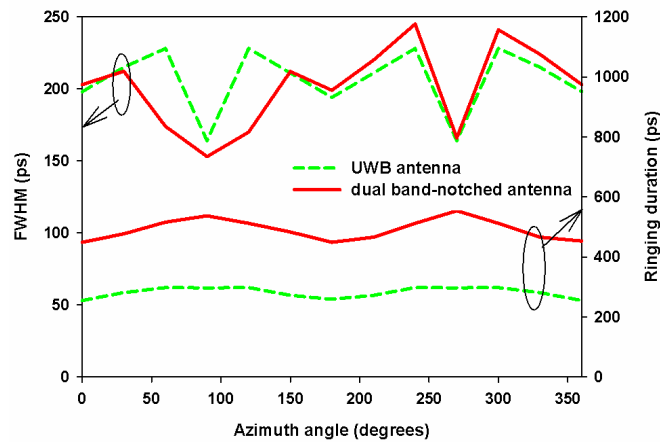
(a)
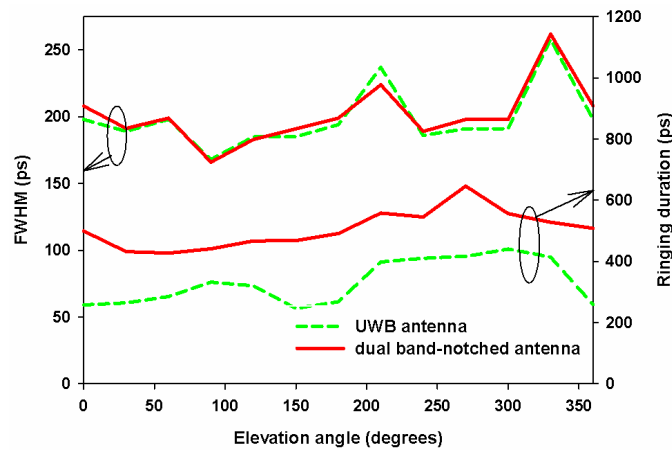
(b)

Fig. 4.28: FWHM and ringing duration of simulated received pulses in (a) azimuth plane and (b) elevation plane

4.4   Experimental results

Reflection coefficient:

Measured reflection coefficient of the proposed UWB antenna shown in Fig. 4.29 (a) covers a band from 3.4 GHz to more than 12 GHz.

(a)

(b)
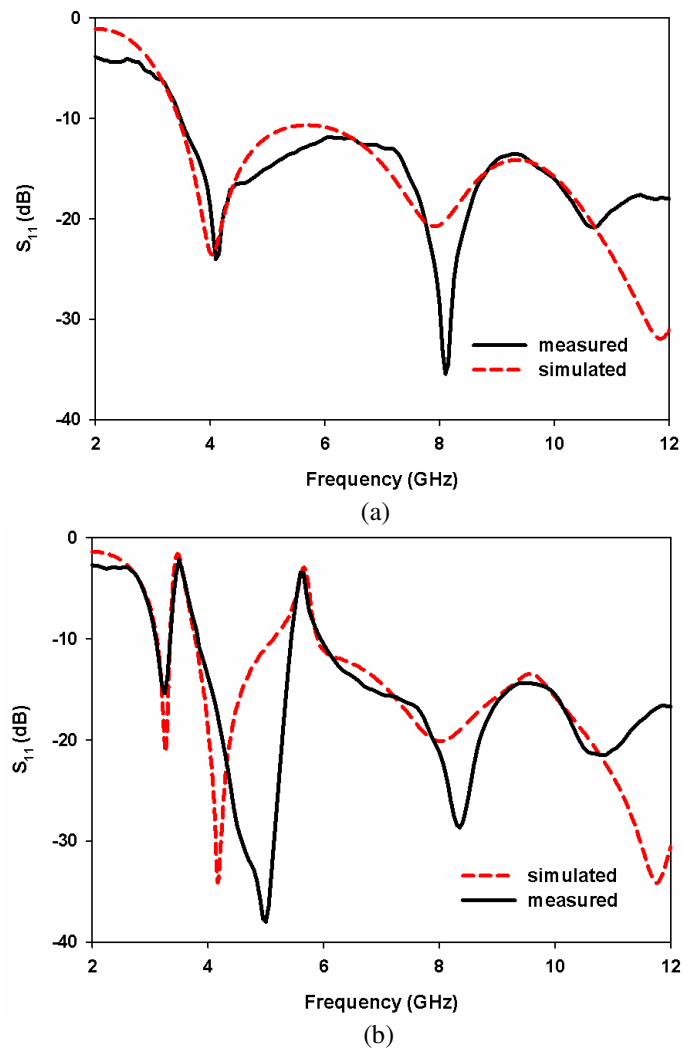
Fig. 4.29: Simulated and measured S_{11} of (a) UWB antenna and (b) dual band- notched UWB antenna

Fig. 4.29 (b) shows the measured S_{11} of the dual band notched UWB antenna which produces notched bands at 3.45 GHz and 5.65 GHz while maintaining the S_{11} response unchanged over the remaining frequency range. The measured results are validated by the simulated results in the respective plots.

Radiation pattern:

Normalised radiation patterns of the dual band-notched UWB antenna at different frequencies in two principal planes, azimuth (xz-plane) and elevation (yz-plane) for co-polarisation and cross-polarisation are shown in Fig. 4.30 (a) - (d). The patterns are similar to that of monopole antenna; non-directional in xz-plane (azimuth plane) and 'figure of eight' in the yz-plane (elevation plane). It is observed that the radiation patterns at different frequencies are similar, which is expected from a wideband antenna. Moreover, cross polarisation of better than 9 dB is observed along the bore sight for all the measured radiation patterns. Measured co-polar radiation patterns for both the planes match well with the simulation results.

xz- plane   **yz-plane**

(a)

cross-polar. simulated
co-polar. simulated
co-polar. measured
cross-polar. measured

(b)
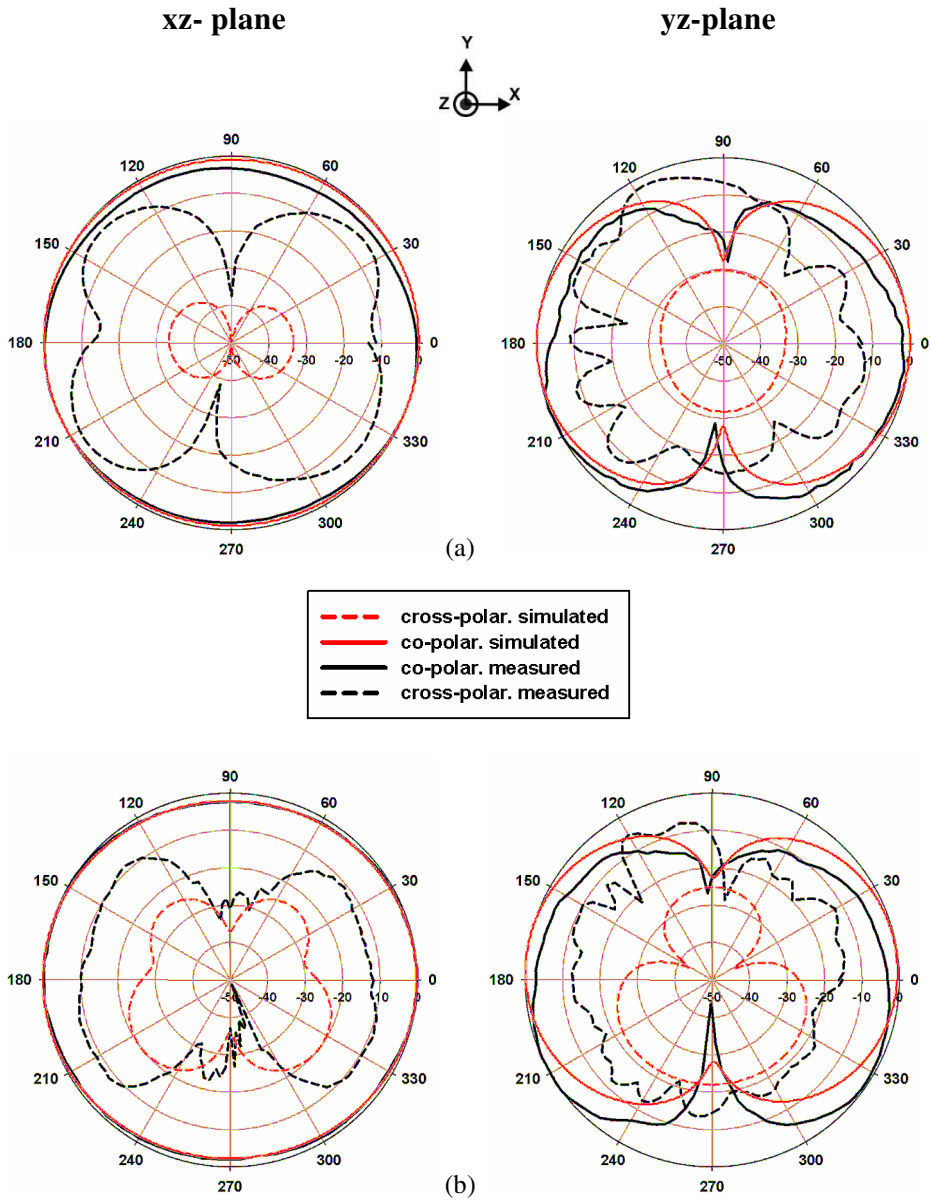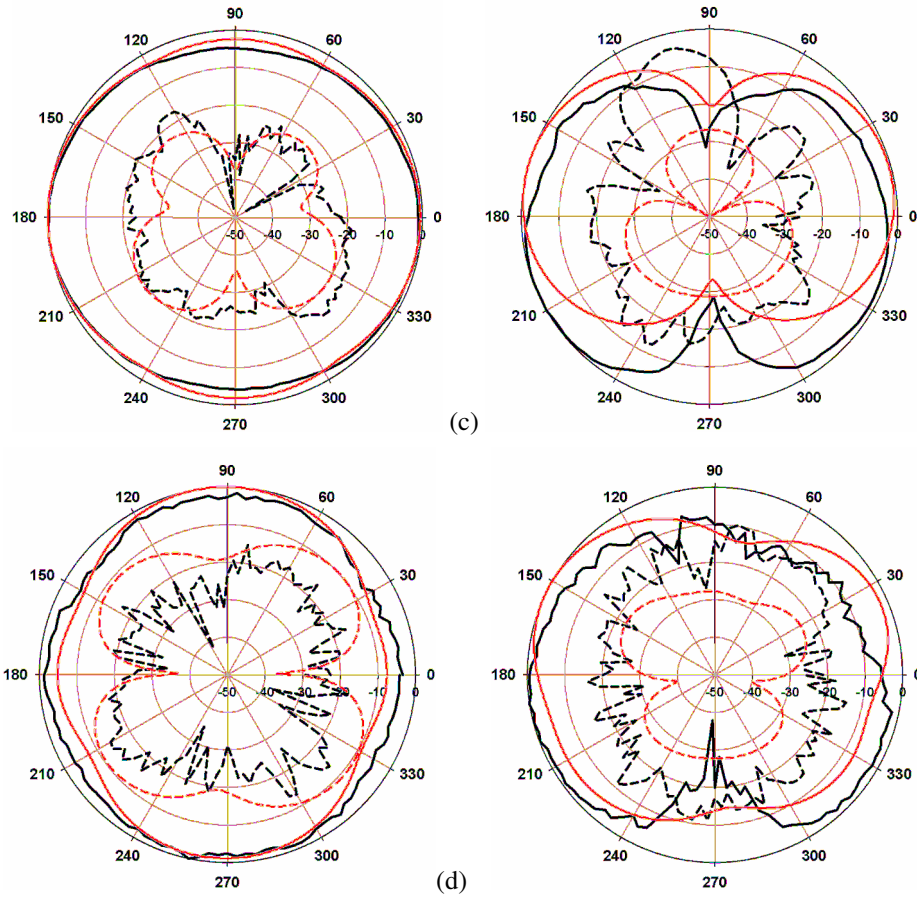
Fig. 4.30: **Simulated and measured radiation patterns of dual band-notched UWB antenna at frequencies (a) 3.1 GHz (b) 6 GHz and (c) 7 GHz and (d) 11 GHz**

Gain and efficiency:

Measured peak gain shown in Fig. 4.31 (a) exhibits an almost flat response throughout the operating band of 3.1 GHz – 10.6 GHz with gain varying from 1.6 dBi to 4.4 dBi. Fig. 4.31 (b) shows the gain response of the dual band-notched antenna where the gain falls to - 5.1 dBi and - 6.8 dBi at 3.45 GHz and 5.65 GHz respectively. Measured

radiation efficiency shown along with the gain possesses values within the range of 73% to 88% over the entire bandwidth. At notched bands sharp decrease in efficiency observed agree well with the dips in the gain response. All the measured results are validated with simulation results in the respective plots.

(a)

(b)
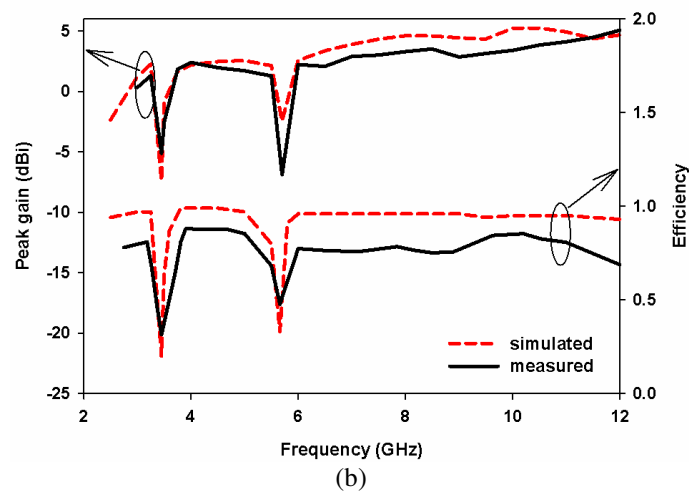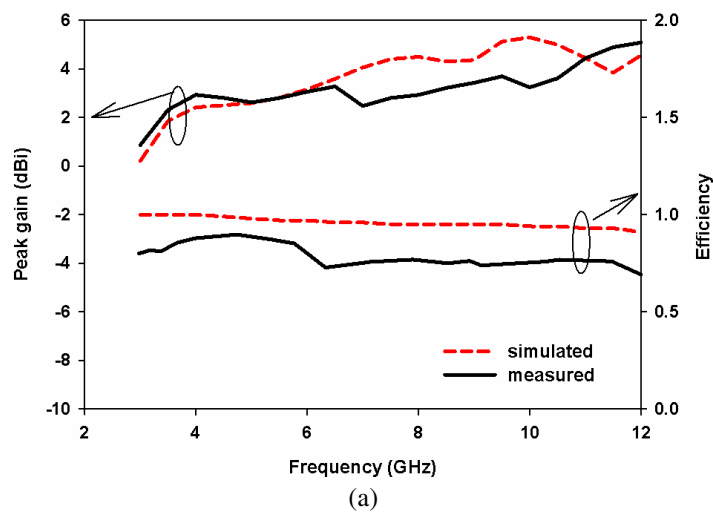
Fig. 4.31: Measured and simulated peak gain and efficiency of (a) UWB antenna and (b) dual band-notched UWB antenna

Time domain analysis:

Response of antenna to narrow pulses (pulse width << 1 ns) are studied using the method described in Chapter 3, section 3.5.2.3. All the measurements based on pulse response check whether the antenna is capable of receiving the source pulse without distortion in all the directions. From the simulated received pulse response shown in Fig. 4.26 & Fig. 4.27, it is clear that the response in the elevation plane is distorted compared to that in the azimuth plane because of the pattern nulls ('figure of eight' pattern) of receiving antenna in the elevation plane. So all the time domain measurements are carried out in the azimuth plane where the antenna is expected to provide uniform response in all the directions.

Antenna transfer function S_{21} and group delay:

Two important parameters considered for the pulse dispersion analysis of UWB antenna are i) antenna transfer function S_{21} and (ii) group delay [11]. The measured antenna transfer function and group delay taken for two extreme orientations of the transmitting and receiving antennas in azimuth plane, (i) face to face and (ii) face to side, are displayed in Fig. 4.32. From Fig. 4.32 (a), the response of the antenna transfer function is almost same for both the orientations except over the frequencies around 7.9 GHz. It indicates that the antenna possesses good radiation characteristics in all the directions in the azimuth plane. The variations in S_{21} response (< 5dB) and group delay (< 1 ns) are within the reasonable levels to assure good spatial radiation properties of the radiated pulses. Sharp variations in S_{21} and group delay responses observed in Fig. 4.32 (b) correspond to the notch bands of the antenna.
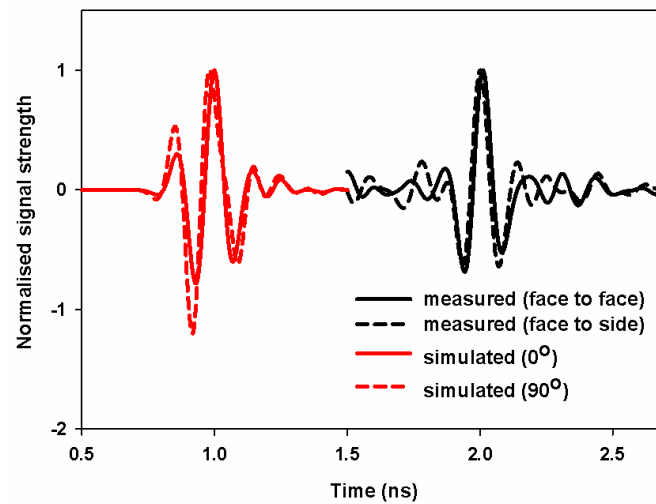
(a)

(b)
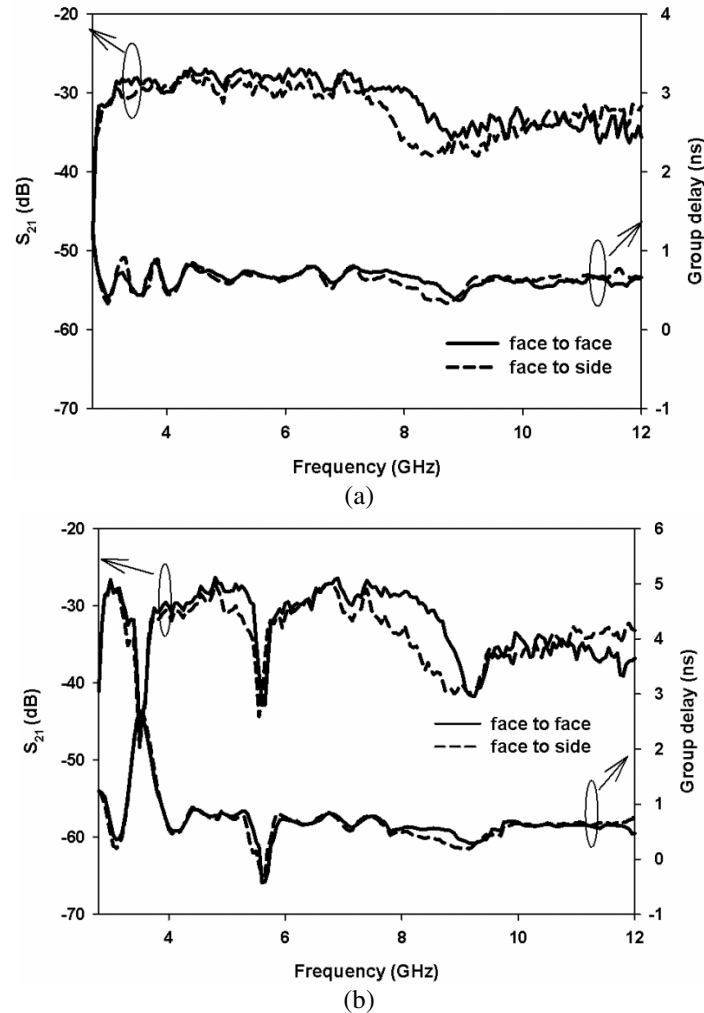
Fig. 4.32: Measured antenna transfer function S_{21} and group delay in azimuth plane of (a) UWB antenna and (b) dual band-notched UWB antenna
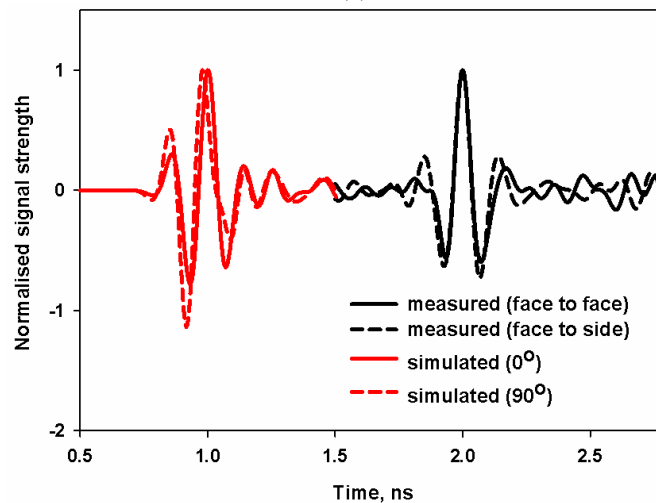
Received pulse:

The normalised received pulses measured for two different orientations of the antennas in the azimuth plane are plotted in Fig. 4.33. Here, 4th order Rayleigh pulse is chosen as the input pulse. The received pulses are derived from the measured antenna transfer function S_{21} by

using (3.24) in Chapter 3, section 3.5.2.1. It is observed in Fig. 4.33 (a) that the measured pulses are almost similar to the simulated pulses for both the orientations. With the notch structures, the shapes of the measured pulses are not much distorted and shown in the Fig. 4.33 (b).

(a)

(b)

Fig. 4.33: Measured and simulated normalised received pulses in azimuth plane of (a) UWB antenna and (b) dual band-notched UWB antenna

Fidelity:

Similarity between the received pulse and the source pulse is measured by a term called fidelity which actually compares the shapes of the pulses not the amplitudes. Fig. 4.34 (a) and (b) compare the measured and simulated fidelity in azimuth plane, calculated using (3.26) in Chapter 3, section 3.5.2.3, for the UWB and band-notched UWB antennas respectively.
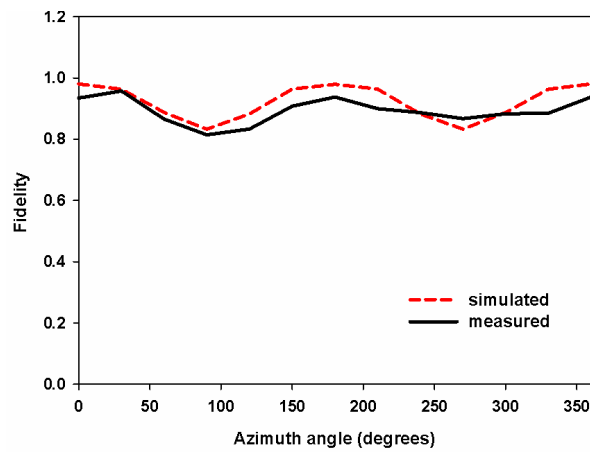
(a)
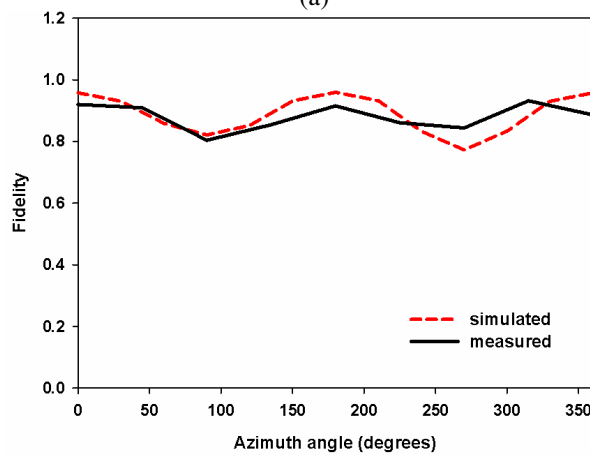
(b)

Fig. 4.34: Simulated and measured fidelity in azimuth plane of (a) UWB antenna and (b) dual band- notched UWB antenna

Fidelity values obtained is greater than 0.8 in both the cases, indicate that the antennas radiate uniformly in all the directions in the azimuth plane. On comparing, the fidelity values for dual band-notched antenna are slightly less than that for the UWB antenna. In Fig. 4.34, lowest fidelity values (0.81 - 0.83) are seen around the angles 90° and 270°, i.e., the received pulses experience maximum distortions in these directions which correspond to face to side orientation of the antennas.

4.5 Conclusion

A coplanar waveguide fed, modified circular disc antenna with improved radiation pattern is presented in this chapter. The antenna exhibits wide impedance bandwidth from 3.4 GHz to greater than 12 GHz with a compact size of 25 mm × 20 mm. The antenna consists of a truncated circular disc and a finite ground plane. In this design, the radiation pattern is improved compared to ref [1] by reducing the ground width and truncating upper edge of the circular disc as discussed in section 4.1.1. The impedance bandwidth of the truncated disc is further improved by including gradual tapering in ground plane near the feed point i.e., adopting elliptical shape for the upper portion of the ground plane. Measured impedance and radiation characteristics reveal that the designed antenna is suitable for UWB applications.

Then the proposed UWB antenna is further modified to eliminate the interference with the co-existing WiMAX and WLAN services. Frequency rejection at these two bands are achieved by inserting a folded U-slot and U-slot of length equal to half of the guide wavelength

at WiMAX and WLAN respectively within the radiating patch. From the impedance and radiation characteristics it is observed that these notch structures reject the unwanted bands very effectively without changing the antenna properties over the remaining portion of the operating bandwidth.

Time domain analysis reveals that the proposed antenna can support impulse radio which uses narrow pulses of duration less than 1 ns as the source/input pulse. Features of the radiated pulses depends on the transfer characteristics of the antenna, thus on the shape of the radiation pattern. In this design the antenna exhibits nearly omnidirectional radiation patterns, thus radiated pulses with almost similar features are expected in all the directions, i.e. independent of space coordinates. From the discussions, it is clear that pattern bandwidth is an important parameter as far as the impulse radio application is concerned.

Features of the radiated pulses are verified by the time domain measurements such as antenna transfer function S_{21} and group delay taken for different orientations of two identical antennas. The extent of pulse distortion by the antenna is further confirmed by fidelity measurement over the azimuth plane and reveals that the antenna is capable of reproducing the narrow input pulses with negligible distortions.

With the above performance studies, the antenna is proved to be a promising candidate for various UWB applications in WiMAX/WLAN environment.

References

[1]   J. Liang, L. Guo, C.C. Chiau, X. Chen and C.G. Parini, "Study of CPW-fed circular disk monopole antenna for ultra-wideband applications", IEE Proc. Microwaves Antennas & Propagation, vol. 152, no. 6, pp.520-526, 2005.

[2]   P. Li, J. Liang, and X. Chen, "Study of printed elliptical/circular slot antennas for Ultra wideband applications", IEEE Transactions on Antennas and Propagation, vol. 54, pp. 1670–1675, 2006.

[3]   P.S. Carter, "Wideband, short wave antenna and transmission line system", U.S. Patent2, 181, 870, December 1939.

[4]   L. Paulsen, J.B West, W.F Perger and J. Kraus, "Recent investigations on the volcano smoke antenna", IEEE Antennas and Propagation International Symposium (Digest), 2003.

[5]   G. M. Yang, R. H. Jin, G. B. Xiao, C. Vittoria, V. G. Harris, and N. X. Sun, "Ultra wideband (UWB) Antennas With Multi resonant Split-Ring Loops", IEEE Transactions on Antennas and Propagation, vol.57, no.1, pp. 256-260, 2009.

[6]   Liang, J., Chiau, C.C., Chen, X., and Parini, C.G.: 'Analysis and design of UWB disc monopole antennas'. IEE Seminar on Ultra Wideband Commun. Technol. Syst. Design, Queen Mary, University of London, pp. 103–106, 2004.

[7]   Z.L. Zhou, L. Li and J.S. Hong, "Compact UWB printed monopole antenna with dual narrow band notches for WiMAX/ WLAN bands", Electronics Letters, vol. 47 no. 20, 2011.

[8]   L. Li, Z.-L. Zhou, J.-S. Hong and B.-Z. Wang, "Compact dual-band-notched UWB planar monopole antenna with modified SRR", Electronics Letters, vol. 47, no. 17, 2011.

[9]   W. Wiesbeck, G. Adamiuk and C. Sturm, "Basic Properties and Design Principles of UWB Antennas", Proceedings of the IEEE, vol. 97, no. 2, pp. 372- 386, 2009.

[10]   W. Sorgel and W. Wiesbeck, "Influence of the Antennas on the Ultra-Wideband Transmission", EURASIP Journal on Applied Signal Processing, Hindawi Publishing Corporation, pp. 296–305, 2005.

[11]   K. Bahadori and Y. Rahmat-Samii, "A miniaturized elliptic-card UWB antenna with WLAN band rejection for wireless communications", IEEE Transactions on Antennas and Propagation, vol. 55, no. 11, pp. 3326 - 3332, 2007.

.....ඎ.....

Chapter 5

DUAL BAND-NOTCHED UWB SLOT ANTENNA

Performance of CPW-fed slot antenna suitable for UWB communication application is discussed in this chapter. The antenna has wide impedance bandwidth from 2.5 GHz to12 GHz which occupies the unlicensed UWB spectrum specified by FCC regulation. The structure is derived from a conventional CPW-fed monopole antenna. The ground plane is extended to surround the patch which act effectively as a slot structure and then modified to introduce multiple resonances. The slot structure supports multiple modes and provides coupling between these modes to enhance the bandwidth of the structure. To notch out the co-existing WiMAX and WLAN bands, a band rejection mechanism for the present structure is also proposed. Studies on both the frequency domain and time domain characteristics are also discussed in this chapter.

5.1   UWB Slot Antenna

5.1.1 Evolution and Geometry of the antenna

5.1.1.1 Evolution of the antenna

The evolution of the proposed antenna from a simple CPW-fed monopole structure is presented. Firstly, a 50 Ω CPW line of width W_f and gap G on a substrate with $\varepsilon_r = 4.4$ and height $h = 1.6mm$ is considered. The geometry and reflection coefficient characteristics (S_{11}) are shown in Fig. 5.1(a) and (b) respectively. CPW line presents severe impedance mismatch over the UWB spectrum and from the radiation studies it is not acting as an antenna.

(a)   (b)
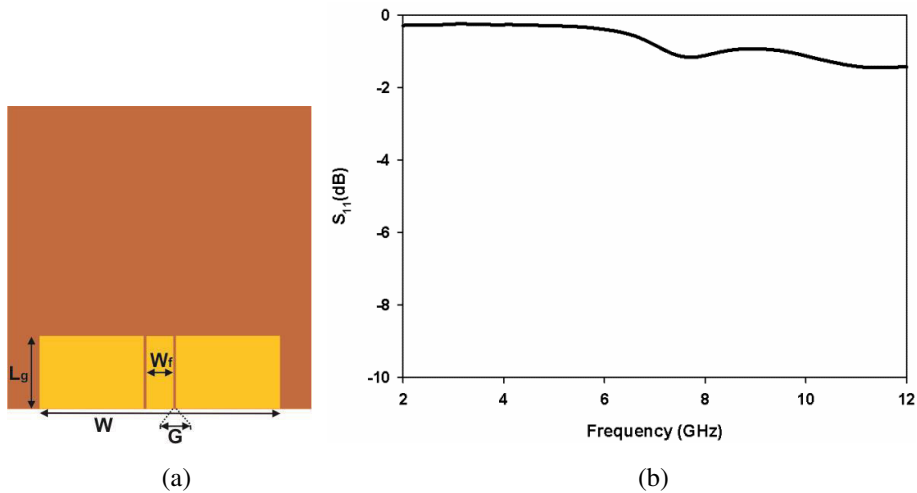
Fig. 5.1: CPW line (W = 1.013λ_{gc}, L$_g$ = 0.307λ_{gc}, W$_f$ = 3 mm, G = 0.3 mm, h =1.6 mm, ε$_r$ = 4.4, where λ_{gc} is the guide wavelength corresponding to the centre frequency of UWB bandwidth)

The length of the feed line is increased to L_m as in Fig. 5.2 (a) resulting in a quarter wavelength monopole structure. The reflection

coefficient characteristic is shown in Fig. 5.2 (b). A well matched resonance which depends on the extended length L_m is produced. The expression for the resonant frequency is $f_r = \dfrac{c}{4\,L_m\sqrt{\varepsilon_{re}}}$; $\varepsilon_{re} = \dfrac{\varepsilon_r + 1}{2}$ where c is the velocity of light in free space, ε_r is the relative permittivity of the substrate. In this case the width of the extended line is equal to the signal strip width of the CPW line.
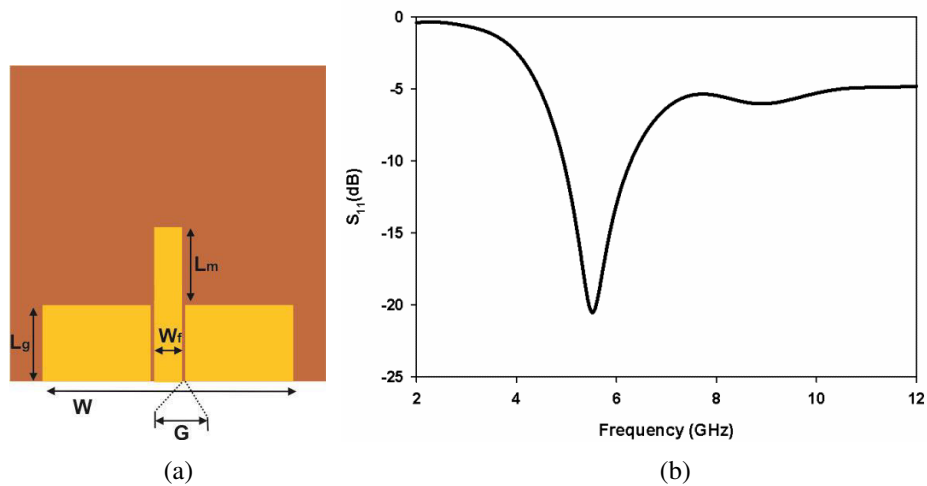

| (a) | (b) |

Fig. 5.2: CPW-fed monopole (W = 1.013λ_{gc}, L$_m$ = 0.311λ_{gc}, L$_g$ = 0.307λ_{gc}, W$_f$ = 3 mm, G = 0.3 mm, h =1.6 mm, ε_r = 4.4)

Width of the extended feed line (L_m) is increased to W_r after leaving a gap g above the ground plane. The geometry and its S_{11} characteristics are shown in Fig. 5.3 (a) and (b) respectively. The S_{11} response is almost similar to that of the previous geometry with slight increment in resonant frequency (because now the length is $L_m - g$).

(a) (b)
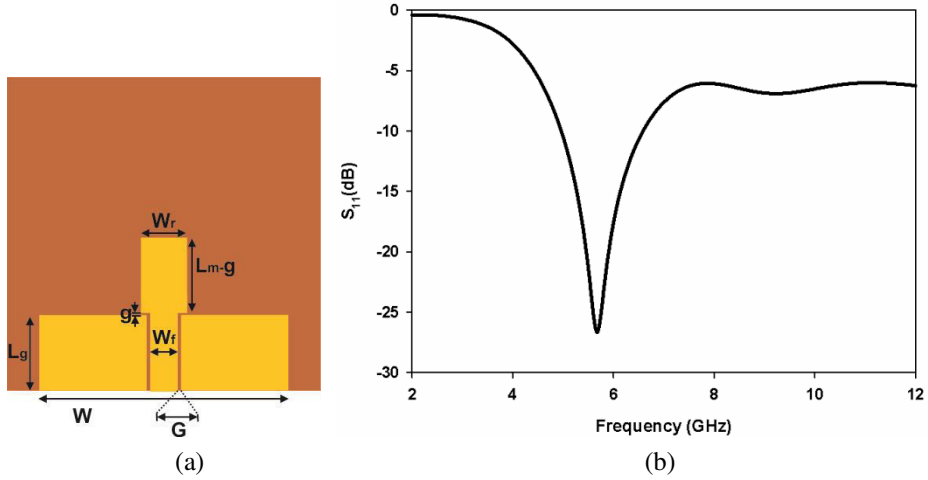
Fig. 5.3: CPW-fed rectangular monopole (W = 1.013λ_{gc}, L$_m$ = 0.311λ_{gc}, W$_r$ = 0.187λ_{gc}, L$_g$ = 0.307λ_{gc}, g = 0.3 mm, W$_f$ = 3 mm, G = 0.3 mm, h =1.6 mm, ε$_r$ = 4.4)

The rectangular patch is modified by bevelling its bottom edge as shown in Fig. 5.4 (a). Here, in the geometry $L_r + L_b = L_m - g$.
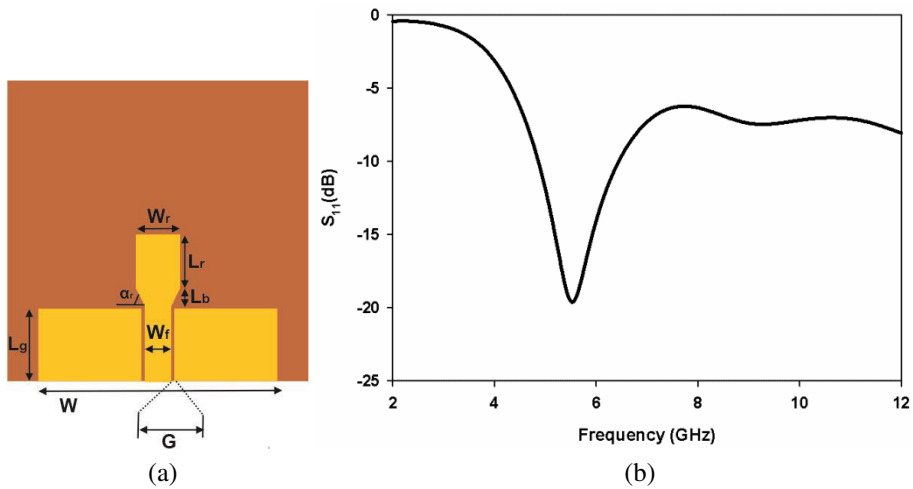

(a) (b)

Fig. 5.4: CPW-fed bevelled rectangular monopole (W = 1.013λ_{gc}, L$_r$ = 0.225λ_{gc}, L$_b$ = 0.075λ_{gc}, W$_r$ = 0.187λ_{gc}, L$_g$ = 0.307λ_{gc}, α$_r$ = 63°, W$_f$ = 3 mm, G = 0.3 mm, h =1.6 mm, ε$_r$ = 4.4)

From the geometry shown, the length of the bevelled patch is $L_r + \frac{L_b}{Sin(\alpha_r)}$, slightly greater than earlier one. So the resonant frequency of the rectangular strip decreases when its bottom edge is bevelled and is confirmed from the S_{11} characteristics shown in Fig. 5.4 (b).

Then the structure is modified by extending the ground plane by a length $L_0 + W_1$ to surround the rectangular patch as shown in Fig. 5.5 (a). It can be seen from Fig. 5.5 (b) that the extended ground lowers the resonant frequency to f_m. The new resonant frequency f_m results from the coupling between the modes due to the extended ground plane and the bevelled rectangular patch. The coupling of these modes is verified by varying the separation d between these elements in the structure in Fig. 5.5 (a). This is clearly demonstrated in Fig. 5.6.

<div align="center">(a)   (b)</div>
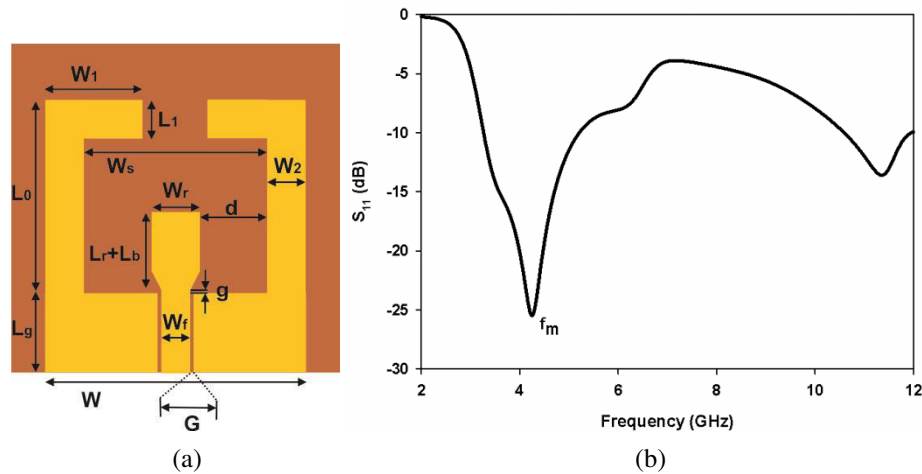
Fig. 5.5: CPW-fed monopole with extended ground. (W = $1.013\lambda_{gc}$, L_r = $0.225\lambda_{gc}$, L_b = $0.075\lambda_{gc}$, W_r = $0.187\lambda_{gc}$, L_0 = $0.818\lambda_{gc}$, L_1 = $0.15\lambda_{gc}$, W_1 = $0.375\lambda_{gc}$, W_2 = $0.15\lambda_{gc}$, L_g = $0.307\lambda_{gc}$, W_s = $0.713\lambda_{gc}$, d = $0.262\lambda_{gc}$, g = 0.3 mm, W_f = 3 mm, G = 0.3 mm, h =1.6 mm, ε_r = 4.4)

Fig. 5.6 illustrates the effect of separation $'d'$ between the extended ground plane and the bevelled rectangular patch. In Fig. 5.6 f_g and f_b represent the resonance due to the extended ground and bevelled rectangular strip respectively. For $d = 12.5\ mm$, these two frequencies are highly separated. From Fig. 5.6, it is seen that as the value of d decreases f_g and f_b come closer due to the coupling between their respective modes. For $d = 7\ mm$ ($0.262\lambda_{gc}$), f_b and f_g are merged to form a single resonance at f_m.
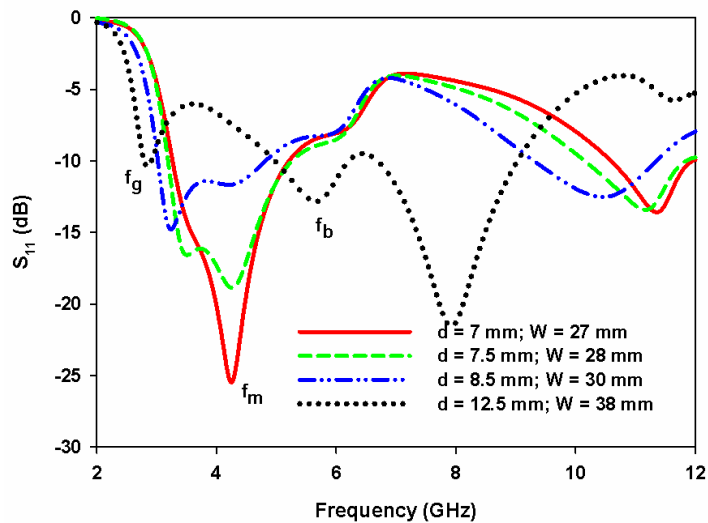
Fig. 5.6: Reflection coefficient of the structure in Fig. 5.5 (a) with varying the separation d. (W = 1.013λ_{gc}, L$_r$ = 0.225λ_{gc}, L$_b$ = 0.075λ_{gc}, W$_r$ = 0.187λ_{gc}, L$_0$ = 0.818λ_{gc}, L$_1$ = 0.15λ_{gc}, W$_1$ = 0.375λ_{gc}, W$_2$ = 0.15λ_{gc}, L$_g$ = 0.307λ_{gc}, W$_s$ = 0.713λ_{gc}, g = 0.3 mm, d = 0.262λ_{gc}, W$_f$ = 3 mm, G = 0.3 mm, h =1.6 mm, ε_r = 4.4)

By cutting slits $W_3 \times L_3$ from the extended ground as shown in Fig. 5.7 (a), the effective current path length in the extended ground is increased. As a result the resonant frequency due to the extended ground plane is retrieved and decreases to f_0 as in Fig. 5.7 (b). i.e., pair of slits $W_3 \times L_3$ cut in the extended ground plays an important role in achieving the lower band of UWB spectrum without increasing the antenna size. This is clear from the parametric analysis of this structure by varying W_3 as shown in Fig. 5.8.

(a) (b)
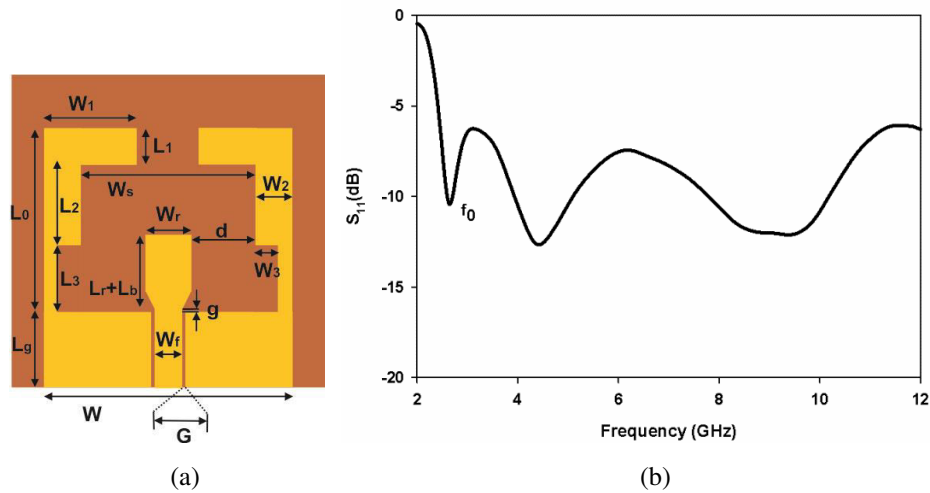
Fig. 5.7: CPW-fed monopole with slits on extended ground. (W = 1.013λ_{gc}, L$_r$ = 0.225λ_{gc}, L$_b$ = 0.075λ_{gc}, W$_r$ = 0.187λ_{gc}, L$_0$ = 0.818λ_{gc}, L$_1$ = 0.15λ_{gc}, W$_1$ = 0.375λ_{gc}, L$_2$ = 0.412λ_{gc}, W$_2$ = 0.15λ_{gc}, L$_3$ = 0.255λ_{gc}, W$_3$ = 0.112λ_{gc}, L$_g$ = 0.307λ_{gc}, W$_s$ = 0.713λ_{gc}, d = 0.262λ_{gc}, g = 0.3 mm, W$_f$ = 3 mm, G = 0.3 mm, h = 1.6 mm, ε_r = 4.4)
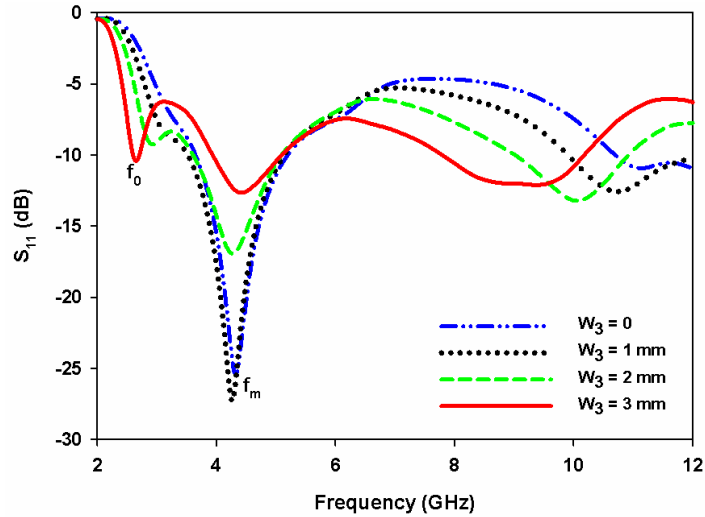
Fig. 5.8: Effect of W_3 on S_{11} characteristics of the structure shown in Fig. 5.7 (a). (W = $1.013\lambda_{gc}$, L_r = $0.225\lambda_{gc}$, L_b = $0.075\lambda_{gc}$, W_r = $0.187\lambda_{gc}$, L_0 = $0.818\lambda_{gc}$, L_1 = $0.15\lambda_{gc}$, W_1 = $0.375\lambda_{gc}$, L_2 = $0.412\lambda_{gc}$, W_2 = $0.15\lambda_{gc}$, L_3 = $0.255\lambda_{gc}$, W_3 = $0.112\lambda_{gc}$, L_g = $0.307\lambda_{gc}$, W_s = $0.713\lambda_{gc}$, d = $0.262\lambda_{gc}$, g = 0.3 mm, W_f = 3 mm, G = 0.3 mm, h =1.6 mm, ε_r = 4.4)

From Fig. 5.8 as the slit width W_3 increases the resonant frequency due to the extended ground decreases to f_0 without changing f_m. The f_m remains unchanged indicate that there is no change in the coupling effect of extended ground on the rectangular strip.

The S_{11} characteristics shown in Fig. 5.7 (b) has poor impedance match over the UWB region. Bevelling is one of the techniques [1] to improve the impedance bandwidth of wide band planar antennas. This is achieved by bevelling the portion of the structure close to the feed probe having high current density, i.e., ground plane corners near the feed probe are bevelled or tapered symmetrically. These bevels provide a considerable improvement in the impedance match of the antenna,

thus results in proposed antenna with broad band response from 2.5 GHz to 12 GHz.

5.1.1.2 Geometry of the proposed antenna

The proposed antenna structure consists of a CPW-fed bevelled rectangular patch with bevel angle α_r and a ground plane extended to a length of $L_0 + W_1$. Then to enhance the impedance bandwidth of the antenna certain modifications are introduced in the extended ground plane.
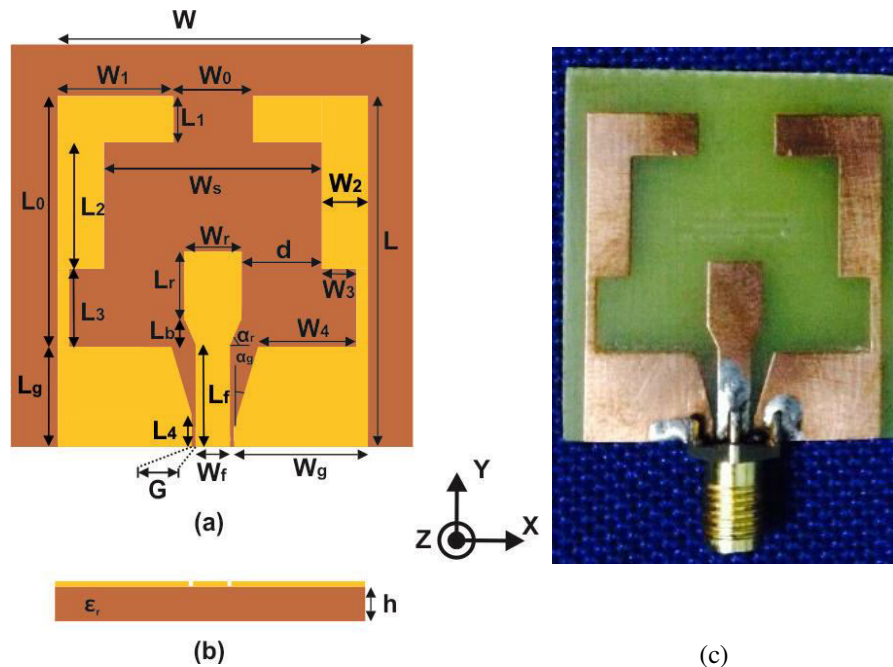

Fig. 5.9: Geometry of the proposed UWB slot antenna (a) top view (b) side view and (c) photograph. (L = $1.126\lambda_{gc}$, W = $1.013\lambda_{gc}$, L_r = $0.225\lambda_{gc}$, W_r = $0.187\lambda_{gc}$, L_b = $0.075\lambda_{gc}$, L_f = $0.319\lambda_{gc}$, L_0 = $0.818\lambda_{gc}$, W_0 = $0.262\lambda_{gc}$, L_1 = $0.15\lambda_{gc}$, W_1 = $0.375\lambda_{gc}$, L_2 = $0.412\lambda_{gc}$, W_2 = $0.15\lambda_{gc}$, L_3 = $0.255\ \lambda_{gc}$, W_3 = $0.112\lambda_{gc}$, W_4 = $0.33\lambda_{gc}$, L_4 = $0.082\lambda_{gc}$, L_g = $0.307\lambda_{gc}$, W_g = $0.437\lambda_{gc}$, W_s = $0.713\lambda_{gc}$, d = $0.262\lambda_{gc}$, W_f = 3 mm, G = 0.3 mm, α_r = 63°, α_g = 16.7^o, h =1.6 mm, ε_r = 4.4)

Pair of rectangular slits $W_3 \times L_3$ inserted in the ground plane extends the lower edge of the band without increasing the overall size of the antenna. By bevelling the ground plane corners near the feed point with a bevel angle α_g, impedance match over the entire bandwidth is obtained. The CPW fed monopole and the ground plane are printed on the same side of a substrate with relative dielectric constant $\varepsilon_r = 4.4$ and thickness $h = 1.6 \, mm$. The geometry and photograph of the proposed antenna are shown in Fig. 5.9.

5.1.2 Simulation, Parametric Analysis and Design

5.1.2.1 Simulation

Reflection coefficient:

The antenna structure is simulated using EM simulation tool CST. Simulated impedance bandwidth extends from 2.5 GHz to 12 GHz with four resonant frequencies as shown in Fig. 5.10. Resonant frequencies observed at 2.6 GHz, 4.0 GHz, 6.9 GHz and 10.7 GHz correspond to the dips in the reflection coefficient characteristics. Like any other UWB antenna the overlapping of the multiple bands centred at these four resonant frequencies results in UWB response.
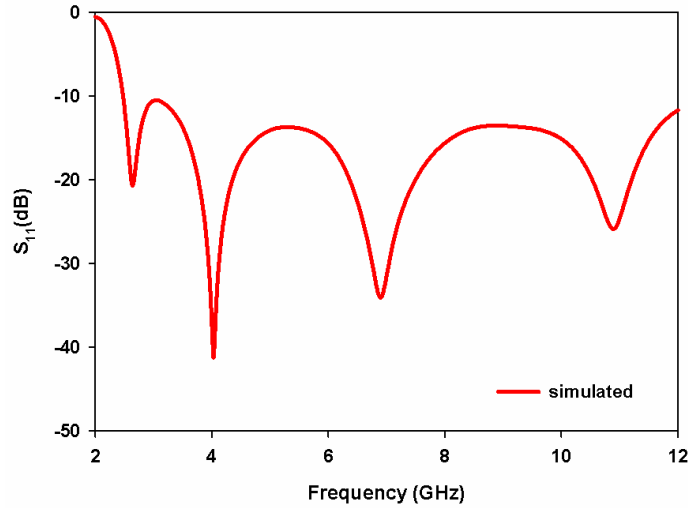
Fig. 5.10: Simulated S_{11} of the UWB slot antenna in Fig. 5.9. (L = 1.126λ_{gc}, W = 1.013λ_{gc}, L_r = 0.225λ_{gc}, W_r = 0.187λ_{gc}, L_b = 0.075λ_{gc}, L_f = 0.319λ_{gc}, L_0 = 0.818λ_{gc}, W_0 = 0.262λ_{gc}, L_1 = 0.15λ_{gc}, W_1 = 0.375λ_{gc}, L_2 = 0.412λ_{gc}, W_2 = 0.15λ_{gc}, L_3 = 0.255 λ_{gc}, W_3 = 0.112λ_{gc}, W_4 = 0.33λ_{gc}, L_4 = 0.082λ_{gc}, L_g = 0.307λ_{gc}, W_g = 0.437λ_{gc}, W_s = 0.713λ_{gc}, d = 0.262λ_{gc}, W_f = 3 mm, G =0.3 mm, α_r = 63°, α_g = 16.7°, h =1.6 mm, ε_r = 4.4)

Surface current distribution and radiation pattern:

Fig. 5.11 shows the simulated current distributions and 3D radiation patterns at four resonant frequencies. Simulated surface current distribution is very useful in the antenna design since it identifies the current path responsible for each resonant frequency within the impedance bandwidth of the antenna.
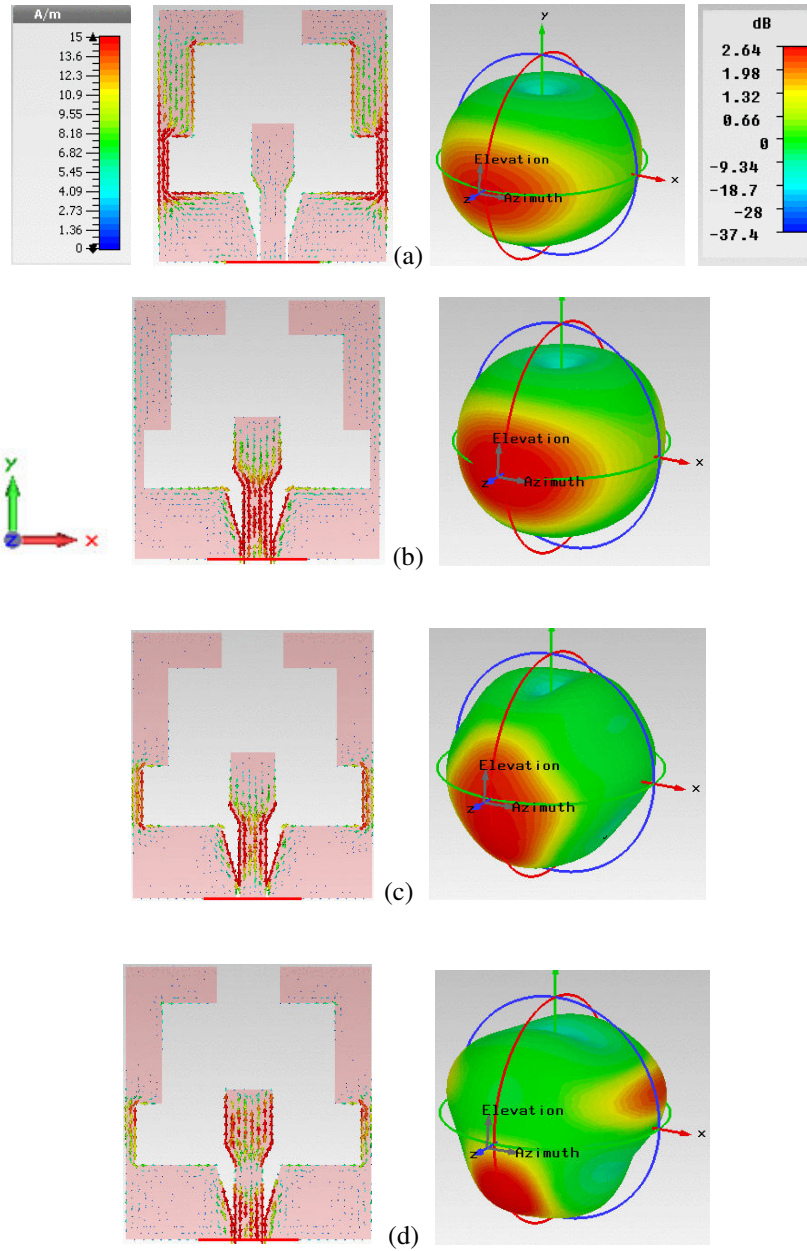
Fig. 5.11: Simulated surface current distribution and 3D radiation pattern at resonant frequencies (a) 2.6 GHz (b) 4 GHz (c) 6.9 GHz and (d) 10.7 GHz

Fig. 5.11 (a) shows that there is a half wavelength surface current variations along the extended ground. So the lowest resonance f_1 is due to this length. This occurs when the length

$$W_4 + L_3 + W_3 + L_2 + (W_1 - W_2) = \frac{\lambda_{g1}}{2} \quad \text{................. (5.1)}$$

where λ_{g1} is the wavelength inside the substrate at 2.6 GHz.

At second resonance, the current distribution in Fig. 5.11 (b) shows a quarter wavelength surface current variations on the bevelled rectangular strip. So the current path length which produces the second resonance f_2 is

$$\frac{L_b}{sin(\alpha_r)} + L_r + \frac{W_r}{2} = \frac{\lambda_{g2}}{4} \quad \text{.................................... (5.2)}$$

where λ_{g2} is the wavelength inside the substrate at 4 GHz.

For the third resonant frequency f_3, high current density present on both the strip and the extended ground simultaneously as in Fig. 5.11 (c). This indicates that the resonance is due to the combined effects of these two structures. Since these currents are in same direction there exists a strong coupling between the fields of these structures which in turn affect the resonant frequency. So the resonant frequency obtained not only depends on the current path lengths but also on the coupling between them.

In Fig. 5.11 (d), current present on the rectangular bevelled strip shows a half wavelength surface current variation; therefore the fourth resonance f_4 is related to the length

$$\frac{L_b}{sin(\alpha_r)} + L_r = \frac{\lambda_{g4}}{2} \quad \text{.. (5.3)}$$

where λ_{g4} is the wavelength inside the substrate at 10.7 GHz.

The expression for the guide wavelength λ_{gr} in terms of resonant frequency f_r given by [2]

$$\lambda_{gr} = \frac{c}{f_r\sqrt{\varepsilon_{re}}} \quad \text{.. (5.4)}$$

where c is the velocity of light and ε_{re} is the effective relative permittivity ($\varepsilon_{re} = \frac{\varepsilon_r + 1}{2}$)

The simulated 3D radiation patterns at different resonant frequencies are also shown along with the current distributions in Fig. 5.11. Compared with other UWB antennas in literature it produces nearly omnidirectional patterns even up to the upper limit of the operating band. From Fig. 5.11, for frequencies more than the centre frequency of the operating band, the direction of maximum radiation is observed along $\phi = 0^o$ in the azimuth plane. At the fourth resonance, the radiation maximum is shifted slightly from the bore sight and forms small radiation lobes in the xy-plane.

5.1.2.2 Parametric Analysis

Effects of various geometric parameters on the reflection coefficient characteristics of the proposed antenna are discussed here.

Effect of extended ground length (L_0):

From the surface current distribution shown in Fig. 5.11(a) and (c), it is evident that the first and the third resonant frequencies are influenced by the length of the extended ground, i.e., the resonant frequency decreases as the length increases.
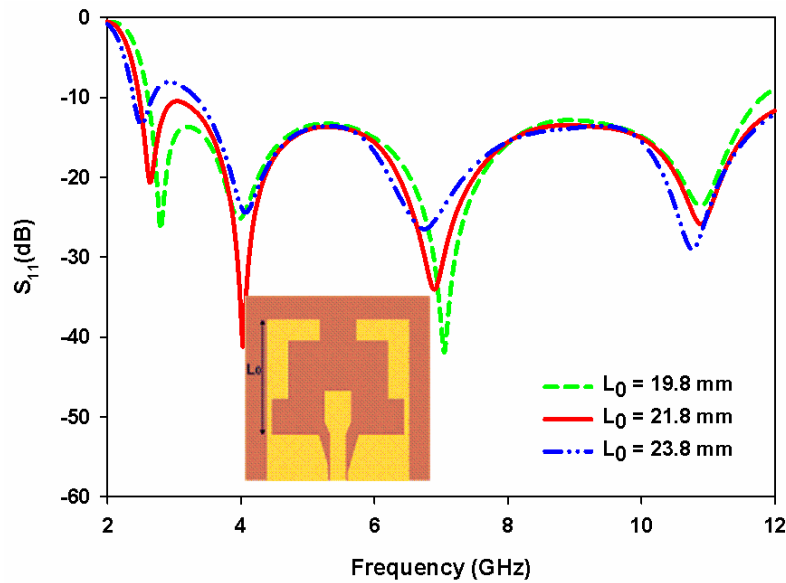

Fig. 5.12: **Effect of extended ground length L_0 on S_{11} (L = 1.126λ_{gc}, W = 1.013λ_{gc}, L_r = 0.225λ_{gc}, W_r = 0.187λ_{gc}, L_b = 0.075λ_{gc}, L_f = 0.319λ_{gc}, L_0 = 0.818λ_{gc}, W_0 = 0.262λ_{gc}, L_1 = 0.15λ_{gc}, W_1 = 0.375λ_{gc}, L_2 = 0.412λ_{gc}, W_2 = 0.15λ_{gc}, L_3 = 0.255 λ_{gc}, W_3 = 0.112λ_{gc}, W_4 = 0.33λ_{gc}, L_4 = 0.082λ_{gc}, L_g = 0.307λ_{gc}, W_g = 0.437λ_{gc}, W_s = 0.713λ_{gc}, d = 0.262λ_{gc}, W_f = 3 mm, G = 0.3 mm, α_r = 63°, α_g = 16.7^o, h =1.6 mm, ε_r = 4.4)**

Effect of extended ground length L_0 on the reflection coefficient is shown in Fig. 5.12. As the length L_0 increases first and third resonant frequencies decrease while the second and fourth resonant frequencies remain almost constant. The first resonant frequency can be calculated using (5.2) in which $L_3 + L_2 = L_0 - L_1$.

Effect of slot width (W_s):

Top end of the extended ground is folded to a length W_1 in order to decrease the first resonant frequency without increasing the overall size of the antenna. Now the structure can be approximated as a slot structure and the effect of widening the slot structure is studied and shown in Fig. 5.13. It is seen that the slot width W_s is an important parameter in determining the bandwidth of the antenna. For slot width W_s less than 15 mm the antenna doesn't cover the entire bandwidth because of the impedance mismatch over the frequency range from 4 GHz to 7 GHz. Similarly for slot width $W_s = 21\ mm$, the impedance match of the S_{11} characteristics drops at the lower band, unable to cover the entire UWB band. So the desired bandwidth performance is obtained for W_s = 19 mm $(0.713\lambda_{gc})$ which is considered as the optimum slot width.
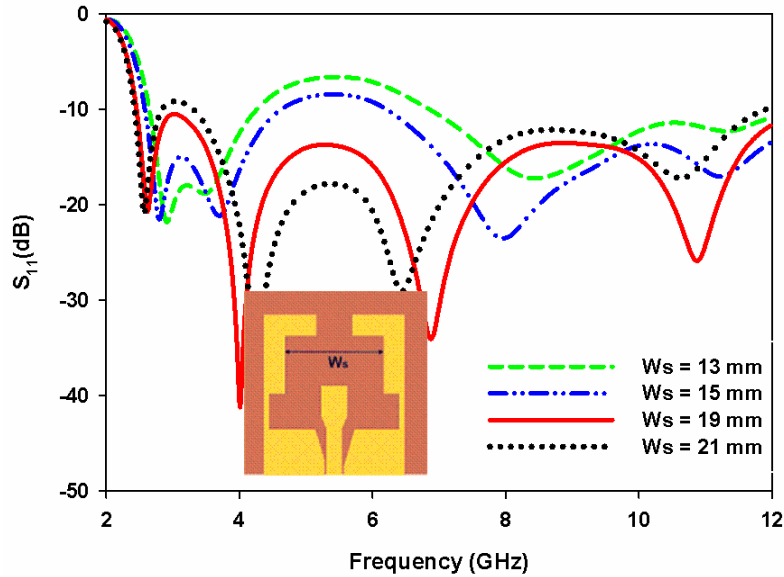
Fig. 5.13: Effect of slot width W_s on S_{11}, (L = 1.126λ_{gc}, W = 1.013λ_{gc},
L_r = 0.225λ_{gc}, W_r = 0.187λ_{gc}, L_b = 0.075λ_{gc}, L_f = 0.319λ_{gc},
L_0 = 0.818λ_{gc}, W_0 = 0.262λ_{gc}, L_1 = 0.15λ_{gc}, W_1 = 0.375λ_{gc},
L_2 = 0.412λ_{gc}, W_2 = 0.15λ_{gc}, L_3 = 0.255 λ_{gc}, W_3 = 0.112λ_{gc},
W_4 = 0.33λ_{gc}, L_4 = 0.082λ_{gc}, L_g = 0.307λ_{gc}, W_g = 0.437λ_{gc},
W_s = 0.713λ_{gc}, d = 0.262λ_{gc}, W_f = 3 mm, G = 0.3 mm, α_r = 63°,
α_g = 16.7°, h =1.6 mm, ε_r = 4.4)

As the slot width W_s varies all the resonant frequencies vary as shown Fig. 5.13. This structure supports two fundamental modes and their harmonics, one is due to the extended ground which acts as a slot structure and the other is due to the bevelled rectangular strip. In the evolution of the structure it is observed that there exists some sort of coupling between these modes which in turn influence the resonant frequencies. The amount of coupling depends on various factors such as slot width, direction and concentration of current present on the strip and the extended ground. So when the slot width W_s increases the first

and second resonances moves away due to variation in coupling between the modes. So the current path lengths at first, second and fourth resonances i.e., (5.1) to (5.3) are valid only for the optimum slot width $W_s = 0.713\lambda_{gc}$.

Effect of bevelled strip length (L_r):

Fig. 5.14 illustrates the effect of strip length L_r on the reflection coefficient characteristics. It is seen that as the strip length L_r increases the second and fourth resonances decrease while the first resonant frequency remains unchanged.
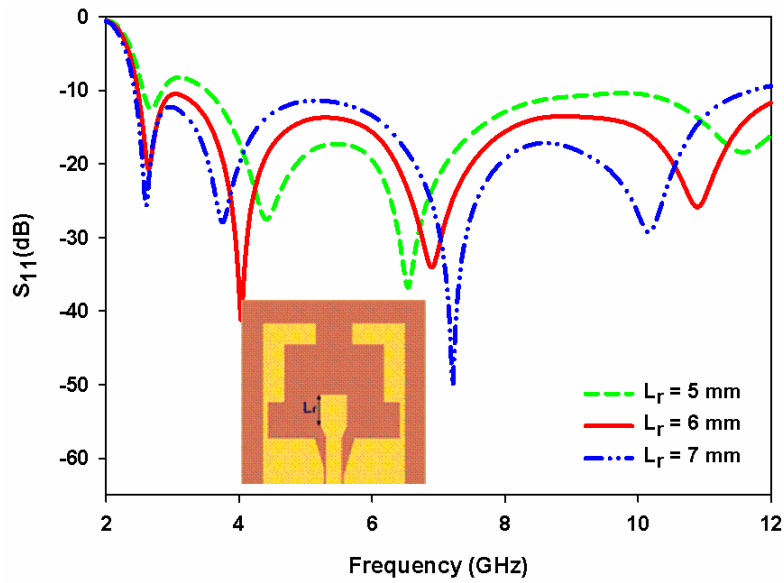
Fig. 5.14: Effect of patch length L_r on S_{11} (L = 1.126λ_{gc}, W = 1.013λ_{gc}, L_r = 0.225λ_{gc}, W_r = 0.187λ_{gc}, L_b = 0.075λ_{gc}, L_f = 0.319λ_{gc}, L_0 = 0.818λ_{gc}, W_0 = 0.262λ_{gc}, L_1 = 0.15λ_{gc}, W_1 = 0.375λ_{gc}, L_2 = 0.412λ_{gc}, W_2 = 0.15λ_{gc}, L_3 = 0.255 λ_{gc}, W_3 = 0.112λ_{gc}, W_4 = 0.33λ_{gc}, L_4 = 0.082λ_{gc}, L_g = 0.307λ_{gc}, W_g = 0.437λ_{gc}, W_s = 0.713λ_{gc}, d = 0.262λ_{gc}, W_f = 3 mm, G = 0.3 mm, α_r = 63°, α_g = 16.7°, h =1.6 mm, ε_r = 4.4)

It indicates that both the second and fourth resonances are controlled by the strip length but in different proportion because the path length of current distribution is quarter wavelength for second resonance and half wavelength for the fourth resonance. The observed results agree well with the surface current distributions shown in Fig. 5.11 (b) and (d). From Fig. 5.14, it is observed that as the strip length L_r increases impedance match over the lower and upper portions of the frequency band improves while over the middle portion degrades. So the dimension L_r is optimized to 6 mm.

The current pattern in Fig. 5.11(c) shows that the third resonance results from the combined effect of extended ground length and the strip length. From Fig. 5.14, it is seen that as the strip length L_r increases the third resonance moves away from the second resonance due to increase in coupling area between the strip and extended ground

Effect of the slit width (W_3):

The effects of the slit width W_3 on the lower resonances are shown in Fig. 5.15. When $W_3 = 0$, i.e., slits are not present, the lowest resonant frequency is 3.65 GHz and the curve exhibits high impedance mismatch over the entire frequency range. As the width W_3 increases, this frequency splits into two slightly different frequencies and start to move apart resulting in first (2.7 GHz) and second (4.0 GHz) resonances when $W_3 = 3 \, mm$.
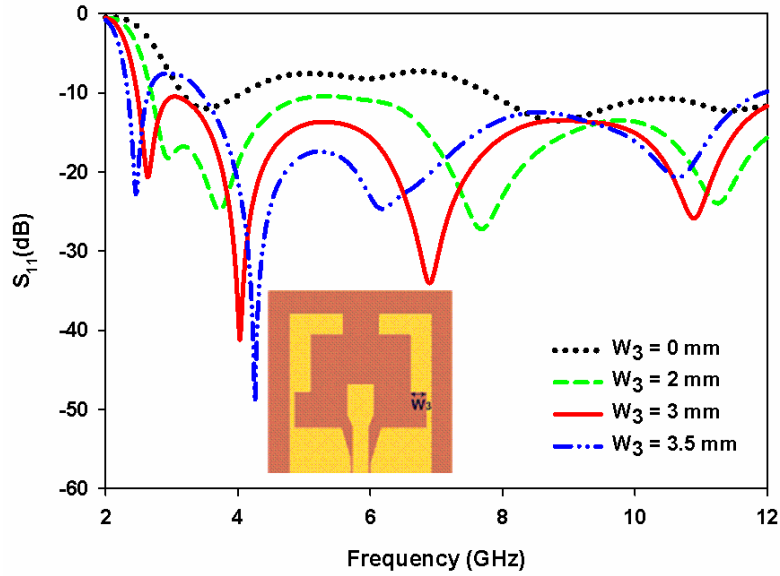
Fig. 5.15: Effect of slit width W_3 on S_{11}, (L = $1.126\lambda_{gc}$, W = $1.013\lambda_{gc}$, L_r = $0.225\lambda_{gc}$, W_r = $0.187\lambda_{gc}$, L_b = $0.075\lambda_{gc}$, L_f = $0.319\lambda_{gc}$, L_0 = $0.818\lambda_{gc}$, W_0 = $0.262\lambda_{gc}$, L_1 = $0.15\lambda_{gc}$, W_1 = $0.375\lambda_{gc}$, L_2 = $0.412\lambda_{gc}$, W_2 = $0.15\lambda_{gc}$, L_3 = 0.255 λ_{gc}, W_3 = $0.112\lambda_{gc}$, W_4 = $0.33\lambda_{gc}$, L_4 = $0.082\lambda_{gc}$, L_g = $0.307\lambda_{gc}$, W_g = $0.437\lambda_{gc}$, W_s = $0.713\lambda_{gc}$, d = $0.262\lambda_{gc}$, W_f = 3 mm, G = 0.3 mm, α_r = 63°, α_g = 16.7°, h =1.6 mm, ε_r = 4.4)

On comparing Fig. 5.13 and Fig. 5.15, the resonant frequencies behave in the same manner as the either W_s or W_3 varies. This indicates that same phenomenon is involved in both the cases. Now the characteristic curve possesses the required impedance matching of $S_{11} < -10 dB$ over the entire operating band. Even though increase in W_3 decreases the lower resonance, it is observed that the width $W_3 = 3.5\ mm$ results in an impedance mismatch at lower frequency region and hence reduces the bandwidth of the antenna. So $W_3 = 3\ mm$ $(0.112\lambda_{gc})$ is taken as optimum dimension.

Fig. 5.16 (a) and (b) show the input impedance behavior of the antenna structure with and without slits on the extended ground plane.
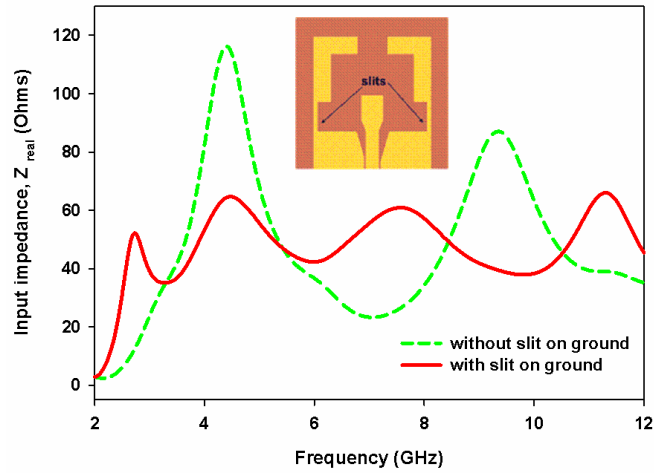
(a)
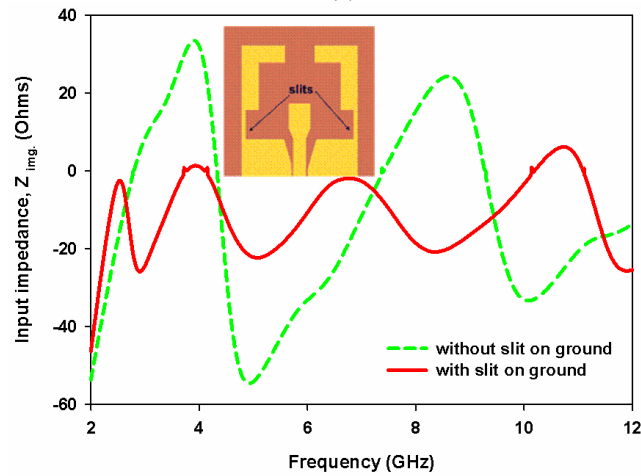
(b)

Fig. 5.16: Simulated input impedance of the antenna with and without slits on ground plane (a) real component and (b) imaginary component

It is found that these slits are actually acting as impedance matching elements for the antenna structure by eliminating sharp variations in

real and imaginary input impedances. Thus forms a major component in determining the operating bandwidth of the proposed antenna.

Effect of the bevelling angle (α_g):

Effects of bevelling angle α_g on the reflection coefficient characteristics are shown in Fig. 5.17. It is observed that the bevelling angle (α_g) on the ground plane has significant effect on the impedance match of the antenna. Without bevelling the S_{11} characteristics exhibits poor impedance match as shown in Fig. 5.17.
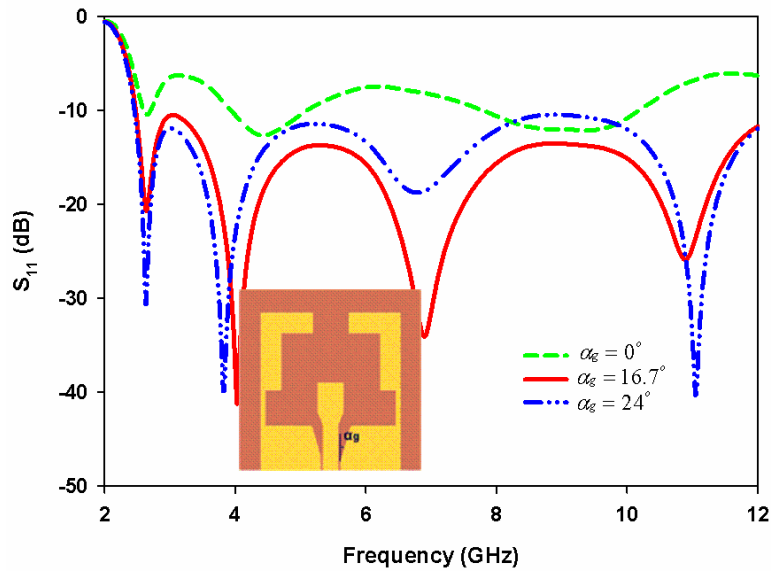
Fig. 5.17: **Effect of bevelling angle α_g on S_{11}, (L = 1.126λ_{gc}, W = 1.013λ_{gc}, L$_r$ = 0.225λ_{gc}, W$_r$ = 0.187λ_{gc}, L$_b$ = 0.075λ_{gc}, L$_f$ = 0.319λ_{gc}, L$_0$ = 0.818λ_{gc}, W$_0$ = 0.262λ_{gc}, L$_1$ = 0.15λ_{gc}, W$_1$ = 0.375λ_{gc}, L$_2$ = 0.412λ_{gc}, W$_2$ = 0.15λ_{gc}, L$_3$ = 0.255 λ_{gc}, W$_3$ = 0.112λ_{gc}, W$_4$ = 0.33λ_{gc}, L$_4$ = 0.082λ_{gc}, L$_g$ = 0.307λ_{gc}, W$_g$ = 0.437λ_{gc}, W$_s$ = 0.713λ_{gc}, d = 0.262λ_{gc}, W$_f$ = 3 mm, G = 0.3 mm, α$_r$ = 63°, α$_g$ = 16.7°, h =1.6 mm, ε$_r$ = 4.4)**

Improved impedance match over the entire band is obtained as the bevelling angle α_g increases and the optimum response is obtained for $\alpha_g = 16.7^o$.
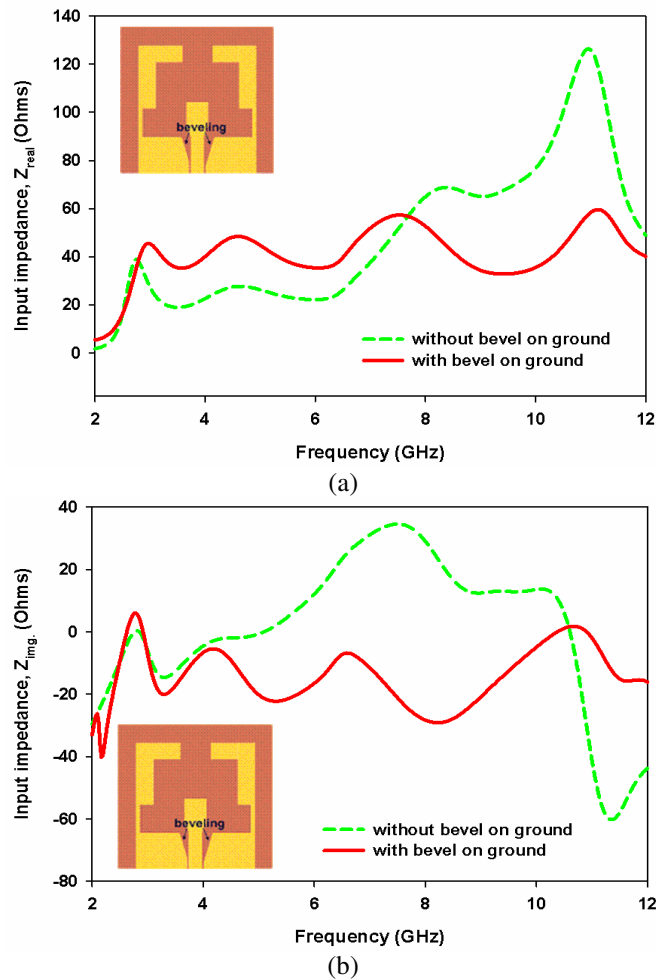

(a)

(b)

Fig. 5.18: Simulated input impedance of the antenna with and without bevels on ground plane (a) real component and (b) imaginary component

Meanwhile, these bevels act as an impedance matching element to control the impedance bandwidth of the proposed antenna. From the

impedance plots in Fig. 5.18 (a) and (b), it is clear that the bevels reduce drastic variations in real and imaginary components of input impedance of the proposed antenna respectively. Thus the bevels play a key role in determining the operating bandwidth of the antenna.

Effect of substrate height (h) *and relative permittivity* (ε_r)**:**

Fig. 5.19 shows the effect of substrate height h on the reflection coefficient characteristics of the antenna. For substrate height from 0.5 mm to 1.6 mm, the antenna exhibits ultra-wide band response.   For height more than 1.6 mm impedance match of the antenna degrades and loses the ultra-wide band response.
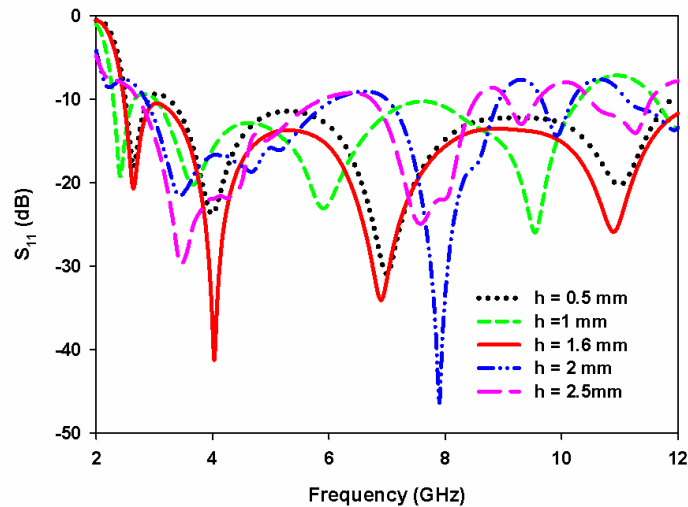

**Fig. 5.19: Effect of substrate height h on S_{11}. (L = $1.126\lambda_{gc}$,
W = $1.013\lambda_{gc}$, L_r = $0.225\lambda_{gc}$, W_r = $0.187\lambda_{gc}$, L_b = $0.075\lambda_{gc}$,
L_f = $0.319\lambda_{gc}$, L_0 = $0.818\lambda_{gc}$, W_0 = $0.262\lambda_{gc}$, L_1 = $0.15\lambda_{gc}$,
W_1 = $0.375\lambda_{gc}$, L_2 = $0.412\lambda_{gc}$, W_2 = $0.15\lambda_{gc}$, L_3 = $0.255 \lambda_{gc}$,
W_3 = $0.112\lambda_{gc}$, W_4 = $0.33\lambda_{gc}$, L_4 = $0.082\lambda_{gc}$, L_g = $0.307\lambda_{gc}$,
W_g = $0.437\lambda_{gc}$, W_s = $0.713\lambda_{gc}$, d = $0.262\lambda_{gc}$, W_f = 3 mm,
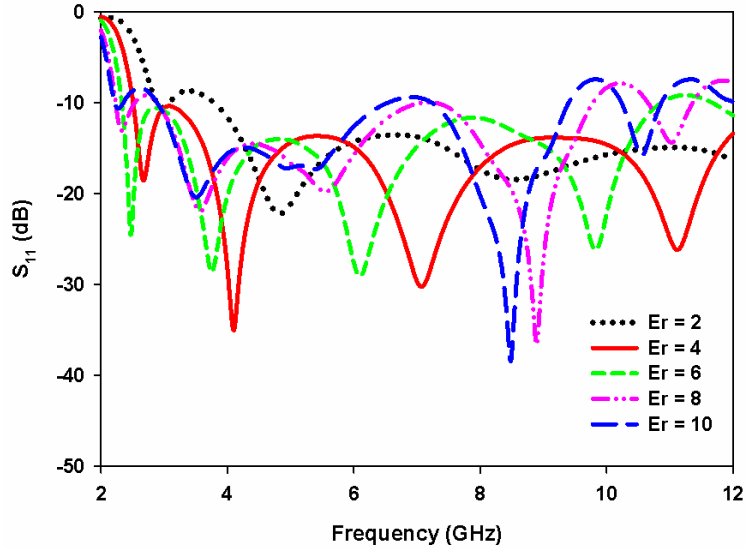G = 0.3 mm, α_r = 63°, α_g = 16.7^o, ε_r = 4.4)**

Fig. 5.20: **Effect of relative permittivity ε_r on S_{11}. (L = 1.126λ_{gc}, W = 1.013λ_{gc}, L$_r$ = 0.225λ_{gc}, W$_r$ = 0.187λ_{gc}, L$_b$ = 0.075λ_{gc}, L$_f$ = 0.319λ_{gc}, L$_0$ = 0.818λ_{gc}, W$_0$ = 0.262λ_{gc}, L$_1$ = 0.15λ_{gc}, W$_1$ = 0.375λ_{gc}, L$_2$ = 0.412λ_{gc}, W$_2$ = 0.15λ_{gc}, L$_3$ = 0.255 λ_{gc}, W$_3$ = 0.112λ_{gc}, W$_4$ = 0.33λ_{gc}, L$_4$ = 0.082λ_{gc}, L$_g$ = 0.307λ_{gc}, W$_g$ = 0.437λ_{gc}, W$_s$ = 0.713λ_{gc}, d = 0.262λ_{gc}, W$_f$ = 3 mm, G = 0.3 mm, α$_r$ = 63°, α$_g$ = 16.7°, h =1.6 mm)**

From Fig. 5.20, it is observed that as the relative permittivity ε_r increases the lower resonant frequency decreases, so the operational bandwidth shifted towards lower frequencies. Moreover, the antenna can maintain its impedance match response for a variation in the relative permittivity from 4 to 6.

5.1.2.3 Design

Based on the above observations the design criterion for the UWB antenna is developed and discussed in the next section. Design procedures for the proposed UWB antenna on any substrates are summarised as follows

- Design a 50-Ω CPW line on a substrate with permittivity ε_r and thickness h

- Calculate the effective relative permittivity for CPW line using

  $$\varepsilon_{re} = \frac{\varepsilon_r + 1}{2}$$

For calculating the dimension of each section of the structure, the centre frequency f_c of the operating band is considered.

- Calculate the guide wavelength λ_{gc} corresponding to the centre frequency f_c.

- The first resonant frequency is determined by the extended ground length as in (5.1).

  Here, a rectangular ground of size $W x L_4$ is extended to a length L_0 as shown in Fig. 5.5 (a) with width W_2 and then folded to a length W_1 with width L_1.

  $$L_4 = 0.307 \, \lambda_{gc} \quad\text{... (5.5)}$$

  $$W = 1.013 \, \lambda_{gc} \quad\text{... (5.6)}$$

  $$L_0 = 0.818 \, \lambda_{gc} \quad\text{.. (5.7)}$$

  $$W_2 = L_1 = 0.15 \, \lambda_{gc} \quad\text{.. (5.8)}$$

  $$W_1 = 0.375 \, \lambda_{gc} \quad\text{... (5.9)}$$

- Insert slits on the extended ground as shown in Fig. 5.7 (a)

  $$L_3 = 0.255 \, \lambda_{gc} \quad\text{.. (5.10)}$$

$$W_3 = 0.112\ \lambda_{gc} \text{...} (5.11)$$

▪ Taper the ground plane corners near the feed point as shown in Fig. 5.9 (a)

$$W_4 = 0.33\ \lambda_{gc} \text{...} (5.12)$$

$$L_5 = 0.082\ \lambda_{gc} \text{..} (5.13)$$

▪ The second and fourth resonances are determined by the length of the bevelled rectangular strip as per (5.2) and (5.3)

Bevelled rectangular strip with CPW feed line:

$$L_r = 0.225\ \lambda_{gc} \text{..} (5.14)$$

$$L_b = 0.075\ \lambda_{gc} \text{..} (5.15)$$

$$W_r = 0.187\ \lambda_{gc} \text{..} (5.16)$$

$$L_f = 0.319\ \lambda_{gc} \text{..} ((5.17)$$

Table 5.1: Description of substrates

Parameters	Rogers 5880	FR4 Epoxy	Rogers RO3006	Rogers 6010LM
h (mm)	1.57	1.6	1.28	0.635
ε_r	2.2	4.4	6.15	10.2
ε_{eff}	1.6	2.7	3.575	5.6
W_f(mm)	4	3	2.58	2.05
G(mm)	0.17	0.35	0.45	0.5

The antenna structure is simulated on different substrates as listed in Table 5.1 with parameters calculated using the above design equations. Fig. 5.21 shows the S_{11} characteristics obtained for different

substrates. From Fig. 5.21 as the substrates changes, the resonant frequencies vary slightly, but exhibit broad impedance bandwidth response, thus validating the design equations.
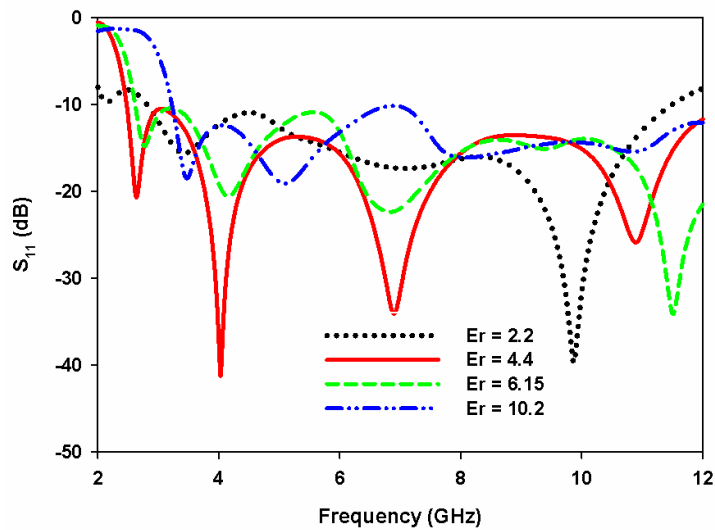

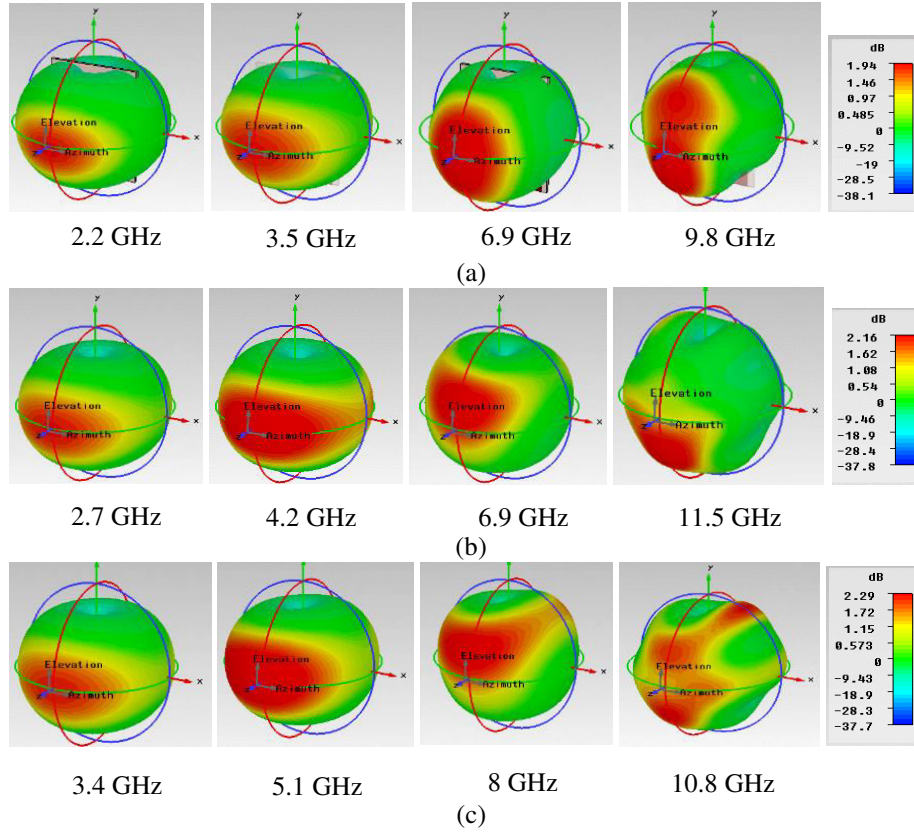**Fig. 5.21: Simulated S_{11} of UWB slot antenna with different substrates.**

Simulated radiation patterns at resonant frequencies of the antennas on different substrates with relative permittivity 2.2, 6.15 and 10.2 are shown in Fig. 5.22 (a) – (c) respectively. It is observed that the maximum radiations for all the antennas are in z-direction over the entire operating bandwidth, indicating that the proposed antenna is characterised by wide pattern bandwidth performance.

Fig. 5.22: Radiation patterns at resonant frequencies of the antennas on different substrates with relative permittivity (a) 2.2 (b) 6.15 and (c) 10.2.

5.2 Dual Band-notched Slot Antenna

Two compact band-reject elements are employed to realise dual band-notched characteristics in planar UWB slot antenna. A meandered line (Z-shaped) parasitic element placed in the radiating aperture of the antenna suppresses the radiation at WiMAX band (3.3 - 3.6 GHz). The meandered structure is actually a microstrip line folded back and forth to lower its resonant frequency with miniaturised size [3]. This requires less

space for implementation compared to the other designs using parasitic strips that are straight and have length comparable to the radiating aperture. A pair of symmetric L-shaped quarter-wavelength stubs attached to the upper edge of the ground plane eliminates the WLAN band (5.2 - 5.75 GHz) effectively. This approach is very efficient for dual/multiple band-notched design as it has the advantage of controlling both the centre frequency and the bandwidth of the each notched-band independently by adjusting the parameters of the corresponding notch structures. The geometry and photograph of the dual band-notched antenna are shown in Fig. 5.23.
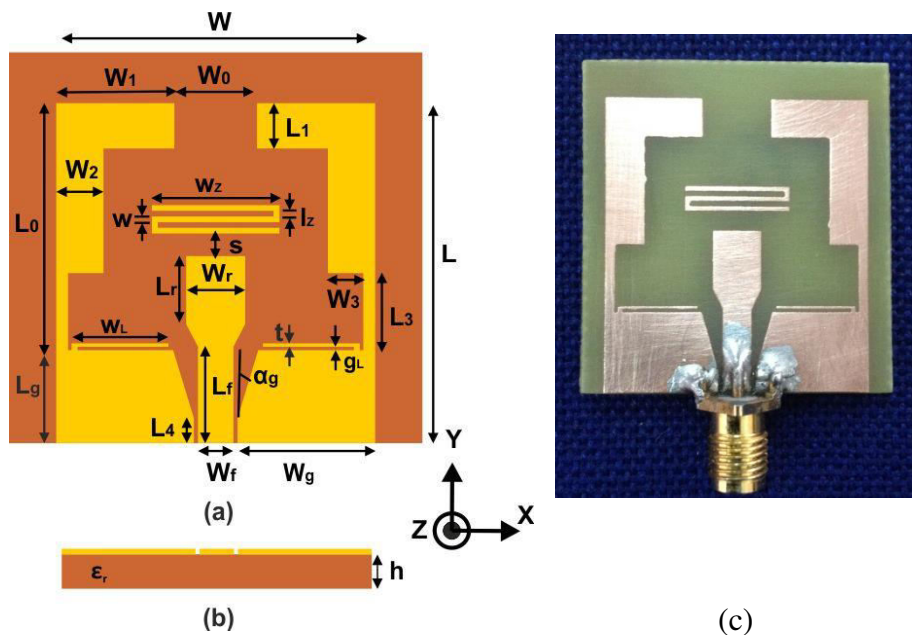
Fig. 5.23: Geometry of the dual band-notched antenna (a) top view (b) side view and (c) photograph. (Z-shaped parasitic element: l_Z = 0.5 mm, w_Z = 0.203λ_{n1}, w = 0.5 mm, s = 2 mm; L-shaped stub: w_L = 0.243λ_{n2}, g_L = 0.3 mm, t = 0.3mm; where λ_{n1} and λ_{n2} are the guide wavelength corresponding to the notch frequencies)

5.2.1 Simulation and Parametric Analysis

5.2.1.1 Simulation

Reflection coefficient:

Fig. 5.24 shows the simulated S_{11}characteristics of the UWB antenna with band-notched elements inserted in it. The impedance bandwidth extends from 2.5 GHz to 11.8 GHz with two rejection bands at 3.3 - 3.6 GHz and 5.2 - 5.75 GHz. Similar to UWB slot antenna, the S_{11} response of band-notched structure also exhibits resonances at 2.6 GHz, 4 GHz, 7 GHz and 10.7 GHz within the operating band.
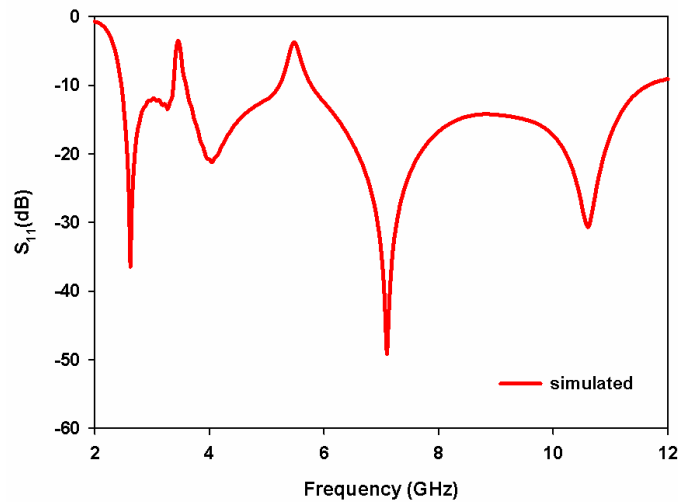

Fig. 5.24: Simulated S_{11} of the dual band-notched UWB slot antenna in Fig. 5.23 (Z-shaped parasitic element: l_Z = 0.5 mm, w_Z = 0.203λ_{n1}, w = 0.5 mm, s = 2 mm; L-shaped stub: w_L= 0.243λ_{n2}, g_L = 0.3 mm, t = 0.3mm)

Radiation pattern and Surface current distribution:

The 3D radiation patterns of dual band-notched antenna at four resonant frequencies are similar to the patterns of the UWB slot antenna and are shown in Fig. 5.25 (a) to (d).
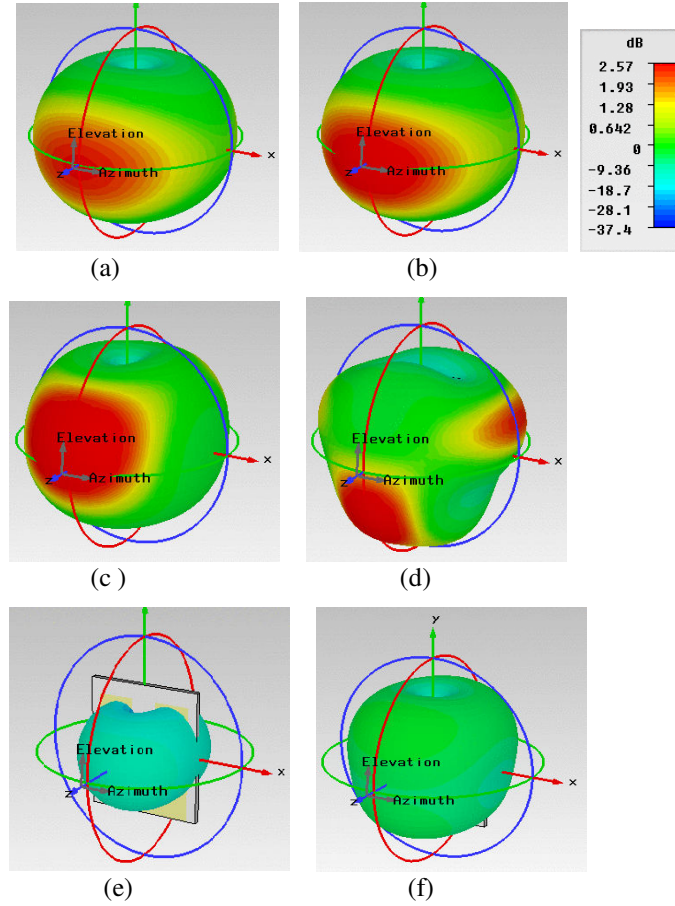
Fig. 5.25: Simulated 3D radiation pattern of the dual band-notched antenna (a) 2.6 GHz (b) 4 GHz (c) 7 GHz (d) 10.7 GHz (e) 3.44 GHz and (f) 5.42 GHz

To study the capability of the notch structures to reject the unwanted bands, radiation pattern at the centre frequencies of WiMAX band ($f_{n1} = 3.44\ GHz$) and WLAN band ($f_{n2} = 5.42\ GHz$) are plotted. From Fig. 5.25 (e) and (f), it is seen that the radiations along all the directions are much reduced w.r.t. the radiation at other resonant frequencies which reveals that the notch structures used are very efficient.

Fig. 5.26 (a) and (b) show the surface current distribution at 3.44 GHz and 5.42 GHz respectively. At the notch frequencies the current is concentrated on the respective notch structures. It is also observed that the current is not present on any portion/part of the antenna, which means antenna does not radiate at these frequencies.

The Z-shaped meandered structure and its parameters are described in Fig. 5.23 (a). At 3.44 GHz, the current is present on the Z-shaped meandered structure alone as in Fig. 5.26(a). Since the spacing between the horizontal strips is small, current on the horizontal strips dominates more compared to that on the vertical strips and are in opposite phase between adjacent horizontal strips. Hence these currents do not contribute much to the radiation. The resonant frequency of a meander line is given by the expression $f_r = \frac{1}{2\pi\sqrt{LC}}$; where L and C are the equivalent inductance and capacitance of the meandered line. The values of L and C depend on the parameters of the meander line [4] - [5].

At 5.42 GHz, the surface current is present not only in the L-shaped stubs but also in the upper edge of the ground plane as shown in Figure 5.26 (b). It is clear that the current present on the upper edge of the ground plane is actually the mirror image of that in the stubs, i.e., these two currents are in opposite phase. These currents do not contribute to the radiation, as done for the Z-shaped meandered structure.
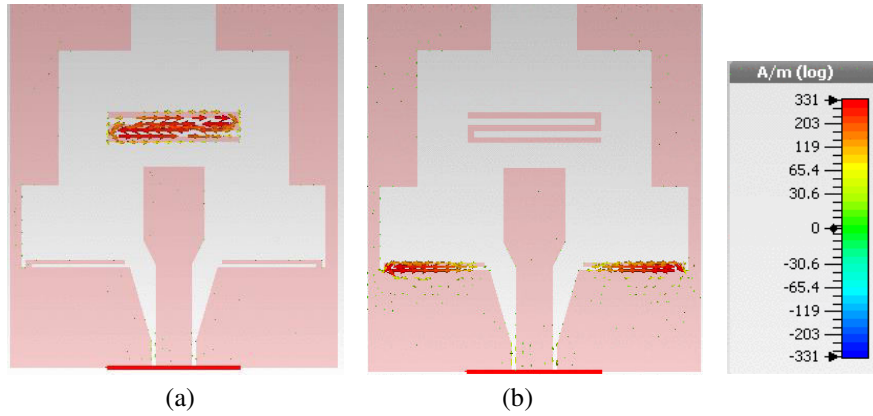
(a)   (b)

Fig. 5.26: Surface current distribution at notch frequencies (a) 3.44 GHz and (b) 5.42 GHz

Here, the L-shaped stub acts as a quarter-wavelength resonator and its approximate length l_{LE} is given by the expression:

$$l_{LE} = \frac{\lambda_{02}}{4\sqrt{\frac{\varepsilon_r+1}{2}}} = \frac{\lambda_{n2}}{4} \quad \dots\dots\dots\dots\dots\dots\dots\dots\dots\dots\dots\dots \text{ (5.18)}$$

where $l_{LE} = (w_L - t) + g_L$; t is the thickness of L-shaped stub ($t = 0.3\,mm$) and λ_{02} is the free space wavelength at the notch frequency f_{n2}.

5.2.1.2 Parametric Analysis

Z-shaped parasitic element - Effects of horizontal strip length (w_Z) and vertical strip length(l_Z):

Fig. 5.27 (a) and (b) illustrate the effect of horizontal strip length w_Z and vertical strip length l_Z on S_{11} characteristics of the antenna respectively.
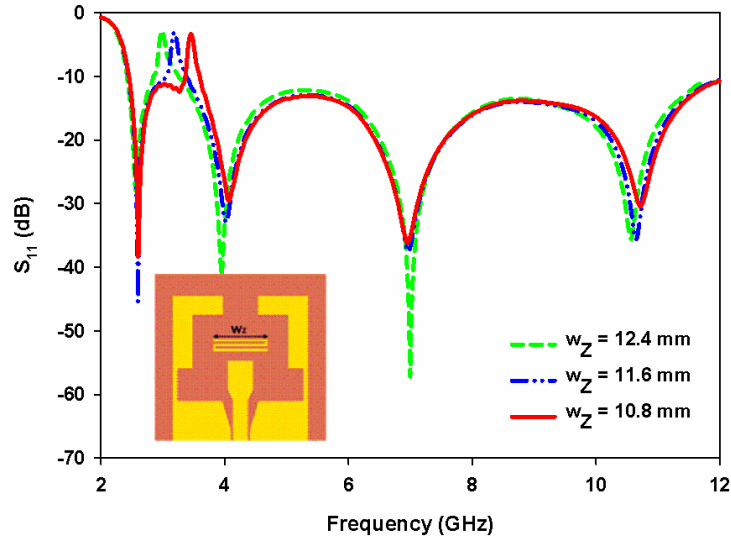
(a)
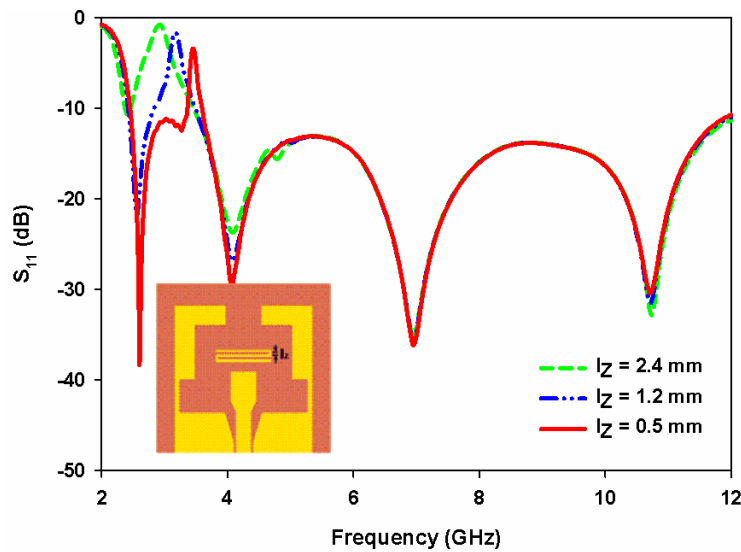
(b)

Fig. 5.27: **Effects of (a) horizontal strip length w_Z and (b) vertical strip length l_Z of Z-shaped parasitic on S_{11} of the single band-notched UWB antenna ($l_Z = 0.5$ mm, $w_Z = 0.203\lambda_{n1}$, w = 0.5 mm)**

It is observed that increasing either w_Z or l_Z decreases the notch frequency (WiMAX) because the inductance increases as the length of

the strip increases. Another important parameter of a meander line is the strip width (w); narrow strip width offers high inductance which in turn lowers the notch frequency again. Therefore, length of the strip required to obtain a given notch frequency can be reduced by using narrow strips, which provides a compact notch structure for WiMAX band. Considering these factors the strip width (w) is chosen as 0.5 mm.

In Fig. 5.27 (b), a significant reduction in notched bandwidth is observed with decreasing l_Z. When l_Z decreases the spacing between the horizontal strips of the meandered structure also decreases. Thus the effective parallel-plate capacitance increases and results in narrowing of rejected bandwidth. From Fig. 5.27 (b), the required notch response is obtained for l_Z = 0.5 mm. After exhaustive simulation studies, with $w = l_Z$ the length of the horizontal strip is given by an empirical expression:

$$w_Z = \frac{0.2\,\lambda_{01}}{\sqrt{\frac{\varepsilon_r+1}{2}}} = 0.2\,\lambda_{n1} \dots\dots\dots (5.19)$$

where λ_{01} is the free space wavelength at the designed notch frequency $f_{n1.}$ From Fig. 5.27 (a), it is found that the desired notch response at WiMAX is attained for $w_Z = 10.8\,mm$.

L-shaped stubs - Effects of horizontal strip length (w_L) and the gap (g_L):

Effects of horizontal strip length w_L and the gap g_L of the L-shaped stub on S_{11} characteristics are described in Fig. 5.28 (a) and (b) respectively. In both the cases, as either w_L or g_L decreases, the notch frequency (WLAN) increases without disturbing the S_{11}

characteristics of the single band- notched UWB antenna discussed in the previous section .
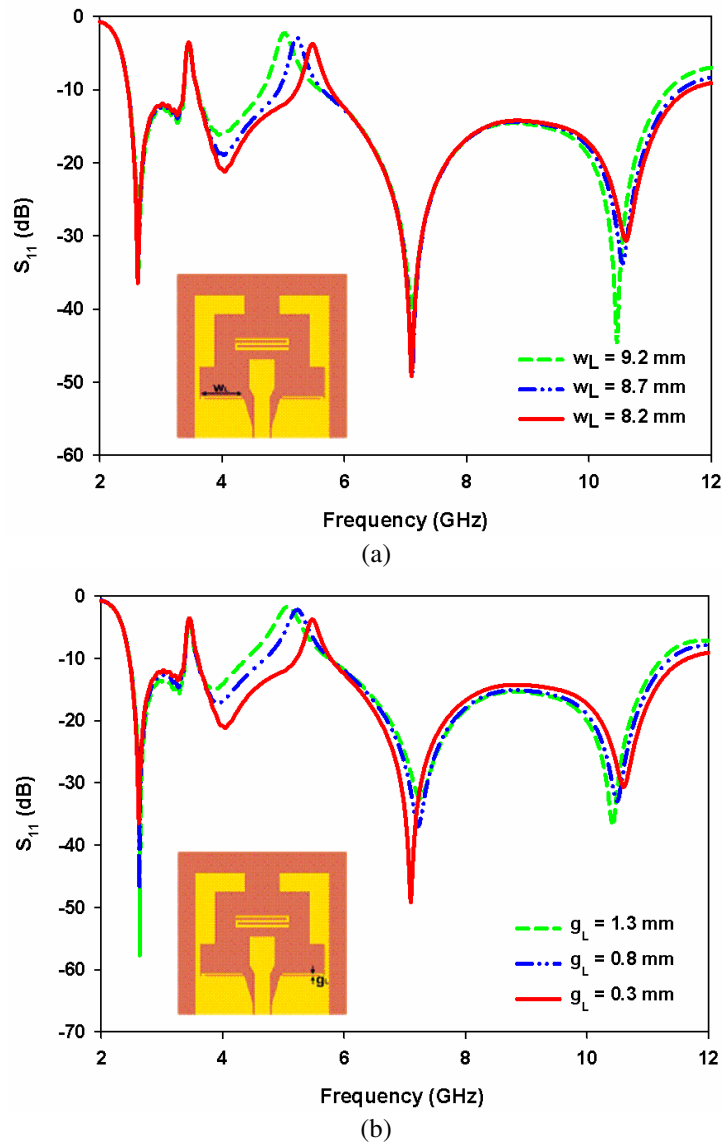

(a)

(b)

Fig. 5.28: Effects of (a) horizontal strip length w_L and (b) gap g_L of L-shaped stub on S_{11} of the proposed antenna (l_Z = 0.5 mm, $w_Z = 0.203\lambda_{n1}$, w = 0.5 mm, s = 2 mm, $w_L= 0.243\lambda_{n2}$, g_L = 0.3 mm, t = 0.3mm)

Fig. 5.28 (b) reveals that the notched (WLAN) bandwidth is mainly determined by the parameter g_L which is actually the spacing between the horizontal strip of L-shaped stub and upper edge of the ground plane. Here, the notched bandwidth decreases as the parameter g_L decreases because of parallel-plate capacitance effect. Fig. 5.28 (a) and (b) show that by choosing $g_L = 0.3\ mm$ and $w_L = 8.2\ mm$, the required notch response at WLAN band can be achieved.

The simulated S_{11} confirm that Z-shaped meandered parasitic element and the L-shaped quarter wavelength stubs operate independently and have little effect on each other. Hence, offers great flexibility in the design of each notched band.

5.3 Transient Analysis

Antenna transfer functions in azimuth and elevation planes obtained from the CST simulations are described in Fig. 5.29 and Fig. 5.30. Transfer function and radiation patterns are two important parameters of UWB antenna. These two parameters are related and from the transfer function it is easy to analyse the distribution of the radiation pattern of the antenna at different frequencies.

Antenna transfer function H(jω):

From Fig. 5.29 (a) it is clear that the antenna possesses nearly non-directional pattern in the azimuth plane over the entire operating bandwidth. For frequencies around 8 GHz, there is a slight reduction in radiation level at angles around 90° and 270°. Transfer function of the dual band-notched antenna is shown in Fig. 5.29 (b) is similar to that in

Fig. 5.29 (a) with sharp reduction in intensity at 3.44 GHz and 5.42 GHz. Fig. 5.29 (b) also shows that these frequencies are effectively notched for all the orientation of the antenna in the azimuth plane.
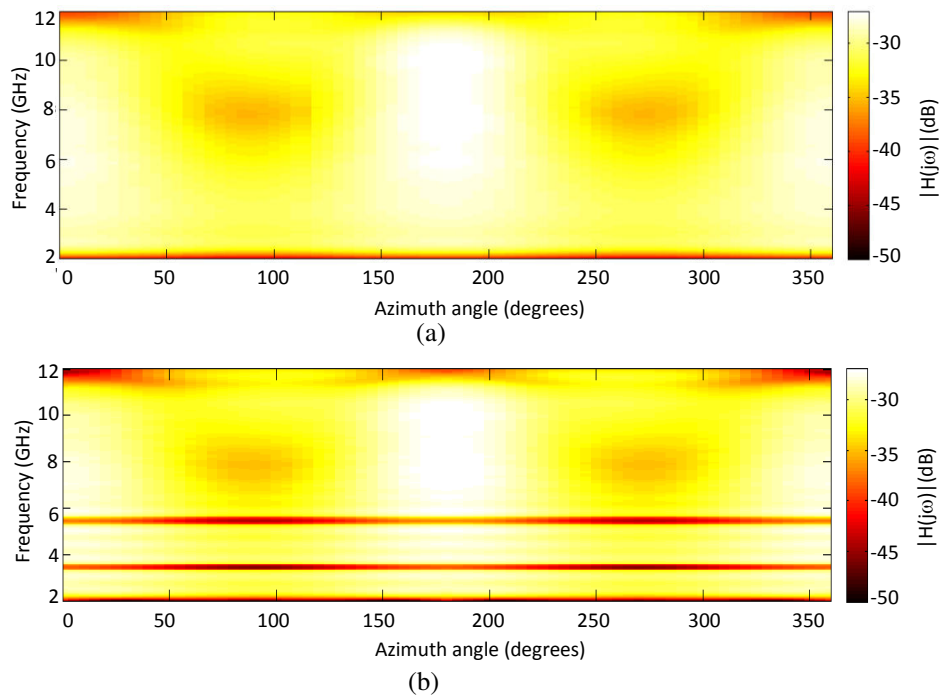

Fig. 5.29: Magnitude of simulated antenna transfer function H($j\omega$) in the azimuth plane (a) UWB antenna and (b) dual band-notched UWB antenna.

Fig. 5.30 (a) and (b) illustrates the transfer function in elevation plane. Black portions in the plots represent the nulls at 90° and 270° of the 'figure of eight pattern' of the antenna in this plane. Notch bands are visible in Fig. 5.30 (b) but not too sharp as in that of Fig. 5.29 (b). Further the transfer function in the elevation plane has more distortion in the vicinity of 90° and 270°.
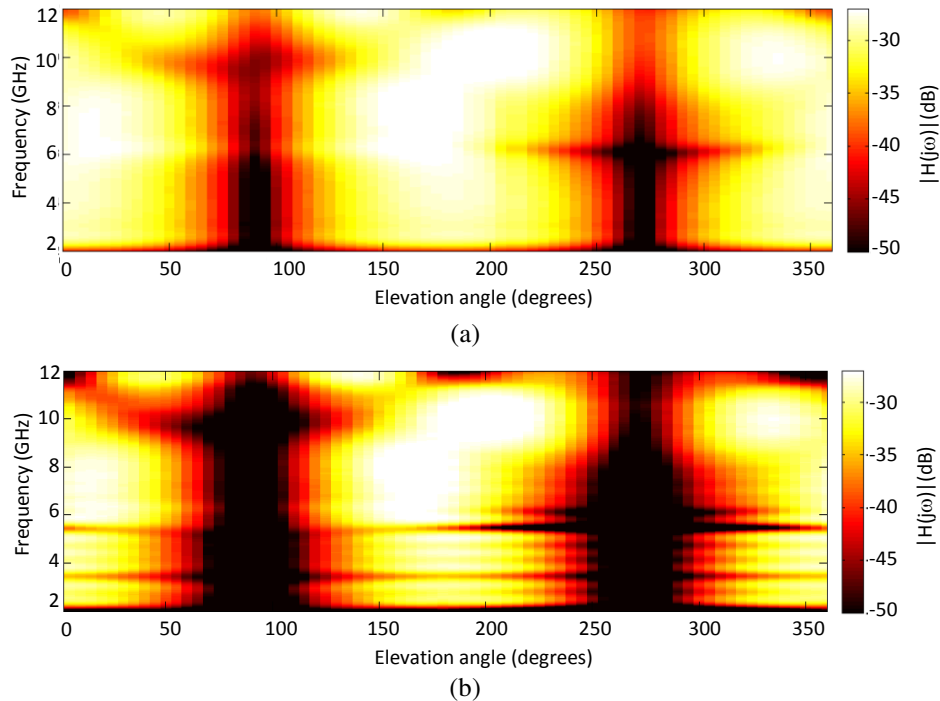
(a)

(b)

Fig. 5.30: Magnitude of simulated antenna transfer function H($j\omega$) in the elevation plane (a) UWB antenna and (b) dual band-notched UWB antenna.

Gain response:

Fig. 5.31 shows the gain of the antenna calculated from the transfer function using (3.19) in Chapter 3. From Fig. 5.31 (a), it is seen that the antenna has flat gain response over the entire operating frequency for all the orientations in the azimuth plane. A sharp reduction in gain is observed at 3.44 GHz and 5.42 GHz in Fig. 5.31 (b) account for the satisfactory rejection of these frequencies.
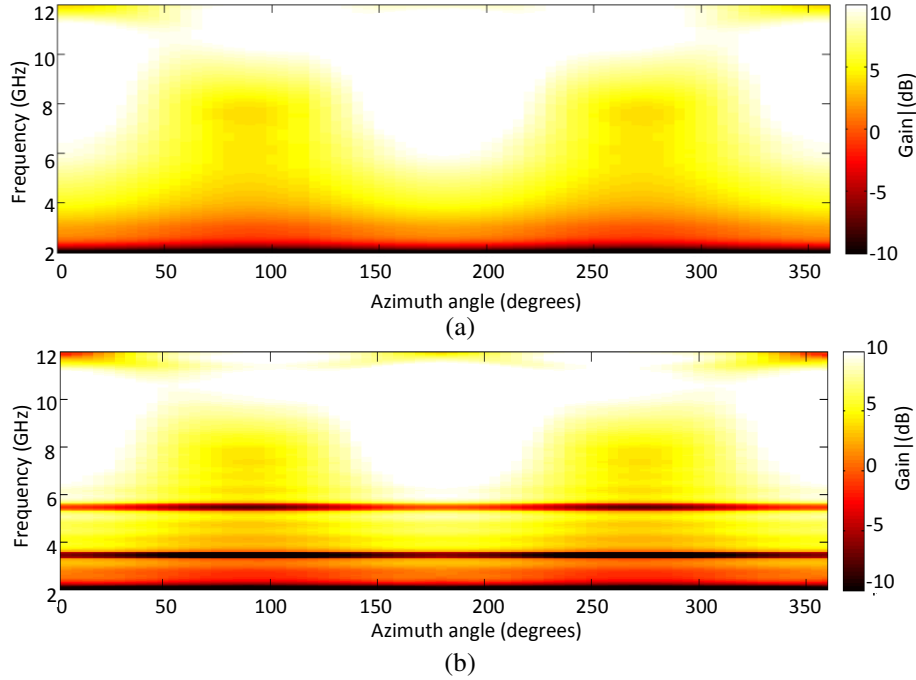
Fig. 5.31: Simulated gain in the azimuth plane (a) UWB antenna and (b) dual band-notched UWB antenna.
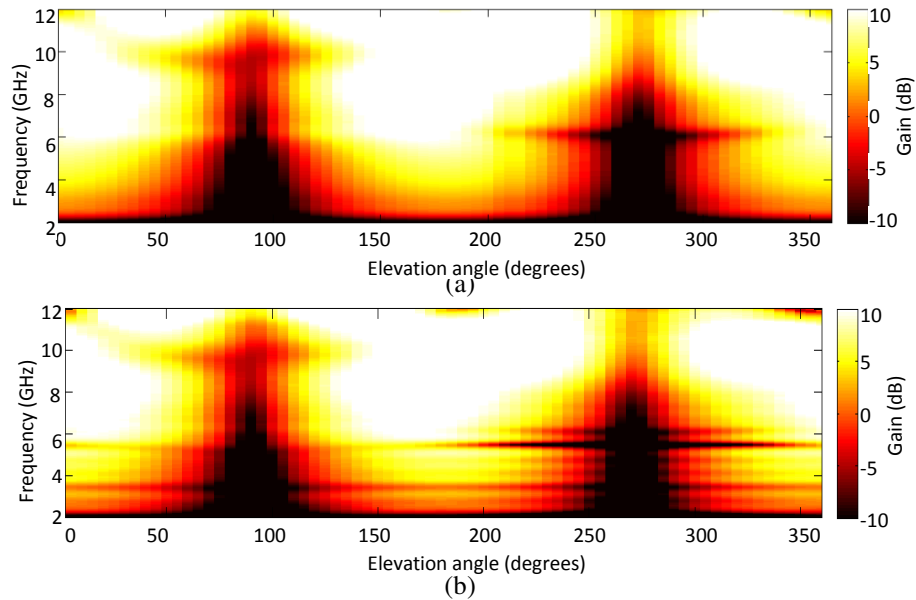

Fig. 5.32: Simulated gain in the elevation plane (a) UWB antenna and (b) dual band-notched UWB antenna.

Fig. 5.32 (a) and (b) show the gain response in the elevation plane which are highly distorted around 90° and 270° corresponding to the null points of the 'figure of eight pattern' in that plane. Gain reductions in the unwanted bands for the elevation plane are not as prominent as that in azimuth plane.

Normalised received pulse:

Fig. 5.33 (a) and (b) illustrates the behaviour of the normalised received pulses in the azimuth plane for different orientations of virtual probes around the antenna in CST. From the Fig. 5.33 (a), it is observed that the received pulses are exact replica of the input Rayleigh pulse and remains unchanged throughout the azimuth plane.
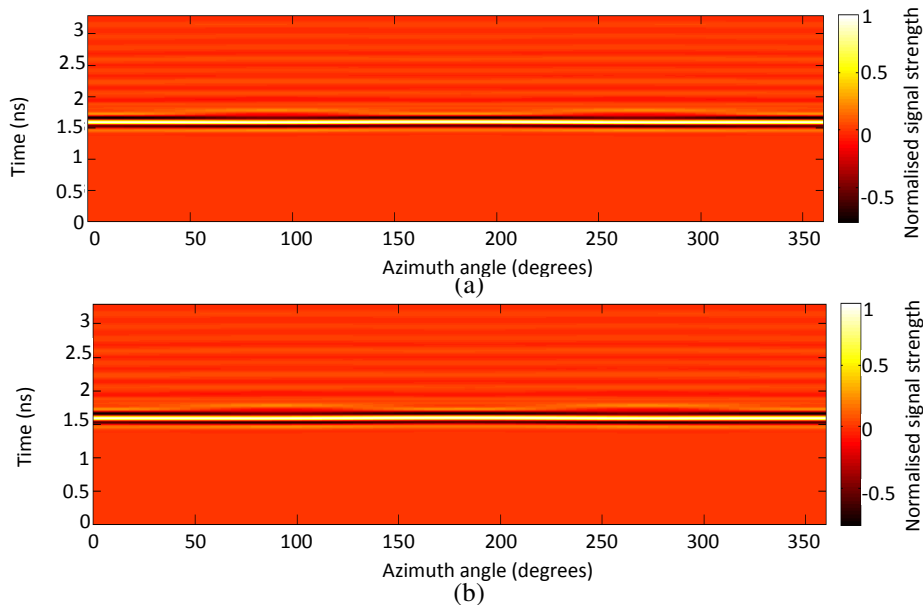

Fig. 5.33: Normalised received pulses in the azimuth plane (a) UWB antenna and (b) dual band-notched UWB antenna.

Fig. 5.33 (b) which corresponds to dual band-notched antenna shows more ringing in the received pulses compared to Fig. 5.33 (a).

Fig. 5.34 (a) and (b) describe the pulse response in the elevation plane. These plots show some distortions around 90° and 270° in the elevation plane. The received pulses are inverted compared to the reference input pulse over the angle from 90° to 270°. Ringing effect is more pronounced in Fig. 5.34 (b) which corresponds to elevation plane of dual band-notched antenna.
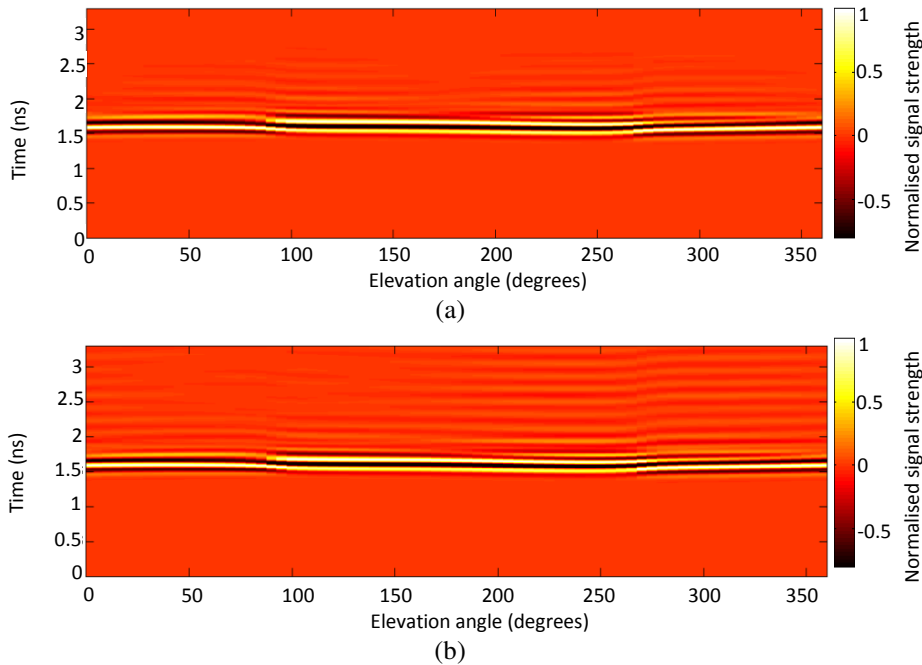

(a)

(b)

Fig. 5.34: Normalised received pulses in the elevation plane (a) UWB antenna and (b) dual band-notched UWB antenna.

Parameters of received pulse:

Fig. 5.35 describes the FWHM and ringing of the received pulses. In the azimuth plane, the variations in FWHM (envelope width) and the ringing w.r.t angle are very small, i.e., almost constant for all the orientations. The ringing duration for dual band-notched antenna is around

300 - 370 ps which is slightly higher than that of the UWB antenna (192 - 260 ps). In elevation plane both the plots exhibits more variations compared to azimuth plane. In both the planes the parameters FWHM and ringing are within the tolerable limits of few hundreds of picoseconds, hence the antenna can support high speed data transmission.
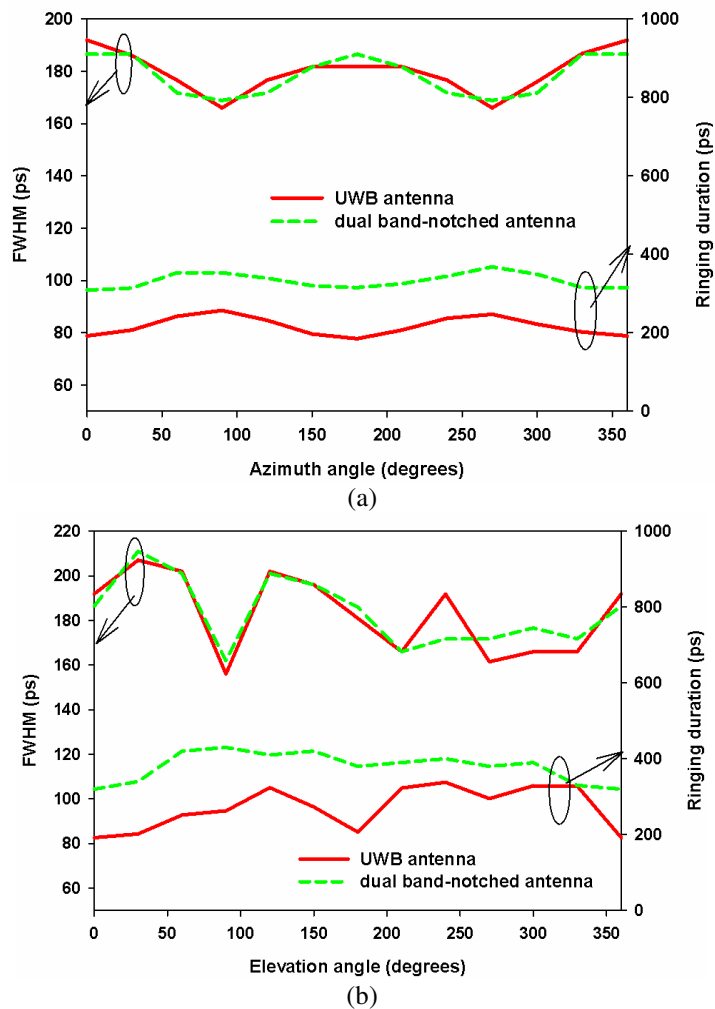

(a)

(b)

Fig. 5.35: FWHM and ringing duration of the simulated received pulses in the (a) azimuth plane and (b) elevation plane.

5.4   Experimental Results

Reflection coefficient:

Measured reflection coefficient of the UWB slot antenna is compared with the simulated result in Fig. 5.36 (a) and agrees reasonably well. The antenna covers frequencies from 2.5 GHz to 12 GHz with four resonant frequencies within the band. Fig. 5.36 (b) shows the reflection
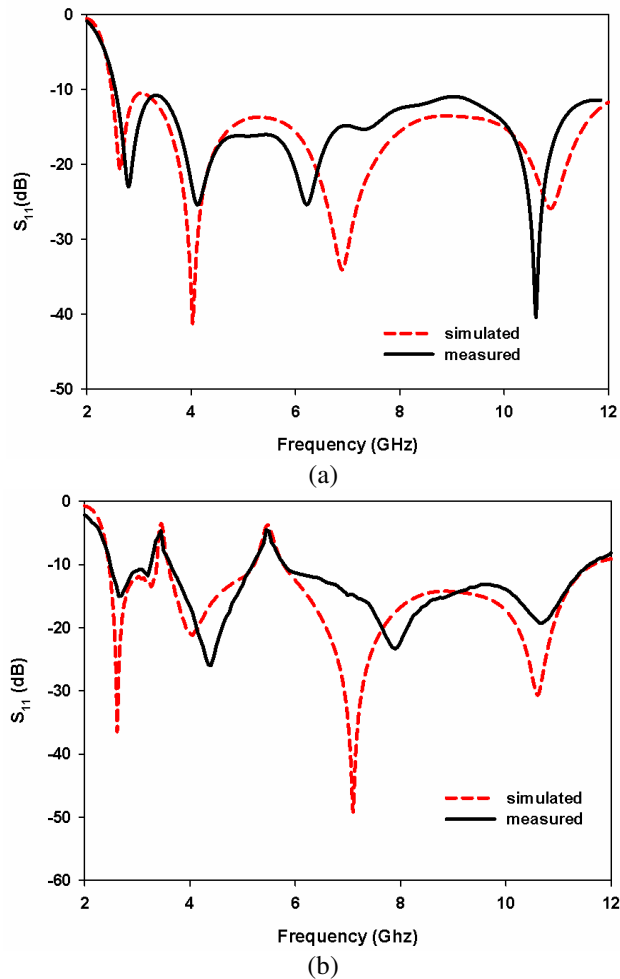

(a)

(b)

Fig. 5.36: Simulated and measured S_{11} of (a) UWB slot antenna and (b) dual band- notched UWB antenna.

coefficient characteristics of the dual band-notched UWB antenna which rejects frequencies in the WiMAX and WLAN bands without changing the characteristics of the UWB antenna in Fig. 5.36 (a). S_{11} can be improved by modelling the coaxial connector in simulation.

Radiation patterns:

Fig 5.37 (a) - (d) displays the normalised radiation patterns of the UWB band-notched slot antenna at four resonant frequencies 2.7 GHz, 4 GHz, 7 GHz and 10.7 GHz within the operating band. The measured radiation patterns are compared with the simulated results and agree reasonably well. Co-polarised patterns in the H-plane (x-z plane) are nearly non-directional and it continues to remain as such till the upper end of the UWB band. Co-polar patterns in the E-plane (y-z plane) follow 'figure of eight" shape over the entire band. i.e., the antenna exhibits nearly omni-directional radiation patterns over a wide bandwidth which is an attractive feature for UWB communication applications.
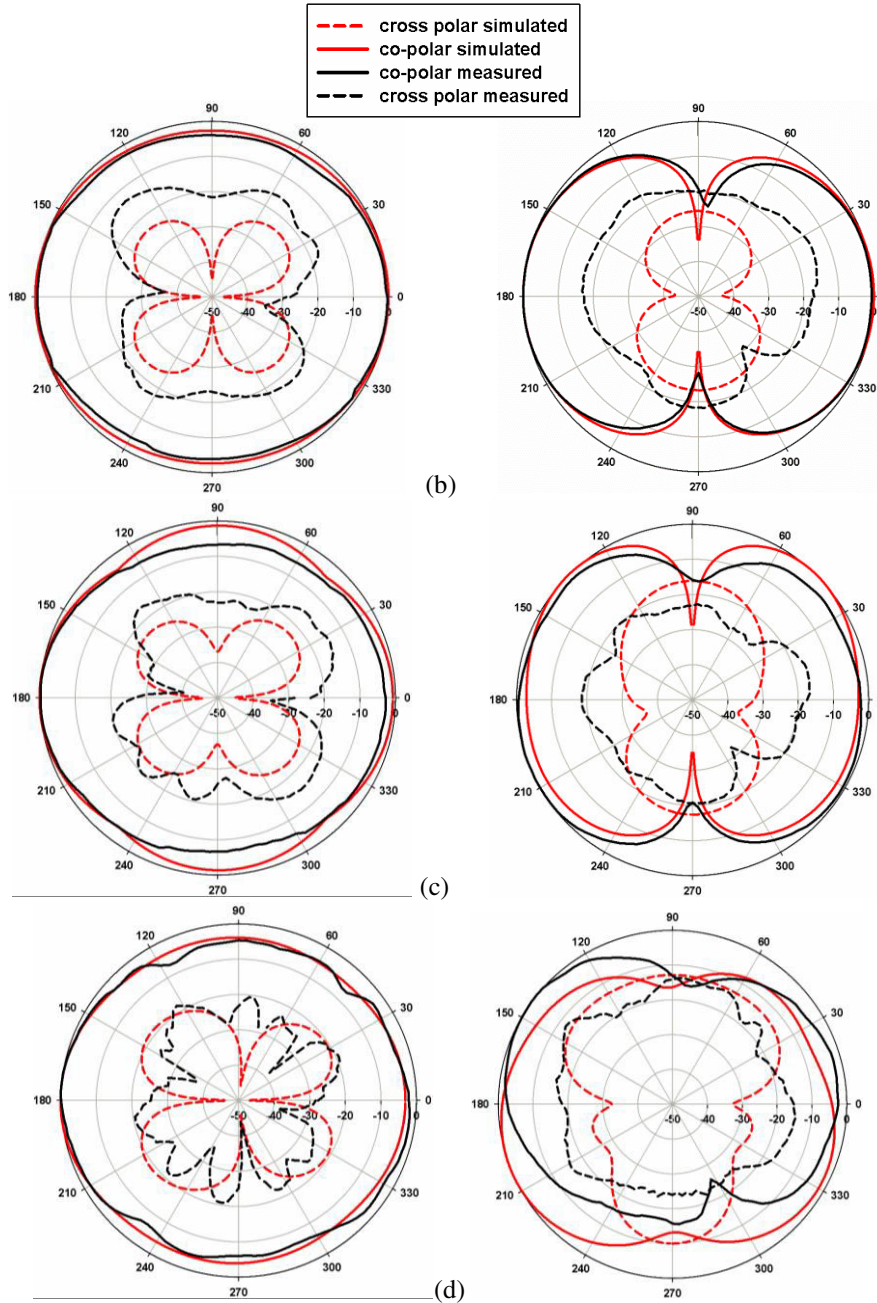

(a)
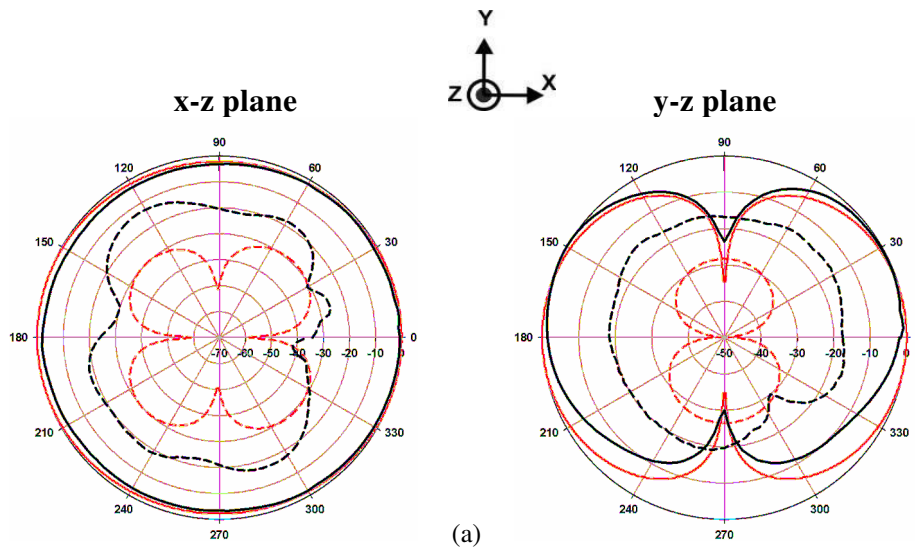
Fig. 5.37: Simulated and measured radiation patterns of the UWB dual band-notched slot antenna at frequencies (a) 2.7 GHz (b) 4 GHz (c) 8 GHz and (d) 10.7 GHz.

It is also observed that the antenna has polarisation discrimination better than -15 dB throughout the operating band in the both the planes along the bore sight. This is because of the current distribution shown in Fig. 5.11 (a) to (d), where at all the resonant frequencies the major part of the current is contributed by the vertical components rather than the horizontal components, thus less cross polar radiations. Deviation in signal strength is less than 5 dB for H-plane patterns.

Gain and efficiency:

Measured gain and efficiency of the UWB antenna are compared with the simulated one in Fig. 5.38 (a). The gain is measured using gain comparison method as mentioned in Chapter 3, section 3.5.1.

The proposed antenna exhibits a moderate gain response with variations less than 2.3 dB throughout the desired UWB frequency band. The radiation efficiency is measured using a wideband Wheeler cap method mentioned in Chapter 3, section 3.5.1 and is found to be varying from 80% to 90% across the operating band. Fig. 5.38 (b) shows the gain and efficiency of dual band-notched antenna. The responses are almost similar to that in Fig. 5.38 (a) with sharp dips in the notched bands. The efficiency also drops to 45% at the notched frequencies. Sharp decrease in gain and efficiency at the notched bands ensures the band-rejection behaviour of the proposed band-notched antenna.
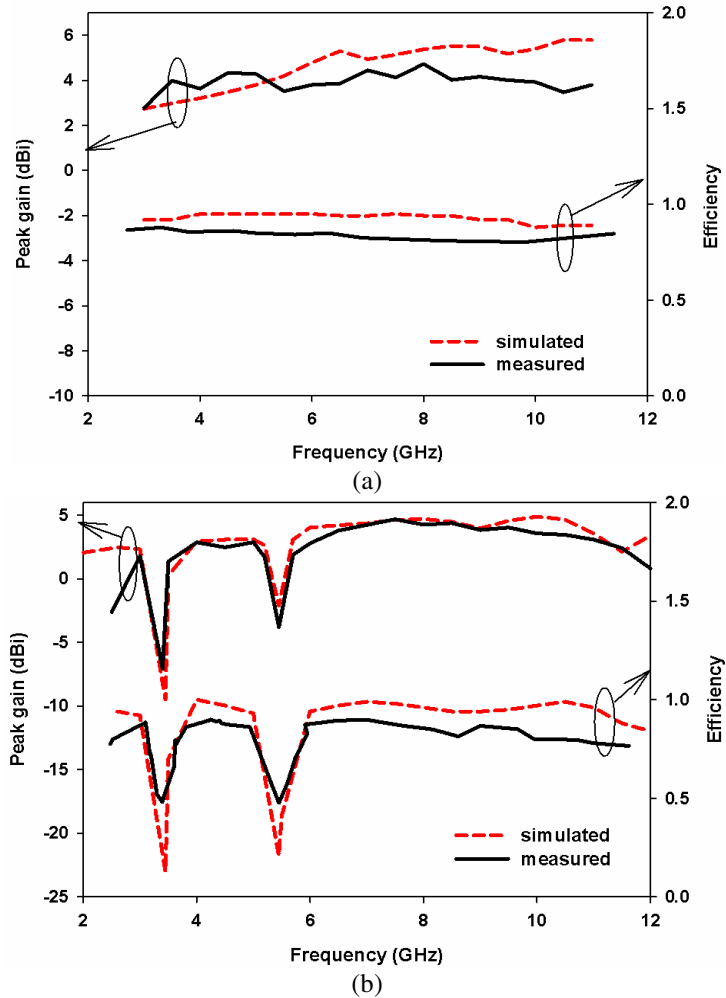
Fig. 5.38: Simulated and measured gain and efficiency of (a) UWB slot antenna and (b) dual band-notched antenna.

Time domain analysis:

Since the UWB antennas are mainly used for short distance pulse communication applications, it is recommendable to evaluate the pulse handling capability of the antenna; i.e., the amount by which the radiated pulse is dispersed by the UWB antenna. Two important parameters which are used to evaluate the amount of pulse dispersion

are antenna transfer function S_{21} and group delay. The pulse related measurements are carried out in the azimuth plane.

Antenna transfer function S_{21} and group delay:

Antenna transfer function and group delay are measured using two identical UWB antennas mounted in two different orientations; face to face and face to side as described in Chapter 3, section 3.5.2.3.
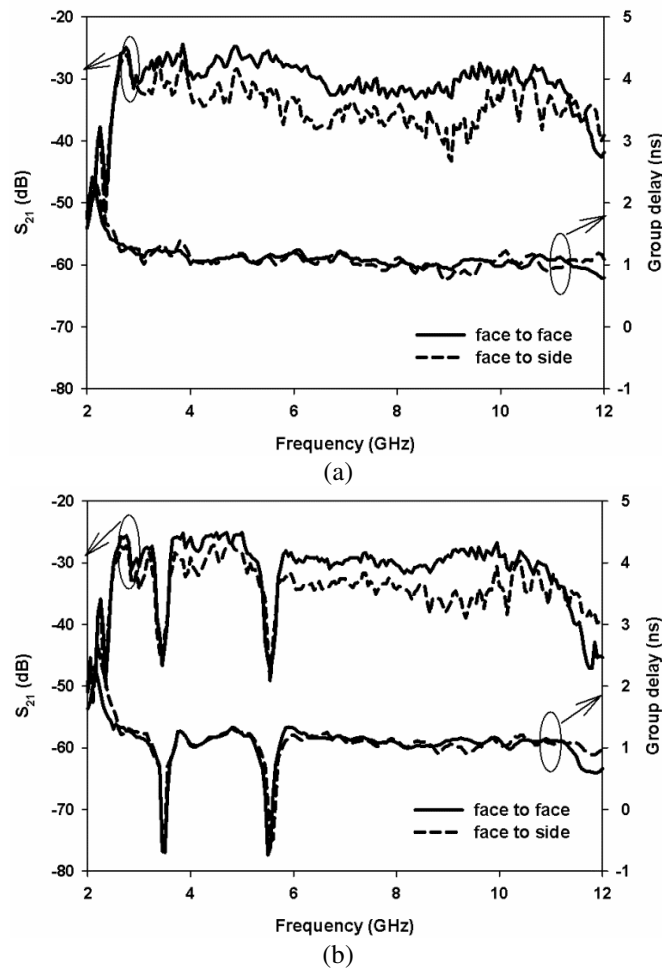

(a)

(b)

Fig. 5.39: Measured antenna transfer function S_{21} and group delay of (a) UWB slot antenna and (b) dual band-notched antenna.

Measured S_{21} and group delays are shown in Fig. 5.39. Antenna transfer function displayed in Fig. 5.39 (a) is almost flat within the operating band while it drops drastically outside the desired band. Group delay response remains almost constant throughout the band. So the pulse dispersion due to the antenna will be negligible. Fig. 5.39 (b) displays the measured values for the dual band-notched antenna. Both S_{21} and group delay are similar to that in Fig. 5.39 (a) except sharp dips at the notched bands. At the notched bands, fluctuations in S_{21} are more than 10 dB and the group delay drops below -0.7 ns. It indicates that the notch functions of the antenna perform reasonably well.

Received pulse:

Fig. 5.40 illustrates the simulated and measured normalised received pulses for the two extreme orientations of the proposed antennas. Measured pulses in Fig. 5.40 (a) are observed to be the replica of the simulated result with negligible ringing tails. Fig. 5.40 (b) shows the received pulses corresponding to the dual band-notched antenna and found to be same as that of UWB antenna without notches but with slight increase in ringing tails. In these plots, the pulses are shifted along the time axis to display them clearly.

(a)

(b)

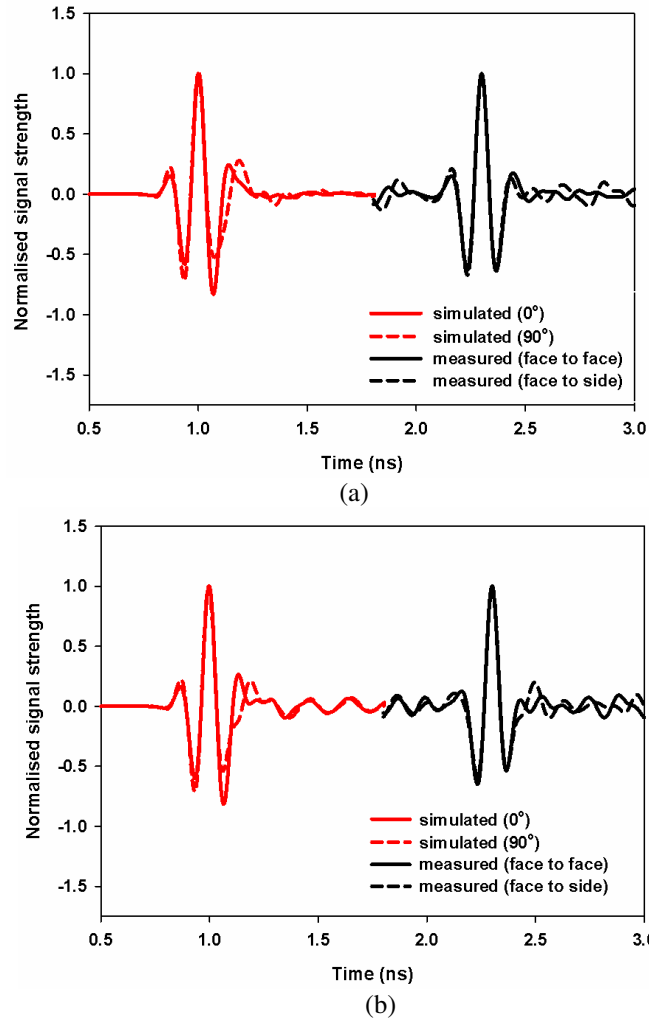**Fig. 5.40: Normalised received pulses of (a) UWB slot antenna and (b) dual band-notched antenna.**

Fidelity:

It measures the extent to which the received pulse is distorted w.r.t. the source pulse. This compares the shape of the received pulse with the source pulse. Fig. 5.41 illustrates fidelity of the received pulse. High fidelity values greater than 0.9 observed in Fig. 5.41 (a) reveal

that the radiated pulse from the UWB antenna is an exact replica of the source pulse. Fig, 5.41 (b) shows the fidelity resulting from dual band notched antenna. High fidelity value is observed i.e., pulse distortions due to the proposed antenna are negligible.
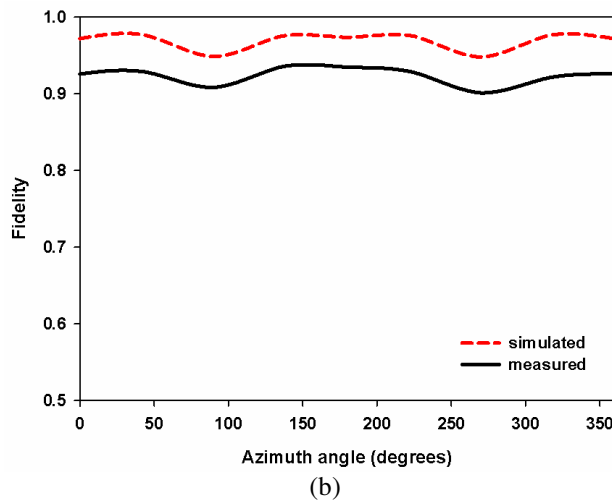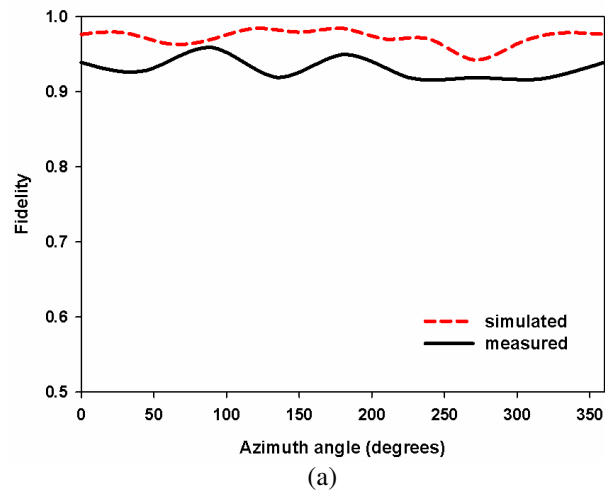

(a)

(b)

Fig. 5.41: Simulated and measured fidelity of (a) UWB slot antenna and (b) dual band-notched antenna

5.5 Conclusion

A CPW-fed slot antenna suitable for UWB applications is presented in this chapter. The bandwidth defined by $S_{11} < -10\ dB$ extends from 2.5 GHz to 12 GHz. Ground plane of a bevelled rectangular strip is extended around the strip to form a slot structure. The slot structure improves the coupling between the modes due to the extended ground and the strip and thus supports multiple modes to derive UWB bandwidth. Slits cut on the extended ground produce resonant frequency at the lower end of the operating band without increasing the size of the antenna. This is equivalent to reducing the overall size of the antenna. Impedance match over the entire bandwidth is obtained by bevelling the ground plane corners near the feed point. By placing Z- shaped parasitic element with in the radiating aperture and attaching quarter wave length stub to the ground plane, co-existing WiMAX and WLAN bands are rejected respectively.

Exhaustive parametric studies are carried out to analyse the properties of resonant frequencies and bandwidth of the proposed structure. Design equations are developed and validated to design the antenna on any substrates. Simulation analysis on antenna transfer function and radiated pulses are performed to evaluate the response of the antenna to the pulse input.

The antenna exhibits broad impedance match, stable radiation pattern and moderate gain response over the entire operating bandwidth as required by UWB communication systems. To verify the suitability

of the antenna for UWB pulse communication applications, time domain analysis are performed. Measured results show that the antenna has flat transfer characteristics S_{21} and constant group delay throughout the band which ensures minimum pulse dispersion. Another parameter called fidelity is also calculated for analysing the amount of pulse distortions due to the antenna. High fidelity value obtained reveals that the antenna is capable of handling the narrow pulses efficiently.

References

[1] M. J. Amman, "Control of the impedance bandwidth of wideband planar monopole antennas using a bevelling technique", Microwave and Optical Technology Letters, vol. 30, no. 4, pp. 229–232, 2001.

[2] C. A. Balanis, Antenna Theory: Analysis and Design, Wiley & Sons, New York, NY, USA, 1996.

[3] Olusola O. Olaode, W. D. Palmer, and W. T. Joines, "Effects of meandering on dipole antenna resonant frequency", IEEE Antennas and Wireless Propagation Letters, vol. 11, pp. 122-126, 2012.

[4] W. X. Tang, H. Zhao, X. Y. Zhou, J. Y. Chin, and T. J. Cui, "Negative index material composed of meander lines and SRRs", Progress In Electromagnetics Research B, vol. 8, pp. 103-114, 2008.

[5] M. R. Booket, M. Kamyab, A. Jafargholi and S. M. Mousavi, "Analytical modelling of the printed dipole antenna loaded with CRLH structures", Progress In Electromagnetics Research B, vol. 20, pp. 167-186, 2010.

.....ೞೞ.....

Chapter **6**

CONCLUSIONS

The thesis describes the outcome on the design and analysis of dual band-notched UWB monopole and slot antennas. This chapter summarises the results of the research work carried out, then follows the suggestions for future work.

6.1   Thesis Summary and Conclusions

The thesis presented a detailed study on the design and characterisation of dual band-notched UWB antennas. Mainly two categories of antennas are considered; monopole and slot antennas. Two UWB designs proposed are truncated circular disc monopole and a slot antenna, both with dual band-notched characteristics.

Firstly, the evolutions of the proposed antenna are considered to learn how UWB impedance band response of the antenna can be achieved. Through structure modifications these antennas are made to support multiple modes. The overlapping of these modes results in

UWB characteristics. Gradual tapering on the radiating patch and ground plane near the feed point is employed for the proposed antennas for enhancing the impedance bandwidth. Gradual transitions from feed to radiator/ground avoid sharp variations in impedance from one resonant mode to another, lead to wide band performance.

Effects of various geometrical parameters of the antenna on reflection coefficient characteristics are analysed. The behaviour of current pattern and radiation pattern at different resonant frequencies are studied. Then based on these observations, simple design equations for the UWB antennas on any substrates are developed and validated using CST.

The proposed UWB antennas are modified by incorporating resonant structures within the radiating patch or ground plane to reject the interferences from co-existing narrow band wireless services. These embedded notch filters avoid the need for separate filter thus make the system bit compact, so suitable for portable wireless devices.

Summary of the proposed dual band notched UWB antennas:

1.   Truncated circular disc monopole antenna

This antenna is derived from a CPW fed conventional circular disc monopole of size 38 mm × 47 mm which exhibits omnidirectional pattern especially at the lower end of the spectrum (limited to 4.5 GHz). By modifying its geometry as described in Chapter 4 the pattern bandwidth (omnidirectional pattern) of the proposed antenna is extended to around 7.5 GHz with a reduction in size to 25 mm × 20 mm.

The antenna has wide impedance bandwidth from 3.4 GHz to more than 12 GHz with gain varies from 1.6 dBi to 4.4 dBi and radiation efficiency not less than 74% over the entire bandwidth.

Half-wavelength resonator slots are incorporated in this design to avoid the interferences from the co-existing narrow band wireless services. By employing multiple slots on the radiator as well as on the ground, multiple notch functions can be achieved. In this design, narrow folded U-slot and U-slot etched on the radiating patch reject the WiMAX band and WLAN band respectively. Band-notched UWB structure operates over a wide bandwidth of 3.1 GHz to more than 12 GHz with rejection bands at 3.45 GHz and 5.65 GHz. The gain response drops to - 5.1 dBi and – 6.8 dBi at the notch frequencies. Similar variations in efficiency is also observed, which decreases to 35% and 50% at the notched bands. The designed notch structures reject the unwanted bands very efficiently. (Chapter 4, pages 154-158)

2. UWB slot antenna

The proposed UWB slot antenna is obtained by employing impedance bandwidth enhancement techniques on a CPW-fed rectangular monopole operating at 5.6 GHz. Bandwidth enhancement techniques involve extension of rectangular ground to surround the monopole to form a slot structure, inserting slits on the extended ground and bevelling the ground plane corners near the feed point. With these geometrical modifications the resultant antenna structure covers a wide impedance bandwidth from 2.5 GHz to more than 12 GHz with omni-directional radiation patterns in the entire band. The

overall size of the antenna is 30 mm × 27 mm. The antenna exhibits a flat gain response (2.1 dBi to 4.3 dBi) with efficiency greater than 80% over the operating bandwidth.

A combination of parasitic element and stub employed in this design facilitate the satisfactory functioning of the antenna even in the midst of WiMAX and WLAN environment. Z-shaped parasitic element in the vicinity of radiating aperture rejects WiMAX band and quarter wavelength stubs connected to the ground plane rejects the WLAN band. The impedance bandwidth of the band-notched antenna extends from 2.5 GHz to more than 12 GHz with rejection bands at 3.44 GHz and 5.42 GHz. A sharp decrease in gain to -7.4 dBi & -4.8 dBi and efficiency to 45% observed at the notch frequencies ensure the frequency rejection capability of the resonant structures employed in this design. (Chapter 5, pages 211- 214)

Since the UWB is an impulse-based technology, the transient response is also considered in addition to the conventional electrical parameter. For analysing the transient response of the antennas, measurements are carried out in frequency domain using a vector network analyser (VNA). The antenna transfer function S_{21} and group delay are measured in the azimuth plane. Flat S_{21} response over the operating bandwidth is obtained for UWB slot antenna and it decreases drastically outside the operating band. Truncated circular disc antenna possess flat response up to around 8 GHz, after that there is a slight decrease in power level. Group delay observed is almost constant with variations less than 1ns for both the antennas. With band-notched

structures, truncated circular disc monopole antenna shows group delay variations of 2.0 ns at 3.45 GHz & -1.5 ns at 5.65 GHz while the UWB slot antenna exhibits -1.8 ns at both the notch frequencies.

Received pulses derived from the measured S_{21} are similar to the excitation pulse and the amount of pulse distortion due to the antenna is calculated using a parameter called fidelity. Fidelity for dual band-notched UWB slot antennas is greater than 0.9 (0.9 -0.95) while for the dual band-notched truncated circular disc it is in the range of 0.78 to 0.88.

The proposed antenna designs can provide ultra wide band response with band-notched functions. The truncated circular disc presented gives an improved performance in terms of radiation pattern compared to conventional circular disc monopole, thus its transient response also. The UWB slot antenna exhibits superior transient response for different space coordinates with fidelity greater than 0.9, owing to their nearly omnidirectional pattern over the whole bandwidth. The band-notched antenna designs proposed in this thesis have good performances in terms of return loss, radiation pattern, gain, efficiency, transient response etc. over the entire ultra wide bandwidth, which make them a promising candidate for UWB pulse communication applications. (Chapter 4, pages 159-163, Chapter 5, pages 215-219)

6.2 Suggestions for Future Work

Dual band-notched UWB antenna designs presented in this thesis have fixed band-notched characteristics once it is fabricated. Since interferences from narrow-band systems vary with environment,

provision to electronically enable or disable the band-notched functions and tune the notch frequencies within the pass-band of a UWB antenna may be investigated in future. This allows the antenna to operate in multiple predefined frequency bands which supports the cognitive radio (CR) concept. When the antenna is in the UWB mode, it can be used for sensing the spectrum and when it is in the reconfigured modes, the antenna can be used for communication purpose. Electronic switching of the notch bands can be realised by loading the resonant structures with RF switches eg. PIN diode or and Micro Electro Mechanical Systems (MEMS) switches. While varactor diodes can be used for achieving tuneable band-notched characteristics.

UWB systems suffer from multipath fading like other wireless communication systems. So design of multiple-input-multiple-output (MIMO) UWB antenna with less mutual coupling may be considered to improve the capacity and link quality of wireless UWB systems.

UWB receiver requires low noise amplifier (LNA) due to the low transmission power level of UWB systems. Co-design and co-optimisation of UWB-LNA architecture may be investigated to get a best compromise between gain and noise figure.

Most of the research on UWB antenna is mainly focussed to improve short distance wireless communication systems which require omnidirectional patterns. But there are applications like through-the-wall radar imaging which need to cover distance up to 3 to 5 m behind a 20 cm thick, solid concrete wall or a 25 m without any obstacles.

Directional antenna with high gain is required in these cases because the power level of the UWB transmitter is limited by the FCC's emission mask. Therefore, research on high gain UWB directional antenna and antenna array may be carried out.

.....ೞೞ.....

EQUIVALENT CIRCUIT MODEL OF BAND-NOTCHED UWB ANTENNAS

1. Introduction

One of the major challenges in the development of UWB communication systems is the co-design of UWB antennas with other function blocks of the system. This is necessary for optimising the performance of the whole system. The front end of a UWB receiver is low noise amplifier (LNA), optimisation of UWB antenna-LNA is to be carried out to get a best compromise between gain and noise figure. So it is necessary to do co-simulation of the antennas with the UWB transmitter and receiver. Since circuit simulation is traditionally done in a time-domain simulator such as SPICE, a general equivalent circuit model of UWB antennas is required [1]. The basic requirements for the equivalent circuit model of UWB antennas is that input impedances or admittances of the equivalent circuit model should match up with those of the modelled antenna.

For UWB antennas, large bandwidth is due to the overlapping of several adjacent resonances and can be represented by serially

connected parallel R-L-C resonant circuits [2] as shown in Fig. 1. Two additional elements, L_0 and C_0 are added to the equivalent circuit model of the UWB antenna to account for the impedance transformation due to probe inductance and the static antenna capacitance [2]. The band-notched functions are realised according to conceptual circuit model by connecting the antenna input impedance with either a parallel or a series R-L-C resonant circuit depending on the impedance characteristics at the notched frequency [3] – [5]. The final element values are obtained by curve fitting the impedance response of the circuit model developed in ADS with the CST simulated impedance.
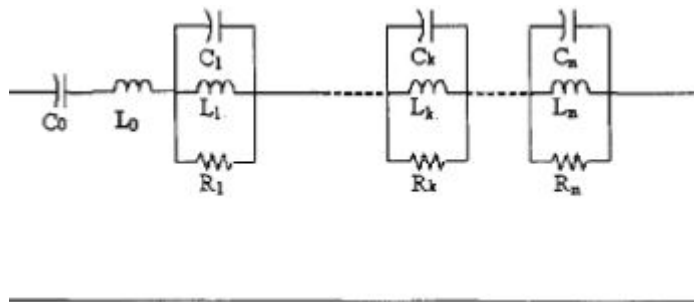

Fig. 1: Equivalent circuit / impedance model of UWB antenna [2]

The modelling procedure begins with the extraction of the R-L-C element values of each of the individual resonances within the bandwidth of UWB antenna without notch structures. This can be derived by transforming the resonant peaks of the simulated input impedance of reference UWB antenna into the equivalent parallel R-L-C resonant circuit using (1) to (3). Here, to determine the values of

R-L-C components the real part of the input impedance alone is considered [2].

$$Q_k = \frac{f_k}{BW_k} \quad \text{..} \quad (1)$$

$$Q_k = R_k\sqrt{\frac{C_k}{L_k}} = \omega_k R_k C_k \quad \text{.............................} \quad (2)$$

$$\omega_k = \frac{1}{\sqrt{L_k C_k}} \quad \text{..} \quad (3)$$

where Q_k is the quality factor, f_k is the resonant frequency, R_k is the real part of the impedance at resonance, BW_k is the range of frequencies where the real part of the input impedance is equal to or greater than 0.707 of the maximum value of the kth resonant peak. The initial values of f_k, R_k and BW_k can be obtained directly from the CST simulated input impedance of the UWB antenna.

2. Equivalent circuit modelling

(a) Dual band-notched truncated circular disc UWB antenna

CST simulated real input impedance of the truncated circular disc UWB antenna discussed in Chapter 4 is shown in Fig. 2. It is observed that the simulated real input impedance of the UWB antenna has four resonance peaks (parallel resonance modes) within the UWB band, so the impedance model of the antenna which thereafter called as reference antenna consists of four parallel resonant circuits as given in Fig. 3. The values of L_0 and C_0 are obtained after exhaustive trial and

error method using ADS. It is observed that these components improve the accuracy of the input impedance characteristics of the circuit model.
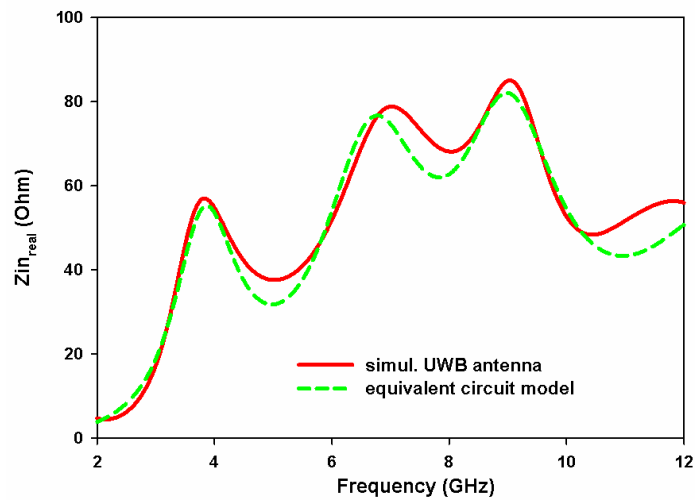

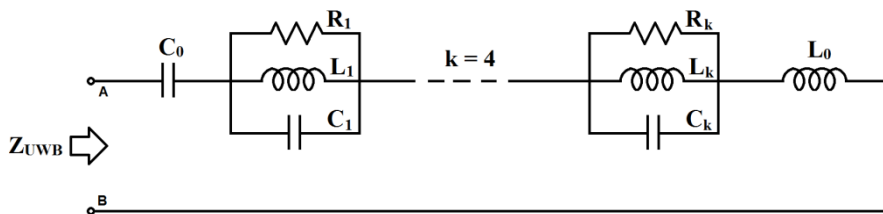**Fig. 2: Real input impedance Z_{in} of truncated disc the UWB antenna**

Fig. 3: Lumped element impedance model of the UWB antenna

The reflection coefficient characteristics obtained from the Fig. 3 is compared with the CST simulated and measured reflection coefficient characteristics in Fig. 4.
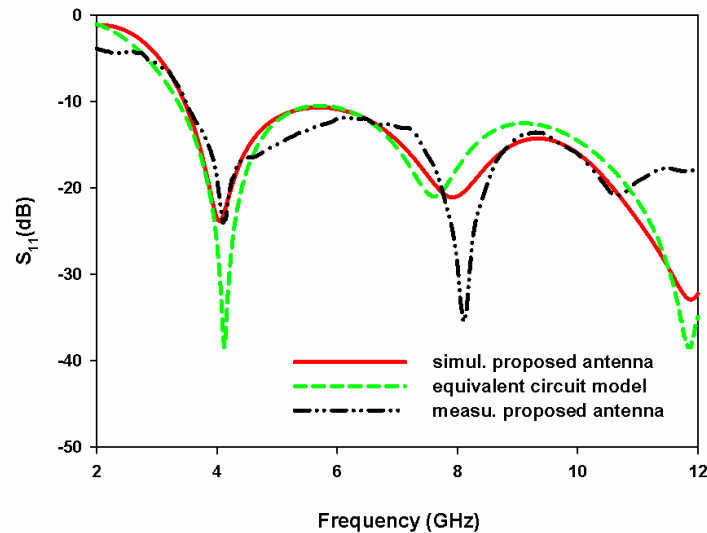
Fig. 4: Comparison of reflection coefficient of the UWB antenna

From the simulated impedances of the truncated circular disc dual band notched antenna shown in Fig. 5 (a) & (b), it is seen that in the WiMAX (3.45GHz) notched frequency band, the imaginary component crosses zero and changes from capacitive to inductive while the real component presents a low resistance (2.078Ω), similar to the behaviour of a series RLC circuit, i.e., the corresponding band rejection structure (folded U-slot) acts as a series RLC circuit. At WLAN (5.65GHz) notched frequency band, the real component has a low resistance (5.10Ω) like series RLC circuit. An additional sharp resistance peak similar to a parallel RLC circuit (75Ω) is observed very close to the notched frequency compared to reference UWB antenna, when the WLAN band is rejected. Here, the imaginary component follows neither parallel RLC characteristic nor series RLC characteristics. So the impedance model of the corresponding band rejection structure

(U-slot) is considered as formed by a combination of a series and a parallel RLC circuits operating close to 5.65 GHz.
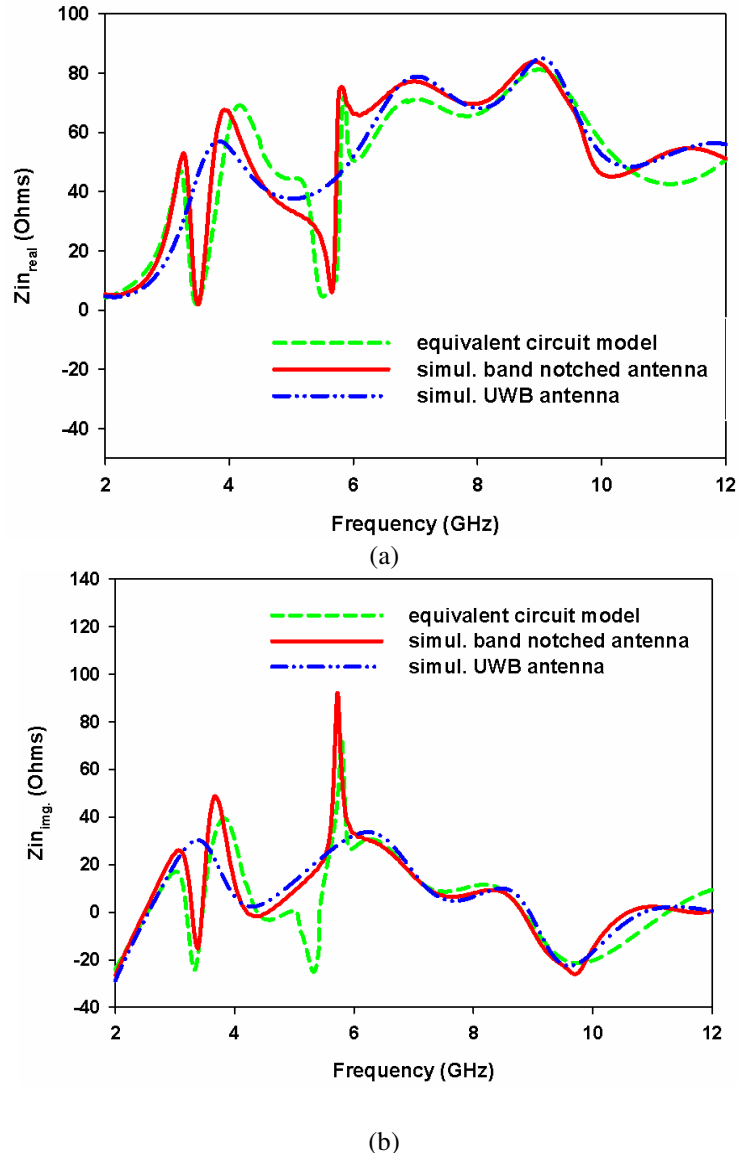

(a)

(b)

Fig. 5: Input impedances Z_{in} of the UWB antenna and dual band-notched antenna (a) real component (b) imaginary component
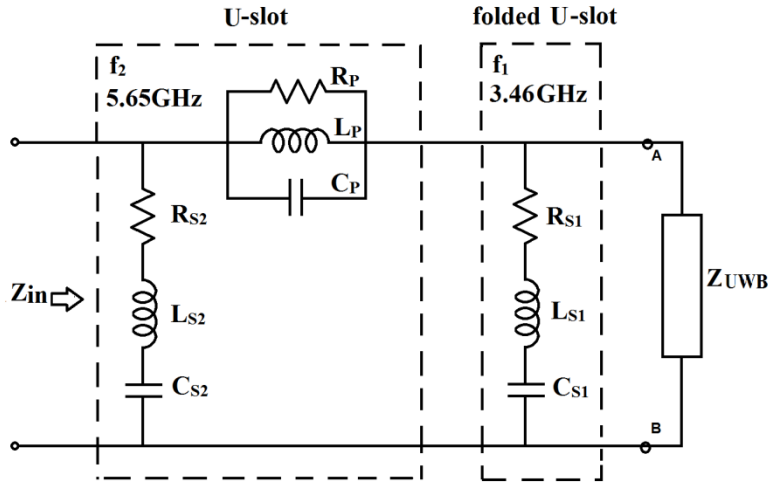
Fig. 6: Equivalent circuit model of the dual band- notched truncated disc UWB antenna in Chapter 4

The equivalent circuit model of the dual band-notched truncated circular disc antenna is shown in Fig. 6. In this model series RLC circuit operating at 3.45 GHz and then the combination of series and parallel RLC circuits operating close to 5.65 GHz are connected in parallel with Z_{UWB}. When the band notched antenna operates at either at WiMAX or WLAN band, the corresponding RLC circuit resonates and leads to high impedance mismatch at that frequency. Consequently, the antenna cannot radiate at this band.

From the CST simulation results in Fig. 5 (a), the initial lumped element values of each resonant circuit are calculated using the standard equations of parallel and series resonant circuits.

For parallel resonant circuits [2]

$$Q_p = R_p \sqrt{\frac{C_p}{L_p}} = R_p C_p \omega_p \quad .... (4)$$

$$\omega_p = \frac{1}{\sqrt{L_p C_p}} \quad \text{...(5)}$$

For series resonant circuits [4]

$$Q_s = \frac{1}{R_s}\sqrt{\frac{L_s}{C_s}} = \frac{1}{R_s C_s \omega_s} \quad \text{.. (6)}$$

$$\omega_s = \frac{1}{\sqrt{L_s C_s}} \quad \text{.. (7)}$$

where Q_p & Q_s represent the quality factors and ω_p & ω_s represent angular resonant frequencies. Then by employing curve fitting approaches [5] the final values of these unknown parameters are obtained and are listed in Table 1.

Table 1: Lumped element values of the equivalent circuit in Fig. 6

Circuits	No.	f(GHz)	R (Ω)	L (nH)	C (pF)
Parallel RLC cells (Z_{UWB})	1	3.92	65.67	0.9427	1.7520
	2	6.6	62.8	0.5797	1.0152
	3	8.9	52.8	0.2483	1.2870
	4	13.0	61.6	0.1829	0.7887
RLC Notch circuits	series 1	3.46	2.078	19.049	0.1105
	series 2	5.5	5.10	17.067	0.04919
	parallel	5.8	200	0.059	0.0126nF
Series LC	L_0	0.42 nH	C_0	1.32 pF	

The input impedance of the proposed band notched antenna by the equivalent circuit model is compared with the CST simulated impedance in Fig. 5 (a) and (b). Further, the reflection coefficient

obtained by the equivalent circuit model is compared with the CST simulated and   measured reflection coefficient of the proposed band-notched antenna in Fig. 7. These plots agree reasonably well over the entire UWB frequency range with minute fluctuations.
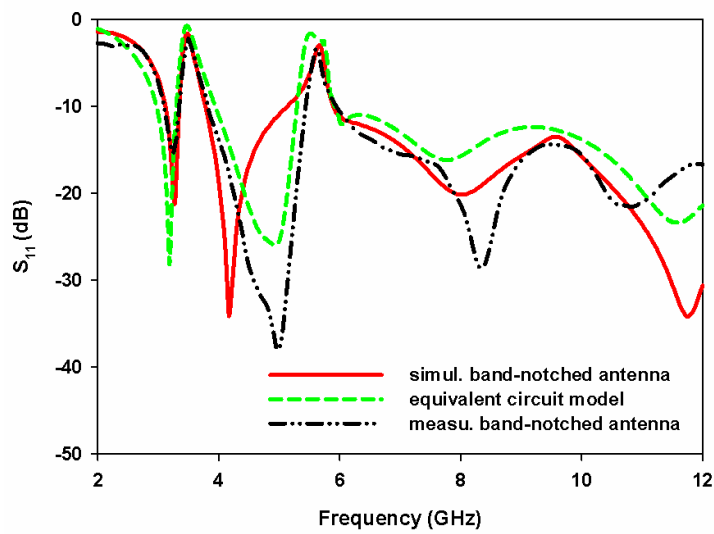

Fig. 7:   Comparison of reflection coefficient of truncated circular disc dual band-notched antenna in Chapter 4

(b)   Dual band-notched UWB slot antenna

Fig. 8 shows the simulated input impedance of the UWB slot antenna and its dual band-notched version presented in Chapter 5. The plot of reference UWB slot antenna (blue colour) has four resonance peaks (parallel resonance modes) within the UWB band, so its impedance model consists of four parallel R-L-C resonant cells.
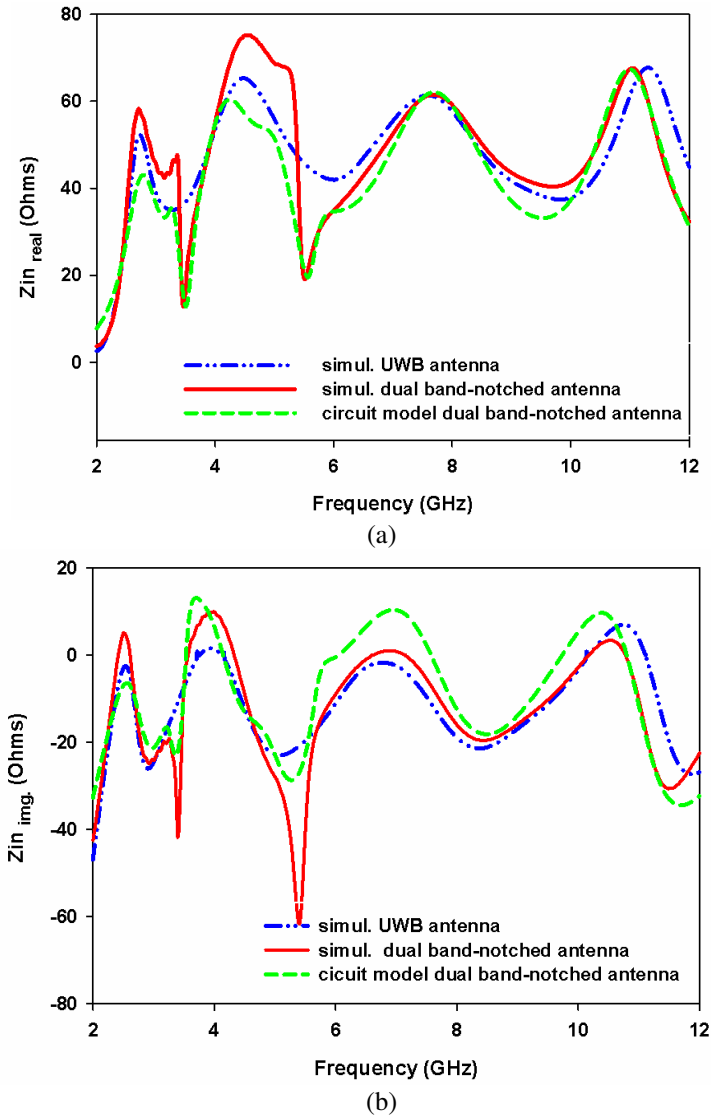
Fig. 8: Input impedances (Zin) of the UWB antenna and dual band-notched antenna (a) real component (b) imaginary component

From Fig. 8, it is seen that at the notched frequencies 3.44 GHz & 5.42 GHz, the real components have a low resistance values of 12.76 Ω and 19.0 Ω respectively like series R-L-C circuit. The values of the

remaining lumped elements L and C are derived by using the standard equations of series R-L-C resonant circuit. Further, it is seen that additional resistance peaks of 47.4 Ω and 68.4 Ω are occurred very close, prior to the notched frequencies 3.44 GHz and 5.42 GHz respectively compared to the reference UWB antenna. These resonance peaks can be approximated to parallel R-L-C circuits where the values of L and C are calculated using the standard equations of parallel R-L-C resonant circuit.

So the circuit model of the corresponding notch structures i.e., Z-shaped parasitic element as well as pair of L-shaped stubs are regarded as formed by the combination of a series R-L-C and parallel R-L-C circuits.
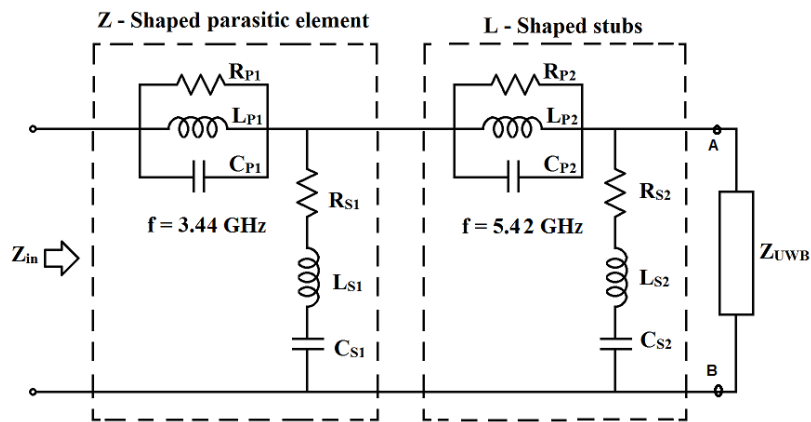

Fig. 9: Lumped element equivalent circuit model of proposed dual band-notched UWB slot antenna in Chapter 5

The equivalent circuit model of the proposed antenna can be considered as the combination of reference UWB antenna (Z_{UWB}), Z-shaped parasitic element and a pair of symmetrical L-shaped stubs

connected as shown in Fig. 9. When the proposed antenna operates at either at WiMAX or WLAN band, the corresponding R-L-C circuits resonate and provide high impedance mismatch at that frequency. Consequently, the antenna cannot radiate at this band.

Table 2: Element values of equivalent circuit model shown in Fig. 9.

R-L-C cells	1	2	3	4
Rk (Ω)	38.62	50.94	52.019	54.199
Lk (nH)	0.6142	0.7662	0.3775	0.1168
Ck (pF)	5.1600	1.8624	1.1912	1.8159
L_0-C_0	$L_0 - 0.48$ nH		$C_0 - 1.049$ pF	
Notch circuits	**Series 1**	**Parallel 1**	**Series 2**	**Parallel 2**
R (Ω)	12.76	11.833	10.13	22.36
L (nH)	28.770	0.0421	14.9755	0.1431
C (pF)	0.0714	55.341	0.0547	7.050

The circuit model is built, tuned and optimized in ADS. The extracted lumped element values of the proposed dual band-notched UWB slot antenna are summarised in Table 2. The input impedance of the proposed antenna by the equivalent circuit model is compared with the CST simulated impedance in Fig. 8 (a) & (b) and the curves agree reasonably well over the entire UWB frequency range with minute fluctuations. For further validation of the extracted equivalent circuit model, the reflection coefficient (dB) of the proposed antenna by circuit model is compared with the measured and CST simulated results in Fig. 10.
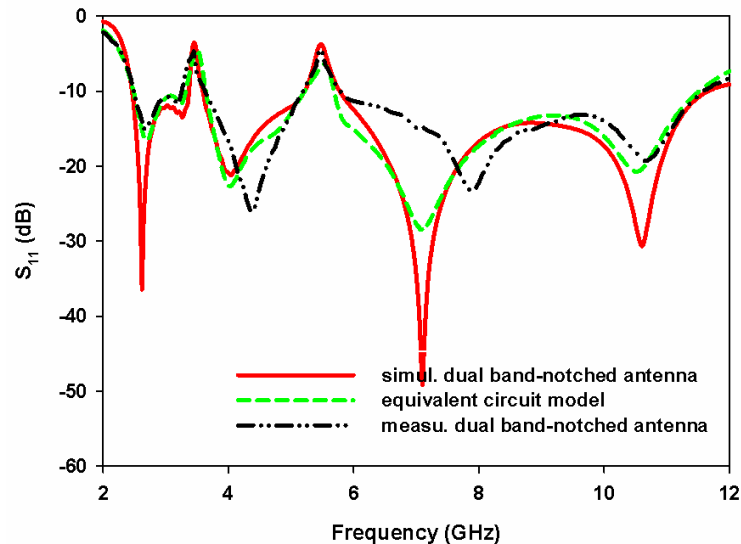
Fig. 10: Comparison of reflection coefficient (dB) of the dual band-notched antenna in Chapter 5

From the impedance models developed behaviour of notch structures can be studied. It is seen that at frequency rejection bands, the notch structures behave either as a parallel R-L-C, series R-L-C resonant circuit or combination of these two. The equivalent circuit developed is very useful for the optimisation of antenna-LNA architecture from the view point of a UWB system designer. It also allow the system designers to consider the effect of the UWB antennas in the simulation of the whole communication system

References

[1]   Y. Wang and J. Z. Li, "An equivalent circuit modelling method for ultra-wideband antennas", Progress In Electromagnetics Research, vol. 82, pp. 433–445, 2008.

[2]   Pele, A. Chousseaud and S. Toutain, "Simultaneous modelling of impedance and radiation pattern antenna for UWB pulse modulation," Proc. IEEE AP-S Int. Symp. pp. 1871–1874, 2004.

[3]   H. J. Zhou, B. H. Sun, Q. Z. Liu and J. Y. Deng, "Implementation and investigation Of U-shaped aperture UWB antenna with dual band-notched characteristics", Electronics Letters, vol. 44, no. 24, pp. 1387-1388, 2008.

[4]   K. Zhang, T. Wang, and L. L. Cheng, "Aanalysis of band-notched UWB printed monopole antennas using a novel segmented structure", Progress In Electromagnetics Research C, vol. 34, pp. 13- 27, 2013.

[5]   F. Zhu, S. Gao, A.T.S Ho, R. A. Abd-Alhameed, C. H See, T.W.C. Brown, J. Li, G. Wei and J. Xu, "Multiple band-notched UWB antenna with band-rejected elements integrated in the feed line", IEEE Transactions on Antennas and Propagation, vol. 61, no. 8, pp. 3952–3958, 2013.

.....ॐ.....

||||| List of Publication |||||

International Journals:

[1] **Sarah Jacob**, A. O. Lindo, C. M. Nijas, C K. Aanandan and P. Mohanan, "Analysis of CPW-Fed UWB Antenna for WiMAX and WLAN Band Rejection", Progress In Electromagnetics Research C, Vol. 52, 83-92, 2014.

[2] **Sarah Jacob**, Anila P.V., S. Mridula, P. Mohanan, "CPW-fed UWB Antenna with WiMAX Band-notched Characteristics" International Journal of Research in Engineering and Technology, Volume: 03 Special Issue: 15, pp. 52-56, Dec-2014, WCPS-2014.

[3] **Sarah Jacob**, V. A. Shameena, S. Mridula, C. K. Anandan, K. Vasudevan, P. Mohanan, "Planar UWB Antenna with Modified Slotted Ground Plane", International Journal of RF and Microwave Computer-Aided Engineering/Vol. 22, No. 5, pp. 594 – 602, September 2012.

[4] Shameena. V.A, **Sarah Jacob**, Mridula. S, Anju Pradeep, Lindo. A.O and P. Mohanan "A Compact CPW fed Slot Antenna for Ultra Wide Band applications", AEUE, International Journal of Electronics and Communication, Vol.56, pp.189-194, March 2012.

[5] Shameena. V.A, **Sarah Jacob**, Mridula. S, C.K. Aanandan, K. Vasudevan and P .Mohanan, A Compact modified ground CPW fed antenna for UWB Applications", Microwave Review Journal, Vol.17, No.1, September2011.

International/ National Conferences:

[1] **Sarah Jacob**, S. Nimisha, P.V. Anila and P. Mohanan, "UWB Antenna with Reconfigurable Band-Notched Characteristics using Ideal Switches", Proc. of IEEE International Microwave and RF Conference, pp. 136-139, IMaRC-2014, Bangalore, Dec. 2014.

[2] **Sarah Jacob,** Anila P.V., S. Mridula, P. Mohanan, "Planar UWB antenna with Dual band-notched characteristics", Proc. of International Symposium on Antennas and Propagation, pp. 232-235, APSYM-2014, Kochi, Dec. 2014.

[3] **Sarah Jacob,** S. Mridula, P. Mohanan, "Truncated Circular Disc UWB Monopole Antenna", Proc. of International Conference on Information Science, pp. 257-260, ICIS-2014, Kochi, July-2014.

[4] **Sarah Jacob** and P. Mohanan, "UWB antenna with Single Notch-Band for WLAN environment", IEEE International Applied Electromagnetic Conference 2011 (AEMC-2011), Calcutta, Dec. 2011.

[5] Shameena V.A, **Sarah Jacob**, C.K. Aanandan, K.Vasudevan and P. Mohanan, "A Compact CPW fed serrated UWB antenna" ICCSP, 2011, NIT Calicut, Kerala.

[6] Shameena.V.A, **Sarah Jacob**, Mridula.S, C.K.Aanandan, K.Vasudevan and P. Mohanan, "A Compact modified ground CPW fed antenna for UWB Applications" URSI GASS,2011, Istanbul, Turkey

[7] **Sarah Jacob**, S.Mridula, V.A. Shameena and P. Mohanan, " Planar UWB Antenna", Proc. of National Symposium on Antennas and Propagation , APSYM-2010, Kochi, Dec. 2010.

.....ॐ.....

▌▌▌ Curriculum Vitae ▌▌▌

Education

- 1993 – 1995, M. Tech (Master of Technology) degree in Electronics, Department of Electronics, Cochin University of Science & Technology, Cochin-22, Kerala.

- 1988-1992, B. Tech. degree in Electronics & Communications, Mar Athanasius College of Engineering, Kothamangalam, Kerala

- 1986-1988, Pre-degree (First group -Maths, Physics & Chemistry), St. Gregorios College, Kottarakkara, Kerala

- 1986, SSLC, Nicholson Syrian High School for Girls, Thiruvalla, Kerala

Awards Received

- 2011 - Awarded with Research Fellowship in Sciences for Meritorious students (RFSMS) by University Grants Commission (UGC), Govt. of India.

- 1993 - Awarded with PG Scholarship (GATE – Graduate Aptitude Test in Engineering), Department of Higher Education, Ministry of Human Resources Development (MHRD), Govt. of India.

Research Interests

- Planar antennas, Microwave communication, Metamaterial antennas, Electromagnetics,

- Biological effects of Microwaves, Dielectric resonator antennas, Microwave material characterisation etc.

Experience

Research

- 2008 – present, Research Scholar at Centre for Research in Electromagnetics and Antennas (CREMA), Department of Electronics, Cochin University of Science and Technology, Cochin - 22, Kerala

- 1995 - Project Trainee at ISRO (VSSC), Govt. of India, Thiruvananthapuram, as a part of the M. Tech. curriculum.

Teaching

- 2007 - Present, Associate Professor in Electronics, Engineering Colleges managed by IHRD, Thiruvananthapuram, Kerala.

- 1997 – 2007, Assistant Professor in Electronics, Engineering Colleges managed by IHRD, Thiruvananthapuram, Kerala.

- 1995 – 1997, Lecturer in Electronics, Applied Science College managed by IHRD, Thiruvananthapuram, Kerala.

Personal Details

Date of birth	:	10th April 1971
Sex	:	Female
Nationality	:	Indian
Religion	:	Christian
Permanent Address	:	Vyramon, Anjilimoodu, Angadical P.O., Chengannur, Kerala, India.

.....ഇൽ.....